Reports of NAS RA

National Academy of Sciences of the Republic of Armenia

ՀՀ ԳԱԱ ՋԵԿՈՒՅՑՆԵՐ

Հայաստանի Հանրապետության Գիտությունների Ազգային Ակադեմիա

Vol. 126 No. 1 2026

Published: 15 January 2026

eISSN: 3045-3151

Reports of NAS RA
National Academy of Sciences of the Republic of Armenia
Vol. 126, No. 1
2026

Editorial Board

Table of Contents

Original Research Articles

Review Articles

Letters to the Editor

Reports of NAS RA
ՀՀ ԳԱԱ Զեկույցներ
NATIONAL ACADEMY OF SCIENCES OF THE REPUBLIC OF ARMENIA
ՀԱՅԱՍՏԱՆԻ ՀԱՆՐԱՊԵՏՈՒԹՅԱՆ ԳԻՏՈՒԹՅՈՒՆՆԵՐԻ ԱԶԳԱՅԻՆ ԱԿԱԴԵՄԻԱ

2026 **Volume 126** **Issue 1** **Article No. 1**

Category: Physics
Type of Paper: Original Research Article
Received: August 24, 2025, **Revised:** November 28, 2025, **Accepted:** December 14, 2025, **Published:** January 16, 2026

DOI: 10.54503/0321-1339-2026.126.1-1

New Equation for a Spin-1/2 Particle with Three Additional Characteristics in the Presence of Electromagnetic and Gravitational Fields

Vasiliy Kisel[1], Elena Ovsiyuk[2], Anton Bury[3], Alina Ivashkevich[3], Viktor Red'kov[3*], and Artur Ishkhanyan[4]

[1]Belarusian State University of Informatics and Radioelectronics, Minsk, 220013 Belarus
[2]Mozyr State Pedagogical University, Mozyr, 247760 Belarus
[3]B.I. Stepanov Institute of Physics of NAS of Belarus, Minsk, 220072 Belarus
[4]Institute for Physical Research of NAS of Armenia, Ashtarak, 0204 Armenia

*Correspondence: v.redkov@ifanbel.bas-net.by

Abstract. Within the general Gel'fand–Yaglom method, starting from the extended 28-component representation of the Lorentz group, we construct a new relativistic P-invariant generalized equation for a spin-1/2 particle possessing three characteristics in addition to the electric charge. The model is first developed for a free particle, where the corresponding system of spinor equations is derived and then transformed into spin-tensor form. In this form, we incorporate the interaction with external electromagnetic fields. By eliminating the accessory variables of the complete wave function, we obtain a minimal four-component Dirac-like equation that contains three new interaction terms, interpreted as arising from the additional electromagnetic characteristics of the particle. This approach is further extended to a Riemann space–time background within the conventional tetrad formalism, leading to additional geometrical interaction terms involving the Ricci scalar $R(x)$, the Ricci tensor $R_{\alpha\beta}$, and the Riemann curvature tensor $R_{\alpha\beta\rho\sigma}(x)$.

Keywords: spin-1/2 particle, relativistic symmetry, generalized equation, additional electromagnetic characteristics, external electromagnetic and gravitational fields

1. Introduction

The general theory of relativistic wave equations has a long history [1]–[26]; for more details, see the recent book [24]. Within the general method of Gel'fand–Yaglom [9], we consider an extended 28-component representation of the Lorentz group, comprising four bispinors and one third-rank spinor. This choice allows the construction of a relativistic system of equations for a spin-1/2 particle that possesses, in addition to electric charge, three further electromagnetic characteristics. The introduction of these characteristics extends the standard Dirac formalism by accommodating additional interaction structures, including higher-order derivatives, within a covariant framework.

We first work in Minkowski space and derive a four-component Dirac-like equation containing the additional interaction terms via couplings to the electromagnetic field tensor. These terms are interpreted as corresponding to the three supplementary electromagnetic characteristics, and their structure goes beyond the minimal-coupling scheme by involving second-order derivatives. The resulting equation therefore generalizes the standard Dirac equation both in algebraic structure and in the types of physical interaction it describes.

The formalism is then extended to a Riemannian space–time background using the tetrad approach, where additional couplings to the curvature appear through the Ricci scalar, Ricci tensor, and Riemann tensor. Finally, the non-relativistic limit is developed for both flat and curved backgrounds, yielding generalized Pauli-type equations in which the same combination of electromagnetic parameters governs both magnetic and curvature-induced interactions. This framework thus provides a unified description of anomalous electromagnetic properties and geometric effects for spin-1/2 particles.

2. The new equation for a spin-1/2 particle

We construct a generalized relativistic equation for a spin-1/2 particle based on an extended 28-component set of irreducible representations of the proper Lorentz group.

$$T = 4\left[(0,1/2)\oplus(1/2,0)\right]\oplus\left[(1/2,1)\oplus(1,1/2)\right], \tag{2.1}$$

with the linking scheme

$$\begin{array}{ccc} 4(0,1/2) & - & 4(1/2,0) \\ | & & | \\ (1/2,1) & - & (1,1/2)\,. \end{array} \tag{2.2}$$

First, we construct a matrix equation for a free particle (applying the *ict* -metric):

$$\left(\Gamma_\mu \partial_\mu + M\right)\Psi = 0, \quad \mu = 1,2,3,4\ . \tag{2.3}$$

In the modified Gel'fand–Yaglom basis, the matrix Γ_4 of the basic equation can be written in the form

$$\Gamma_4 = \begin{vmatrix} c^{(1/2)} \otimes \gamma_4 & 0 \\ 0 & c^{(3/2)} \otimes I_2 \otimes \gamma_4 \end{vmatrix}, \tag{2.4}$$

where the spin blocks $c^{(1/2)}$ and $c^{(3/2)}$ have the structure (corresponding to the linking scheme (2.2))

$$c^{(1/2)} = \begin{vmatrix} c_{11}^{(1/2)} & c_{12}^{(1/2)} & c_{13}^{(1/2)} & c_{14}^{(1/2)} & c_{15}^{(1/2)} \\ c_{21}^{(1/2)} & c_{22}^{(1/2)} & c_{23}^{(1/2)} & c_{24}^{(1/2)} & c_{25}^{(1/2)} \\ c_{31}^{(1/2)} & c_{32}^{(1/2)} & c_{33}^{(1/2)} & c_{34}^{(1/2)} & c_{35}^{(1/2)} \\ c_{41}^{(1/2)} & c_{42}^{(1/2)} & c_{43}^{(1/2)} & c_{44}^{(1/2)} & c_{45}^{(1/2)} \\ c_{51}^{(1/2)} & c_{52}^{(1/2)} & c_{53}^{(1/2)} & c_{54}^{(1/2)} & c_{55}^{(1/2)} \end{vmatrix}, \quad c^{(3/2)} = c_{55'}^{(3/2)}, \tag{2.5}$$

and I_2 is the 2×2 unit matrix. The involved irreducible representations are enumerated as follows:

$$1,2,3,4 \Rightarrow \left(0,1/2\right), \quad 1',2',3',4' \Rightarrow \left(1/2,0\right), \quad 5 \Rightarrow \left(1,1/2\right), \quad 5' \Rightarrow \left(1/2,1\right). \tag{2.6}$$

Below we use shorter λ and β notations:

$$\begin{aligned} &\lambda_1 = c_{11'}, \quad \lambda_2 = c_{22'}, \quad \lambda_3 = c_{33'}, \quad \lambda_4 = c_{44'}, \\ &\frac{\beta_1}{\sqrt{2}} = -ic_{15'}, \quad \frac{\beta_2}{\sqrt{2}} = -ic_{25'}, \quad \frac{\beta_3}{\sqrt{2}} = -ic_{35'}, \quad \frac{\beta_4}{\sqrt{2}} = -ic_{45'}, \\ &\frac{\beta_5}{\sqrt{2}} = ic_{51'}, \quad \frac{\beta_6}{\sqrt{2}} = ic_{52'}, \quad \frac{\beta_7}{\sqrt{2}} = ic_{53'}, \quad \frac{\beta_8}{\sqrt{2}} = ic_{54'}. \end{aligned} \tag{2.7}$$

The involved parameters obey a number of quadratic constraints, which follow from standard physical requirements on the equation:

$$\lambda_1+\lambda_2+\lambda_3+\lambda_4=1,$$
$$\lambda_1\lambda_2+\lambda_1\lambda_3+\lambda_1\lambda_4+\lambda_2\lambda_3+\lambda_2\lambda_4+\lambda_3\lambda_4+\frac{3}{2}(\beta_1\beta_5+\beta_2\beta_6+\beta_3\beta_7+\beta_4\beta_8)=0,$$
$$\lambda_1\lambda_2\lambda_3+\lambda_1\lambda_2\lambda_4+\lambda_1\lambda_3\lambda_4+\lambda_2\lambda_3\lambda_4+$$
$$\frac{3}{2}[(\lambda_2+\lambda_3+\lambda_4)\beta_1\beta_5+(\lambda_1+\lambda_3+\lambda_4)\beta_2\beta_6+(\lambda_1+\lambda_2+\lambda_4)\beta_3\beta_7+(\lambda_1+\lambda_2+\lambda_3)\beta_4\beta_8]=0, \quad (2.8)$$
$$\lambda_1\lambda_2\lambda_3+\lambda_1\lambda_2\lambda_4+\lambda_1\lambda_3\lambda_4+\lambda_2\lambda_3\lambda_4+$$
$$\frac{3}{2}[(1-\lambda_1)\beta_1\beta_5+(1-\lambda_2)\beta_2\beta_6+(1-\lambda_3)\beta_3\beta_7+(1-\lambda_4)\beta_4\beta_8]=0,$$
$$2\lambda_1\lambda_2\lambda_3\lambda_4+3\beta_1\beta_5(\lambda_2\lambda_3+\lambda_2\lambda_4+\lambda_3\lambda_4)+3\beta_2\beta_6(\lambda_1\lambda_3+\lambda_1\lambda_4+\lambda_3\lambda_4)+$$
$$3\beta_3\beta_7(\lambda_1\lambda_2+\lambda_1\lambda_4+\lambda_2\lambda_4)+3\beta_4\beta_8(\lambda_1\lambda_2+\lambda_1\lambda_3+\lambda_2\lambda_3)=0.$$

3. The presence of electromagnetic fields

We omit the technical details and start with the resulting first-order equations in the presence of external electromagnetic fields ($D_\mu=\partial_\mu-ieA_\mu$):

$$(M+\lambda_1\hat{D})\Psi^{(1)}-i2\beta_1\{D_\mu\Psi_\mu-\frac{1}{4}\hat{D}(\gamma_\mu\Psi_\mu)\}=0,$$
$$(M+\lambda_2\hat{D})\Psi^{(2)}-i2\beta_2\{D_\mu\Psi_\mu-\frac{1}{4}\hat{D}(\gamma_\mu\Psi_\mu)\}=0,$$
$$(M+\lambda_3\hat{D})\Psi^{(3)}-i2\beta_3\{D_\mu\Psi_\mu-\frac{1}{4}\hat{D}(\gamma_\mu\Psi_\mu)\}=0, \quad (3.1)$$
$$(M+\lambda_4\hat{D})\Psi^{(4)}-i2\beta_4\{D_\mu\Psi_\mu-\frac{1}{4}\hat{D}(\gamma_\mu\Psi_\mu)\}=0,$$
$$-i\left(D_\lambda-\frac{1}{4}\gamma_\lambda\hat{D}\right)(\beta_5\Psi^{(1)}+\beta_6\Psi^{(2)}+\beta_7\Psi^{(3)}+\beta_8\Psi^{(4)})+M\{\Psi_\lambda-\frac{1}{4}\gamma_\lambda(\gamma_\mu\Psi_\mu)\}=0$$

where the four bispinors and one vector–bispinor are defined as

$$\Psi^{(k)}=\begin{vmatrix}\Psi^{(k)\dot{a}}\\ \Psi^{(k)}_a\end{vmatrix},\quad \Psi_\mu=\begin{vmatrix}\Psi^{\dot{a}}_\mu\\ \Psi_{a\mu}\end{vmatrix},\quad k=1,2,3,4. \quad (3.2)$$

The linear combination of four bispinors is denoted by Ψ:

$$\Psi=\beta_5\Psi^{(1)}+\beta_6\Psi^{(2)}+\beta_7\Psi^{(3)}+\beta_8\Psi^{(4)}. \quad (3.3)$$

From these equations we can derive (with $\hat{D}=\gamma_\mu D_\mu$):

$$\left(M+\lambda_1 D\right)\Psi^1+\frac{2\beta_1}{M}\left(D^2-\frac{1}{4}\hat{D}\hat{D}\right)\Psi=0, \quad (3.4)$$

$$\left(M+\lambda_2 D\right)\Psi^2+\frac{2\beta_2}{M}\left(D^2-\frac{1}{4}\hat{D}\hat{D}\right)\Psi=0, \quad (3.5)$$

$$\left(M+\lambda_3 D\right)\Psi^3+\frac{2\beta_3}{M}\left(D^2-\frac{1}{4}\hat{D}\hat{D}\right)\Psi=0, \tag{3.6}$$

$$\left(M+\lambda_4 D\right)\Psi^4+\frac{2\beta_4}{M}\left(D^2-\frac{1}{4}\hat{D}\hat{D}\right)\Psi=0. \tag{3.7}$$

Next, we act

$$\text{on 3.4 by } \beta_5\left(M+\lambda_2\hat{D}\right)\left(M+\lambda_3\hat{D}\right)\left(M+\lambda_4\hat{D}\right), \tag{3.8}$$

$$\text{on 3.5 by } \beta_6\left(M+\lambda_1\hat{D}\right)\left(M+\lambda_3\hat{D}\right)\left(M+\lambda_4\hat{D}\right), \tag{3.9}$$

$$\text{on 3.6 by } \beta_7\left(M+\lambda_1\hat{D}\right)\left(M+\lambda_2\hat{D}\right)\left(M+\lambda_4\hat{D}\right), \tag{3.10}$$

$$\text{on 3.7 by } \beta_8\left(M+\lambda_1\hat{D}\right)\left(M+\lambda_2\hat{D}\right)\left(M+\lambda_3\hat{D}\right), \tag{3.11}$$

and sum the results. Using the identities

$$\hat{D}\hat{D}=D^2-ieF_{\rho\lambda}J_{\rho\lambda},\quad D^2=D_\mu D_\mu,\quad \gamma_\mu\gamma_\nu\gamma_\rho=\delta_{\mu\nu}\gamma_\rho-\delta_{\mu\rho}\gamma_\nu+\delta_{\nu\rho}\gamma_\mu+\text{ò}_{\mu\nu\rho\eta}\gamma_5\gamma_\eta, \tag{3.12}$$

and taking into account the constraints on the λ parameters, we obtain the basic equation:

$$\left\{M+\gamma_\rho D_\rho-\frac{ie}{M}\mu F_{\mu\beta}J_{\mu\beta}-\frac{ie}{M^2}\sigma\hat{D}F_{\mu\beta}J_{\mu\beta}+\right.$$

$$\left.\frac{1}{M^3}\eta\left(-ie^2D^2F_{\alpha\beta}J_{\alpha\beta}-e^2F_{\alpha\beta}F_{\beta\rho}\gamma_\alpha\gamma_\rho-e^2\frac{1}{2}F_{\alpha\beta}F_{\alpha\beta}-e^2\frac{1}{4}\gamma_5\text{ò}_{\rho\lambda\alpha\beta}F_{\rho\lambda}F_{\alpha\beta}\right)\right\}\Psi=0, \tag{3.13}$$

where

$$\mu=\frac{4}{3}\left(\lambda_1\lambda_2+\lambda_1\lambda_3+\lambda_1\lambda_4+\lambda_2\lambda_3+\lambda_2\lambda_4+\lambda_3\lambda_4\right), \tag{3.14}$$

$$\sigma=\frac{4}{3}\left(\lambda_1\lambda_2\lambda_3+\lambda_1\lambda_2\lambda_4+\lambda_1\lambda_3\lambda_4+\lambda_2\lambda_3\lambda_4\right),\quad \eta=\frac{4}{3}\lambda_1\lambda_2\lambda_3\lambda_4. \tag{3.15}$$

This equation describes a spin-$1/2$ particle which, in addition to its electric charge, possesses three additional electromagnetic characteristics μ, σ, and η. The structure of the resulting equation differs significantly from the known Dirac equation because it contains second-order derivatives in the additional interaction terms.

4. The presence of gravitational fields

Assuming the use of the relativistic interval in real-valued form $ds^2 = c^2dt^2 - dx^2 - dy^2 - dz^2$, one should use the following form of the basic equation in flat Minkowski space:

$$\left\{ i\gamma^\rho D_\rho - M + \frac{e\mu}{M} F_{\alpha\beta} j^{\alpha\beta} + \frac{e\sigma}{M^2} \hat{D} F_{\alpha\beta} j^{\alpha\beta} + \right.$$

$$\left. \frac{\eta}{M^3} \left(-ie^2 D^2 F_{\alpha\beta} j^{\alpha\beta} - e^2 \gamma^\alpha F_{\alpha\beta} F^\beta_\rho \gamma^\rho - e^2 \frac{1}{2} F_{\alpha\beta} F^{\alpha\beta} - e^2 \frac{1}{4} \gamma_5 \dot{o}^{\rho\lambda\alpha\beta} F_{\rho\lambda} F_{\alpha\beta} \right) \right\} \Psi = 0. \qquad (4.1)$$

We now extend this approach to a space–time models with Riemannian structure. To this end, we start with the system:

$$\left(M + \lambda_1 \hat{D} \right) \Psi^{(1)} - 2i\beta_1 \left(D^\mu \Psi_\mu - \frac{1}{4} \hat{D} \left(\gamma^\mu \Psi_\mu \right) \right) = 0, \qquad (4.2)$$

$$\left(M + \lambda_2 \hat{D} \right) \Psi^{(2)} - 2i\beta_2 \left(D^\mu \Psi_\mu - \frac{1}{4} \hat{D} \left(\gamma^\mu \Psi_\mu \right) \right) = 0, \qquad (4.3)$$

$$\left(M + \lambda_3 \hat{D} \right) \Psi^{(3)} - 2i\beta_3 \left(D^\mu \Psi_\mu - \frac{1}{4} \hat{D} \left(\gamma^\mu \Psi_\mu \right) \right) = 0, \qquad (4.4)$$

$$\left(M + \lambda_4 \hat{D} \right) \Psi^{(4)} - 2i\beta_4 \left(D^\mu \Psi_\mu - \frac{1}{4} \hat{D} \left(\gamma^\mu \Psi_\mu \right) \right) = 0, \qquad (4.5)$$

$$-i \left(D_\lambda - \frac{1}{4} \gamma_\lambda \hat{D} \right) \left(\beta_5 \Psi^{(1)} + \beta_6 \Psi^{(2)} + \beta_7 \Psi^{(3)} + \beta_8 \Psi^{(4)} \right) + M \left(\Psi_\lambda - \frac{1}{4} \gamma_\lambda \left(\gamma^\mu \Psi_\mu \right) \right) = 0, \qquad (4.6)$$

where $\Psi^{(a)}$, $a = 1,2,3,4$ are covariant bispinors, and Ψ_μ is a covariant vector–bispinor. We apply the generalized derivative D_μ, which accounts for the presence of both electromagnetic fields and a curved space–time background. The symbol ∇_μ denotes the covariant derivative, $\Gamma_\mu(x)$ is the bispinor connection, and $\gamma_\mu(x)$ are the local Dirac matrices:

$$D_\mu = \nabla_\mu - ieA_\mu(x) + \Gamma_\mu(x), \quad \hat{D} = \gamma^\mu D_\mu = \gamma^\mu(x) \left(\nabla_\mu - ieA_\mu + \Gamma_\mu \right). \qquad (4.7)$$

We have

$$\hat{D}\hat{D} = \left(\gamma^\alpha D_\alpha \right) \left(\gamma^\beta D_\beta \right) = D_\alpha \frac{\gamma^\alpha \gamma^\beta + \gamma^\beta \gamma^\alpha}{2} D_\beta + D_\alpha \frac{\gamma^\alpha \gamma^\beta - \gamma^\beta \gamma^\alpha}{2} D_\beta = \qquad (4.8$$

$$g^{\alpha\beta}(x) D_\alpha D_\beta = D^\alpha D_\alpha + j^{\alpha\beta}(x) [D_\alpha, D_\beta]_- = D^2 + \sigma^{\alpha\beta}(x) M_{\alpha\beta}(x),$$

where

$$D^2 = D^\alpha D_\alpha, M_{\alpha\beta}(x) = [D_\alpha, D_\beta]_-, \quad j^{\alpha\beta}(x) = \frac{\gamma^\alpha(x)\gamma^\beta(x) - \gamma^\beta(x)\gamma^\alpha(x)}{4}. \qquad (4.9)$$

We then derive

$$\left\{M + \hat{D} + \frac{\mu}{M} j^{\alpha\beta} M_{\alpha\beta} + \frac{\sigma}{M^2}\hat{D} j^{\alpha\beta} M_{\alpha\beta} + \frac{\eta}{M^3}\left(D^2 j^{\alpha\beta} M_{\alpha\beta} + j^{\rho\sigma} j^{\alpha\beta} M_{\rho\sigma} M_{\alpha\beta}\right)\right\}\Psi = 0, \quad (4.10)$$

where the involved additional terms are

$$M_{\alpha\beta}\Psi = \left(D_\alpha D_\beta - D_\beta D_\alpha\right)\Psi = \left(ieF_{\alpha\beta} + \frac{1}{2} j^{\nu\rho} R_{\nu\rho\alpha\beta}\right)\Psi, \qquad (4.11)$$

$$\frac{\mu}{M} j^{\alpha\beta} M_{\alpha\beta}\Psi = \frac{\mu}{M}\left(ieF_{\alpha\beta} j^{\alpha\beta} - \frac{1}{4}R(x)\right)\Psi, \qquad (4.12)$$

$$\frac{\sigma}{M^2}\hat{D} j^{\alpha\beta} M_{\alpha\beta}\Psi = \frac{1}{M^2}\sigma\left(\gamma^\rho D_\rho\right)\left(ieF_{\alpha\beta} j^{\alpha\beta} - \frac{1}{4}R(x)\right)\Psi, \qquad (4.13)$$

$$\frac{\eta}{M^3} j^{\rho\sigma} j^{\alpha\beta} M_{\rho\sigma} M_{\alpha\beta} = \frac{\eta}{M^3}\Big[(ieF_{\rho\sigma} j^{\rho\sigma} - \frac{1}{4}R)^2 +$$

$$\frac{ie}{2}F_{\alpha\beta}\left(-2 j^{\rho\alpha} R^\beta_\rho - 2 j^{\nu\rho} R^{\beta\,\alpha}_{\nu\rho} - 2i\gamma^5 j^{\rho\delta}\dot{o}^{\sigma\alpha\nu}_\delta R^\beta_{\nu\rho\sigma}\right) + R^\beta_{\nu\rho\sigma} R_{\dot{o}\tau\alpha\beta} j^{\rho\sigma} j^{\alpha\nu} j^{\dot{o}\tau}\Big]. \qquad (4.14)$$

Thus, the final form of the basic equation is:

$$\left\{\left(\gamma^\sigma D_\sigma + M\right) + \frac{\mu}{M}\left(ieF_{\alpha\beta} j^{\alpha\beta} - \frac{1}{4}R\right) + \frac{\sigma}{M^2}\left(\gamma^\rho D_\rho\right)\left(ieF_{\alpha\beta} j^{\alpha\beta} - \frac{1}{4}R\right) +\right.$$

$$\frac{\eta}{M^3}\Big[D^\sigma D_\sigma\left(ieF_{\alpha\beta} j^{\alpha\beta} - \frac{1}{4}R\right) + \left(ieF_{\rho\sigma} j^{\rho\sigma} - \frac{1}{4}R\right)^2 +$$

$$\left.\frac{ie}{2}F_{\alpha\beta}\left(2 j^{\alpha\rho} R^\beta_\rho - 2 j^{\nu\rho} R^{\beta\,\alpha}_{\nu\rho} - 2i\gamma^5 j^{\rho\delta}\dot{o}^{\alpha\nu\sigma}_\delta R^\beta_{\nu\sigma\rho}\right) - \left(R^\beta_{\nu\rho\sigma} j^{\rho\sigma}\right) j^{\nu\alpha}\left(R_{\alpha\beta\dot{o}\tau} j^{\dot{o}\tau}\right)\Big]\right\}\Psi = 0. \quad (4.15)$$

In order to have a standard presentation for Dirac equation, we should multiply the above equation by imaginary unit i, and make replacement $M \Rightarrow iM$, so, we obtain

$$\left\{\left(i\gamma^\sigma D_\sigma - M\right) + \frac{\mu}{M}\left(ieF_{\alpha\beta} j^{\alpha\beta} - \frac{1}{4}R\right) + \frac{-i\sigma}{M^2}\left(\gamma^\rho D_\rho\right)\left(ieF_{\alpha\beta} j^{\alpha\beta} - \frac{1}{4}R\right) +\right.$$

$$\frac{-\eta}{M^3}\Big[D^\sigma D_\sigma\left(ieF_{\alpha\beta} j^{\alpha\beta} - \frac{1}{4}R\right) + \left(ieF_{\rho\sigma} j^{\rho\sigma} - \frac{1}{4}R\right)^2 +$$

$$\left.\frac{ie}{2}F_{\alpha\beta}\left(2 j^{\alpha\rho} R^\beta_\rho - 2 j^{\nu\rho} R^{\beta\,\alpha}_{\nu\rho} - 2i\gamma^5 j^{\rho\delta}\dot{o}^{\alpha\nu\sigma}_\delta R^\beta_{\nu\sigma\rho}\right) - \left(R^\beta_{\nu\rho\sigma} j^{\rho\sigma}\right) j^{\nu\alpha}\left(R_{\alpha\beta\dot{o}\tau} j^{\dot{o}\tau}\right)\Big]\right\}\Psi = 0. \quad (4.16)$$

Equation (4.16) differs from (4.15) only in the formal change of notations:

$$\mu = \mu, \quad \sigma \Rightarrow -i\sigma, \quad \eta \Rightarrow -\eta, \quad M > 0, \tag{4.17}$$

till now the symbols μ, σ, η are just formal notations; some of them may be even imaginary (see in the end of the next Section)

As seen, a number of additional geometrical interaction terms arise through the Ricci scalar $R(x)$, the Ricci tensor $R_{\alpha\beta}$, and the Riemann curvature tensor $R_{\alpha\beta\rho\sigma}(x)$. The contributions from the Ricci tensor and Riemann tensor are zero only if the third parameter η vanishes.

5. The non-relativistic equation in flat space

Let us perform the $(3+1)$-splitting of the above equation. Using the identities

$$\begin{gathered} F_l^n F_n^l = 2\left(\vec{E}^2 - \vec{B}^2\right), \quad F_{kl} F_n^l j^{kn} \equiv 0, \\ \frac{1}{2} F_{kl} F^{kl} = \vec{B}^2 - \vec{E}^2, \quad \frac{1}{4}\gamma_5 \varepsilon^{mnkl} F_{mn} F_{kl} = \gamma^5 \vec{E}\,\vec{B}, \end{gathered} \tag{5.1}$$

and the notations $(K_i) = \left(j^{01}, j^{02}, j^{03}\right)$, $(J_i) = \left(j^{23}, j^{31}, j^{12}\right)$, we can write the main equation in the form

$$\begin{gathered} \{i\left(\gamma^0 D_0 + \gamma^j D_j\right) - M + \frac{2ei\mu}{M}\left(\vec{E}\,\vec{K} + \vec{B}\vec{J}\right) + \frac{2e\sigma}{M^2}\left(\gamma^0 D_0 + \gamma^j D_j\right)\left(\vec{E}\,\vec{K} + \vec{B}\vec{J}\right) - \\ \frac{e\eta}{M^3}\left(2i\left(D_0^2 - D_j D_j\right)\left(\vec{E}\,\vec{K} + \vec{B}\vec{J}\right) + \left(\vec{E}^2 - \vec{B}^2\right) + \gamma^5 \vec{E}\,\vec{B}\right)\Psi = 0. \end{gathered} \tag{5.2}$$

It is convenient to use the Pauli representation for the Dirac matrices:

$$\gamma^0 = \begin{vmatrix} I & 0 \\ 0 & -I \end{vmatrix}, \quad \gamma^j = \begin{vmatrix} 0 & \sigma_j \\ -\sigma_j & 0 \end{vmatrix}, \quad \gamma^5 = -i\gamma^0\gamma^1\gamma^2\gamma^3 = \begin{vmatrix} 0 & -I \\ -I & 0 \end{vmatrix}, \tag{5.3}$$

$$\sigma_0 = \begin{vmatrix} 1 & 0 \\ 0 & 1 \end{vmatrix}, \quad \sigma_1 = \begin{vmatrix} 0 & 1 \\ 1 & 0 \end{vmatrix}, \quad \sigma_2 = \begin{vmatrix} 0 & -i \\ i & 0 \end{vmatrix}, \quad \sigma_3 = \begin{vmatrix} 1 & 0 \\ 0 & -1 \end{vmatrix}. \tag{5.4}$$

The generators $j^{ab} = \frac{1}{4}\left(\gamma^a\gamma^b - \gamma^b\gamma^a\right)$ are given by

$$K_1 = \frac{1}{2}\begin{vmatrix} \sigma_1 & 0 \\ 0 & -\sigma_1 \end{vmatrix}, \quad K_2 = \frac{1}{2}\begin{vmatrix} \sigma_2 & 0 \\ 0 & -\sigma_2 \end{vmatrix}, \quad K_3 = \frac{1}{2}\begin{vmatrix} \sigma_3 & 0 \\ 0 & -\sigma_3 \end{vmatrix}, \tag{5.5}$$

$$J_1 = -\frac{i}{2}\begin{vmatrix} \sigma_1 & 0 \\ 0 & \sigma_1 \end{vmatrix}, \quad J_2 = -\frac{i}{2}\begin{vmatrix} \sigma_2 & 0 \\ 0 & \sigma_2 \end{vmatrix}, \quad J_3 = -\frac{i}{2}\begin{vmatrix} \sigma_3 & 0 \\ 0 & \sigma_3 \end{vmatrix}. \tag{5.6}$$

To define large and small components, we apply the projection operators:

$$P_+ = P_1 = \frac{I+\gamma^0}{2} = \begin{vmatrix} I & 0 \\ 0 & 0 \end{vmatrix}, \quad P_- = P_2 = \frac{I-\gamma^0}{2} = \begin{vmatrix} 0 & 0 \\ 0 & I \end{vmatrix}, \tag{5.7}$$

we write

$$\Psi = \begin{vmatrix} \varphi_+(x) \\ \varphi_-(x) \end{vmatrix}, \quad \Psi_1 = P_1\Psi = \begin{vmatrix} \varphi_+(x) \\ 0 \end{vmatrix}, \quad \Psi_2 = P_2\Psi = \begin{vmatrix} 0 \\ \varphi_-(x) \end{vmatrix}. \tag{5.8}$$

In the non-relativistic limit, $\varphi_+(x)$ is the large component and $\varphi_-(x)$ the small one.

Presenting the main equation in block form, we obtain the coupled equations:

$$\begin{aligned} &\left(iD_0 - M\right)\varphi_+ + iD_k\sigma_k\varphi_- + \frac{ei\mu}{M}\left(\vec{E}\vec{\sigma} - i\vec{B}\vec{\sigma}\right)\varphi_+ + \\ &\frac{e\sigma}{M^2}\left[D_0\left(\vec{E}\vec{\sigma} - i\vec{B}\vec{\sigma}\right)\varphi_+ + D_k\sigma_k\left(-\vec{E}\vec{\sigma} - i\vec{B}\vec{\sigma}\right)\varphi_-\right] - \\ &-\frac{e\eta}{M^3}\left[\left(D_0^2 - D_jD_j\right)\left(\vec{E}\vec{\sigma} - i\vec{B}\vec{\sigma}\right)\varphi_+ + \left(\vec{E}^2 - \vec{B}^2\right)\varphi_+ - \left(\vec{E}\,\vec{B}\right)\varphi_-\right] = 0, \end{aligned} \tag{5.9}$$

$$\begin{aligned} &-iD_k\sigma_k\varphi_+ + \left(-iD_0 - M\right)\varphi_- + \frac{ei\mu}{M}\left(-\vec{E}\vec{\sigma} - i\vec{B}\vec{\sigma}\right)\varphi_- + \\ &\frac{e\sigma}{M^2}\left[-D_k\sigma_k\left(\vec{E}\vec{\sigma} - i\vec{B}\vec{\sigma}\right)\varphi_+ - D_0\left(-\vec{E}\vec{\sigma} - i\vec{B}\vec{\sigma}\right)\varphi_-\right] - \\ &\frac{e\eta}{M^3}\left[\left(D_0^2 - D_jD_j\right)\left(-\vec{E}\vec{\sigma} - i\vec{B}\vec{\sigma}\right)\varphi_- + \left(\vec{E}^2 - \vec{B}^2\right)\varphi_- - \left(\vec{E}\,\vec{B}\right)\varphi_+\right] = 0. \end{aligned} \tag{5.10}$$

We now separate the rest energy by the substitutions:

$$D_0 \Rightarrow \left(D_0 - iM\right), \quad iD_0 \Rightarrow \left(iD_0 + M\right), \quad D_0^2 \Rightarrow \left(D_0^2 - 2iMD_0 - M^2\right). \tag{5.11}$$

We then obtain

$$\begin{aligned} &i\frac{1}{M}D_0\varphi_+ + i\frac{1}{M}D_k\sigma_k\varphi_- + \frac{ei\mu}{M^2}\left(\vec{E}\vec{\sigma} - i\vec{B}\vec{\sigma}\right)\varphi_+ + \\ &\frac{e\sigma}{M^2}\left[\left(\frac{1}{M}D_0 - i\right)\left(\vec{E}\vec{\sigma} - i\vec{B}\vec{\sigma}\right)\varphi_+ + \frac{1}{M}D_k\sigma_k\left(-\vec{E}\vec{\sigma} - i\vec{B}\vec{\sigma}\right)\varphi_-\right] - \\ &\frac{e\eta}{M^2}\left[\left(\frac{1}{M^2}D_0^2 - 2i\frac{1}{M}D_0 - 1 - \frac{1}{M^2}D_jD_j\right)\left(\vec{E}\vec{\sigma} - i\vec{B}\vec{\sigma}\right)\varphi_+ + \right. \\ &\left. + \frac{1}{M^2}\left(\vec{E}^2 - \vec{B}^2\right)\varphi_+ - \frac{1}{M^2}\left(\vec{E}\,\vec{B}\right)\varphi_-\right] = 0, \end{aligned} \tag{5.12}$$

$$-i\frac{1}{M}D_k\sigma_k\varphi_+ + \left(-i\frac{1}{M}D_0 - 2\right)\varphi_- + \frac{ei\mu}{M^2}\left(-\vec{E}\vec{\sigma} - i\vec{B}\vec{\sigma}\right)\varphi_- +$$

$$\frac{e\sigma}{M^2}\left[-\frac{1}{M}D_k\sigma_k\left(\vec{E}\vec{\sigma}-i\vec{B}\vec{\sigma}\right)\varphi_+-\left(\frac{1}{M}D_0-i\right)\left(-\vec{E}\vec{\sigma}-i\vec{B}\vec{\sigma}\right)\varphi_-\right]-$$

$$\frac{e\eta}{M^2}\left[\left(\frac{1}{M^2}D_0^2-2i\frac{1}{M}D_0-1-\frac{1}{M^2}D_jD_j\right)\left(-\vec{E}\vec{\sigma}-i\vec{B}\vec{\sigma}\right)\varphi_-+\right.$$

$$\left.\left(\vec{E}^2-\vec{B}^2\right)\varphi_--\frac{1}{M^2}\left(\vec{E}\,\vec{B}\right)\varphi_+\right]=0. \qquad (5.13)$$

It is known (for instance, see [3, 4]) that we should assume the following orders of smallness for the involved quantities (magnetic components B_j arise from commutators $D_{[kl]}$, electric components E_k from commutators $D_{[0k]}$, whence follow their smallness orders):

$$\varphi_+\sim 1,\varphi_-\sim x,\quad \frac{1}{M}D_j\sim x,\quad \frac{1}{M}D_0\sim x^2,\quad \frac{B_j}{M^2}\sim x^2,\quad \frac{E_j}{M^2}\sim x^3. \qquad (5.14)$$

In both equations, we will preserve only the terms of order x and x^2. In this way we obtain:

$$x^2:\quad i\frac{1}{M}D_0\varphi_++i\frac{1}{M}D_k\sigma_k\varphi_-+\frac{e\mu}{M^2}\left(\vec{B}\vec{\sigma}\right)\varphi_+-\frac{e\sigma}{M^2}\left(\vec{B}\vec{\sigma}\right)\varphi_+-i\frac{e\eta}{M^2}\left(\vec{B}\vec{\sigma}\right)\varphi_+=0; \qquad (5.15)$$

$$x:\quad \varphi_-=-i\frac{1}{2M}D_k\sigma_k\varphi_+=0. \qquad (5.16)$$

Eliminating the small component φ_-, we derive (changing the notations $\sigma\Rightarrow i\sigma,\ \eta\Rightarrow-\eta$):

$$iD_0\varphi_++\frac{1}{2M}\left(D_k\sigma_k\right)\left(D_n\sigma_n\right)\varphi_++\frac{e}{M}\left(+\mu-\sigma-i\eta\right)\left(\vec{B}\vec{\sigma}\right)\varphi_+=0. \qquad (5.17)$$

Keeping in mind the multiplication rule for Pauli matrices, we arrive at the equation (let $\psi=\Psi_+$, by physical reason we should assume the replacements: $\mu\Rightarrow\mu,\ \sigma=\sigma,\ -i\eta\Rightarrow\eta$):

$$iD_0red\psi+\frac{1}{2M}D^2\psi+\frac{e}{2M}\left(\vec{B}\vec{\sigma}\right)\psi+\frac{e}{M}\left(\mu+\sigma+\eta\right)\vec{B}\vec{\sigma}\psi=0. \qquad (5.18)$$

Thus, in the non-relativistic limit, the generalized equation takes the form of the ordinary Pauli equation for a spin-1/2 particle with anomalous magnetic moment due to additional $\left(\mu+\sigma+\eta\right)$-term.

6. The non-relativistic approximation in presence of curved space background

The detailed structure of the basic equation within the tetrad formalism reads as

$$\left\{ i\gamma^c (e^\sigma_{(c)} \left(\partial_\sigma + ieA_\sigma + \Gamma_\sigma \right) - M + \frac{\mu}{M} \left(ieF_{[kl]} j^{[kl]} - \frac{1}{4} R \right) + \right.$$

$$\frac{-i\sigma}{M^2} \gamma^c \left(e^\sigma_{(c)} \partial_\sigma + \Gamma_c \right) \left(ieF_{[kl]} j^{[kl]} - \frac{1}{4} R \right) +$$

$$\frac{-\eta}{M^3} \left[D^\sigma D_\sigma \left(ieF_{[kl]} j^{[kl]} - \frac{1}{4} R \right) + (ieF_{[kl]} j^{[kl]} - \frac{1}{4} R)^2 + \right.$$

$$\frac{ie}{2} F_{[kl]} \left(\left(j^{[kc]} R^l_c - j^{[lc]} R^k_c \right) - j^{[nc]} \left(R^{lk}_{nc} - R^{lk}_{cn} \right) - i\gamma^5 j^{[cd]} \delta^{kns}_d \left(R^l_{nsc} - R^l_{snc} \right) \right) -$$

$$\left. \left. \left(R^b_{ncs} j^{[cs]} \right) j^{[na]} \left(R_{abkl} j^{[kl]} \right) \right] \right\} \Psi = 0, \qquad (6.1)$$

where $D_c = e^\sigma_{(c)} \partial_\sigma + ieA_c + \frac{1}{2} \gamma_{[mn]c} j^{[mn]}, e^\sigma_{(c)}$ is a tetred and the symbols $\gamma_{[mn]c}$ stand for Ricci rotation coefficients. The Latin letters designate the tetrad components. Equation (6.1) contains the scalar and tensor Ricci quantities.

In order to develop the non-relativistic approximation (this is possible only for the non-relativistic metric, $dS^2 = dx_0^2 + g_{kl} dx^l dx^l$, we need to fix the smallness orders of the involved geometrical quantities:

$$R_{abcd} = \left(\gamma_{abc,d} - \gamma_{abd,c} \right) + \left(\gamma_{abf} \gamma^f_{cd} - \gamma_{abf} \gamma^f_{dc} \right) + \left(\gamma_{afc} \gamma^f_{bd} - \gamma_{afd} \gamma^f_{bc} \right), \qquad (6.2)$$

$$R_{mn} = R^a_{mcn} = \left(\gamma^c_{mc,n} - \gamma^c_{mn,c} \right) + \left(\gamma^c_{bf} \gamma^f_{cd} - \gamma^c_{bf} \gamma^f_{dc} \right) + \left(\gamma^c_{fc} \gamma^f_{bd} - \gamma^c_{fd} \gamma^f_{bc} \right). \qquad (6.3)$$

In the non-relativistic equations, only the components of the Ricci tensor with spatial indices are present, so we get the simpler formula

$$R_{bd} = \left(\gamma^i_{bi,d} - \gamma^i_{bd,i} \right) + \left(\gamma^i_{bf} \gamma^f_{id} - \gamma^i_{bf} \gamma^f_{di} \right) + \left(\gamma^i_{fi} \gamma^f_{bd} - \gamma^i_{fd} \gamma^f_{bi} \right). \qquad (6.4)$$

In the Ricci rotation coefficients, only the following appear: $\gamma_{[ij]0}$ and $\gamma_{[ij]k}$. Therefore, expressions for the generalized derivatives are simplified (note that $n, m, k, l \in \{1, 2, 3\}$):

$$D_0 = \partial_0 + ieA_0 + \frac{1}{2} \gamma_{[kl]0} j^{[kl]}, \quad D_m = e^n_{(m)} \left(\partial_n + ieA_n \right) + \frac{1}{2} \gamma_{[kl]m} j^{[kl]}. \qquad (6.5)$$

So, in the non-relativistic metric, we have:

$$R_{00} = 0, \quad R_{01} = 0, \quad R_{02} = 0, \quad R_{02} = 0, \qquad (6.6)$$

$$
\begin{aligned}
R_{11} &= (\gamma^i_{1i,1} - \gamma^i_{11,i}) + (\gamma^i_{1k}\gamma^k_{i1} - \gamma^i_{1k}\gamma^k_{1i}) + (\gamma^i_{ki}\gamma^k_{11} - \gamma^i_{k1}\gamma^k_{1i}),\\
R_{22} &= (\gamma^i_{2i,2} - \gamma^i_{22,i}) + (\gamma^i_{2k}\gamma^k_{i2} - \gamma^i_{2k}\gamma^k_{2i}) + (\gamma^i_{ki}\gamma^k_{22} - \gamma^i_{k2}\gamma^k_{2i}),\\
R_{33} &= (\gamma^i_{3i,3} - \gamma^i_{33,i}) + (\gamma^i_{3k}\gamma^k_{i3} - \gamma^i_{3k}\gamma^k_{3i}) + (\gamma^i_{ki}\gamma^k_{33} - \gamma^i_{k3}\gamma^k_{3i}),\\
R_{23} &= (\gamma^i_{2i,3} - \gamma^i_{23,i}) + (\gamma^i_{2k}\gamma^k_{i3} - \gamma^i_{2k}\gamma^k_{3i}) + (\gamma^i_{ki}\gamma^k_{23} - \gamma^i_{k3}\gamma^k_{2i}),\\
R_{31} &= (\gamma^i_{3i,1} - \gamma^i_{31,i}) + (\gamma^i_{3k}\gamma^k_{i1} - \gamma^i_{3k}\gamma^k_{1i}) + (\gamma^i_{ki}\gamma^k_{31} - \gamma^i_{k1}\gamma^k_{3i}),\\
R_{12} &= (\gamma^i_{1i,2} - \gamma^i_{12,i}) + (\gamma^i_{1k}\gamma^k_{i2} - \gamma^i_{1k}\gamma^k_{2i}) + (\gamma^i_{ki}\gamma^k_{12} - \gamma^i_{k2}\gamma^k_{1i}).
\end{aligned}
\tag{6.7}
$$

Similarly, for non-vanishing components of the curvature tensor we have (indices belong to $\{1,2,3\}$):

$$
R_{klmn} = \left(\gamma_{klm,n} - \gamma_{kln,m}\right) + \left(\gamma_{klj}\gamma^j_{mn} - \gamma_{klj}\gamma^j_{nm}\right) + \left(\gamma_{kjm}\gamma^j_{ln} - \gamma_{kjn}\gamma^j_{lm}\right). \tag{6.8}
$$

The smallness orders of the involved quantities are:

$$
\begin{aligned}
&\frac{D_n}{M} \sim \frac{\gamma_{kln}}{M} \sim x,\ \ \frac{D_0}{M} \sim x^2,\ \ \frac{B_n}{M^2} \sim x^2,\ \ \frac{B_n^2}{M^4} \sim x^4,\ \ \frac{E_n}{M^2} \sim x^3,\ \ \frac{E_n^2}{M^4} \sim x^6,\\
&\frac{\gamma_{kl0}}{M} \sim x^2,\ \ \frac{R_{kl}}{M^2} \sim x^2,\ \ \frac{R}{M^2} \sim x^2,\ \ \frac{R_{klmn}}{M^2} \sim x^2,\ \ \frac{R_{klmn}}{M^2} \times \frac{R_{klmn}}{M^2} \sim x^4.
\end{aligned}
\tag{6.9}
$$

Further, making the needed calculations, we arrive at a generalized Pauli-like equation

$$
\left(i\partial_0 - eA_0(x) + \frac{1}{2}G_{n0}(x)\sigma_n\right)\Psi = -\frac{1}{2M}(\sigma_m e^n_{(m)}(x)\left(\partial_n + ieA_n(x)\right) -
$$

$$
\frac{i}{2}\sigma_m\sigma_n G_{mn}(x))^2\Psi + \frac{1}{M}(\mu+\sigma+\eta)\left(eB_n\sigma_n - \frac{1}{4}R\right)\Psi. \tag{6.10}
$$

where we apply shortening notations for Ricci rotation coefficients:

$$
\left(\gamma_{[01]0}, \gamma_{[02]0}, \gamma_{[03]0}\right) = G_{j0}(x), \left(\gamma_{[23]m}, \gamma_{[02]m}, \gamma_{[03]m}\right) = G_{nm}(x).
$$

Thus, in the presence of a curved space–time background, the Pauli-like equation takes the form of the ordinary Pauli equation for a spin-1/2 particle with anomalous magnetic moment $(\mu+\sigma+\eta)$, and the same coefficient appears in the geometrical term proportional to the Ricci scalar R.

7. Conclusions

Starting from the extended 28-component representation of the Lorentz group for a spin-1/2 particle, we have constructed a new relativistic equation that incorporates, in addition to the electric charge, three further electromagnetic characteristics. The derivation leads to a generalized 4-component Dirac-like equation in which three new interaction terms appear

explicitly. Each of these additional terms can be naturally interpreted as corresponding to one of the new electromagnetic characteristics of the spin-1/2 particle, thereby extending the range of possible interactions beyond those described by the standard Dirac formalism.

The approach has been further generalized to the case of a Riemannian space–time background, where the formulation is carried out within the tetrad formalism. In this generalized setting, the presence of curvature introduces a number of additional geometrical interaction terms into the basic equation. These terms involve contributions from the Ricci scalar $R(x)$, the Ricci tensor $R_{\alpha\beta}(x)$, and the Riemann curvature tensor $R_{\alpha\beta\rho\sigma}(x)$. The resulting framework thus provides a unified description of spin-1/2 particles with anomalous electromagnetic properties, applicable in both flat and curved space–time, and explicitly shows how electromagnetic and geometrical interactions can be incorporated simultaneously into the relativistic dynamics of the particle.

References

1. Dirac, P.A.M.: The quantum theory of the electron. *Proc. R. Soc. A* **117**, 610–624 (1928);The quantum theory of the electron. Part II. *Proc. R. Soc. A* **118**, 351–361 (1928).
2. Fierz, M., Pauli, W.: On relativistic wave equations for particles of arbitrary spin in an electromagnetic field. *Proc. R. Soc. Lond. A* **173**, 211–232 (1939).
3. Rarita, W., Schwinger, J.: On a theory of particles with half-integral spin. *Phys. Rev.* **60**, 61–64 (1941).
4. Ginzburg, V.L.: To the theory of excited states of elementary particles. *Zh. Eksp. Teor. Fiz.* **13**, 33–58 (1943) (in Russian).
5. Davydov, A.S.: Wave equations of a particle with spin 3/2 in the absence of a field. *Zh. Eksp. Teor. Fiz.* **13**, 313–319 (1943) (in Russian).
6. Bhabha, H.J.: Relativistic wave equations for elementary particles. *Rev. Mod. Phys.* **17**, 200–215 (1945).
7. Bhabha, H.J.: The theory of the elementary particles. *Rep. Prog. Phys.* **10**, 253–271 (1946).
8. Harish-Chandra: Relativistic equations for elementary particles. *Proc. R. Soc. Lond. A* **192**, 195–218 (1948).
9. Gel'fand, I.M., Yaglom, A.M.: General relativistic invariant equations and infinite-dimensional representations of the Lorentz group. *Zh. Eksp. Teor. Fiz.* **18**, 703–733 (1948).
10. Fradkin, E.E.: On the theory of particles with higher spins. *Zh. Eksp. Teor. Fiz.* **20**, 27–38 (1950).
11. Bhabha, H.J.: An equation for a particle with two mass states and positive charge. *Philos. Mag.* **43**, 33–47 (1952).
12. Fedorov, F.I.: Generalized relativistic wave equations. *Dokl. Akad. Nauk SSSR* **82**, 37–40 (1952).
13. Fainberg, V.Ya.: On the interaction of higher-spin particles with electromagnetic and meson fields. *Tr. Fiz. Inst. Akad. Nauk SSSR* **6**, 269–332 (1955).
14. Ginzburg, V.L.: On relativistic wave equations with a mass spectrum. *Acta Phys. Pol.* **15**, 163–175 (1956).

15. Shimazu, H.: A relativistic wave equation for a particle with two mass states of spin 1 and 0. *Prog. Theor. Phys.* **16**, 285–298 (1956).
16. Buchdahl, H.A.: On the compatibility of relativistic wave equations for particles of higher spin in a gravitational field. *Nuovo Cimento* **10**, 96–103 (1958).
17. Shelepin, L.A.: Covariant theory of relativistic wave equations. *Nucl. Phys.* **33**, 580–593 (1962).
18. Aurilia, A., Umezawa, H.: Theory of high spin fields. *Phys. Rev.* **182**, 1682–1694 (1969).
19. Kisel, V.V., Pletyukhov, V.A.: Wave equations with repeated representations of the Lorentz group: Half-integer spin. *Proc. Natl. Acad. Sci. Belarus, Phys.-Math. Ser.* **3**, 78–83 (1970).
20. Capri, A.Z.: Electromagnetic properties of a new spin-1/2 field. *Prog. Theor. Phys.* **48**, 1364–1374 (1972).
21. Khalil, M.A.K.: Properties of a 20-component spin-1/2 relativistic wave equation. *Phys. Rev. D* **15**, 1532–1539 (1977).
22. Mathews, P.M., Vijayalakshmi, B.: On admissible Lorentz group representations in unique-mass relativistic wave equations. *Phys. Lett. A* **92**, 157–160 (1982).
23. Mathews, P.M., Vijayalakshmi, B.: On inequivalent classes of unique-mass relativistic wave equations with repeated irreducible representations. *J. Math. Phys.* **25**, 1080–1087 (1984).
24. Kisel, V.V., et al.: *Elementary Particles with Internal Structure in External Fields*, Vols. I–II. Nova Science Publishers, New York (2018).
25. Ovsiyuk, E.M., et al.: Spin-1/2 particle with anomalous magnetic moment in a uniform magnetic field. *Nonlinear Phenom. Complex Syst.* **19**, 153–165 (2016).
26. Kisel, V.V., et al.: Spin-1/2 particle with two mass states interacting with external fields. *Nonlinear Phenom. Complex Syst.* **20**, 404–423 (2017).

Author Contributions: The authors equally contributed to this work in the conceptualization of the study, in the mathematical derivations, and in the writing of the manuscript. All authors have read and agreed to the published version of the manuscript.

Funding: The work by A.M. Ishkhanyan was supported by the Armenian State Committee of Science (grant No. 21AG-1C064).

Data Availability Statement: No data were generated or analyzed in this research.

Conflicts of Interest: The authors declare no conflict of interest.

ԱՄՓՈՓԱԳԻՐ

Երեք լրացուցիչ բնութագրերով 1/2 սպին ունեցող մասնիկի համար նոր հավասարում էլեկտրամագնիսական և գրավիտացիոն դաշտերի դեպքում

Վասիլի Կիսել[1], Ելենա Օվսիյուկ[2], Անտոն Բուրի[3], Ալինա Իվաշկևիչ[3], Վիկտոր Ռեդկով[3*], Արթուր Իշխանյան[4]

[1]Ինֆորմատիկայի և ռադիոէլեկտրոնիկայի բելառուսական պետական համալսարան, Մինսկ, 220013 Բելառուս
[2]Մոզիրի պետական մանկավարժական համալսարան, Մոզիր, 247760 Բելառուս
[3]Բելառուսի ԳԱԱ Բ.Ի.Ստեպանովի անվան ֆիզիկայի ինստիտուտ, Մինսկ, 220072 Բելառուս
[4]ՀՀ ԳԱԱ ֆիզիկական հետազոտությունների ինստիտուտ, Աշտարակ, 0204 Հայաստան

* Հաղորդակցության համար՝ v.redkov@ifanbel.bas-net.by

Գելֆանդ–Յագլոմի ընդհանուր մեթոդի շրջանակներում, ելնելով Լորենցի խմբի ընդլայնված՝ 28 բաղադրիչ ունեցող ներկայացումից, մենք կառուցում ենք նոր ռելատիվիստական P-ինվարիանտ ընդհանրացված հավասարում 1/2 սպին ունեցող մասնիկի համար, որը էլեկտրական լիցքից բացի, օժտված է ևս երեք բնութագրերով։ Մոդելը նախ կառուցվում է ազատ մասնիկի համար, որի դեպքում ստացվում է համապատասխան սպինորային հավասարումների համակարգ, որն այնուհետև վերափոխվում է սպին–թենզորային ձևի։ Ապա այս ներկայացման մեջ ներառվում է արտաքին էլեկտրամագնիսական դաշտերի հետ փոխազդեցությունը։ Լրիվ ալիքային ֆունկցիայի լրացուցիչ փոփոխականների արտաքսման արդյունքում ստացվում է նվազագույն՝ չորս բաղադրիչ ունեցող Դիրակի տիպի հավասարում, որը պարունակում է փոխազդեցության երեք նոր անդամ՝ մեկնաբանվող որպես մասնիկի լրացուցիչ էլեկտրամագնիսական բնութագրերից ծագող։ Այս մոտեցումը հետագայում ընդլայնվում է Ռիմանի տարածաժամանակային ֆոնի վրա՝ ավանդական տետրադային ֆորմալիզմի շրջանակներում, ինչի արդյունքում առաջանում են երկրաչափական փոխազդեցության լրացուցիչ անդամներ՝ ներառյալ Ռիչիի $R(x)$ սկալարը, Ռիչիի $R_{\alpha\beta}$ թենզորը և Ռիմանի $R_{\alpha\beta\rho\sigma}(x)$ կորության թենզորը։

Բանալի բառեր՝ 1/2 սպին ունեցող մասնիկ, ռելատիվիստական համաչափություն, ընդհանրացված հավասարում, լրացուցիչ էլեկտրամագնիսական բնութագրեր, արտաքին էլեկտրամագնիսական և գրավիտացիոն դաշտեր

Reports of NAS RA
ՀՀ ԳԱԱ Զեկույցներ
NATIONAL ACADEMY OF SCIENCES OF THE REPUBLIC OF ARMENIA
ՀԱՅԱՍՏԱՆԻ ՀԱՆՐԱՊԵՏՈՒԹՅԱՆ ԳԻՏՈՒԹՅՈՒՆՆԵՐԻ ԱԶԳԱՅԻՆ ԱԿԱԴԵՄԻԱ

2026 **Volume 126** **Issue 1** **Article No. 2**

Category: Biological Sciences
Type of Paper: Original Research Article
Received: October 1, 2025, **Revised:** December 23, 2025, **Accepted:** January 5, 2026
Published: January 30, 2026

DOI: 10.54503/0321-1339-2026.126.1-2

Persistence of Western Diet-Associated Pathway Activity Profiles in Ventricular Tissues

Tamara Sirunyan[1,2,#], Gisane Lazaryan[1,2,#], Siras Hakobyan[1,3], Suren Davitavyan[1,2], Roksana Zakharyan[1,2], Ani Stepanyan[1], Agnieszka Brojakowska[4,5], Mary K. Khlgatian[5], Malik Bisserier[6], Shihong Zhang[4], David A. Goukassian[4], Arsen Arakelyan[1,2,3,*]

[1]Institute of Molecular Biology NAS RA, Yerevan, Armenia; e-mail@e-mail.com
[2]Russian-Armenian University, Yerevan, Armenia; e-mail@e-mail.com
[3]Armenian Bioinformatics Institute, Yerevan, Armenia
[4]Cardiovascular Research Institute, Icahn School of Medicine at Mount Sinai, NY, USA
[5]Department of Cell Biology, Yale School of Medicine, New Haven, CT, USA
[6]Department of Cell Biology and Anatomy and Physiology, New York Medical College, Valhalla, NY, USA

[#]Equal contribution
[*]Correspondence: a_arakelyan@mb.sci.am

Running title: Western Diet-Associated Pathway Activity Profiles in Ventricular Tissues

Abstract

The consumption of a Western diet (WD), characterized by high levels of fats and sugars, is strongly associated with adverse cardiovascular outcomes. In this case-control study, we evaluated long-term alterations in signaling pathway activities in the left (LV) and right (RV) ventricular tissues of C57Bl/6J mice that were exposed to WD starting at 300 days of age for 125 days before switching to a normal diet (ND). LV and RV tissues were collected at 530 days and subjected to RNA sequencing. Pathway activity for 40 signaling pathways (comprising 709 pathway branches/sinks) was calculated using the topology-aware Pathway Signal Flow (PSF) algorithm, which assesses signal propagation along a pathway based on gene expression levels of its components and their interactions. We observed significant perturbations in 14 pathway branches specifically in LV tissue of male mice, 105 days after the ND switch. These alterations included the downregulation of cardioprotective VEGF signaling and the upregulation of pro-fibrotic TGF-beta signaling, suggesting lasting cardiovascular risks. Furthermore, strong signaling was detected in the cGMP-PKG and FOXO pathways linked to cardiac failure. Finally, pro- and anti-apoptotic signals were simultaneously upregulated, accompanied by the downregulation of cell cycle inhibitors. Notably, no significant gene expression changes were detected in the left ventricular tissue of females, and no significant differences were observed in right ventricular tissue in either sex. These findings suggest that the effects of a Western diet may persist even after transitioning to a healthier diet. Further studies are needed to elucidate the diet-associated risks and develop strategies to mitigate these long-term effects.

Keywords: Western diet, left ventricle, right ventricle, RNA sequencing, transcriptomics, signaling pathways, Pathway Signal Flow

1. Introduction

The long-term impact of dietary habits on cardiovascular health remains a critical area of research, particularly in the context of metabolic memory and disease predisposition [1]. While the detrimental effects of prolonged consumption of a high-fat and high-sugar Western diet (WD) on cardiovascular function are well-documented [2], less is known about the persistence of these effects following a transition to a healthier diet. In real-world scenarios, individuals may consume a WD for extended periods, such as during early adulthood, before adopting healthier dietary patterns later in life.

We have previously demonstrated that prior WD consumption induces sex-specific alterations in cardiac function and transcriptomic profiles in the left ventricular (LV) in mice [3]. This study aims to investigate the long-term effects of WD on both heart ventricles, with a particular focus on the persistence of signaling pathway alterations following a transition to a normal diet. We applied a topology-aware Pathway Signal Flow (PSF) algorithm, a computational method for pathway activity analysis incorporating gene expression and pathway topology (interaction between pathway nodes) [4]. Using RNA sequencing data from left (LV) and right (RV) ventricular tissues of male and female mice previously subjected to a WD, we assessed whether prior dietary exposure leaves persistent imprints on signaling network activity profiles.

2. Materials and Methods

Animals and Diet

Three-month-old male and female C57BL/6J mice were stratified into two dietary groups: case - a Western diet (WD) (n=20, males/females: 10/10) received a modified Teklad diet containing 42% fat (TD.88137, Envigo, Madison, WI), and control - a standard rodent chow as a control (Normal diet, ND) (n=20, males/females: 10/10). WD was introduced at 300 days of age for 125 days, then animals switched to ND. Our previous publication extensively described animal handling, diet exposure, tissue collection, and RNA sequencing [3]. Animal protocols adhered to the National Institutes of Health guidelines and were approved by the Institutional Animal Care and Use Committees at Brookhaven National Laboratory (BNL) (Upton, NY) (BNL IACUC Protocol #502) and the Icahn School of Medicine at Mount Sinai (NY, NY) (ISMMS IACUC Protocol #2019-0017).

Pathway Signal Flow analysis of transcriptome perturbations

The PSF algorithm computes the activity state of pathway nodes (genes or gene groups) using relative gene expression values of a node in a pathway and its interactions with upstream nodes. It begins with input nodes and propagates to terminal nodes, computing node signal values based on fold changes, upstream signals, interaction weights, and activation/inhibition impacts. For each node in a pathway, a signal value is computed as the product of its expression fold change and the weighted contributions of signals arriving from upstream nodes. At each node, incoming signal from upstream nodes is combined proportionally: the contribution of an upstream node is normalized by the total incoming signal. Activating edges transmit upstream signal multiplicatively, whereas inhibitory edges invert the signal by applying a negative impact factor. The detailed description of algorithm is presented in our previous publication [4].

Raw RNA-seq read counts were normalized with the DESeq2 R package (version 1.44.0). Gene expression fold changes against mean expression across all samples were computed from a normalized gene count matrix and used as an input for the PSF algorithm [4].

We calculated the PSF activity values of 40 signaling pathways (709 pathway branches/sinks) in the LV and RV tissues in the studied groups. For each pathway sink, PSF activity values were compared between experimental groups using linear regression models. A pathway sink was considered significant if the absolute log2PSF value exceeded 1 and the false discovery rate-adjusted p value (FDR) was < 0.05.

To orthogonally validate the PSF-based findings, we performed conventional differential gene expression analysis using the limma R package, followed by overrepresentation analysis (ORA) of Gene Ontology gene sets using the enrichR package. We then evaluated the concordance between ORA results and PSF sink significance.

3. Results

We performed a topology-aware analysis of pathway activity in the LV and RV heart ventricles in animals with prior exposure to WD. Our findings indicated significant (absolute log2PSF > 1 and pFDR < 0.05) perturbations of 14 pathway branch activities at 530 days (105 days after switching to ND) in the LV tissue of male rats (Figure 1A, Additional Figures S1-S11, Additional Tables S1-S4). However, we did not detect significant perturbations in female animals' LV or both sexes' RV tissues (Figure 1B-D).

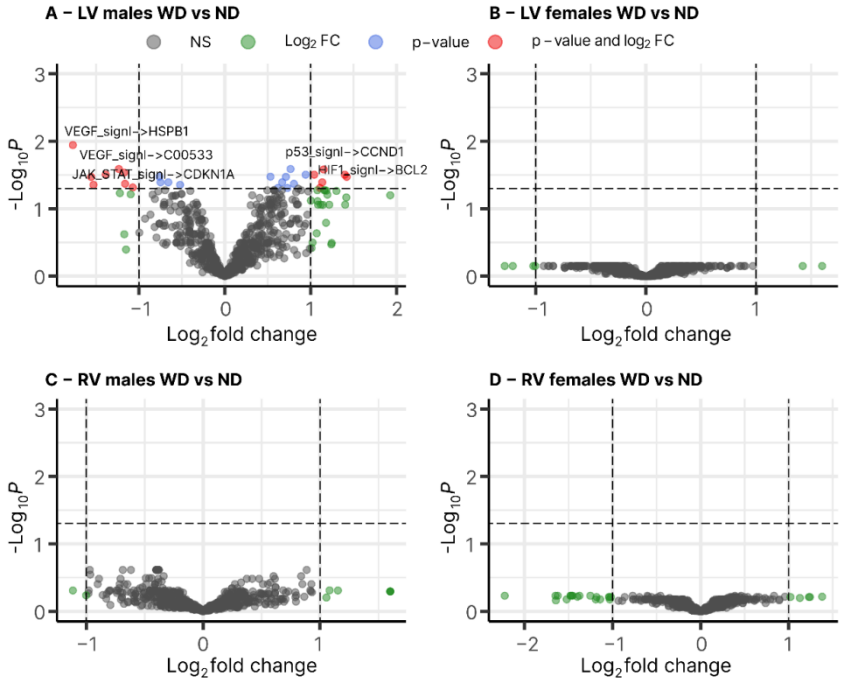

Figure 1. Signaling pathway activity perturbations (log2PSF) in LV and RV tissues associated with Western diet. The results of differential pathway deregulation analysis are presented as Volcano plots. The horizontal line represents the -log10 FDR adjusted p-value threshold equal to 0.05 (-log10(0.05) = 1.30). Vertical lines represent log2PSF = ±1 threshold. A) Pathway deregulation profiles in LV of WD-exposed male mice. B) Pathway deregulation profiles in LV of WD-exposed female mice. C) Pathway deregulation profiles in RV of WD-exposed male mice. D) Pathway deregulation profiles in RV of WD-exposed female mice.

In WD-fed males we observed downregulation of pathway signals in 4 branches of VEGF signaling pathway associated with focal adhesion (VEGF_signl → PXN log2PSF = -1.38, pFDR = 0.031), actin reorganization (VEGF_signl → HSPB1, log2PSF = -1.77, pFDR = 0.011), NO production (VEGF_signl → C00533, log2PSF = -1.23, pFDR = 0.026), angiogenic response (VEGF_signl → SHC2, log2PSF = -1.17, pFDR = 0.029). The Erbb signaling pathway converged at the downregulated signal at cyclin-dependent kinase inhibitors associated with cell cycle control (ErbB_signl → CDKN1A, log2PSF = -1.16, pFDR = 0.042) and JAK-STAT (JAK_STAT_signl → CDKN1A, log2PSF = -1.53, pFDR = 0.044). Furthermore, downregulation was observed for the pathway signal at the mitochondrial permeability transition node in the cGMP-PKG signaling pathway (cGMP_PKG_signl → PPIF, log2PSF = -1.56, pFDR = 0.034). Finally, in the Endocrine resistance

pathway, we observed downregulation of apoptosis machinery signal converged at the BIK node (Endocrine_res → BIK, log2PSF = -1.07, pFDR = 0.048).

Upregulated pathway signals in LV tissue of male mice were mostly associated with TGF-beta (TGFb_signl → ROCK1, log2PSF = 1.40, pFDR = 0.031), FOXO (FoxO_signl → ATM, log2PSF = 1.42, pFDR = 0.034), HIF-1 (HIF1_signl → BCL2, logPSF = 1.14, pFDR = 0.041), cAMP (cAMP_signl → PTCH1, log2PSF = 1.11, pFDR = 0.049), p53 (p53_signl → CCND1, log2PSF = 1.15, pFDR = 0.026), and Apoptosis (Apoptosis → TP53AIP1, log2PSF = 1.04, pFDR = 0.031).

4. Discussion

In this paper, we studied the long-term effects of WD on the signaling activity state in the ventricular tissue of the heart. Our findings show that the WD consumption, even for some time, still leaves the footprint of pathway deregulation on the left ventricular tissue of male mice (Figure 2).

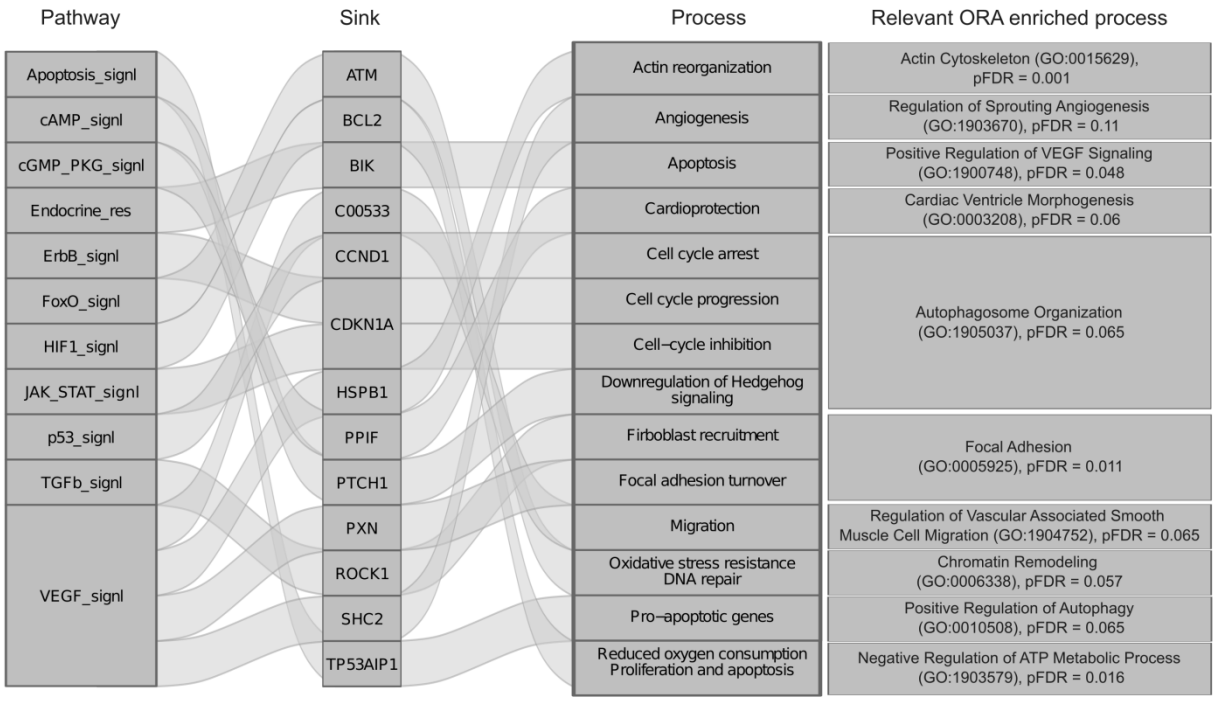

Figure 2. Association of significantly deregulated pathways with biological processes in LV tissues of WD-exposed males. The results are presented as Sankey plots connecting a pathway to its sink node and the sink node to the associated biological process. Information about pathway node-node and node-process interactions was retrieved from the KEGG Pathway database (https://www.genome.jp/kegg/pathway.html). The results of over-representation analysis with conventional differential expression analysis are also presented (right column). The full list of differentially expressed genes and enriched GO terms are presented in Additional tables S5 and S6.

Orthogonal validation using conventional differential gene expression analysis followed by functional enrichment confirmed that biological processes associated with significantly altered PSF sinks were enriched at the Gene Ontology process level (Additional Tables S5 and S6). No differences in pathway perturbation levels were observed for LV tissue in females and RV tissues in both males and females. Furthermore, neither LV in females nor RV tissues for both sexes showed significant pathway deregulation. This finding is well aligned with our previous results showing the massive deregulation in LV transcriptome at 530 days in male mice (~1500 differentially expressed genes

(DEGs) compared to females 8 DEGs), and a small number of DEGs in RV for both sexes, as it is evident from our preliminary results [3,5].

In male animals, we observed strong pathway branch deregulations promoting cardiac damage in the LV tissue. VEGF signaling pathway is known to play an important role in cardioprotection [6,7]; here we observed the downregulated pathway activity for branches associated with focal adhesion, cytoskeleton rearrangement, and NO production, all playing an important role in cardiac function recovery [8,9]. Furthermore, the activation of the TGFbeta-ROCK cascade can further exacerbate heart damage through fibrotic remodeling [10] as also shown in our previous study [3]. The cGMP-PKG pathway showed a strong inhibitory signal at *PPIF* (cyclophilin D) associated with mitochondrial permeability transition [11]. It has been shown that $Ppif^{-/-}$ mice are more prone to metabolic heart failure [12], supporting our observations. Furthermore, we also observed activation signals of IGF1 and EGF1 branches in the FOXO pathway that converged on the *ATM* gene previously implicated in cardiac failure associated with a high-fat, high-sugar diet [13].

We observed a variety of pro- and anti-apoptotic signals coming from different pathways. The observed upregulation of pro-apoptotic signals alongside anti-apoptotic signals and the downregulation of cell cycle inhibitors (Figure 2).

This balance may represent a compensatory mechanism where the tissue attempts to mitigate damage by promoting cell survival pathways, while also activating apoptotic pathways to eliminate severely damaged cells [14,15]. The net effect on cardiac function would depend on the predominance of these opposing signals and the heart's ability to manage cellular stress. These results are consistent with previously reported HFrEF phenotype in males later in life [16]. The absence of significant changes in RV and LV tissue in females can be connected to differences in sex-specific responses to a high-fat, high-sugar diet [17] and structural and functional differences between the heart’s ventricles [18].

It should be noted that we did not consider the individual levels of gene expression. Instead, we performed a systems-level analysis focusing on signal propagation through signaling pathway branches [6]. This allowed us to detect significant perturbations within pathways induced by small but orchestrated changes in expression values and affected by interactions between pathway components [19].

The apparent limitation of our study is the small number of samples in the experimental groups. Moreover, because of the limited number of pathways in the analysis, we may overlook other effects in RV tissues or in female animals associated with other pathways not included in this study. Another limitation of our study is the absence of gene expression data during the WD feeding period and immediately after switching from WD to ND, which prevents direct tracking of early diet-associated molecular events. However, previous characterization of this cohort during the active Western Diet (WD) feeding phase (14–28 days) revealed systolic dysfunction and transient hypertrophic signaling in male animals [20]. Furthermore, independent research has shown that even short-term WD exposure in male mice induces hypertrophy coordinated by repressor element 1-silencing transcription factor at the level of chromatin [21]. Finally, aligned with our results, other studies indicate that while a dietary switch causes reversal of metabolic gene signatures, structural and functional remodeling pathways are less plastic [22].

Our topology-aware pathway analysis reveals long-term perturbations in signaling pathway branches that influence cardiac function in the left ventricular tissue of male mice exposed to a Western diet. These findings suggest that the impact of diet may persist even after transitioning to a healthier diet, warranting further studies to elucidate diet-associated risks and develop strategies for their mitigation.

References

[1] Anand, S. S.; Hawkes, C.; de Souza, R. J.; Mente, A.; Dehghan, M.; Nugent, R.; et al. Food Consumption and Its Impact on Cardiovascular Disease: Importance of Solutions Focused on the Globalized Food System: A Report from the Workshop Convened by the World Heart Federation. J. Am. Coll. Cardiol. 2015, 66, 1590–1614. https://doi.org/10.1016/j.jacc.2015.07.050.

[2] Oikonomou, E.; Psaltopoulou, T.; Georgiopoulos, G.; Siasos, G.; Kokkou, E.; Antonopoulos, A.; et al. Western Dietary Pattern Is Associated with Severe Coronary Artery Disease. Angiology 2018, 69, 339–346. https://doi.org/10.1177/0003319717721603.

[3] Stepanyan, A.; Brojakowska, A.; Zakharyan, R.; Hakobyan, S.; Davitavyan, S.; Sirunyan, T.; et al. Evaluating Sex-Specific Responses to Western Diet across the Lifespan: Impact on Cardiac Function and Transcriptomic Signatures in C57BL/6J Mice at 530 and 640/750 Days of Age. Cardiovasc. Diabetol. 2024, 23, 454. https://doi.org/10.1186/s12933-024-02565-9.

[4] Hakobyan, S.; Stepanyan, A.; Nersisyan, L.; Binder, H.; Arakelyan, A. PSF Toolkit: An R Package for Pathway Curation and Topology-Aware Analysis. Front. Genet. 2023, 14, 1264656. https://doi.org/10.3389/fgene.2023.1264656.

[5] Stepanyan, A.; Hakobyan, S.; Brojakowska, A.; Bisserier, M.; Zakharyan, R.; Davitavyan, S.; Sirunyan, T.; Khachatryan, G.; Khlgatian, M. K.; Zhang, S.; et al. Long-Term Impact of Western Diet on Right Ventricular Transcriptome: Uncovering Sex-Specific Patterns in C57BL/6J Mice. Int. J. Mol. Sci. 2026, 27, 259. https://doi.org/10.3390/ijms27010259.

[6] Braile, M.; Marcella, S.; Cristinziano, L.; Galdiero, M. R.; Modestino, L.; Ferrara, A. L.; et al. VEGF-A in Cardiomyocytes and Heart Diseases. Int. J. Mol. Sci. 2020, 21, 5294. https://doi.org/10.3390/ijms21155294.

[7] Mallick, R.; Ylä-Herttuala, S. Therapeutic Potential of VEGF-B in Coronary Heart Disease and Heart Failure: Dream or Vision? Cells 2022, 11, 4134. https://doi.org/10.3390/cells11244134.

[8] Schulz, R.; Kelm, M.; Heusch, G. Nitric Oxide in Myocardial Ischemia/Reperfusion Injury. Cardiovasc. Res. 2004, 61, 402–413. https://doi.org/10.1016/j.cardiores.2003.09.019.

[9] Casarella, S.; Ferla, F.; Di Francesco, D.; Canciani, E.; Rizzi, M.; Boccafoschi, F. Focal Adhesion's Role in Cardiomyocyte Function: From Cardiomyogenesis to Mechanotransduction. Cells 2024, 13, 664. https://doi.org/10.3390/cells13080664.

[10] Shi, J.; Zhang, L.; Wei, L. Rho-Kinase in Development and Heart Failure: Insights from Genetic Models. Pediatr. Cardiol. 2011, 32, 297–304. https://doi.org/10.1007/s00246-011-9920-0.

[11] Javadov, S.; Jang, S.; Parodi-Rullán, R.; Khuchua, Z.; Kuznetsov, A. V. Mitochondrial Permeability Transition in Cardiac Ischemia–Reperfusion: Whether Cyclophilin D Is a Viable Target for Cardioprotection? Cell. Mol. Life Sci. 2017, 74, 2795–2813. https://doi.org/10.1007/s00018-017-2502-4.

[12] Elrod, J. W.; Wong, R.; Mishra, S.; Vagnozzi, R. J.; Sakthievel, B.; Goonasekera, S. A.; et al. Cyclophilin D Controls Mitochondrial Pore-Dependent Ca^{2+} Exchange, Metabolic Flexibility, and Propensity for Heart Failure in Mice. J. Clin. Invest. 2010, 120, 3680–3687. https://doi.org/10.1172/JCI43171.

[13] Wang-Heaton, H.; Wingard, M. C.; Dalal, S.; Shook, P. L.; Connelly, B. A.; Johnson, P.; et al. ATM Deficiency Differentially Affects Expression of Proteins Related to Fatty Acid Oxidation and Oxidative Stress in a Sex-Specific Manner in Response to Western-Type Diet Prior to and Following Myocardial Infarction. Life Sci. 2024, 342, 122541. https://doi.org/10.1016/j.lfs.2024.122541.

[14] Zhang, Q.; Wang, L.; Wang, S.; Cheng, H.; Xu, L.; Pei, G.; et al. Signaling Pathways and Targeted Therapy for Myocardial Infarction. Signal Transduct. Target. Ther. 2022, 7, 38. https://doi.org/10.1038/s41392-022-00925-z.

[15] Mustafa, M.; Ahmad, R.; Tantry, I. Q.; Ahmad, W.; Siddiqui, S.; Alam, M.; et al. Apoptosis: A Comprehensive Overview of Signaling Pathways, Morphological Changes, and Physiological Significance and Therapeutic Implications. Cells 2024, 13, 1838. https://doi.org/10.3390/cells13221838.
[16] Noll, N. A.; Lal, H.; Merryman, W. D. Mouse Models of Heart Failure with Preserved or Reduced Ejection Fraction. Am. J. Pathol. 2020, 190, 1596–1608. https://doi.org/10.1016/j.ajpath.2020.04.006.
[17] Shetty, S.; Duesman, S. J.; Patel, S.; Huynh, P.; Toh, P.; Shroff, S.; et al. Sex-Specific Role of High-Fat Diet and Stress on Behavior, Energy Metabolism, and the Ventromedial Hypothalamus. Biol. Sex Differ. 2024, 15, 55. https://doi.org/10.1186/s13293-024-00628-w.
[18] Sanz, J.; Sánchez-Quintana, D.; Bossone, E.; Bogaard, H. J.; Naeije, R. Anatomy, Function, and Dysfunction of the Right Ventricle. J. Am. Coll. Cardiol. 2019, 73, 1463–1482. https://doi.org/10.1016/j.jacc.2018.12.076.
[19] Subramanian, A.; Tamayo, P.; Mootha, V. K.; Mukherjee, S.; Ebert, B. L.; Gillette, M. A.; et al. Gene Set Enrichment Analysis: A Knowledge-Based Approach for Interpreting Genome-Wide Expression Profiles. Proc. Natl. Acad. Sci. U.S.A. 2005, 102, 15545–15550. https://doi.org/10.1073/pnas.0506580102.
[20] Brojakowska, A.; Jackson, C. J.; Bisserier, M.; Khlgatian, M. K.; Jagana, V.; Eskandari, A.; et al. Lifetime Evaluation of Left Ventricular Structure and Function in Male ApoE Null Mice after Gamma and Space-Type Radiation Exposure. Front. Physiol. 2023, 14, 1292033. https://doi.org/10.3389/fphys.2023.1292033.
[21] Medford, H. M.; Cox, E. J.; Miller, L. E.; Marsh, S. A. Consuming a Western Diet for Two Weeks Suppresses Fetal Genes in Mouse Hearts. Am. J. Physiol. Regul. Integr. Comp. Physiol. 2014, 306, R519–R526. https://doi.org/10.1152/ajpregu.00253.2013.
[22] Lytle, K. A.; Jump, D. B. Is Western Diet-Induced Nonalcoholic Steatohepatitis in Ldlr$^{-/-}$ Mice Reversible? PLoS One 2016, 11, e0146942. https://doi.org/10.1371/journal.pone.0146942.

Supplementary Materials: Additional tables and figures associated with this study are deposited in the Zenodo repository (See Data Availability Section).

Author Contributions: Conceptualization - A.A., D.A.G.; Formal analysis - T.S., G.Kh., S.H., S.D., R.Z., A.S.; Funding acquisition - D.A.G., A.A.; Investigation - A.B., M.K.Kh., M.B., Sh.Zh.; Resources - D.A.G.; Supervision - D.A.G., A.A.; Visualization - S.D.; Writing – original draft and Writing – review and editing - all authors.

Funding: This study was funded by the ADVANCE Research Grant provided by the Foundation for Armenian Science and Technology (D.A.G.), 25FAST-1F004 by the Higher Education and Science Committee of MESCS RA (D.A.G. and A.A.), and by the grant No: 80NSSC19K1079 from NASA Human Research Program to D.A.G.

Institutional Review Board Statement: Animal protocols adhered to the National Institutes of Health guidelines and were approved by the Institutional Animal Care and Use Committees at Brookhaven National Laboratory (BNL) (Upton, NY) (BNL IACUC Protocol #502) and the Icahn School of Medicine at Mount Sinai (NY, NY) (ISMMS IACUC Protocol #2019-0017).

Informed Consent Statement: Not applicable.

Data and Code Availability Statement: The raw sequencing data is available in the Gene Expression Omnibus (Accession: GSE272168). Additional tables and figures associated with this study are deposited in the Zenodo repository (https://zenodo.org/records/17879619).

Acknowledgments: During the preparation of this work, the authors used the ChatGPT 4-o service to improve language and readability. After using this service, the authors reviewed and edited the content as needed and take full responsibility for the content of the publication.

Conflicts of Interest: All authors declare no conflict of interest.

ԱՄՓՈՓԱԳԻՐ

«Արևմտյան» սննդակարգով պայմանավորված կենսաբանական ուղիների երկարատև ակտիվությունը սրտի փորոքային հյուսվածքներում

Թամարա Սիրունյան[1,2,#], Գիսանե Խաչատրյան[1,2,#], Սիրաս Հակոբյան[1,3], Սուրեն Դավիթավյան[1,2], Ռոքսանա Զախարյան[1,2], Անի Ստեփանյան[1], Ագնեշկա Բոոյակովսկա[4,5], Մերի Խլղաթյան[5], Մալիկ Բիսիրեր[6], Շիհոնգ Ժանգ[4], Դավիթ Ղուկասյան[4], Արսեն Առաքելյան[1,2,3,*]

[1]ՀՀ ԳԱԱ մոլեկուլային կենսաբանության ինստիտուտ, Երևան, ՀՀ
[2]Ռուս-Հայկական համալսարան, Երևան, ՀՀ
[3]Հայաստանի կենսաինֆորմատիկայի ինստիտուտ, Երևան, ՀՀ
[4]Սրտանոթային հետազոտությունների ինստիտուտ, Մաունթ Սայնայի Իքանի բժշկության դպրոց, Նյու Յորք, Նյու Յորք, ԱՄՆ
[5]Բջջային կենսաբանության ամբիոն, Յելի համալսարանի բժշկության դպրոց, Նյու Հեյվեն, Կոնեկտիկուտ, ԱՄՆ
[6]Բջջային կենսաբանության, անատոմիայի և ֆիզիոլոգիայի ամբիոն, Նյու Յորքի բժշկական քոլեջ, Վալհալա, Նյու Յորք, ԱՄՆ

[#]Հավասար ներդրում
[*]Հաղորդակցության համար՝ a_arakelyan@mb.sci.am

«Արևմտյան սննդակարգը» (ԱՍ), որը բնորոշվում է ճարպերի և շաքարների բարձր պարունակությամբ, սերտորեն ասոցացված է սրտանոթային հիվանդությունների բարձր ռիսկի հետ: Սույն հետազոտությունում գնահատվել են կենսաբանական ազդանշանային ուղիների ակտիվությունների երկարատև փոփոխությունները 125 օր ԱՍ-ով կերակրված, ապա նորմալ սննդակարգի (ՆՍ) անցած C57Bl/6J մկների ձախ (ՁՓ) և աջ (ԱՓ) փորոքների հյուսվածքներում: ՁՓ և ԱՓ հյուսվածքները հավաքվել են 530-րդ օրը՝ ՆՍ-ին անցնելուց 105 օր անց, և ենթարկվել ՌՆԹ սեքվենավորման: Քառասուն ազդանշանային ուղիների ակտիվությունը հաշվարկվել է մեր կողմից մշակված Pathway Signal Flow (PSF) ալգորիթմի միջոցով, որը գնահատում է կենսաբանանական ազդակի տարածումը ուղու երկայնքով՝ հիմնվելով ուղու բաղադրիչների գենային էքսպրեսիայի մակարդակների և այդ բաղադրիչների փոխազդեցությունների վրա: Արդյունքների համաձայն՝ ՆՍ-ին անցնելուց 105 օր անց արու մկների ՁՓ հյուսվածքում հայտնաբերվել են ակտիվության էական շեղումներ ազդանշանային ուղիների 14 ճյուղերում: Մասնավորապես, նկատվել է կարդիոպրոտեկտոր VEGF ազդանշանային ուղու ակտիվության նվազում և ֆիբրոզ խթանող TGF-beta ուղու ակտիվացում, ինչը վկայում է սրտանոթային ռիսկերի երկարաժամկետ պահպանման մասին: Բացի այդ, հայտնաբերվել է cGMP-PKG և FOXO ուղիներում ազդանշանի ակտիվացում, ինչը կարող է կապված լինել սրտային անբավարարության հետ: Միաժամանակ նկատվել է ինչպես հարապոպտոտիկ, այնպես էլ հակաապոպտոտիկ ուղիների ակտիվացում, որն ուղեկցվում է բջջային ցիկլի արգելակիչների ակտիվության նվազմամբ: Հատկանշական է, որ էական փոփոխություններ չեն հայտնաբերվել էգ մկների ՁՓ հյուսվածքում և երկու սեռերի ԱՓ-ի հյուսվածքում: Ստացված արդյունքները ցույց են տալիս, որ ԱՍ-ի բացասական

ազդեցությունները կարող են պահպանվել նույնիսկ առողջ սննդակարգի անցնելուց հետո: Անհրաժեշտ են հետագա ուսումնասիրություններ՝ սննդակարգի հետ կապված ռիսկերը պարզաբանելու և այդ երկարաժամկետ ազդեցությունները մեղմելու արդյունավետ ռազմավարություններ մշակելու համար:

Բանալի բառեր՝ արևմտյան սննդակարգ, ձախ փորոք, աջ փորոք, ՌՆԹ սեքվենավորում, տրանսկրիպտոմիկա, ազդանշանային ուղիներ, Pathway Signal Flow

Reports of NAS RA
ՀՀ ԳԱԱ Զեկույցներ
NATIONAL ACADEMY OF SCIENCES OF THE REPUBLIC OF ARMENIA
ՀԱՅԱՍՏԱՆԻ ՀԱՆՐԱՊԵՏՈՒԹՅԱՆ ԳԻՏՈՒԹՅՈՒՆՆԵՐԻ ԱԶԳԱՅԻՆ ԱԿԱԴԵՄԻԱ

2026 **Volume 126** **Issue 1** **Article No. 3**

Category: Mathematics
Type of Paper: Review Article
Received: January 2, 2026, **Revised:** January 29, 2026, **Accepted:** January 29, 2026
Published: February 13, 2026

DOI: 10.54503/0321-1339-2026.126.1-3

Aggrandization of spaces: a new general approach and application

Alexey Karapetyants[1,*]

[1] Southern Federal University, Rostov-on-Don, Russia

[*]Correspondence: karapetyants@gmail.com

Abstract
Our study is based on recent results concerning the so-called local aggrandization of Lebesgue spaces. We extend this framework to the case of arbitrary Banach spaces of functions on metric spaces. Furthermore, we demonstrate that grand spaces of holomorphic functions can be equivalently defined through aggrandization associated exclusively with the boundary. This paper review presents recent results obtained in collaboration with Stefan Samko and provides a concise introduction to the classical theory of grand spaces for comparative analysis. We also discuss the underlying motivation for investigating these spaces.

Keywords: Grand spaces, Holomorphic functions, Aggrandization
AMS MSC: 47G10, 47B38, 46E30

1. Introduction

Drawing on recent results concerning the so-called local aggrandization of Lebesgue spaces (see e.g., [7,8,9]), we present a new approach to the construction of grand spaces. This framework was recently introduced and developed in [5] in the case of arbitrary Banach spaces of functions on metric spaces. By examining specific classes of analytic functions, we demonstrate that grand spaces of holomorphic functions can be equivalently defined via an aggrandization associated solely with the boundary. Although the problem of aggrandizing analytic spaces was the initial objective for this research, it became immediately apparent that this concept could be applied to a wide range of Banach spaces of functions on metric spaces.

To better illustrate the underlying concept, we consider the specific case of p-integrable holomorphic functions on the unit disc in the complex plane. By applying the general method of local aggrandization to such spaces, we establish the following equivalence of norms:

$$\sup_{0<\varepsilon<p-1} \varepsilon^{\theta} \left(\int_{\mathbb{D}} |f(z)|^{p-\varepsilon} \, \mathrm{dA}(z) \right)^{\frac{1}{p-\varepsilon}}$$

$$\eqsim \sup_{0<\varepsilon<l} \varepsilon^{\theta} \left(\int_{\mathbb{D}} |f(z)|^{p} \left(1-|z|\right)^{\lambda\varepsilon} \, \mathrm{dA}(z) \right)^{\frac{1}{p}}$$

for all $\lambda > 0$ and $l > 0$. In fact, we prove more general statement with $(1-|z|)^{\lambda\varepsilon}$ replaced by $a(1-|z|)^{\varepsilon}$, under some assumptions on the function a, called aggrandizer.

Naturally, this theory allows for further development, particularly through the selection of specific function spaces. Our objective here, however, is not to pursue these extensions, but rather to illustrate the core idea using a fundamental case, while simultaneously presenting the definition in the most general setting to date.

As previously noted, the main definition of the aggrandization and proofs of the theorems presented in Sections 3, 4 originally appeared in [5]; we refer to this source for more details and generalizations.

2. Classical approach. Definitions and some results

We do not aim to provide a comprehensive survey of the vast literature on classical grand spaces; we mention only a few key works: [1,2,3,4].

2.1. What is Grand Lebesgue space over finite measure domain Ω

Given an open set $\Omega \subset \mathbb{R}^n$, $|\Omega| = 1$, $1 < p < \infty$, and $\theta > 0$, the grand Lebesgue space $L^{p),\theta}(\Omega)$ consists of all measurable on Ω functions f such that

$$\| f \|_{p),\theta} = \sup_{0<\varepsilon<p-1} \left(\varepsilon^{\theta} \int_{\Omega} |f(x)|^{p-\varepsilon} \, dx \right)^{\frac{1}{p-\varepsilon}}. \tag{2.1}$$

Let us outline basic relations with Lebesgue spaces. For a finite measure domain Ω we have:

$$L^p \subset L^{p)} \subset L^{p-\varepsilon}, \quad L^{p+\varepsilon} \subset L^{(p} \subset L^p, \quad L^p \subset L^{p,\infty} \subset L^{p)}$$

$$L^p \subset L^p \log^{-1} L \subset L^{p)} \subset \cap_{\alpha>1} L^p \log^{-\alpha} L$$

The fundamental function provides insight into how grand and small Lebesgue spaces differ from the classical Lebesgue space. The following result can be inferred from the work of Alberto Fiorenza; however, its formulation in terms of the Lambert function first appeared in a paper by S. Umarkhadzhiev.

Lemma 2.1 ([6]). Let $1 < p < \infty$, $\theta > 0$, Ω be an open set in $\mathbb{R}^n$, $|\Omega| = 1$, and E be an open set in Ω with $|E| = \eta$. Then

$$\| \chi_E \|_{p),\theta} = \begin{cases} e^{\frac{\theta}{p} W_-\left(-\frac{p\eta^{1/\theta}}{e}\right)}, & 0 < \eta^{\frac{1}{\theta}} < \dfrac{1}{p-1} e^{-\frac{1}{p-1}}, \\ (p-1)^{\theta}\eta, & \dfrac{1}{p-1} e^{-\frac{1}{p-1}} \leqslant \eta^{\frac{1}{\theta}} < 1, \end{cases} \tag{2.2}$$

where W_- is the branch of Lambert function W, which yields

$$\| \chi_E \|_{p),\theta} \simeq \eta^{\frac{1}{p}} \ln^{-\frac{\theta}{p}} \frac{e}{\eta}, \qquad \| \chi_E \|_{(p,\theta} \simeq \eta^{\frac{1}{p}} \ln^{\frac{\theta}{p'}} \frac{e}{\eta}.$$

2.2. Whether there is a difference between a space of p - integrable holomorphic functions and its grand counterpart

The answer is affirmative for $\mathcal{A}^p(\mathbb{D})$ and $\mathcal{A}^{p),\theta}(\mathbb{D})$. More precisely,

$$\frac{1}{(1-z)^{\lambda}} \in \mathcal{A}^p(\mathbb{D}) \Leftrightarrow \lambda < \frac{2}{p},$$

see Duren and Schuster book (2004), while it is easily checked that

$$\frac{1}{(1-z)^{\frac{2}{p}}} \in \mathcal{A}^{p),\theta}\left(\mathbb{D}\right), \quad \theta = 1.$$

Moreover, we know that (see [10]):

$$g_\theta\left(z\right) = \frac{1}{(1-z)^{\frac{2}{p}}} \ln^{\frac{\theta-1}{p}} \frac{e}{1-z} \in \mathcal{A}^{p),\theta}\left(\mathbb{D}\right)$$

under the proper choice of the branch of logarithmic function.

3. Local aggrandization of function spaces over metric spaces: a general approach

Let $\left(\Lambda, d\right)$ be a metric space and $\mathcal{D} = \operatorname{diam}\Lambda, \quad 0 < \mathcal{D} \leqslant \infty$. Given a closed non empty subset $F \subset \Lambda,$ denote

$$\delta_F\left(x\right) = \inf_{y \in F} d\left(x, y\right), \quad x \in \Lambda.$$

Let $X = X\left(\Lambda\right)$ be an arbitrary normed space of functions $f : \Lambda \to \mathbb{C}$ and $\|\cdot\|_X$ be its norm.

With the space X we associate the normed space $X_w = X\left(\Lambda, w\right)$ depending on a functional parameter $w : \Lambda \to \mathbb{R}_+,$ and assume that $X_w = X,$ for $w = 1.$ By $\|\cdot\|_{X,w}$ we denote the norm in $X_w.$ We assume that w is nonnegative. Also, in what follows we assume that the space X_w possesses the following property (lattice property with respect to weights): for any two weights u, v such that $u \leqslant v$, the following inequality holds

$$\| f \|_{X,u} \leqslant \| f \|_{X,v}.$$

Definition 3.1. Let $F \subset \Lambda$ be a closed non-empty set. For a positive almost increasing function $a \in L^\infty\left(0, \mathcal{D}\right), \quad a\left(0+\right) = 0,$ we define the local grand space

$$X^g_{F,a,\theta} = X^g_{F,a,\theta}\left(\Lambda\right)$$

related to the space $X,$ by the norm

$$\| f \|_{X^g_{F,a,\theta}} = \sup_{0<\varepsilon<l}\left(\varepsilon^\theta \| f \|_{X,(a\circ\delta_F)^\varepsilon}\right), \ l > 0. \tag{3.3}$$

The function a used in definition of $X^g_{F,a,\theta}$ will be referred to as aggrandizer. The embedding

$$X \subset X^g_{F,a,\theta} \tag{3.4}$$

holds because $a \in L^\infty\left(0, \mathcal{D}\right)$ by definition.

4. Application to the space of holomorphic functions

4.1. Let us recall classical definitions

Let $\Lambda = \mathbb{D}$ be the unit disc in $\mathbb{C}$. We identify $\mathbb{R}^2 \equiv \mathbb{C}$ so that $\left(x, y\right) = z.$ Let $\mathrm{dA}\left(z\right) = \frac{1}{\pi} dxdy$. Let $\rho = \rho\left(t\right)$. In the sequel we always assume that for arbitrary $\delta \in \left(0,1\right)$

$$0 < \inf_{t \in (\delta,1)} \rho\left(t\right) \leq \sup_{t \in (\delta,1)} \rho\left(t\right) < \infty.$$

The weighted Lebesgue space $L^p(\mathbb{D},\rho)$ is defined by the norm

$$\| f \|_{L^p(\mathbb{D},\rho)} = \left(\int_{\mathbb{D}} |f(z)|^p \, \rho(1-|z|) \, \mathrm{dA}(z) \right)^{1/p}, \quad 1 \leqslant p < \infty.$$

Let $\mathcal{A}^p(\mathbb{D},\rho)$ stand for the subspace of $L^p(\mathbb{D},\rho)$, which consist of functions holomorphic in $\mathbb{D}$.

For $1 < p < \infty$ and $\theta > 0$, the (classical weighted) grand Lebesgue space $L^{p),\theta}(\mathbb{D},\rho)$ consists of all functions f measurable on $\mathbb{D}$ such that

$$\| f \|_{L^{p),\theta}(\mathbb{D},\rho)} := \sup_{0<\varepsilon<p-1} \varepsilon^\theta \| f \|_{L^{p-\varepsilon}(\mathbb{D},\rho)} < \infty. \tag{4.5}$$

The corresponding subspace of holomorphic functions will be denoted by $\mathcal{A}^{p),\theta}(\mathbb{D},\rho)$.

4.2. Local aggrandization of the space $L^p(\mathbb{D},\rho)$

We take $F = \mathbb{T}$, $\delta_{\mathbb{T}}(z) = 1-|z|$. We find it convenient to use the notation $L^{p)}_{\mathbb{T},a,\theta}(\mathbb{D},\rho)$ for the aggrandized space for $L^p(\mathbb{D},\rho)$. Same for $\mathcal{A}^{p)}_{\mathbb{T},a\theta}(\mathbb{D},\rho)$. Hence,

$$\| f \|_{L^{p)}_{\mathbb{T},a,\theta}(\mathbb{D},\rho)} = \sup_{0<\varepsilon<l} \left(\varepsilon^\theta \| f \|_{L^p(\mathbb{D},\rho),(a\circ\delta_{\mathbb{T}})^\varepsilon} \right)$$

$$= \sup_{0<\varepsilon<l} \left(\varepsilon^\theta \int_{\mathbb{D}} |f(z)|^p \, (a\circ\delta_{\mathbb{T}})(z)^\varepsilon \, \rho(1-|w|) \, \mathrm{dA}(z) \right)^{\frac{1}{p}},$$

where $l > 0$ (we will assume that $l < p-1$).

4.3. The inclusions between classical grand spaces and spaces constructed via local aggrandization

Here, we illustrate our approach by comparing classical grand spaces with those constructed via the local method, specifically for the case of weighted spaces of holomorphic functions. In fact, this comparison demonstrates that under minimal assumptions, the spaces coincide, up to equivalence of norms. This allows for the interchangeability of norms in applications and further research, enabling the choice of the most suitable or productive norm for each specific case.

Recall, that a function φ satisfies the reverse doubling condition if there exists $c_{(2)} > 0$ such that $\varphi(t) \leqslant c_{(2)} \varphi(2t)$, $t > 0$.

Theorem 4.3. The following statements hold true.

(1) Let there exist $\delta > 0$ such that

$$\int_0^1 \frac{\rho(t)}{a(t)^\delta} dt < \infty.$$

Then

$$\mathcal{A}^{p)}_{\mathbb{T},a,\theta}(\mathbb{D},\rho) \hookrightarrow \mathcal{A}^{p),\theta}(\mathbb{D},\rho).$$

(2) Let any of the two following conditions be satisfied:

(a) the function $\rho = \rho(t)$ is almost decreasing and satisfying the reverse doubling condition and there exist $\eta > 0$, $c_a > 0$ and $\varepsilon_0 \in (0, p-1)$ such that

$$a(t)\leqslant c_a\left(t^{\frac{2}{p}}\rho(t)^{\frac{1}{p-\varepsilon_0}}\right)^{\eta},\qquad t\in(0,1),$$

(b) the function $\rho=\rho(t)$ is almost increasing and $M(\rho)<p-1$, and there exist $\eta>0$ and $c_a>0$, such that

$$a(t)\leqslant c_a\left(t^{\frac{2}{p}}\rho(t)^{\frac{1}{p}}\right)^{\eta},\qquad t\in(0,1).$$

Then

$$\mathcal{A}^{p),\theta}(\mathbb{D},\rho)\hookrightarrow\mathcal{A}^{p)}_{\mathbb{T},a,\theta}(\mathbb{D},\rho).$$

The case of a power weight is of particular interest.

Theorem 4.4. Let $\rho(t)=t^{\gamma}$, $-1<\gamma<p-1$, and there exists $\delta>0$ such that

$$\int_0^1\frac{t^{\gamma}dt}{a(t)^{\delta}}<\infty,$$

and there exist $C>0$ and $\eta>0$ such that

$$a(t)\leqslant Ct^{\eta}.$$

Then the space $\mathcal{A}^{p),\theta}(\mathbb{D},\rho)$ coincides with the space $\mathcal{A}^{p)}_{\mathbb{T},a,\theta}(\mathbb{D},\rho)$, up to equivalence of norms.

We single out particular corollary for the unweighed case: $\rho=1$. We use symbols $\mathcal{A}^{p),\theta}(\mathbb{D})$ and $\mathcal{A}^{p)}_{\mathbb{T},a,\theta}(\mathbb{D})$ for the unweighed spaces.

Theorem 4.5. The space $\mathcal{A}^{p),\theta}(\mathbb{D})$ coincides with the space $\mathcal{A}^{p)}_{\mathbb{T},a,\theta}(\mathbb{D})$ with any aggrandizer a satisfying $m(a)>0$, up to equivalence of norms.

References

[1] Iwaniec, T.; Sbordone, C. On the Integrability of the Jacobian under Minimal Hypotheses. *Arch. Ration. Mech. Anal.* **1992**, *119*, 129–143. https://doi.org/10.1007/BF00375119.

[2] Greco, L.; Iwaniec, T.; Sbordone, C. Inverting the *p*-Harmonic Operator. *Manuscr. Math.* **1997**, *92*, 249–258. https://doi.org/10.1007/BF02678192.

[3] Di Fratta, G.; Fiorenza, A. A Direct Approach to the Duality of Grand and Small Lebesgue Spaces. *Nonlinear Anal.* **2009**, *70*, 2582–2592. https://doi.org/10.1016/j.na.2008.03.044.

[4] Fiorenza, A.; Karadzhov, G. E. Grand and Small Lebesgue Spaces and Their Analogs. *Z. Anal. Anwend.* **2004**, *23*, 657–681. https://doi.org/10.4171/ZAA/1215.

[5] Karapetyants, A.; Samko, S. Aggrandization of Spaces of Holomorphic Functions Reduces to Aggrandization on the Boundary. *Math. Notes* **2024**, *116*, 1292–1305. https://doi.org/10.1134/S000143462411035X.

[6] Samko, S. G.; Umarkhadzhiev, S. M. On Iwaniec–Sbordone Spaces on Sets Which May Have Infinite Measure. *Azerb. J. Math.* **2011**, *1* (1), 67–84.

[7] Rafeiro, H.; Samko, S.; Umarkhadzhiev, S. Local Grand Lebesgue Spaces on Quasi-Metric Measure Spaces and Some Applications. *Positivity* **2022**, *26*, 53. https://doi.org/10.1007/s11117-022-00915-z.

[8] Rafeiro, H.; Samko, S. Local Grand Variable Exponent Lebesgue Spaces. *Z. Anal. Anwend.* **2023**, *42*, 1–15. https://doi.org/10.4171/ZAA/1719.
[9] Samko, S. G.; Umarkhadzhiev, S. M. Local Grand Lebesgue Spaces. *Vladikavkaz Math. J.* **2021**, *23*, 96–108. https://doi.org/10.46698/e4624-8934-5248-n.
[10] Karapetyants, A. N.; Samko, S. G. On Grand and Small Bergman Spaces. *Math. Notes* **2018**, *104*, 431–436. https://doi.org/10.4213/mzm12114.

Funding: The research is supported by the Regional Mathematical Center of Southern Federal University under the program of the Ministry of Education and Science of the Russian Federation, agreement No. 075-02-2025-1720.
Data and Code Availability Statement: The author confirms that all data generated or analyzed during this study are included in this article.
Conflicts of Interest: The author declares no conflicts of interest.

Reports of NAS RA
ՀՀ ԳԱԱ Զեկույցներ
NATIONAL ACADEMY OF SCIENCES OF THE REPUBLIC OF ARMENIA
ՀԱՅԱՍՏԱՆԻ ՀԱՆՐԱՊԵՏՈՒԹՅԱՆ ԳԻՏՈՒԹՅՈՒՆՆԵՐԻ ԱԶԳԱՅԻՆ ԱԿԱԴԵՄԻԱ

2026 **Volume 126** **Issue 1** **Article No. 4**

Category: Chemistry
Type of Paper: Review Article
Received: November 6, 2025, **Revised:** January 14, 2026, **Accepted:** February 13, 2026
Published: February 19, 2026

DOI: 10.54503/0321-1339-2026.126.1-4

Modern Synthetic Approaches to Cubebene and Related Sesquiterpene Frameworks

William C. Croydon[1], Andrei V. Malkov[1,*]

[1]Department of Chemistry, Loughborough University, Loughborough, LE11 3TU, UK

[*]Correspondence: A.Malkov@lboro.ac.uk

Abstract

Cubebenes and related sesquiterpenes, featuring a tricyclo[4.4.0.0^{1},^{5}]decane framework, exhibit notable structural complexity and diverse bioactivity. This review highlights key synthetic approaches toward these molecules, including diazo-mediated cyclopropanation, metal-catalysed enyne cyclisation, bicycloannulation cascades, and photochemical rearrangements. Mechanistic and stereochemical aspects are discussed, highlighting progress in diastereo- and enantioselective methodologies. Although substantial advances have been achieved, efficient access to higher cubebene analogues remains a synthetic challenge. Integration of bioinspired design, modern synthetic methods, and asymmetric catalysis is expected to further advance concise and stereoselective synthesis of these complex architectures.

Keywords: Asymmetric synthesis, Cyclopropanation, Enyne cyclisation, Sesquiterpenes, Transition-metal catalysis

1. Introduction

Cubebenes were first isolated from *Piper cubera* berries and later also found in several pine species. Natural cubebenes **1-4** and their structural analogues **5-8** (Figure 1)[1,2] represent a distinctive class of sesquiterpenes with the tricyclo[4.4.0.0^{1,5}]decane ring system that have attracted the attention of researchers owing to their diverse biological activities and the unique tricyclic framework.

The synthesis of cubebene analogues holds both practical and academic significance: on one hand, their occurrence in essential oils and reported antimicrobial, anti-inflammatory, and antioxidant properties position them as promising leads for drug discovery and fine chemical applications; on the other, the complex stereochemical architecture of cubebene represents an attractive challenge for the development of efficient synthetic methodologies and strategies for selective functionalisation. Therefore, research on cubebene analogues not only contributes to the understanding of structure–activity relationships within sesquiterpenes but also advances modern approaches in terpene synthesis, catalysis, and molecular design. To date, several total synthesis strategies have been reported for compounds **1-3**.[3,4] However, compounds **4-8** have yet to be made. Herein, we review the general strategies employed for the construction of 6-3-5 ring systems.

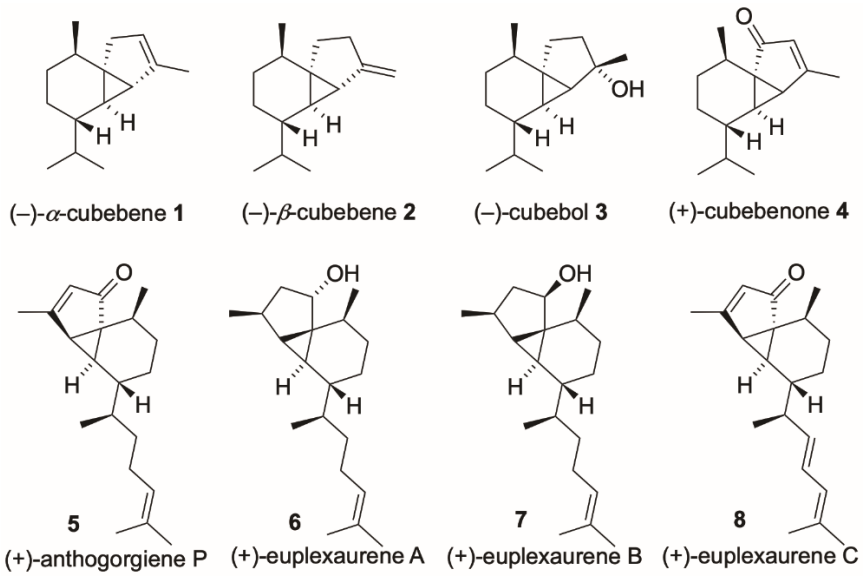

Figure 1. Natural products featuring cubebene tricyclic framework.

2. Synthesis of cubebenes and related scaffolds

2.1. Biosynthesis

The biosynthesis of cubebene has been studied through deuterium labelling (Scheme 1).[5] Depyrophosphorylation of farnesyl pyrophosphate **9** followed by [1,10] ring closure of cation **10**, 1,3-hydride shift in **11,** and proton elimination frim **12** yields (*S*)-(-)-germacrene D **13** as an intermediate. Protonation of the exo-alkene (**14**) followed by electrophilic [1,6] ring closure gives the cardinyl cation **15**. A 1,2-hydride shift to cation **16** and then a [1,5] ring closure give the 6,3,5-ring system **17**. Then, the outcome depends on the subsequent reactions. Thus, endo-proton elimination gives *α*-cubebene **1**, exo-proton elimination leads to *b*-cubebene **2**, whereas hydrolysis gives rise to cubebol **3**.[5,6]

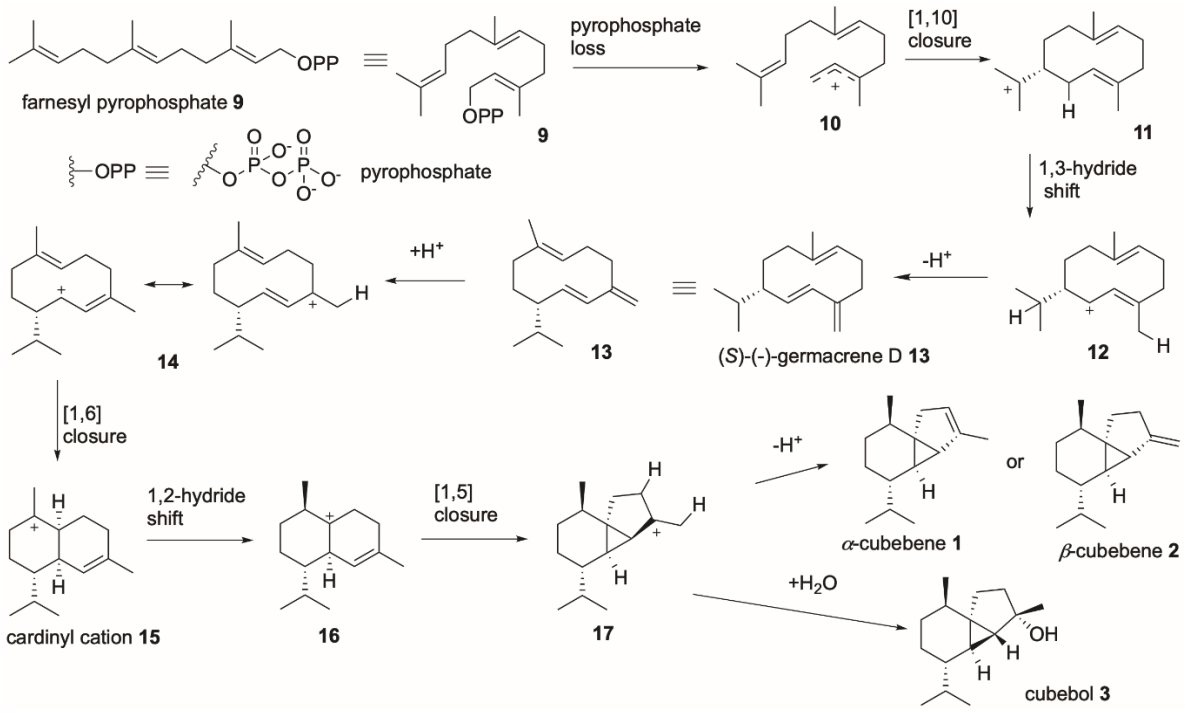

Scheme 1. Biosynthesis of cubebenes.

For the most recent additions to the cubebene family, the analogues of anthogorgiene P **5**-**8**, biosynthesis has not been elucidated in detail, but a proposed biosynthetic pathway is thought to involve the depyrophosphorylation of geranylgeranyl pyrophosphate **18** followed by ring closure between the C1/C10 and C1/C6, followed by oxidation to the serrulatane scaffold **10** (Scheme 2). The tetrahydronaphthalene is thought to then undergo aromatic rearrangement and oxidation to Anthogorgiene P **5**.[2]

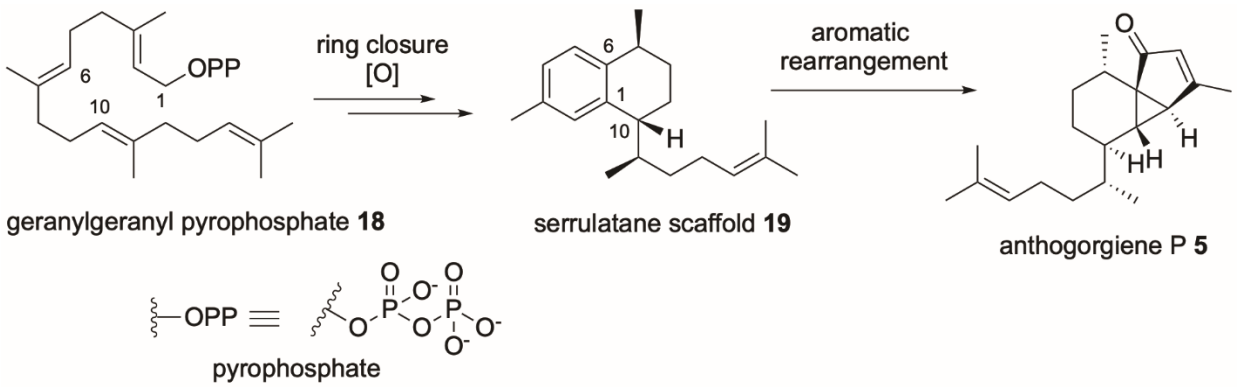

Scheme 2. Proposed biosynthesis of anthogorgiene P.

Over the past 50 years, several methodologies have been developed towards the synthesis of the cubebenes. The typical synthetic strategy involves modifying a cyclic monoterpenoid that can undergo intramolecular cyclopropanation, although there are notable exceptions. In the next sections, we shall survey the reported strategies for the synthesis of cubebene analogues.

2.2. Diazo-based strategies

In 1969 and 1971, the De Waal group published the first total synthesis of *b*-cubebene **2,** which also constituted a formal synthesis of *a*-cubebene **1** (Scheme 3).[7,8] The synthesis commenced with menthone **20,** yielding within 11 steps a-diazo ketone **21**. The cyclopropanation was performed using stoichiometric amounts of copper(II) sulphate in cyclohexane and afforded a 38:62 mixture of **22** and **23**, respectively, with a 78% combined yield, favouring the unnatural isomer **23**. The practicality of this methodology suffers from poor selectivity and the use of stoichiometric metal salt. However, after isolation, the minor isomer **22** was subjected to Wittig alkenylation to achieve the first total synthesis of *b*-cubebene **2**.

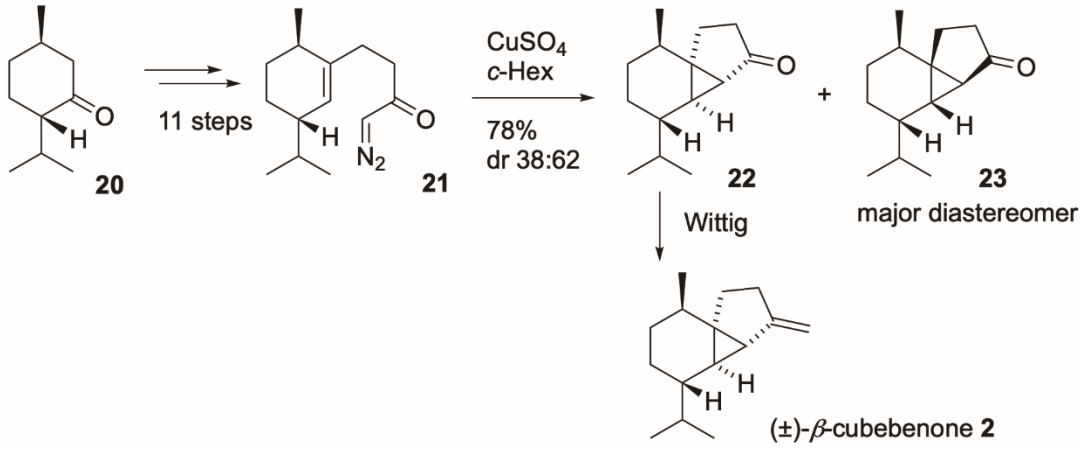

Scheme 3. Key steps of De Waals' synthesis of racemic cubebenes.

The synthetic sequence reported by Yoshikoshi[9] resembles that of De Waals[8] (Scheme 1.4), but has a more efficient synthesis of the key a-diazo ketone intermediate **25**. Starting from (–)-*trans*-caran-2-one **24,** the diazo intermediate was successfully synthesised in 7 steps. The intramolecular cyclopropanation, however, provided a lower yield compared to the De Waals protocol but showed marginally better diastereoselectivity for the desired isomer **26** (dr 44:56)**.** For the stoichiometric copper reagent, Yoshikoshi deployed copper powder instead of copper(II) sulphate. The diastereoselectivity still favoured the cyclopropane being *anti* to the methyl group, as in **27**.

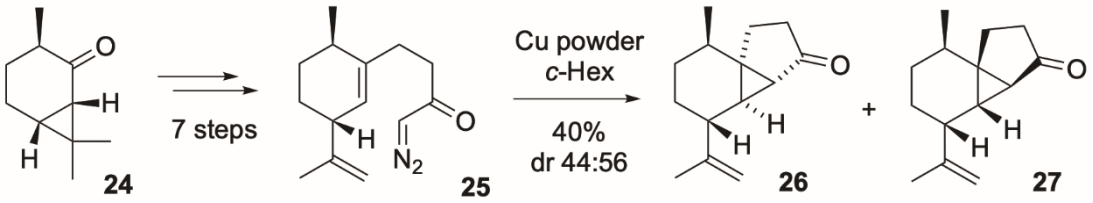

Scheme 4. Key steps of Yoshikoshi's synthesis of cubebenes.

Hosokawa worked on the total synthesis of exigurin **28** and a formal total synthesis of boneratamide A **29** (Scheme 5).[10] Both routes relied on a tricyclo[4.4.0.0^{1,5}]decane intermediates **32** and **34**, analogous to the cubebene nucleus. Similar to the works of De Waal[8] and Yoshikoshi,[9] the synthesis involved intramolecular cyclopropanation of a diazo intermediate. Instead of using an a-diazo ketone, they deployed an *a*-diazo-*b*-keto sulphone. This sulphone was required for the total synthesis but also provided sizeable steric bulk. In this approach, to carry out intramolecular cyclopropanation, stoichiometric copper reagents were replaced by catalytic quantities of complex **30**.

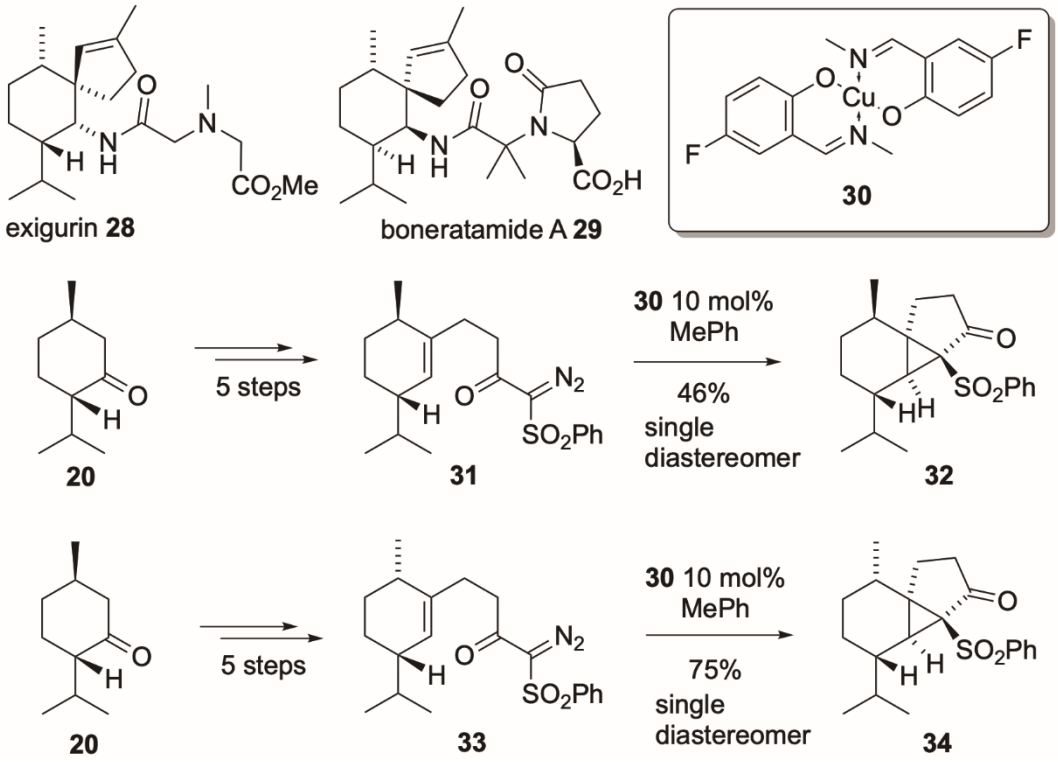

Scheme 5. Key steps in the synthesis of exigurin **28** and bonertamide **A 29**.

The synthesis of the *a*-diazo-*b*-keto sulphone for both the *anti*-**31** and *syn*-**33** methyl and isopropyl menthone analogues started with menthone **20**. The intermediates were formed in 5 steps each and isolated as single diastereomers. The copper-catalysed intramolecular cyclopropanation proved to be highly diastereoselective for the construction of the tricyclo[4.4.0.0^{1,5}]decane ring system; this was owed to the steric hindrance between the phenyl sulphone and the isopropyl group, enabling high facial selectivity for the cyclopropanation as illustrated by **32** and **34**. For the *syn-a*-diazo-*b*-keto sulphone **33,** the cyclopropanation gave a 75% yield of **34** as a single diastereomer. However, the *anti-a*-diazo-*b*-keto sulphone **31** provided a significantly lower yield of **32**, 46%, but still as a single diastereomer. In both instances, the cyclopropanation installed the cyclopropane on the opposite face to the isopropyl group.

2.3. Bicycloannulation

Hagiwara[11–13] developed a bicycloannulation of 3-OTMS 1,3-dienes **35a-c** with methyl 2-bromopropenoates **36,** which undergo a cascade of two Michael additions and terminate with a substitution giving cyclopropanes within a tricyclic system **37** (Scheme 6). The reaction is initiated with the formation of the kinetic lithium enolate generated upon treatment of **36a** with MeLi. The reaction required the use of the silyl enol ether because the generation of the enolate from the ketone with LDA provided no yield in the reaction. Another version of this methodology employed unsaturated enone **35b** and methyl 2,3-dichloropropenoate **38**.[13] In this modification, the lithium enolate and methyl 2-chloropropenoate are generated in situ with LiHMDS; it provides higher yields and does not require the generation of a Michael acceptor ex-situ nor conversion of the enone to the silyl enol ether. Mechanistically, the reaction goes through a stepwise Michael-Michael cascade rather than a [4+2] cycloaddition (Scheme 7). The initial intermolecular Michael addition of **40** to **36a** generated the second enolate **41** that undergoes an intramolecular Michael addition to form **42,** and the cascade terminates with the final enolate undergoing substitution of the bromide yielding the tricyclic system **37aa**. The facial selectivity of the intramolecular Michael addition and sequential ring closure can be controlled by the stereocenter on C-3 on the cyclohexene ring, as in **35b**, which can inhibit the *syn* facial approach of the second Michael addition and drive the formation of an *anti*-conformation of the C-3 substituent and cyclopropane **39**. When this methodology was applied in the total synthesis of cubebene with silylenol ether **43,** there was no conversion to the desired scaffold. The only recovered product was an intermediate from the initial Michael addition **44,** at which the cascade was terminated (Scheme 8).

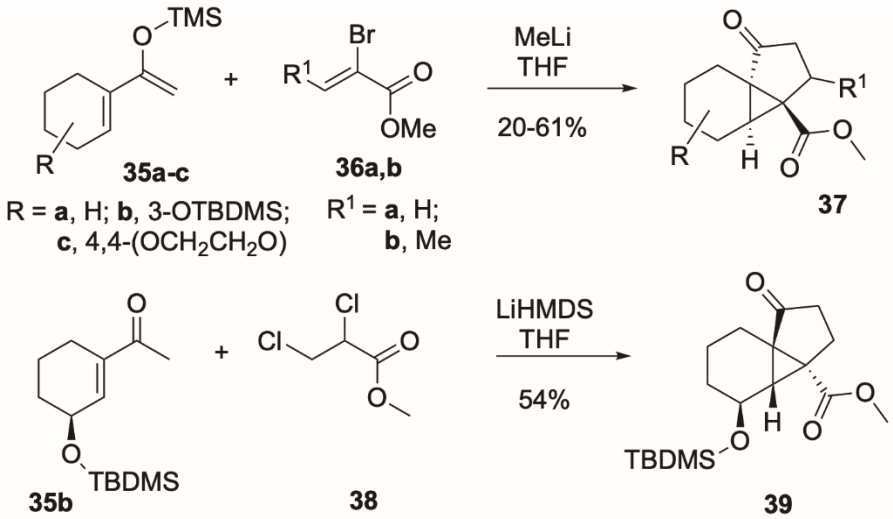

Scheme 6. Bicycloannulation cascade.

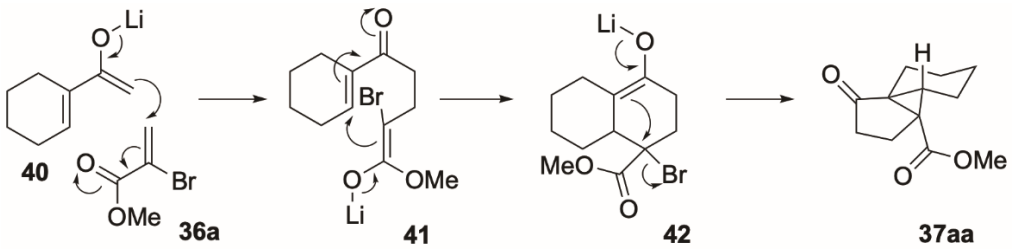

Scheme 7. Proposed mechanistic pathway for the bicycloannulation cascade.

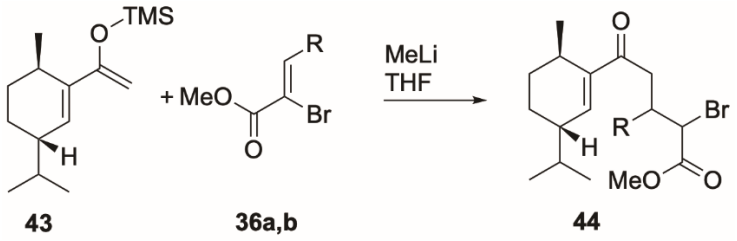

Scheme 8. Unsuccessful attempt at a synthesis of the cubebene scaffold.

2.4. Enyne cyclisation strategies

This is the group of the most successful strategies, where the formation of the cyclopropane ring relies on 1,5-enyne cyclisation catalysed by transition metals of 10-11 groups.

The synthesis by the Furstner group[14] commenced with (*R*)-(–)-carvone **45,** and in 7 steps produced a mixture of two diastereoisomeric acetates, (*S*)-**46** and (*R*)-**47** (dr 63:35)**,** with strategically positioned double and triple bonds (Scheme 9). The key step in the synthesis was a platinum(II) chloride-catalysed cyclopropanation. Importantly, the (*S*)-enantiomer **46** gave the desired product **48** in 92% yield as a single diastereomer. At the same time, cyclisation of the (*R*)-enantiomer **47** under the same conditions proceeded with a lower yield of 79% and with a complete lack of diastereoselectivity to afford a 50:50 mixture **of 48** and **49**.

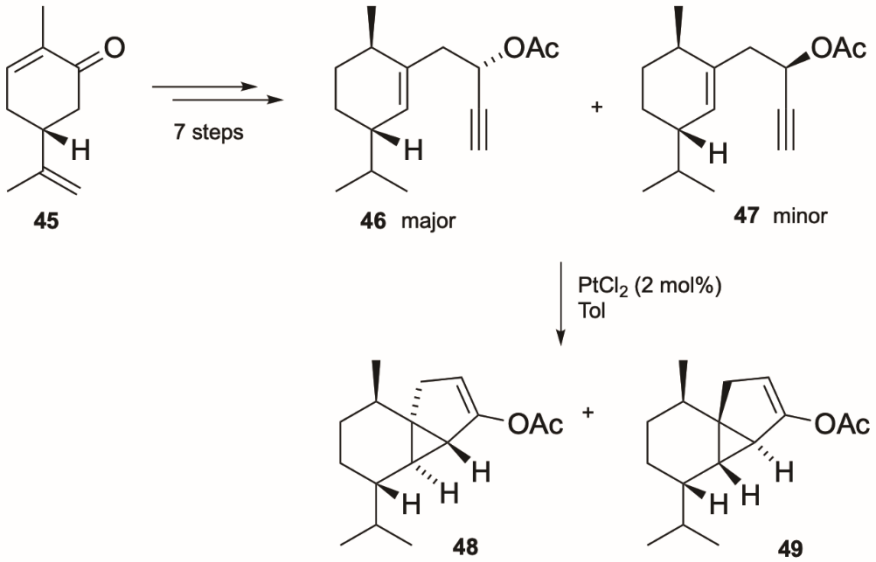

Scheme 9. Key steps in Furstner's synthesis of cubebene.[14]

Mechanistically, the high selectivity with (*S*)-enantiomer **46** and the lack of selectivity with the (*R*)-enantiomer **47** prompt an important query (Scheme 10). The dramatic difference in selectivity

suggests that at least 2 potential mechanisms might be in operation.[14,15] In path 1, the propargyl acetate **50** promotes the formation of platinum carbene **52** through a rearrangement of vinyl acetate **51**. The carbene **52** can then undergo cyclopropanation with the tethered olefin to give the cyclopropane product **53.** In path 2, the tethered olefin undergoes electrophilic attack on the activated alkyne to form an intermediate cation **50a**, followed by ring closure to the cyclopropane **54**. The resultant platinum carbene then promotes the acetate rearrangement through the dioxolane cation **55** and platinum elimination to give the target vinyl acetate **53.** Of the two mechanistic pathways, the high selectivity of the (*S*)-enantiomer **46** suggests it goes through path 2 due to the non-planarised acetate group inducing stereo control. In contrast, the lack of any selectivity for the (*R*)-enantiomer **47** suggests that path 1 could play a role, due to the planarisation of the acetate group. Computational mechanistic studies have shown that path 2 is generally energetically more preferred and that the mechanistic pathway is substrate-dependent.[15]

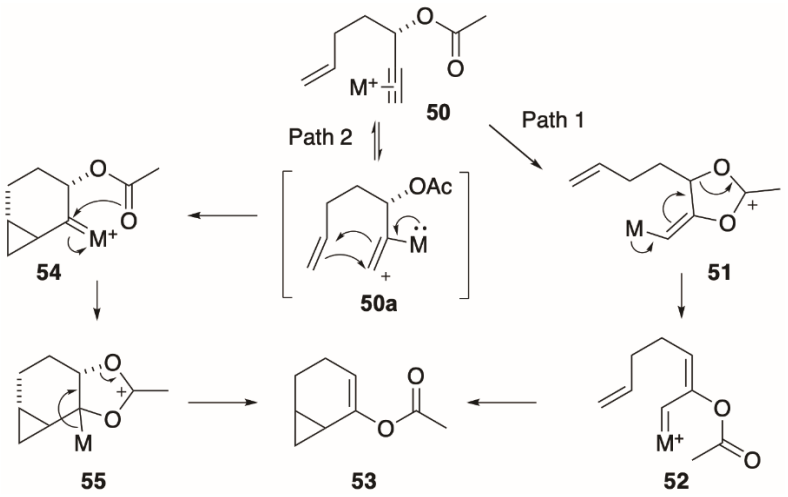

Scheme 10. Possible mechanistic pathways for cyclopropanation using propargyl acetate.

Synthesis of cubebol **3** by Fehr[16,17] has the same key step as in Furstner's[14] route. However, the synthesis of the 1,5-enyne was achieved using tetrahydrocarvone **56,** and a pivalate was used in place of an acetate (Scheme 11). The protected propargylic alcohols **57** and **58** were obtained as an 88:12 mixture, but the two isomers were separated chromatographically. An investigation was conducted into the influence of the catalyst and the stereochemical purity of the 1,5-enyne on the reaction selectivity (Table 1).

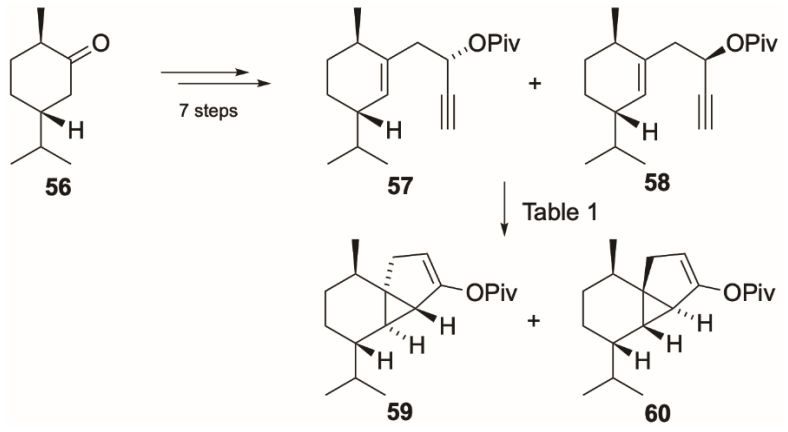

Scheme 11. Acyl promoted metal-catalysed cyclopropanation of 1,5-enyne.[17]

Table 1. Metal-catalysed cyclopropanation of 1,5-enynes **57** and **58**.

Entry	**57:58**	Conditions	**59:60**	Yield [%]
1	9:91	$PtCl_2$ (2 mol%), DCE, 70°C, 9h	60:40	80
2	9:91	$AgSbF_6/AuCl(PPh_3)$ (2 mol%), DCM, RT, 40min	47:53	65
3	70:30	$PtCl_2$ (2 mol%), DCE, 70°C, 9h	86:14	-[a]
4	88:12	$PtCl_2$ (2 mol%), DCE, 70°C, 9h	94:6	81
5	98:2	$PtCl_2$ (2 mol%), DCE, 70°C, 9h	99:1	-[a]
6	98:2	$Cu(CH_3CN)_4BF_4$ (2 mol%), PhMe, 60°C, 9h	99:1	77

[a]Not determined

The use of Pt(II) chloride mirrored the results observed by Furstner[14,] confirming that **57** showed high selectivity and **58** was non-selective (Table 1, entries 1,3-5). $Au(PPh_3)SbF_6$ and $Cu(CH_3CN)_4BF_4$ were tested as alternative catalysts, where the Au(I) provided a lower yield and little selectivity (Table 1, entry 2), whereas the Cu(I) catalyst behaved similarly to Pt(II) but in slightly lower yield (Table 1, entry 6).

A method for the formation of cyclopropanes from 1,5-enynes catalysed by Au(I) complexes was reported by the group of Ji[18,19] (Scheme 12). They employed *P,N*-ligand **67** and 8-methyl quinoline *N*-oxide **68** as an external oxidant. In this work, two examples of a tricyclo[4.4.0.0^{1,5}]decane ring system were reported. The methodology provides a high-yielding access to tricylco[4.4.0.0^{1,5}]decanes. However, diastereoselectivity remained poor. Compounds **62** and **63** were obtained in 92% combined yield as a 37:63 mixture from the TIPS-protected homopropargyl alcohol **61**. Quaternisation of the alcoholic centre, as in **64**, gave rise to compounds **65** and **66** in a 95% yield with no diastereoselectivity. Additionally, the effect of the conformational rigidity of the amine in the ligand was investigated. Steric interaction between the *cis* dimethyl groups in ligand **67** prevents *N*-inversion, making the non-bonded sp^3 orbital of the nitrogen more accessible to cationic gold species.[18]

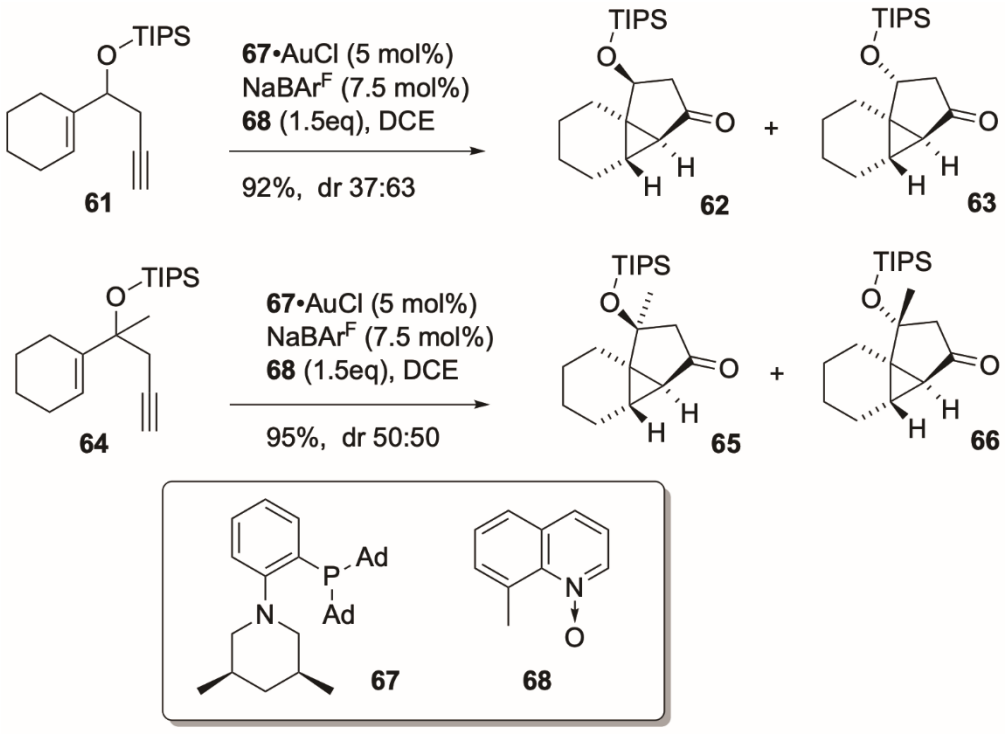

Scheme 12. *N*-oxide promoted Au(I)-catalysed cyclopropanation of 1,5-enyne[18]

2.5. Miscellaneous strategies

Hodgson reported a 7-step total synthesis of cubebol **3** and, by extension, a formal total synthesis of *a*-cubebene **1** and *b*-cubebene **2**.[20] The key step involved a stereospecific lithium amide-induced cyclopropanation of a bishomoallyic epoxide. When either chlorohydrin **69** or epoxide **70** were exposed to LiTMP, there was an efficient transformation to the tricyclo[4.4.0.0^{1,5}]decane nucleus of cubebene **71,** which in another two steps was converted to (–)-cubebol **3** (Scheme 13).

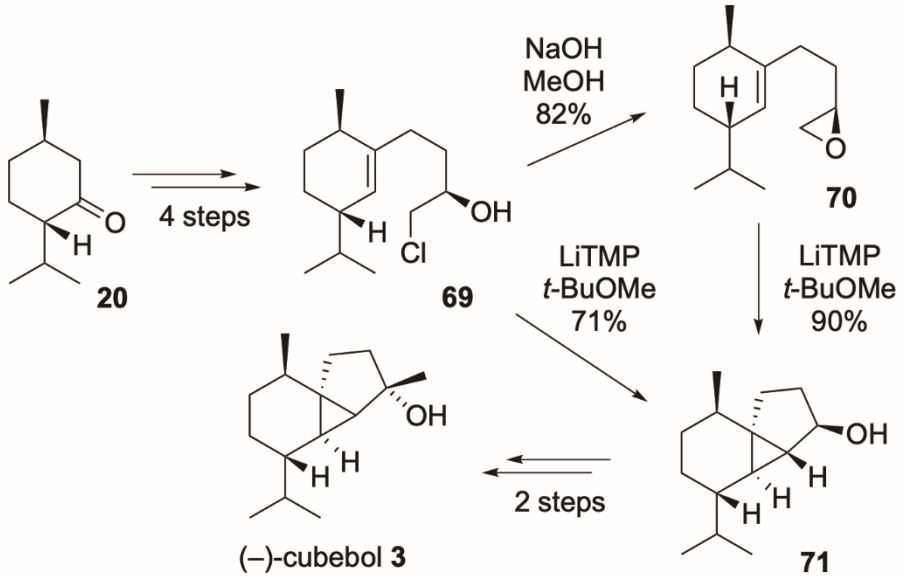

Scheme 13. Key steps in Hodgson's synthesis of cubebol **3**.[20]

The stereoselectivity of this reaction strongly depends on the absolute configuration of the epoxide and the *cis* or *trans* configuration of the alkene. Mechanistically, the lithium amide deprotonates the terminal epoxide **72**, which then forms a chair-like transition state **73** where the epoxide lies equatorially, making the *cis* substituent on the alkene sit axially and the *trans* substituent lies equatorially. With this method, the alcohol always sits *anti* to the cyclopropane ring in **74**. When diastereomerically pure epoxide **72** is used, an efficient chirality transfer in **73** results in a single stereoisomer of the alcoholic bicyclo[3.1.0]hexane ring system (Scheme 14).

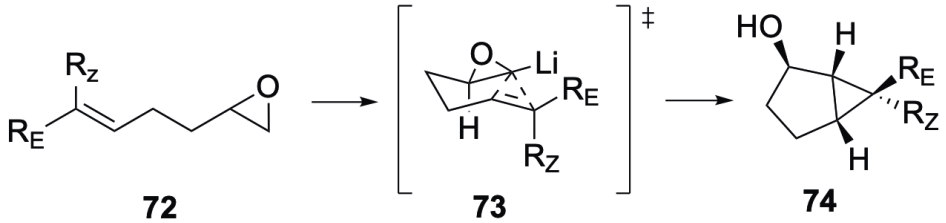

Scheme 14. Stereochemical course of the cyclopropanation of bishomoallylic epoxides.

Derksen[21] reported a method for a photochemical 1,4-sigmatropic rearrangement of the diastereomeric divinyl ketone species **75** and **78**, based on earlier literature precedents.[22] Both of these compounds can be prepared in 5 steps from tetrahydrocarvone **56**. In this photochemical rearrangement, the stereoselectivity is determined by the configuration of the cyano-group in the diastereomers **75** and **78**. Under UV irradiation, **75** was converted to tricyclo[4.4.0.0^{1,5}]decane **76** as well as a tricyclo[4.3.1.0^{2,10}]decane ring system **77**. Notably, **76** features the tricyclic system as found

in cubebene with the *syn* arrangement of the methyl and the cyclopropane**.** Unfortunately, the rearrangement of **75** heavily favours the unwanted tricyclic system **77** with the highest ratio of 18:82 for **76** and **77**, respectively (Table 2). Stereoisomer **78** showed increased preference towards **79** with a 91:9 ratio of **79** and **80** (Table 3). For obtaining cubebene scaffolds **76** and **79,** the best results were observed using UV-C light, 235-280 nm, see Table 2, entries 10-11, and Table 3, entries 8-9.

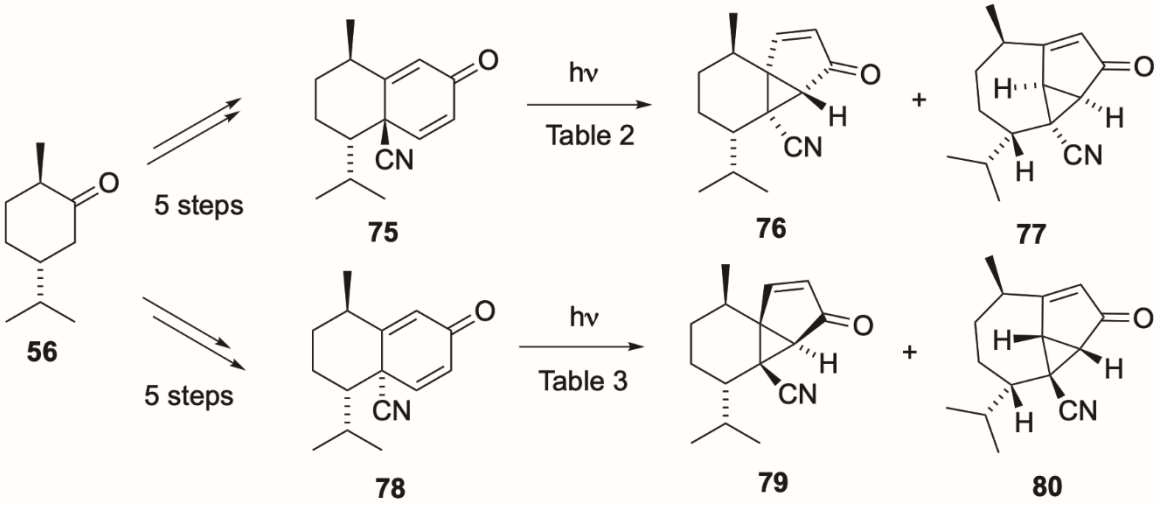

Scheme 15. Photochemical rearrangement for the synthesis of tricyclodecane ring systems.

The computational studies on the mechanism of the photochemical rearrangement revealed that the initial step involves excitation of the a,b-unsaturated ketone **75,** giving the allylic enol diradical **81**, which can then undergo ring closure, forming the cyclopropane diradical **82**, followed by ring cleavage of the cyclopropane, forming the spirocyclic a-cyano enolic diradical **83.** The reaction then terminates through ring closure between the radicals, giving stereospecifically tricyclo[4.4.0.0^{1,5}]decane ring system **76**. The reaction provides complete chirality transfer, but unfortunately, the poor conversion and selectivity for the cubebene nucleus **76** means that it would be an inefficient key step for the total synthesis of cubebene (Scheme 16).

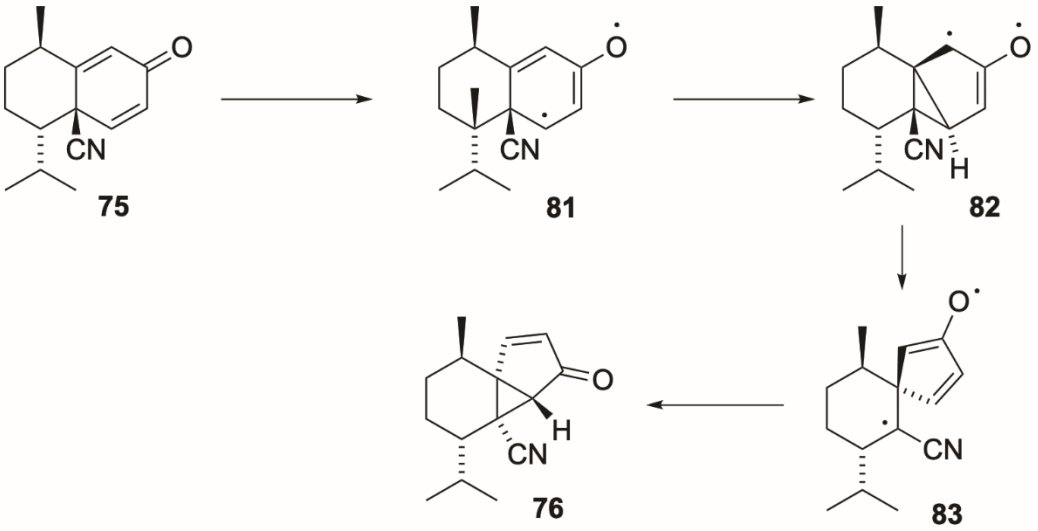

Scheme 16. Proposed mechanistic pathway for the photochemical rearrangement.

Table 2. Photochemical rearrangement of **75**.

Entry	Light	Time (h)	**76:77**
1	Visible	100	0:100
2	UV-A	2	0:100
3	UV-B	2	0:100
4	Visible	20	10:90
5	Visible	44	5:95
6	Visible	80	0:100
7	UV-A	3	0:100
8	UV-A	9	0:100
9	UV-B	2	9:91
10	UV-C	0.8	18:82
11	UV-C	3	18:82

Table 3. Photochemical rearrangement of **78**.

Entry	Light	Time (h)	**79:80**
1	Visible	24	66:34
2	UV-A	0.5	66:34
3	UV-B	2	75:25
4	UV-B	4	75:25
5	Visible	2	80:20
6	UV-A	2	75:25
7	UV-B	2	75:25
8	UV-C	0.7	91:9
9	UV-C	2	91:9

While working on the total synthesis of *b*-copaene **84,** Wenkert[23] discovered a cationic ring contraction of the copaene skeleton leading to the tricyclic cubebene scaffold (Scheme 17).

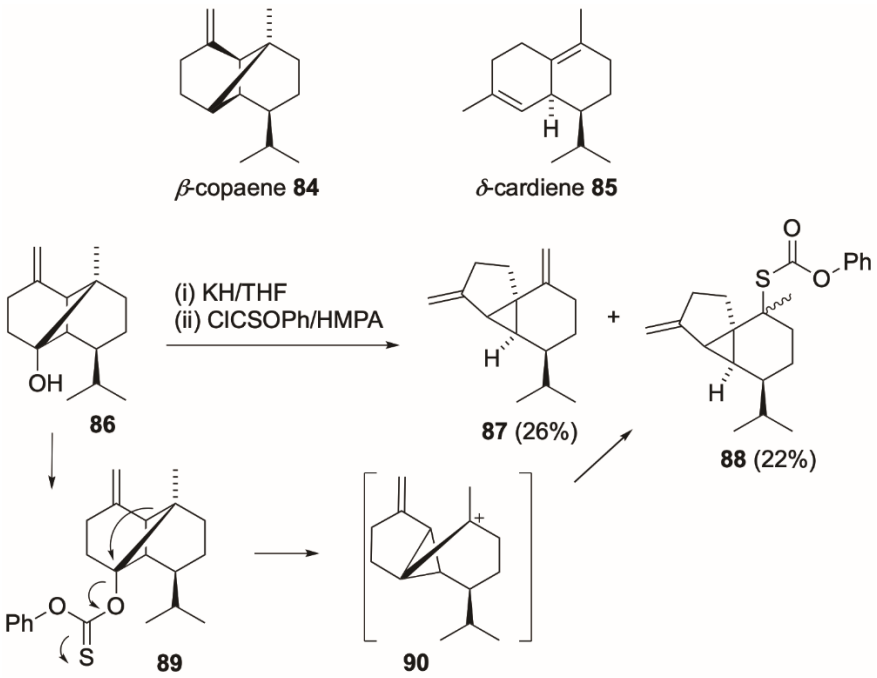

Scheme 17. Ring contraction of copaenol **86**, yielding the 6,3,5-tricyclic ring system.

When alcohol **86** was converted into a leaving group, *O*-phenyl carbonothioate **89**, the cyclobutene underwent spontaneous ring contraction, the resultant cation could then either promote a-proton elimination to **87** or undergo trapping of the residual *O*-phenyl thiocarbonate **88**. An attempt has been made to synthesize *b*-cubebene **2** by desulphurisation of **88** with Raney nickel, but this led to further skeletal rearrangement to *d*-cadiene **85**.

3. Discussion

The synthetic efforts towards cubebene and related sesquiterpenes demonstrate the challenges of constructing compact, highly strained carbocyclic frameworks while maintaining control of stereochemistry. The evolution of synthetic methodologies in this area reflects the existing trends in terpene synthesis, moving from long sequences relying on stoichiometric reagents toward catalytic, mechanistically informed strategies.

Cyclopropanations using diazo compounds, pioneered by De Waal and Yoshikoshi, provided the first practical access to cubebene frameworks and demonstrated the fundamental feasibility of constructing the desired tricyclic core. However, these methods suffer from low efficiency, the need for stoichiometric metal salts, and modest diastereoselectivity. Subsequent modifications using α-diazo-β-ketosulfones improved stereocontrol, taking advantage of steric constraints; however, they remain limited by the substrate scope and the challenges of handling diazo precursors.

Transition-metal-catalysed 1,5-enyne cyclisations represented a conceptual breakthrough, offering catalytic, high-yielding routes with improved stereochemical fidelity. Platinum(II)- and copper(I)-mediated reactions displayed good diastereoselectivity, as exemplified by the work of Fürstner and Fehr, whereas gold(I) catalysis provided complementary reactivity under milder reaction conditions. Nevertheless, the mechanistic dichotomy between carbene-type and electrophilic pathways makes it difficult to predict the stereochemical outcome, and there are only limited enantioselective variants of these processes.

Alternative approaches, such as multistep bicycloannulation cascades, photochemical sigmatropic rearrangements, and cationic ring contractions, further expand the synthetic toolbox but remain context-specific. For example, photochemical transformations, though elegant and mechanistically intriguing, often deliver mixtures of rearranged products with limited synthetic utility. Cationic rearrangements of some terpene scaffolds offer access to the desired tricyclic core, but their lack of selectivity and sensitivity to even minute variation of electronic effects hinder general application.

Overall, even with the advanced methodological diversity, achieving a unified, enantioselective, and scalable synthesis of higher cubebene analogues remains a challenging task. Advances in asymmetric catalysis, photoredox activation, and computationally informed synthetic design are expected to narrow the gap between conceptual innovation and synthetic practicality.

4. Conclusions

The synthesis of cubebene and its analogues continues to attract the attention of researchers as a benchmark for innovative synthetic development in terpene chemistry, serving as a testing ground for new catalytic, stereochemical methodologies, and mechanistic insights. While classical diazo-based intramolecular cyclopropanations pioneered by De Waal and Yoshikoshi laid the foundational strategies, subsequent advances, particularly transition-metal-catalysed enyne cyclisations, have significantly expanded the synthetic toolbox. Each approach provides notable advantages in selectivity, step economy, or mechanistic understanding. However, the total synthesis of higher cubebene analogues (compounds **4**–**8**) remains an open challenge. Future progress will likely depend on integrating bioinspired cascade reactions, modern synthetic methods, and asymmetric catalysis to achieve efficient, stereocontrolled construction of the tricyclo[4.4.0.0^{1,5}]decane framework. These

developments not only promise access to unexplored natural and non-natural cubebene derivatives but also enrich our understanding of the complex natural carbocyclic systems.

References

(1) Ohta, Y.; Sakai, T.; Hirose, T. Sesquiterpene Hydrocarbons from the Oil of Cubeb α-Cubebene and β-Cubebene. *Tetrahedron Lett.* **1966**, *7* (51), 6365–6370. https://doi.org/10.1016/S0040-4039(00)70179-1.

(2) Cao, F.; Shao, C.-L.; Liu, Y.-F.; Zhu, H.-J.; Wang, C.-Y. Cytotoxic Serrulatane-Type Diterpenoids from the Gorgonian Euplexaura Sp. and Their Absolute Configurations by Vibrational Circular Dichroism. *Sci. Rep.* **2017**, *7* (1), 12548. https://doi.org/10.1038/s41598-017-12841-2.

(3) Chen, D. Y. K.; Pouwer, R. H.; Richard, J. A. Recent Advances in the Total Synthesis of Cyclopropane-Containing Natural Products. *Chem. Soc. Rev.* **2012**, *41* (13), 4631–4642. https://doi.org/10.1039/C2CS35067J.

(4) Stathakis, C. I.; Gkizis, P. L.; Zografos, A. L. Metal-Catalyzed Cycloisomerization as a Powerful Tool in the Synthesis of Complex Sesquiterpenoids. *Nat. Prod. Rep.* **2016**, *33* (9), 1093–1117. https://doi.org/10.1039/C6NP00026F.

(5) Könen, P. P.; Wüst, M. Analysis of Sesquiterpene Hydrocarbons in Grape Berry Exocarp (Vitis Vinifera L.) Using in Vivo-Labeling and Comprehensive Two-Dimensional Gas Chromatography–Mass Spectrometry (GC×GC–MS). *Beilstein J. Org. Chem.* **2019**, *15* (1), 1945–1961. https://doi.org/10.3762/BJOC.15.190.

(6) Li, Z.; Howell, K.; Fang, Z.; Zhang, P. Sesquiterpenes in Grapes and Wines: Occurrence, Biosynthesis, Functionality, and Influence of Winemaking Processes. *Compr. Rev. Food Sci. Food. Saf.* **2020**, *19* (1), 247–281. https://doi.org/10.1111/1541-4337.12516.

(7) Piers, E.; Britton, R. W.; de Waal, W. α-Cubebene and β-Cubebene. Synthetic Proof of Gross Structure. *Tetrahedron Lett.* **1969**, *10* (16), 1251–1253. https://doi.org/10.1016/S0040-4039(01)87855-2.

(8) Piers, E.; Britton, R. W.; Waal, W. De. Total Synthesis of (±)-α-Cubebene and (±)-β-Cubebene. *Can. J. Chem.* **1971**, *49* (1), 12–19. https://doi.org/10.1139/v71-003.

(9) Tanaka, A.; Tanaka, R.; Uda, H.; Yoshikoshi, A. Synthesis of Cubebane-Type Sesquiterpenoids and the Stereochemistry of Cubebol. *J. Chem. Soc., Perkin Trans. 1* **1972**, No. 0, 1721–1727. https://doi.org/10.1039/P19720001721.

(10) Hosokawa, S.; Nakanishi, K.; Udagawa, Y.; Maeda, M.; Sato, S.; Nakano, K.; Masuda, T.; Ichikawa, Y. Total Synthesis of Exigurin: The Ugi Reaction in a Hypothetical Biosynthesis of Natural Products. *Org. Biomol. Chem.* **2020**, *18* (4), 687–693. https://doi.org/10.1039/C9OB02249J.

(11) Hagiwara, H.; Abe, F.; Uda, H. Bicycloannulation Leading to the Tricyclo[4.4.0.01,5]Decane Framework and Its Congeners. *J. Chem. Soc., Chem. Commun.* **1991**, No. 16, 1070. https://doi.org/10.1039/c39910001070.

(12) Hagiwara, H. Annulation via Sequential Multifold Michael Reaction. One Aspect of Terpenoid Synthesis. *J. Synth. Org. Chem. Jpn.* **1992**, *50* (8), 713–725. https://doi.org/10.5059/yukigoseikyokaishi.50.713.

(13) Hagiwara, H.; Abe, F.; Uda, H. Bicycloannulation of α-Bromo α,β-Unsaturated Esters; Synthesis of the Tricyclo[4.4.0.0 ^{1,5}]Decane Framework and Its Congeners. *J. Chem. Soc., Perkin Trans. 1* **1993**, No. 21, 2651–2655. https://doi.org/10.1039/P19930002651.

(14) Fürstner, A.; Hannen, P. Platinum- and Gold-Catalyzed Rearrangement Reactions of Propargyl Acetates: Total Syntheses of (-)-α-Cubebene, (-)-Cubebol, Sesquicarene and Related Terpenes. *Chem. Eur. J.* **2006**, *12* (11), 3006–3019. https://doi.org/10.1002/CHEM.200501299.
(15) Soriano, E.; Ballesteros, P.; Marco-Contelles, J. Theoretical Investigation on the Mechanisms of the PtCl2-Mediated Cycloisomerization of Polyfunctionalized 1,6-Enynes. 2. Propargylic Carboxylates. *Organometallics* **2005**, *24* (13), 3182–3191. https://doi.org/10.1021/OM050134R.
(16) Fehr, C.; Winter, B.; Magpantay, I. Synthesis of (-)-Cubebol by Face-Selective Platinum-, Gold-, or Coppercatalyzed Cycloisomerization: Evidence of Chirality Transfer and Mechanistic Insights. *Chem. Eur. J.* **2009**, *15* (38), 9773–9784. https://doi.org/10.1002/CHEM.200901292.
(17) Fehr, C.; Galindo, J. Synthesis of (-)-Cubebol by Face-Selective Platinum-, Gold-, or Copper-Catalyzed Cycloisomerization: Evidence for Chirality Transfer. *Angew. Chem. Int. Ed.* **2006**, *45* (18), 2901–2904. https://doi.org/10.1002/ANIE.200504543.
(18) Ji, K.; Zhang, L. A Non-Diazo Strategy to Cyclopropanation via Oxidatively Generated Gold Carbene: The Benefit of a Conformationally Rigid P,N-Bidentate Ligand. *Org. Chem. Front.* **2014**, *1* (1), 34–38. https://doi.org/10.1039/C3QO00080J.
(19) Ji, K.; Zheng, Z.; Wang, Z.; Zhang, L. Enantioselective Oxidative Gold Catalysis Enabled by a Designed Chiral P,N-Bidentate Ligand. *Angew. Chem. Int. Ed.* **2015**, *54* (4), 1245–1249. https://doi.org/10.1002/ANIE.201409300.
(20) Hodgson, D. M.; Salik, S.; Fox, D. J. Stereocontrolled Syntheses of (-)-Cubebol and (-)-10-Epicubebol Involving Intramolecular Cyclopropanation of a-Lithiated Epoxides. *J. Org. Chem.* **2010**, *75* (7), 2157–2168. https://doi.org/10.1021/JO9022974.
(21) Gorobets, E.; Wong, N. E.; Paton, R. S.; Derksen, D. J. Divergent Photocyclization/1,4-Sigmatropic Rearrangements for the Synthesis of Sesquiterpenoid Derivatives. *Org. Lett*. **2017**, *19* (3), 484–487. https://doi.org/10.1021/acs.orglett.6b03635.
(22) Greene, A. E.; Edgar, M. T. Synthesis of Oxoisodehydroleucodin: A Novel Guaianolide from Montanoa Imbricata. *J. Org. Chem.* **1989**, *54* (6), 1468–1470. https://doi.org/10.1021/jo00267a049.
(23) Wenkert, E.; Bookser, B. C.; Arrhenius, T. S. Total Syntheses of (±)-a- and (±)-b-Copaene and Formal Total Syntheses of (±)-Sativene, (±)-Cis-Sativenediol, and (±)-Helminthosporal. *J. Am. Chem. Soc.* **2002**, *114* (2), 644–654. https://doi.org/10.1021/JA00028A034.

Author Contributions: Writing – original draft and Writing – review and editing - all authors.
Funding: This study was funded by Loughborough University.
Conflicts of Interest: All authors declare no conflict of interest.

Reports of NAS RA
ՀՀ ԳԱԱ Զեկույցներ
NATIONAL ACADEMY OF SCIENCES OF THE REPUBLIC OF ARMENIA
ՀԱՅԱՍՏԱՆԻ ՀԱՆՐԱՊԵՏՈՒԹՅԱՆ ԳԻՏՈՒԹՅՈՒՆՆԵՐԻ ԱԶԳԱՅԻՆ ԱԿԱԴԵՄԻԱ

2026 **Volume 126** **Issue 1** **Article No. 5**

Category: Chemistry
Type of Paper: Original Research Article
Received: October 31, 2025, **Revised:** February 2, 2026, **Accepted:** February 3, 2026
Published: March 2, 2026

DOI: 10.54503/0321-1339-2026.126.1-5

Study of Various Aspects of the Mechanism of Cα-Alkylation of α-Amino Acids under Phase-Transfer Salen Catalysis Conditions

Anna S. Tovmasyan[1,*], Anna F. Mkrtchyan[1,2], Ashot S. Saghyan[1,2]

[1]Scientific and Production Center "Armbiotechnology" NAS RA, 14 Gyurjyan Str., Yerevan 0056, Armenia
[2]Yerevan State University, 1 Alex Manoogian Str., Yerevan 0025, Armenia

[*]Correspondence: anna.tovmasyan1@edu.isec.am

Abstract

The stereodifferentiating ability of salen complexes of Cu(II), Ni(II), and Zn(II) ions in Cα-alkylation reactions of amino acids as phase-transfer catalysts (PTC) has been investigated. We found that substituents in the 3-position of the aromatic ring of the salicylidene moiety of the complexes have a particularly strong effect on catalytic activity. The highest efficiency was observed for the 3-methoxy-substituted salen complex of the Zn (II) — ee > 90%. DFT calculations showed that the stereodifferentiating ability of the catalyst depends on the ratio of propeller-like and cross-like conformational structures of dimeric binuclear salen complex molecules in the alkylation transition state. It was demonstrated that propeller-like conformational isomers, which predominate in the dimeric binuclear structure of 3-allyl-substituted salen complexes, correspond to the catalytically inactive form and inhibit asymmetric catalysis. In contrast, cross-like isomers, which dominate in the dimeric binuclear structure of 3-methoxy-substituted salen complexes, ensure high stereodifferentiating activity and promote asymmetric catalysis. The DFT calculation data correlates clearly with the experimental results.

Keywords: phase transfer catalysis, asymmetric catalysis, salen complexes, alkylation, amino acids

1. Introduction

α-Amino acids are an important class of physiologically and pharmacologically active compounds. The demand for amino acids is steadily increasing due to their wide use in biotechnology, medicine, pharmaceutical and food industries, and other fields of science and technology, among which non-proteinogenic α-amino acids occupy a special place [1, 2]. The synthesis of non-proteinogenic α-amino acids is also in high demand due to their wide application in synthetic chemistry and chemistry of materials [3–9]. The development of efficient and straightforward methods for the synthesis of enantiomerically enriched non-proteinogenic α-amino acids is an extremely important task, since they are successfully used as irreversible enzyme inhibitors in numerous biomedical applications [10–12]. Among non-proteinogenic amino acids, various α, α-disubstituted amino acids — both in isolated form and as part of peptides — exhibit potential pharmacological activity [13–17]. One of the simple methods for synthesizing non-physiological α-amino acids is α-C(sp^3)–H alkylation of α-amino acids or their derivatives. However, only a few examples have been described, including the works of Zhaon [18], Yamamoto [19], and Yazaki and Ohshima [20, 21], which require the use of catalysts and

additives. On the other hand, numerous methods for the catalytic asymmetric synthesis of unnatural amino acids have been described, including hydrogenation of olefins and imines [22, 23], electrophilic amination of enolates [24, 25], electrophilic alkylation of glycine derivatives [26], and nucleophilic addition to α-imino esters [27]. In practice, chiral phase-transfer catalysts such as derivatives of cinchonine, TADDOL, NOBIN, and the Maruoka and Lygo catalysts have been successfully applied for the preparation of enantiomerically enriched non-proteinogenic amino acids [28]. Chiral salen complexes of transition metal ions Cu(II) and Ni(II), have also shown relatively high catalytic activity in phase-transfer asymmetric alkylation reactions of amino acid enolates [29].

2. Results and Discussion

We investigated the influence of substituents on the salicylaldehyde moiety of the complexes and the benzylidene amino acid substrates on the stereodifferentiating ability of the catalyst, with the aim of developing the most efficient catalytic system for the asymmetric synthesis of α-amino acids. To this end, numerous salen complexes of Cu(II), Ni(II) and Zn(II) ions, derived from the Schiff Base of chiral cyclohexyldiamine and substituted salicylaldehides, containing various substituents in different positions of the aromatic ring of the salicylaldehyde moiety were synthesized: methyl, allyl, *tert*-butyl, methoxy, ethoxy groups (Figure 1) [30]. As an analog of the O'Donnell substrate, the Schiff bases of the *iso*-propyl ester of aminoacids and substituted benzaldehydes were synthesized.

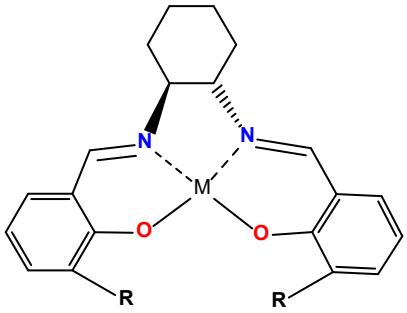

M=Cu, R=H (**1**)
M=Cu, R=OCH3(**2**)
M=Cu, R=Allyl(**3**)
M=Zn, R=H(**4**)
M=Zn, R=Allyl(**5**)
M=Zn, R=OCH3(**6**)
M=Ni, R=H(**7**)
M=Ni, R=Allyl(**8**)
M=Ni, R=OCH3(**9**)

Figure 1. Schematic structure of the complexes explored in this work.

To the best of our knowledge, most of these compounds were synthesized for the first time, in particular, all zinc salen complexes, fluorine-containing substrates and others. As a model reaction for evaluating the catalytic ability of the complexes, the alkylation of unsubstituted alanine substrate with benzyl bromide was chosen (Scheme 1).

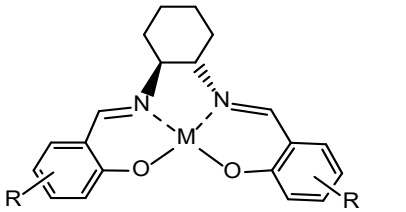

M= Cu(II), Ni(II), Zn(II)

R=Me, t-Bu, Allyl, MeO, EtO

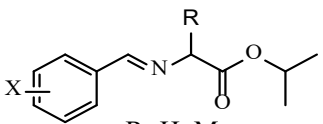

R=H, Me

X = H, Cl, F, Br

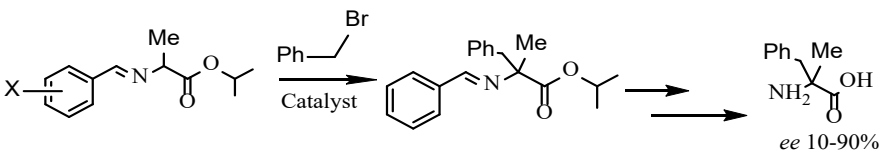

ee 10-90%

Scheme 1. Asymmetric alkylation of amino acid enolates under PTC with benzyl bromide.

The obtained results indicated that the synthesized complexes exhibit high catalytic activity, and for some complexes the enantiomeric excess of products reaches 90%. However, it was evident that the substituents in position 3 of the salicylaldehyde moiety have a particularly strong influence on the catalytic activity of salen complexes. Therefore, in subsequent experiments, we focused on salen complexes containing allylic and methoxy groups at position 3 of the salicylaldehyde moiety. For comparison, unsubstituted salen complexes of the same ions were also investigated [31] (Figure 2).

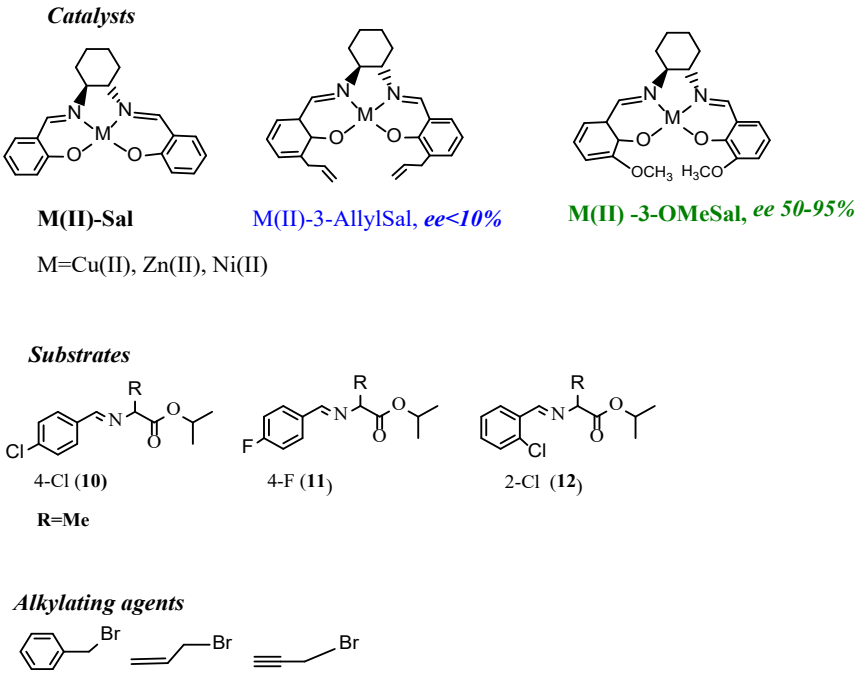

Figure 2. The structures of the salen complexes, amino acid substrates and alkylating agents.

As amino acid substrates, *o*-chlorine, *p*-chlorine and *p*-fluorine-substituted benzylidene derivatives were investigated, as an alkylating agent, benzyl bromide, allyl bromide and propargyl bromide were used. The results in the case of allylation reaction of alanine substrates are summarized in the Table 1.

Table 1. Conversion rates (c.r.) and enantiomeric excesses (ee) for the Cα-alkylation of substrates 10–12 with allyl bromide using PTC.

Catalyst	Substrate **10** *c.r. (%)**	*ee (%)***	Substrate **11** *c.r. (%)*	*ee (%)*	Substrate **12** *c.r. (%)*	*ee (%)*
1	80	74	55	32	85	70
2	10	<5	16	10	10	<5
3	**90**	**87**	**60**	**34**	**94**	**88**
4	10	<5	11	<5	10	<5
5	**15**	**10**	**20**	**12**	**10**	**<5**
6	95	90	75	54	95	93
7	45	56	34	22	64	58
8	**10**	**0**	**10**	**<5**	**10**	**0**
9	50	58	25	16	75	66

**- Conversion rates (c.r.) were determined by NMR spectroscopy*
***- Enantiomeric excesses (ee) were determined by chiral HPLC analysis of isolated products.*
The reactions were carried out using allyl bromide as the alkylating agent. Values reported as '<5' indicate enantiomeric excess below the reliable detection limit.

The obtained data showed that all complexes containing an allyl group at the 3-position of salicylaldehyde moiety in all alkylation reactions provide low stereoselectivity, not more than the 10% enantiomeric excess of the products, regardless of the nature of the alkylating agent and substrate. The opposite picture is observed in the case of salen complexes, containing a methoxy group at position 3 of the salicylaldehyde fragment. Practically in all alkylation reactions these complexes showed high stereo differentiation ability, regardless of the nature of the substrate and the alkylating agent. The most effective was the 3-methoxy-substituted zinc ion complex, which provides on average 90% enantiomeric excess of alkylated products.

The observed trends are summarized in the allylation reactions are presented in the Figure 3. Notably in the series of unsubstituted salen complexes, the catalytic activity of metal ions decreases in the following order: copper complexes are the most active ones, followed by nickel and then zinc complexes. In addition, transitioning from unsubstituted salen complexes to 3-allyl-substituted complexes leads to a significant inhibition of the catalytic activity.

In contrast, the transition from unsubstituted complexes to 3-methoxy-substituted complexes leads to increase of the catalytic activity. In series of these complexes the catalytic activity of metal ions decreases in the following order: zinc complexes are the most active – *ee 94%*, followed by copper complexes – *ee 87%* and then nickel complexes – *ee 58%.* These results indicate that strong increase in catalytic activity is observed in the case of zinc ion complexes.

In the series of substrates, efficiency decreases in the following order: ortho-chlorine, then para-chlorine and para-fluorine-substituted substrates.

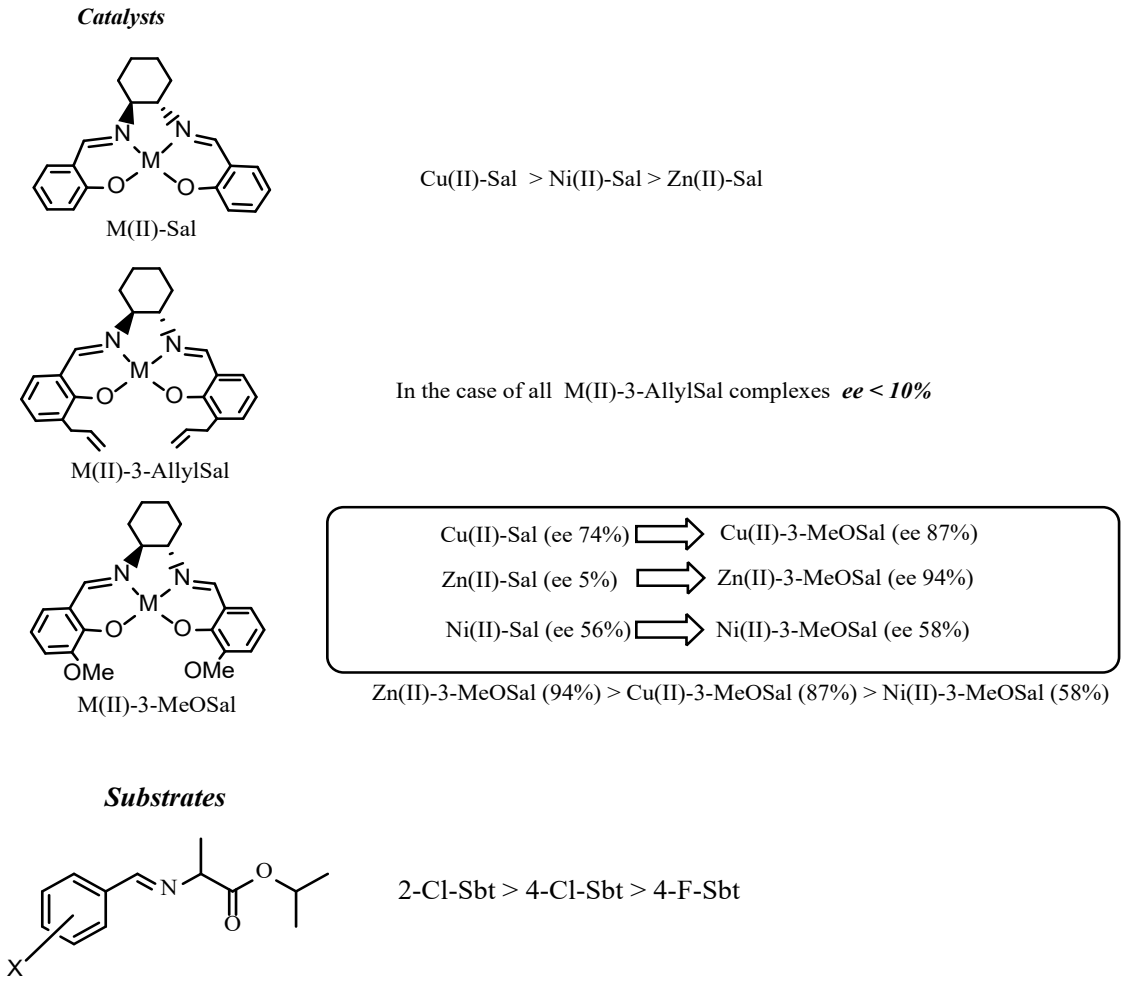

Figure 3. The identified patterns observed in the allylation reactions.

Summarizing the results, we can state that the introduction of an allyl group into position 3 of the salicylaldehyde moiety inhibits the catalytic activity of the complexes, whereas the introduction of a methoxy group at the same position, on the contrary, stimulates asymmetric catalysis.

An explanation for this phenomenon can be found based on the hypothetical model of the alkylation reaction mechanism proposed by Y.N. Belokon and M. North. [32, 33] (Figure 4).

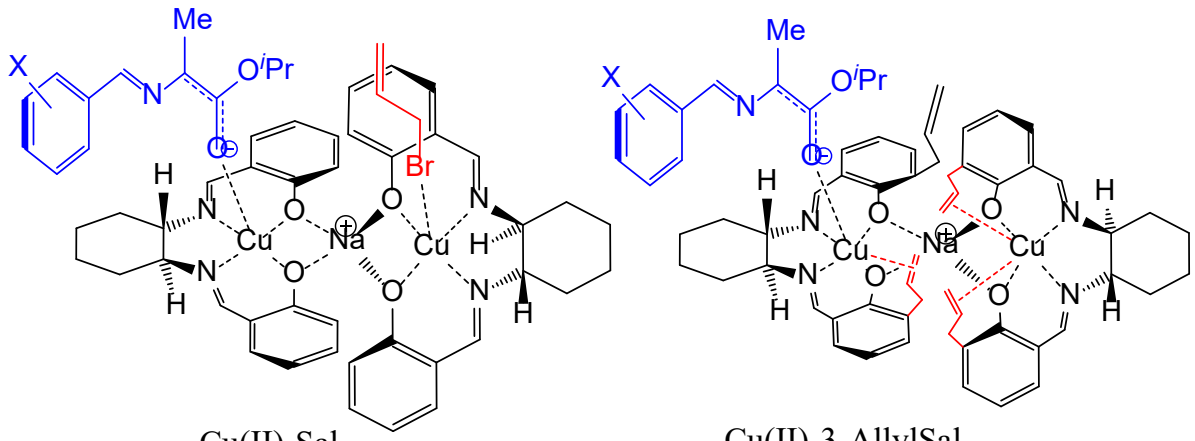

Figure 4. The proposed structure of the dimeric binuclear complex-catalyst in the transition state of alkylation: **a)** unsubstituted salicylidene complex; **b)** 3-allylsalicylidene complex.

According to this mechanism, in the transition state of alkylation, the catalyst takes part in the form of a dimeric binuclear derivative, which is formed due to additional coordination of oxygen atoms of the salen part of the complexes with the sodium ion. In the formed dimeric structure, both transition metal ions are coordinated to the ionized substrate and the alkylating agent. Their interaction occurs on a single coordination plane of the dimeric complex (Figure 4). This represents an active catalytic state.

To evaluate the experimental data, a conformational analysis of binuclear dimeric molecules formed from mononuclear salen complexes in the transition state of alkylation was performed using DFT calculations. For this purpose, changes in Gibbs free energy and Hirschfeld charges concentrated on the transition metal ions were determined (see Table 2), as well as the distance between the central transition metal ions during the dimerization of the complexes.

Table 2. Changes in electronic energy (ΔE) and Gibbs free energy (ΔG) during the formation of a binuclear structure from two mononuclear molecules.

	Zn(II)-H	**Zn(II)-OMe**	**Zn(II)-Allyl**	**Cu(II)-H**	**Cu(II)-OMe**	**Cu(II)-Allyl**
Δ***E***	-129.66	-182.24	-178.47	35.82	-14.38	3.44
Δ***G***	-56.55	-103.31	-94.94	102.05	69.02	87.86

DFT calculations showed that the Gibbs free energy of unsubstituted complexes of Cu(II), Ni(II), and Zn(II) ions is significantly higher than that of their 3-allyl-substituted analogs.

To evaluate the contribution of allyl fragment coordination to the transition metal ion, a conformational analysis of the resulting binuclear complex was performed [34].

Two dynamically stable conformers were identified: in one of them three out of four allyl fragments are coordinated to the transition metal ions, while in the other, only one out of four possible allyl fragments is coordinated (Figure 4b). This indicates that in solution, the conformation with coordinated allyl fragments predominates significantly, thereby hindering further reaction progress, which is supported by experimental data on reagent conversion.

The chemical nature of such allyl fragment coordination is also confirmed by the calculated Hirshfeld charges concentrated on the transition metal ions [35].

For example, in zinc complexes the charge increases from +0.40 to +0.48 upon dissociation of the allyl fragment, and in copper complexes from +0.20 to +0.24. Based on previously published studies, asymmetric alkylation of enolates catalyzed by a salen complex proceeds via an asynchronous S_N2-type reaction with the primary role of the catalyst being to enhance the nucleophilicity of the enolate [36].

This explains why the enantiomeric excess decreases when moving from Cu(II) to Zn(II) complexes, as the overall charge of the metal ion is reduced.

However, within the series of salicylidene Zn(II) complexes, the following phenomenon is observed. In case of the unsubstituted and 3-allyl-substituted Zn(II) complexes, the hypothesis holds true, as the asymmetric yield is much lower than that of other complexes.

But in the case of the 3-methoxy-substituted Zn(II) complex, the enantiomeric yield is high and exceeds that of all other complexes. Based on some observations from the work of Kostakis, we propose that the introduction of a methoxy group at the 3-position of the aromatic ring of the salicylaldehyde fragment in the metal complex enhances the rigidity of the intramolecular structure of the bimetallic derivative due to additional coordination with the sodium ion, thereby promoting asymmetric induction [37] (Figure 5).

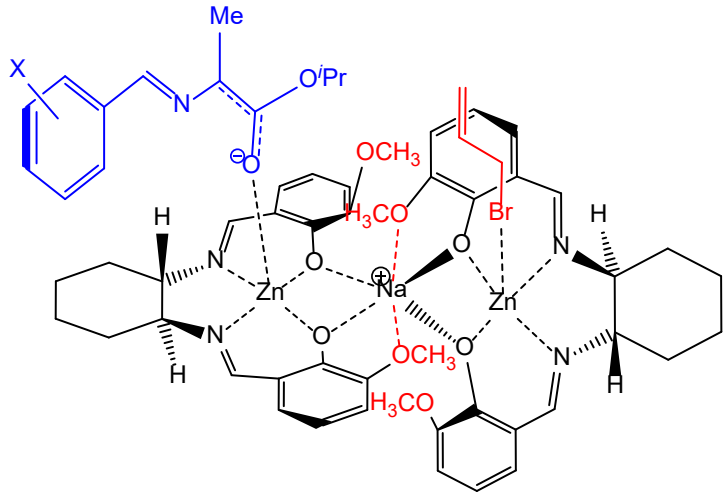

Figure 5. Possible intramolecular stabilization of the dimeric structure of the 3-methoxy-substituted Zn(II) salen complex in the transition state of alkylation.

Based on the analysis of DFT calculation data, it might be concluded that during the formation of dimeric complexes from monomeric salen complexes, the dimeric molecules are in the form of two conformational isomeric structures, Propeller-like structure and Cross-like structure (Figure 6).

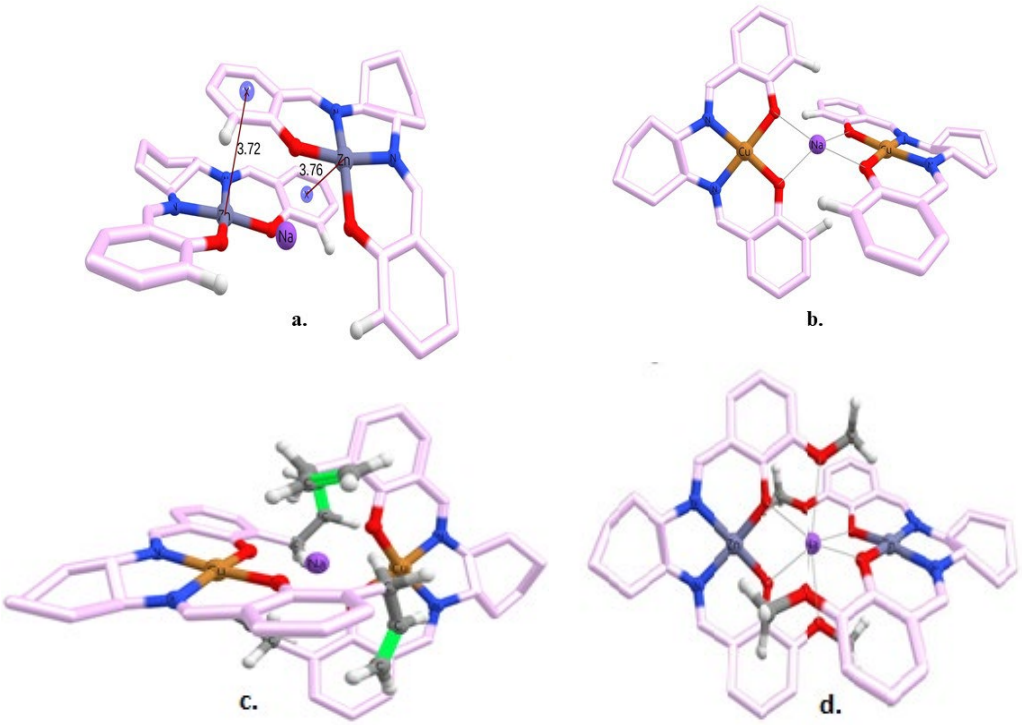

Figure 6. DFT optimized structures of binuclear complexes: **a.** propeller-like structure of unsubstituted Zn(II) complex; **b.** cross-like structure of unsubstituted Cu(II) complex; **c.** propeller-like structure of 3-allylsubstituted Cu(II) complex; **d.** cross-like structure of 3-methoxysubstituted Zn(II) complex.

In the case of the Propeller-like structure, a relatively small change in the Gibbs free energy during dimerization and a relatively large distance between the metal ions are fixed. Such data indicate a low catalytic ability of these salen complexes. In contrast, in the case of the Cross-like structure, the difference in Gibbs free energy between the dimeric and monomeric molecules is relatively large, and the distance between the metal ions is comparatively low. This arrangement of groups in the dimeric structure indicates high catalytic activity of salen complexes.

DFT calculations have shown that in the dimeric structure of 3-allyl-substituted salen complex three out of four molecules have Propeller-like structure. In the dimeric structure of 3-methoxy-substituted salen complex of Zn(II) ion, all particles have Cross-like structure. Cross-like structure was also found in the dimeric structure of the unsubstituted salen complex of Cu(II) ion, but the unsubstituted salen complex of Zn(II) ion predominantly contains Propeller-like structures. Both Propeller-like and Cross-like structural isomers were found in the dimeric structure of other salen complexes, and depending on their ratio, these complexes can be active or passive catalysts.

Thus, the analysis of the DFT-calculation data indicates that Cross-like conformational structures of dimeric salen complexes promote enantioselective catalysis, while Propeller-like structures, on the contrary, inhibit the catalytic ability of the complexes. These data clearly correlate with the experimental data.

Summarizing the obtained data on salen catalysis, it might be stated that indeed in the transition state of alkylation the complex-catalyst takes part in the form of an ionically bound dimeric molecule. Based on these arguments, covalently bound dimeric binuclear salen Cu(II) complexes were synthesized and tested in reaction of alkylation of unsubstituted alanine substrate with benzylbromide, as phase transfer catalyst (*ee*>80%) [31] (Figure 7).

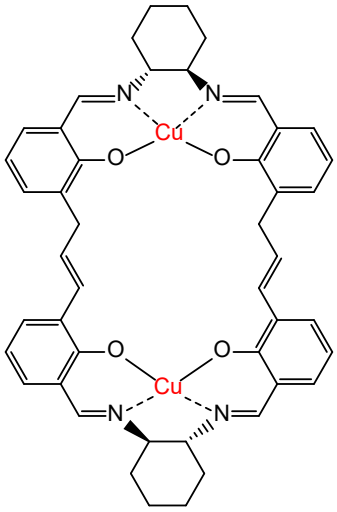

Figure 7. The structure of covalently bound dimeric binuclear salen complexs of Cu(II) ion.

At present, the most promising synthesized salen complexes of Cu(II) and Zn(II) ions are being studied in the alkylation reaction of valine substrates - Schiff bases of isopropyl ester of D,L-valine and substituted benzaldehydes. Importantly, that all previous attempts to alkylate the valine moiety using both stoichiometric and catalytic methods, including phase-transfer salen catalysis, have been unsuccessful [29]. The newly synthesized, the most promising salen complex catalysts are also being investigated in Michael nucleophilic addition reactions to the C=C bond of dehydroalanine analog of O'Donnell's substrate. Research on the synthesis and modification of salen complexes and amino acid substrates, as well as the optimization of phase-transfer catalysis methods is ongoing.

3. Conclusions

The stereodifferentiating ability of salen complexes of Cu(II), Ni(II) and Zn(II) ions, derived from Schiff bases of chiral 1,2-cyclohexyldiamine and substituted salicylaldehydes (PTC), was studied in Cα-alkylation reactions of amino acid substrates — specifically, Schiff bases of the *iso*-propyl ester of D,L-alanine and substituted benzaldehydes.

The chosen alkylating agents were MeI, BnBr, AllylBr and PropargylBr. We found that substituents at the 3-position of the aromatic ring in the salicylidene fragment of the complexes have a particularly strong influence on the stereodifferentiating ability of the catalyst. These findings contribute to a deeper understanding of structure–activity relationships in salen-mediated asymmetric catalysis.

Specifically, it was shown that the allyl substituent strongly inhibits catalytic activity, whereas the methoxy group significantly enhances it. The most efficient catalyst was identified as the 3-methoxy-substituted Zn(II) salen complex, achieving *ee*>90%. DFT calculations demonstrated that the stereodifferentiating ability of the catalyst depends on the ratio of Propeller-like and Cross-like conformational isomers in the dimeric binuclear structure of the salen complex-catalysts in the transition state of the alkylation reaction.

In the dimeric binuclear structure of 3-allyl-substituted salen complexes, the Propeller-like conformational isomers dominate (3/4), which, according to DFT calculations, correspond to a catalytically less active form. In contrast, the dimeric binuclear structures of 3-methoxy-substituted salen complexes that contain only Cross-like conformational isomers according to DFT calculation are catalytically active forms. Depending on the ratio of Propeller-like and Cross-like conformational isomers of the dimeric binuclear structures, a salen complex may act as an active or inactive phase-transfer catalyst. The DFT calculation results correlate clearly with the experimental data. Analysis of the obtained data confirms that the salen complex catalyst participates in the transition state of the

alkylation reaction in the form of ionically bound dimeric binuclear molecules, which served as a basis for the synthesis of covalently linked dimeric binuclear salen complexes with a more rigid intramolecular structure.

4. Experimental and note

4.1. Materials

All reagents were obtained from commercial sources and used without further purification. Thin-layer chromatography (TLC) was carried out on aluminum foil backed sheets precoated with 0.2 mm Kielselgel 60 F254 (Merck, Darmstadt, Germany). The spots were visualized by UV irradiation (λ=254 nm). Column chromatography was performed on Fluka silica gel 60 (0.063–0.200 mm, 70–320 mesh) on a glass column.

4.2. Instrumentation

Melting points (mp) were determined by digital melting point instrument Stuart SMP30 Melting Point (Bibby Scientific Limited, Staffordshire England, UK). NMR spectra were recorded in deuterated solvents using Varian Mercury Vx 300 MHz (USA, Palo-Alto) and BRUKER AVANCE NEO 400 in the case of the 15 compound. Chemical shifts (δ) are reported in parts per million (ppm) relative to tetramethyl silane. Signals were referenced to the residual solvent peak 7.26 (CDCl3), 3.31 (CD3OD), 4.79 (D2O), 2.50 ((CD3)2SO) for 1H and 77.10 (CDCl3), 49.15 (CD3OD), 39.52 ((CD3)2SO) for 13C NMR spectra. The 13C NMR spectra were measured with proton decoupling. Coupling constants are reported in Hertz (Hz). Abbreviations for splitting patterns are as follows: s, singlet; d, doublet; t, triplet; q, quartet; qt, quintet; sext, sextet; hept, heptet; m, multiplet; br., broad. The optical rotation was measured on a Perkin Elmer-341 polarimeter (Waltham, Massachusetts, USA). Elemental analysis was performed by “Euro EA3000” elemental analyzer (Eurovector, Pavia, Italy). For the cation exchange a Dowex-50 (H+ form) column was used. The chromatographic system used to determine the enantiomeric purity of the amino acids was a Waters Alliance 2695e Separation Module HPLC system equipped with PDA detector (Waters Corporation, Milford, Massachusetts, USA). The separation was accomplished in isocratic mode on a Nautilus-E 5μ” 4.0 × 250 mm column (BioChimMac ST Company, Moscow, Russia) at 30 ◦C. The mobile phase consisted of methanol and monosodium phosphate buffer (25 mmol/L). The compounds enantiomeric yield was proved by chiral HPLC analysis of the isolated amino acids. The RAMAN analysis was done by Senterra II Raman Microscope (Bruker, Germany). The IR analysis was done by IR Tracer-100, equipped with GladiATR 10, Shimadzu corporation, Japan and NICOLET AVATAR 330 FT-IR. The asymmetric yield is calculated as the value of three measurements.

4.3. Theoretical calculation methodology

All theoretical calculations were performed in the framework of density functional theory (DFT) using the hybrid functional B3LYP [38] in the ORCA 5.0.3 program [39]. The effect of the solvent was designed using the dielectric polarizable continuum model CPCM [40] with the dielectric constant corresponding to CH2Cl2 solvent, as implemented in ORCA 5.0.3. The optimized geometries were obtained using the def2-TZVP basis set of the Alrich’s def2 family [41] with the def2/J auxiliary set. To calculate the vibrational energy of the resulting def2-TZVP geometries, the basis was retained only for the atoms included in the core of the transition metal complex, i.e. for *Cu/Zn, O, N, Na*, and for the rest of the hydrocarbon core the lighter def2-SVP was used. The dispersion correction to the electronic energy D3BJ was also taken into account according to Grimme, et al. [42]. Computations were performed on the NVIDIA DGX A100 cluster which was acquired by the RA MES State Committee of Science grant project N◦10–3/22Eq-10.

The synthesis of (1*S*,2*S*)-diaminocyclohexane was performed following a previously reported method [43]. The synthesis of salen complexes of Cu(II), Ni(II) and Zn(II) ions, as well as amino acid substrates, was carried out according to previously developed methods [29, 32–33].

References

(1) Izumi, Y.; Chibata, I. Production and Utilization of Amino Acids. *Angew. Chem., Int. Ed.* **1978**, *17*, 176–183. https://doi.org/10.1002/anie.197801761.

(2) Saghyan, A.; Langer, P. Asymmetric Synthesis of Non-Proteinogenic Amino Acids. Wiley-VCH, **2016,** 359pp. https://doi.org/10.1002/9783527804498.

(3) Fik-Jaskółka, M. A.; Mkrtchyan, A. F.; Saghyan, A. S.; et al. Spectroscopic and SEM evidences for G4-DNA binding by a synthetic alkyne-containing amino acid with anticancer activity. *Spectrochim. Acta, Part A* **2020**, *229*, 117884. https://doi.org/10.1016/j.saa.2019.117884.

(4) Palumbo, R.; Simonyan, H.; Roviello, G. N. Advances in Amino Acid-Based Chemistry. *Pharmaceuticals* **2023**, *16*, 1490. https://doi.org/10.3390/ph16101490.

(5) Scognamiglio, P. L.; Riccardi, C.; Palumbo, R.; Gale, T. F.; Musumeci, D.; Roviello, G. N. Self-assembly of thyminyl l-tryptophanamide (TrpT) building blocks for the potential development of drug delivery nanosystems. *J. Nanostruct. Chem.* **2024**, *14*. https://doi.org/10.1007/s40097-023-00523-7.

(6) Hickey, J. L.; Sindhikara, D.; Zultanski, S. L.; Schultz, D. M. Beyond 20 in the 21st Century: Prospects and Challenges of Non-Canonical Amino Acids in Peptide Drug Discovery. *ACS Med. Chem. Lett.* **2023**, *14*, 557–565. https://doi.org/10.1021/acsmedchemlett.3c00037.

(7) Yasser, N.; Mazrou, Y. S. A.; El-Gammal, N. A.; et al. Non-proteinogenic amino acids mitigate oxidative stress and enhance the resistance of common bean plants against *Sclerotinia sclerotiorum*. *Front. Plant Sci.* **2024**, *15*, 1385785. https://doi.org/10.3389/fpls.2024.1385785.

(8) Oeller, M.; Ryan, B. H. L.; et al. Sequence-based prediction of the intrinsic solubility of peptides containing non-natural amino acids. *Nat. Commun.* **2023**, *14*. https://doi.org/10.1038/s41467-023-42940-w.

(9) Simonyan, H.; Palumbo, R.; Petrosyan, S.; et al. BSA Binding and Aggregate Formation of a Synthetic Amino Acid with Potential for Promoting Fibroblast Proliferation: An In Silico, CD Spectroscopic, DLS, and Cellular Study. *Biomolecules* **2024**, *14*, 579. https://doi.org/10.3390/biom14050579.

(10) Wei, L.; Zhu, Q.; Xu, S. M.; Chang, X.; Wang, C. J. Stereodivergent Synthesis of α,α-Disubstituted α-Amino Acids via Synergistic Cu/Ir Catalysis. *J. Am. Chem. Soc.* **2018**, *140*, 1508–1513. https://doi.org/10.1021/jacs.7b12174.

(11) Nowak, M. G.; Skwarecki, A. S.; Milewska, M. J. Amino Acid-Based Antimicrobial Agents—Synthesis and Properties. *ChemMedChem* **2021**, *16*, 3513–3544. https://doi.org/10.1002/cmdc.202100503.

(12) Wang, X.; Yang, X.; Wang, Q.; Meng, D. Unnatural amino acids: promising implications for the development of new antimicrobial peptides. *Crit. Rev. Microbiol.* **2022**. https://doi.org/10.1080/1040841X.2022.2047008.

(13) Szcześniak, P.; Pieczykolan, M.; Stecko, S. The Synthesis of α,α-Disubstituted α-Amino Acids via Ichikawa Rearrangement. *J. Org. Chem.* **2016**, *81*, 1057–1074. https://doi.org/10.1021/acs.joc.5b02628.

(14) Oba, M.; Kunitake, M.; Kato, T.; Ueda, A.; Tanaka, M. Enhanced and Prolonged Cell-Penetrating Abilities of Arginine-Rich Peptides by Introducing Cyclic α,α-Disubstituted α-Amino Acids with Stapling. *Bioconjugate Chem.* **2017**, *28*, 1801–1806. https://doi.org/10.1021/acs.bioconjchem.7b00190.

(15) Wang, C.; Qi, R.; Wang, R.; Xu, Z. Photoinduced C(sp^3)–H Functionalization of Glycine Derivatives: Preparation of Unnatural α-Amino Acids and Late-Stage Modification of Peptides. *Acc. Chem. Res.* **2023**, *56*, 2110–2125. https://doi.org/10.1021/acs.accounts.3c00260.

(16) Wang, Q.; Wang, L. New Methods Enabling Efficient Incorporation of Unnatural Amino Acids in Yeast. *J. Am. Chem. Soc.* **2008**, *130*, 6066–6067. https://doi.org/10.1021/ja800894n.

(17) Yu, Y.; Hu, C.; Xia, L.; Wang, J. Artificial Metalloenzyme Design with Unnatural Amino Acids and Non-Native Cofactors. *ACS Catal.* **2018**, *8*, 1851–1863. https://doi.org/10.1021/acscatal.7b03754.
(18) Ji, P.; Li, J.; Tao, Y.; et al. Direct Asymmetric α-Alkylation of NH_2-Unprotected Amino Acid Esters Enabled by Biomimetic Chiral Pyridoxals. *ACS Catal.* **2023**, *13*, 9150–9157. https://doi.org/10.1021/acscatal.3c01770.
(19) Yamamoto, H.; Ramakrishna, I. Alkylation of Glycine Derivatives to Access Nonnatural Amino Acids. *Synfacts* **2020**, *16*, 1119. https://doi.org/10.1055/s-0040-1705860.
(20) Tsuji, T.; Hashiguchi, K.; Yoshida, M.; et al. α-Amino acid and peptide synthesis using catalytic cross-dehydrogenative coupling. *Nat. Synth.* **2022**, *1*, 304–312. https://doi.org/10.1038/s44160-022-00037-0.
(21) Matsumoto, Y.; Sawamura, J.; Murata, Y.; Nishikata, T.; Yazaki, R.; Ohshima, T. Amino Acid Schiff Base Bearing Benzophenone Imine as a Platform for Highly Congested Unnatural α-Amino Acid Synthesis. *J. Am. Chem. Soc.* **2020**, *142*, 8498–8505. https://doi.org/10.1021/jacs.0c02707.
(22) Noda, H.; Shibasaki, M. Recent Advances in the Catalytic Asymmetric Synthesis of β^2- and $\beta^{2,2}$-Amino Acids. *Eur. J. Org. Chem.* **2020**, 2350–2361. https://doi.org/10.1002/ejoc.201901596.
(23) Cabré, A.; Verdaguer, X.; Riera, A. Recent Advances in the Enantioselective Synthesis of Chiral Amines via Transition Metal-Catalyzed Asymmetric Hydrogenation. *Chem. Rev.* **2021**, *122*, 269–339. https://doi.org/10.1021/acs.chemrev.1c00496.
(24) O'Neil, L. G.; Bower, J. F. Electrophilic Aminating Agents in Total Synthesis. *Angew. Chem., Int. Ed.* **2021**, *60*, 25640–25666. https://doi.org/10.1002/anie.202102864.
(25) Greck, C.; Drouillat, B.; Thomassigny, C. Asymmetric Electrophilic α-Amination of Carbonyl Groups. *Eur. J. Org. Chem.* **2004**, 1377–1385. https://doi.org/10.1002/ejoc.200300657.
(26) Zhang, S.; Li, D.; Wang, B.; et al. Palladium-Catalyzed Asymmetric Trifluoromethylated Allylic Alkylation of N-Substituted Glycine Ethyl Esters with α-(Trifluoromethyl)alkenyl Acetates. *Eur. J. Org. Chem.* **2023**. https://doi.org/10.1002/ejoc.202300593.
(27) Liu, Z.-C.; Wang, Z.-Q.; Zhang, X.; Yin, L. Copper(I)-catalyzed asymmetric alkylation of α-imino esters. *Nat. Commun.* **2023,** *14*, 2187. https://doi.org/10.1038/s41467-023-37967-y.
(28) Belokon, Y. N.; North, M.; Churkina, T. D.; Ikonnikov, N. S.; Maleev, V. I. Chiral salen–metal complexes as novel catalysts for the asymmetric synthesis of α-amino acids under phase transfer catalysis conditions. *Tetrahedron* **2001**, *57*, 2491–2498. https://doi.org/10.1016/S0040-4020(01)00072-2.
(29) Tovmasyan, A. S.; Mkrtchyan, A. F.; Khachatryan, H. N.; et al. Synthesis, Characterization, and Study of Catalytic Activity of Chiral Cu(II) and Ni(II) Salen Complexes in the α-Amino Acid C-α Alkylation Reaction. *Molecules* **2023**, *28*, 1180. https://doi.org/10.3390/molecules28031180.
(30) Hovhannisyan, A. M.; Tovmasyan, A. S.; Mkrtchyan, A. F.; et al. Synthesis and evaluation of new mono- and binuclear salen complexes for the Cα-alkylation reaction of amino acid substrates as chiral phase transfer catalysts. *Mol. Catal.* **2024**, *569*, 114618. https://doi.org/10.1016/j.mcat.2024.114618.
(31) Belokon, Y. N.; Bhave, D.; D'Addario, D.; Groaz, E.; North, M.; Tagliazucca, V. Copper(II)salen catalysed, asymmetric synthesis of α,α-disubstituted amino acids. *Tetrahedron* **2004**, *60*, 1849–1861. https://doi.org/10.1016/j.tet.2003.12.031.
(32) Banti, D.; Belokon, Y. N.; Fu, W. L.; Groaz, E.; North, M. Mechanistic studies on the asymmetric alkylation of amino ester enolates using a copper(ii)salen catalyst. *Chem. Commun.* **2005**, 2707–2709. https://doi.org/10.1039/b500813a.
(33) Mazurek, A.; Szeleszczuk, Ł.; Pisklak, D. M. Periodic DFT Calculations—Review of Applications in Pharmaceutical Sciences. *Pharmaceutics* **2020**, *12*, 415. https://doi.org/10.3390/pharmaceutics12050415.

(34) Liu, S. C.; Zhu, X. R.; Liu, D. Y.; Fang, D. C. DFT calculations in solution systems: solvation energy, dispersion energy and entropy. *Phys. Chem. Chem. Phys.* **2023**, *25*, 913–931. https://doi.org/10.1039/D2CP04720A.
(35) Hirshfeld, F. L. Bonded-atom fragments for describing molecular charge densities. *Theor. Chim. Acta* **1977**, *44*, 129–138. https://doi.org/10.1007/BF00549096.
(36) Trost, B. M.; Xu, J.; Schmidt, T. Palladium-Catalyzed Decarboxylative Asymmetric Allylic Alkylation of Enol Carbonates. *J. Am. Chem. Soc.* **2009**, *131*, 18343–18357. https://doi.org/10.1021/ja9053948.
(37) Sampani, S. I.; Aubert, S.; Cattoen, M.; et al. Dinucleating Schiff base ligand in Zn/4f coordination chemistry: synthetic challenges and catalytic activity evaluation. *Dalton Trans.* **2018**, *47*, 4486–4493. https://doi.org/10.1039/C8DT00538A.
(38) Becke, A. D. Density-functional thermochemistry. I. The effect of the exchange-only gradient correction. *J. Chem. Phys.* **1992**, *96*, 2155–2160. https://doi.org/10.1063/1.462066.
(39) Vosko, S. H.; Wilk, L.; Nusair, M. Accurate spin-dependent electron liquid correlation energies for local spin density calculations: a critical analysis. *Can. J. Phys.* **1980**, *58*, 1200–1211. https://doi.org/10.1139/p80-159.
(40) Neese, F. Software update: The ORCA program system—Version 5.0. *WIREs Comput. Mol. Sci.* **2022**. https://doi.org/10.1002/wcms.1606.
(41) Barone, V.; Cossi, M. Quantum Calculation of Molecular Energies and Energy Gradients in Solution by a Conductor Solvent Model. *J. Phys. Chem. A* **1998**, *102*, 1995–2001. https://doi.org/10.1021/jp9716997.
(42) Weigend, F.; Ahlrichs, R. Balanced basis sets of split valence, triple zeta valence and quadruple zeta valence quality for H to Rn: Design and assessment of accuracy. *Phys. Chem. Chem. Phys.* **2005**, *7*, 3297–3305. https://doi.org/10.1039/B508541A.
(43) Larrow, J. F.; Jacobsen, E. N.; Gao, Y.; Hong, Y.; Nie, X.; Zepp, C. M. A Practical Method for the Large-Scale Preparation of [N,N′-Bis(3,5-di-tert-butylsalicylidene)-1,2-cyclohexanediaminato(2-)]manganese(III) Chloride, a Highly Enantioselective Epoxidation Catalyst. *J. Org. Chem.* **1994**, *59*, 1939–1942. https://doi.org/10.1021/jo00086a062.

Author's Contributions: Anna S. Tovmasyan: Methodology, Investigation. Anna F. Mkrtchyan: Conceptualization, Funding acquisition, Writing—review and editing. Ashot S. Saghyan: Conceptualization, Funding acquisition, Project administration, Resources, Supervision, Writing—original draft, Writing—review and editing.

Funding: Computations were performed on the NVIDIA DGX A100 cluster obtained through grant project No. 10–3/22Eq-10 from the Higher Education and Science Committee of the RA MoESCS. Additional support was provided by joint research projects SCS 21AG-1D013 and ISTC AM-2705 from the same committee.

Informed Consent Statement: Not applicable.

Data and Code Availability Statement: Not applicable.

Acknowledgments: We sincerely thank the Optical Spectroscopy and the NMR Magnetic Resonance Spectroscopy Laboratories of the Scientific Technological Center of Organic and Pharmaceutical Chemistry of the National Academy of Sciences of the Republic of Armenia for their invaluable support in conducting Raman, FTIR, and NMR measurements. We also thank the Analysis Laboratory and the Laboratory of BAS Purification and Certification of the SPC "Armbiotechnology" NAS RA for performing the elemental analysis. Their expertise and access to cutting-edge facilities were instrumental to this work. We are also grateful to Professor Yu. N. Belokon for insightful consultations and guidance throughout the study.

Institutional Review Board Statement: Not applicable.

Conflicts of Interest: The authors declare no conflicts of interest.

Reports of NAS RA
ՀՀ ԳԱԱ Զեկույցներ
NATIONAL ACADEMY OF SCIENCES OF THE REPUBLIC OF ARMENIA
ՀԱՅԱՍՏԱՆԻ ՀԱՆՐԱՊԵՏՈՒԹՅԱՆ ԳԻՏՈՒԹՅՈՒՆՆԵՐԻ ԱԶԳԱՅԻՆ ԱԿԱԴԵՄԻԱ

ԱՄՓՈՓԱԳԻՐ

α-Ամինաթթուների Cα-ալկիլացման մեխանիզմի տարբեր ասպեկտների ուսումնասիրությունը միջֆազային քիրալ սալենային կատալիզատորների պայմաններում

Աննա Ս. Թովմասյան[1,*], Աննա Ֆ. Մկրտչյան[1,2], Աշոտ Ս. Սաղյան[1,2]

[1] «Հայկենսատեխնոլոգիա» ԳԱԿ, Գյուրջյան 14, Երևան 0056, ՀՀ
[2] Երևանի պետական համալսարան, Ալեք Մանուկյան 1, Երևան 0025, ՀՀ

* Հաղորդակցության համար՝ anna.tovmasyan1@edu.isec.am

Անցումային շարքի մետաղների՝ Cu(II), Ni(II) և Zn(II) քիրալ սալենային կոմպլեքսների ստերեոդիֆերենցող հատկությունները ուսումնասիրվել են ամինաթթվային սուբստրատների Cα-ալկիլացման ասիմետրիկ ռեակցիաներում՝ որպես քիրալային կատալիզատորներ: Ստացված արդյունքները ցույց են տվել, որ սալենային կոմպլեքսների կատալիտիկ և ստերեոդիֆերենցող ակտիվությունը զգալիորեն կախված է սալիցիլալդեհիդային հատվածում՝ արոմատիկ օղակի 3-րդ դիրքում գտնվող տեղակալիչի բնույթից: Հետազոտության տվյալների համաձայն՝ առավել բարձր կատալիտիկ արդյունավետություն ցուցաբերել է Zn(II)-ի սալենային կոմպլեքսը, որի սալիցիլիդենային օղակի 3-րդ դիրքում տեղակալված է մեթօքսի խումբ: Այս կոմպլեքսը ցուցաբերել է մինչև 90% կատալիտիկ ակտիվություն: Քիրալ սալենային կոմպլեքսների ստերեոդիֆերենցող ակտիվության մեխանիզմի բացատրության համար իրականացվել են DFT (Density Functional Theory) հաշվարկներ: Ըստ հաշվարկների՝ կատալիզատորների ակտիվությունը պայմանավորված է դիմերիկ երկմիջուկ կառուցվածքով կոմպլեքսների պրոպելլերանման (propeller-like) և խաչաձև (cross-like) կոնֆորմացիոն իզոմերների հարաբերակցությամբ՝ ալկիլացման անցումային վիճակում: Պարզվել է, որ պրոպելլերանման կոնֆորմացիաները, որոնք գերակշռում են արոմատիկ օղակի 3-րդ դիրքում ալիլային խումբ պարունակող սալենային կոմպլեքսներում, համապատասխանում են կատալիտիկ ոչ ակտիվ ձևին և արգելակում են ասիմետրիկ կատալիզը: Իսկ խաչաձև կոնֆորմացիաները, որոնք գերակշռում են 3-րդ դիրքում մեթօքսի խումբ պարունակող անալոգներում, ապահովում են բարձր ստերեոդիֆերենցող ակտիվություն և նպաստում են արդյունավետ ասիմետրիկ կատալիզին: DFT հաշվարկներով ստացված արդյունքները համընկնում են փորձարարական տվյալների հետ:

Բանալի բառեր՝ ոչ սպիտակուցային ամինաթթուներ, քիրալային կատալիզատորներ, ասիմետրիկ կատալիզ, սալենային կոմպլեքսներ, ստերեոսելեկտիվություն

Reports of NAS RA
ՀՀ ԳԱԱ Զեկույցներ
NATIONAL ACADEMY OF SCIENCES OF THE REPUBLIC OF ARMENIA
ՀԱՅԱՍՏԱՆԻ ՀԱՆՐԱՊԵՏՈՒԹՅԱՆ ԳԻՏՈՒԹՅՈՒՆՆԵՐԻ ԱԶԳԱՅԻՆ ԱԿԱԴԵՄԻԱ

2026 **Volume 126** **Issue 1** **Article No. 6**

Category: Mathematics
Type of Paper: Original Research Article
Received: November 30, 2025, **Revised:** January 30, 2026, **Accepted:** February 13, 2026
Published: April 16, 2026

DOI: 10.54503/0321-1339-2026.126.1-6

On Conditionally Universal Functions with respect to the Walsh system

Martin Grigoryan[1,*]

[1]Yerevan State University, 1 Alek Manoogian St, Yerevan 0025, Armenia

[*]Correspondence: gmarting@ysu.am

Abstract
This paper proves theorems on the existence of conditionally **universal functions** and **universal triads** with respect to the Walsh system defined by the author. The proof method of these theorems provides a new approach to constructing universal series in the Walsh system: by varying its values on a certain set of arbitrarily small measure, any measurable almost everywhere finite function can be turned into a function such that, after choosing the corresponding signs for the terms of the Fourier-Walsh series of the changed function, we can achieve the fact that the obtained series is universal in the class of all measurable functions.

Keywords: Universal function, Fourier series, Walsh system
MSC (2010): 42B05, 42C10, 43A15

1. Introduction

This article continues the author's studies on establishing the existence and describing the structure of functions (**universal functions)**, which are universal with respect to a given classical system for various function classes (see [1-15]).

We also consider the problem of the existence of **universal pairs** and **universal triads** with respect to the Walsh system for the class of all Lebesgue measurable functions on $[0,1]$.

We need some standard notation.

Let $|E|$ be the Lebesgue measure of a measurable set $E \subseteq [a,b]$ ($[a,b]=[-\pi,\pi]$ or $[0,1]$).

Let $L^p(E)$, $p>0$ be the class of all measurable functions f on E with finite integral $\int_E |f(x)|^p\,dx$ and $L^0(E)$ be the class of all almost everywhere finite, Lebesgue measurable functions on E.

We denote by $M(E)$ the class of all Lebesgue measurable functions on E.

The sequence of functions $\{f_k(x)\}_{k=1}^{\infty} \subset L^0(E)$ is said to converge to f in $L^0(E)$ (in $M(E)$), if $\{f_k(x)\}_{k=1}^{\infty}$ converges to $f(x)$ almost everywhere on E.

The sequence of functions $\{f_k\}_{k=1}^{\infty} \subset L^p(E)$ is said to converge to f in $L^p(E)$, if it converges to f in the $L^p(E)$ metric, that is

$$\lim_{k\to\infty} \int_E |f_k(x) - f(x)|^p \, dx = 0.$$

Let

$$a_k(f) = \frac{1}{\pi}\int_{-\pi}^{\pi} f(x)\cos kx\,dx, \quad b_k(f) = \frac{1}{\pi}\int_{-\pi}^{\pi} f(x)\sin kx\,dx, \quad k \geq 0$$

be the Fourier coefficients of function $f \in L^1[-\pi,\pi]$ with respect to the trigonometric system and let

$$S_N(x,f) = \frac{a_0(f)}{2} + \sum_{k=0}^{N-1} a_k(f)\cos kx + b_k(f)\sin kx$$

be the N-th partial sum of the function f of the Fourier series.

Let $\Phi := \{\varphi_k(x)\}$ be an orthonormal system on $[a,b]$ and let $f \in L^1[a,b]$.

We denote by $c_k(f)$ the Fourier coefficients of function $f \in L^1[a,b]$ with respect to the system Φ, that is

$$c_k(f) = \int_a^b f(x)\varphi_k(x)\,dx, \quad S_n(x,f) = \sum_{k=1}^{n-1} c_k(f)\varphi_k(x).$$

Below S will denote one of the spaces $M(E)$ or $L^p(E)$, $p \geq 0$.

Definition 1^0. A series $\sum_{k=0}^{\infty} f_k(x)$, $(f_k \subset S,\ k = 0,1,2,...)$, is called universal in S (universal in the usual sense), if for each function $f \in S$ there exists a growing subsequence of natural numbers $\{N_m\}_{m=1}^{\infty} \nearrow$, so that the subsequence $\{\sum_{k=0}^{N_m} f_k(x)\}_{m=1}^{\infty}$ of partial sums of that series converges to f in S.

The existence of functions and series which are universal (in one sense or another) in various classes of functions has been studied by many mathematicians working in the theory of functions of real or complex variables (see [16-29]).

The first example is due to Birkhoff [16] in 1929, who proved the existence of an entire function $f(z)$ with the property that for an arbitrary entire function $g(z)$ and every $r > 0$ there exists a subsequence $\{n_k\}_{k=1}^{\infty}$ of the natural numbers, such that $\{f(z+n_k)\}_{k=1}^{\infty}$ converges to $g(z)$, uniformly on the disc $\{z \in C:\ |z| \leq r\}$.

In 1935 Marcinkiewicz [17] proved that for any (converging to zero) sequence $h_n \to 0$ there exists a continuous function $F \in C[0,1]$ $F:\ [0,1] \to \mathcal{R}$ having the property: for any measurable function $f(x):\ [0,1]$, there is a subsequence $n_k \nearrow^{\infty}$ such that

$$\frac{F(x+h_{n_k}) - F(x)}{h_{n_k}} \to g(x)$$

as $k \to \infty$ almost everywhere on $[0,1]$ (see also [18]).

This continuous function F is called a universal primitive function with respect to the given sequence $\{h_n\}_{n=1}^{\infty}$.

In 1952 MacLane [19] proved the existence of a universal entire function $g(z)$ with respect to derivatives. Namely, for every entire function $f(z)$ and every $r > 0$ one can choose an increasing sequence $\{n_k\}_{k=1}^{\infty}$ in such a way that the sequence of derivatives $\{g^{(n_k)}(z)\}_{k=1}^{\infty}$ converges to $f(z)$ uniformly on the disc $|z| \le r$.

In 1986 Luh [20] proved a theorem on the universality of power series $\sum_{k=0}^{\infty} c_k z^k$. Namely, if let $r \ge 0$, there exists a power series $\sum_{k=0}^{\infty} c_k z^k$ of radius of convergence r such that for every compact set K in $\{z \in C : |z| > r\}$ with connected complement and every function $h(z)$ that is continuous on K and holomorphic on the interior of K there exists an increasing sequence $\{N_m\}_{m=1}^{\infty}$ such that

$$\sum_{k=0}^{N_m} c_k z^k \to h(z)$$

as $m \to \infty$ uniformly on K.

We note that the first universal real power series was constructed as early as 1914 by Fekete [21], who in particular proved the existence of a real power series $\sum_{k=0}^{\infty} a_k x^k$ with the following property. For every continuous function $g(x)$ on $[-1,1]$ with $g(0) = 0$ there is an increasing sequence of positive integers $\{n_k\}_{k=1}^{\infty}$ such that $\sum_{j=0}^{n_k} a_j x^j$ converges to $g(x)$ uniformly on $[-1,1]$.

In 1987 Grosse-Erdman [22] proved the existence of an infinitely differentiable function $h(x)$ with universal Taylor expansion. Namely, there exists an infinitely differentiable function h on $(-\infty,\infty)$ with $h(0) = 0$ function $h(x) \in C^{\infty}(-\infty,\infty)$ with $h(0) = 0$ such that the Taylor series at $x_0 = 0$ is locally uniformly universal in $C(R)$; that is for each function $f(x) \in C(R) = C(-\infty,\infty)$ with $f(0) = 0$ and any number $r > 0$ there exists a subsequence

$$S_{n_k}(h,0) = \sum_{m=1}^{n_k} \frac{h^{(m)}(0)}{m!} x^m$$

of partial sums of the Taylor series $\sum_{m=1}^{\infty} \frac{h^{(m)}(0)}{m!} x^m$ of $h(x)$ which converges to $f(x)$ uniformly on the $[-r,r]$.

It is not difficult to see that from this result it follows that for every measurable function $f(x)$ on $[-\pi,\pi]$ there is an increasing sequence $\{m_q\} \nearrow \infty$ of positive integers such that the subsequence of partial sums

$$\sum_{m=1}^{m_q} \frac{h^{(m)}(0)}{m!} x^m$$

converges to $f(x)$ as $q \to \infty$ almost everywhere on $[-\pi, \pi]$.

The notion of a universal series in $M[-\pi, \pi]$ in the trigonometric and by general orthonormal systems is due to Men'shov [23] in 1947 and Talalyan [24] in 1957 (see also [25]-[30]). In this direction, important results were obtained by them and their students.

The first construction of universal trigonometric series in the class of all measurable functions in the sense of convergence almost everywhere was given by Men'shov. He proved the following fundamental theorem.

Theorem (Men'shov). There is a trigonometric series

$$\frac{a_0}{2} + \sum_{k=1}^{\infty} a_k \cos kx + b_k \sin kx, \quad |a_k| + |b_k| \to 0 \quad \text{as} \quad k \to \infty$$

with the following property. For every measurable function $f(x)$ on $[-\pi, \pi]$ there is an increasing sequence $\{m_q\}_{q=1}^{\infty}$ of positive integers such that the subsequence of partial sums

$$\frac{a_0}{2} + \sum_{k=1}^{m_q} a_k \cos kx + b_k \sin kx,$$

converges to $f(x)$ as $q \to \infty$ almost everywhere on $[-\pi, \pi]$ (that is this series is universal in $M[-\pi, \pi]$.)

Theorem (Talalyan). Let $\Phi := \{\varphi_k(x)\}_{k=1}^{\infty}, x \in [0,1]$ be an orthonormal system. There is a series in the system $\{\varphi_k(x)\}_{k=1}^{\infty}$:

$$\sum_{k=1}^{\infty} d_k \varphi_k(x), \; d_k \to 0 \quad \text{as} \quad k \to \infty,$$

which is universal in $M[0,1]$.

Remark 1. As noted above, there is an infinitely differentiable function with universal Taylor series, **but there is no function** $U \in L^1[-\pi, \pi]$, whose Fourier series in the trigonometric system is universal in $M[-\pi, \pi]$:

Otherwise, if there were a function $U \in L^1[-\pi, \pi]$ whose Fourier series in the trigonometric system is universal in $M[-\pi, \pi]$, then for the function $f(x) = 2U(x)$ one could find a growing subsequence of natural numbers $\{N_m\} \nearrow \infty$ such that

$$S_{N_m}(x, U) = \frac{a_0(U)}{2} + \sum_{k=1}^{N_m - 1} a_k(U) \cos kx + b_k(U) \sin kx$$

converges to $2U(x)$ as $q \to \infty$ almost everywhere on $[-\pi, \pi]$.

On the other hand, from a **well-known theorem of Kolmogorov [31] (the Fourier series in the trigonometric system of any integrable function converges to it in** $L^p[-\pi, \pi], p \in (0,1)$, in

particular $\lim_{m\to\infty}\int_{-\pi}^{\pi}\left|S_{N_m}(x,U)-U(x)\right|^p dx=0$), it follows that for some subsequence $\{N_{m_q}\}_{q=1}^{\infty}$ of sequence $\{N_m\}_{m=1}^{\infty}$ the subsequence

$$S_{N_{m_q}}(x,U)=\frac{a_0(U)}{2}+\sum_{k=1}^{N_{m_q}}a_k(U)\cos x+b_k(U)\sin kx$$

converges to $U(x)$ as $q\to\infty$ almost everywhere on $[-\pi,\pi]$.

Hence, we see that $U(x)=2U(x)$ almost everywhere on $[-\pi,\pi]$.

This contradiction shows that there does not exist a function $U\in L^1[-\pi,\pi]$ which is universal for the class $M[-\pi,\pi]$ with respect to the trigonometric system.

Remark 2. A similar analysis shows that there does not exist an integrable function U, whose Fourier series in the other classical systems (Walsh system, Haar system, Franklin system, Vilenkin system) is universal in $M[0,1]$.

The above considerations suggest the following question, the answer to which is unknown:

Question 1. Do there exist an orthonormal system of bounded functions and an integrable function U(x) that is universal for the space $M[0,1]$ with respect to the system $\{\varphi_k(x)\}_{k=1}^{\infty}$?

Despite the fact that, as Men'shov proved, there is a universal trigonometric series in the class $M[-\pi,\pi]$ and (as we indicated above) there is no function $U\in L^1[-\pi,\pi]$ whose Fourier series in the trigonometric system is universal in the class $M[-\pi,\pi]$.

Nevertheless, we managed to construct an integrable function U and prove that after a suitable choice of signs $\{\delta_k;\ \delta_k=\pm1\}_{k=0}^{\infty}$ for the Fourier coefficients of this function U, it is possible to achieve that the newly obtained series $\frac{a_0(U)}{2}+\sum_{k=0}^{\infty}\delta_k\left(a_k(U)\cos kx+b_k(U)\sin kx\right)$ would be universal in $M[-\pi,\pi]$.

Before formulating the main result of the paper, we give corresponding definitions.

Let $\Phi:=\{\varphi_k(x)\}$ **be an orthonormal system on** $[a,b]$.

Definition 1. We say that a function $U\in L^1[a,b]$ and a sequence $\delta=\{\delta_k=\pm1,k=0,1,2,\dots\}$ of signs form **universal pairs:** (U,δ) for space S with respect to this system $\{\varphi_k(x)\}_{k=1}^{\infty}$ in sense of universal series, if the series $\sum_{k=0}^{\infty}\delta_k c_k(f)\varphi_k(x)$ is universal in S.

Definition 2. We say that a function $U\in L^1[a,b]$ and a measurable set $E\subset[a,b]$ form **universal pairs:** (U,E) with respect to the system $\{\varphi_k(x)\}_{k=0}^{\infty}$ in sense of modification, if for each function $f\in L^1[a,b]$ one can find such a function $g\in L^1[a,b]$ coinciding with f on E, and such that

$$\left|c_k(g)\right|=\left|c_k(U)\right|,\quad k=0,1,2,\dots$$

Definition 3. We say that a function $U\in L^1[a,b]$, a sequence $\delta=\{\delta_k=\pm1,k=0,1,2,\dots\}$ of signs and a measurable set $E\subset[a,b]$ form **universal triads:** (U,δ,E) for space S with respect

to the system $\{\varphi_k(x)\}_{k=0}^{\infty}$, if partial sums of the series $\sum_{k=0}^{\infty}\delta_k c_k(f)\varphi_k(x)$ are universal in S and for each function $f\in L^1[a,b]$ one can find such a function $g\in L^1[a,b]$ coinciding with f on E, and such that

$$|c_k(g)|=|c_k(U)|,\quad k=0,1,2,...$$

Definition 4. We say that a function $U\in L^1[a,b]$ is

1) **universal for** a space S with respect to the system $\{\varphi_k(x)\}_{k=0}^{\infty}$, if the Fourier series of the function U with respect to this system is universal in S,

2) **conditionally universal** for a space S with respect to the system $\{\varphi_k(x)\}_{k=0}^{\infty}$, if there exists a sequence of signs $\delta_k=\pm1$ such that the series $\sum_{k=0}^{\infty}\delta_k c_k(U)\varphi_k(x)$ is universal in S,

3) **quasiuniversal** for a space S with respect to the system $\{\varphi_k(x)\}_{k=0}^{\infty}$, if there exists a sequence of signs $\delta_k=\pm1$, with $d_\Lambda(\Omega^+)=1$, such that the series $\sum_{k=0}^{\infty}\delta_k c_k(U)\varphi_k(x)$ is universal in S, where

$$d_\Lambda(\Omega^+):=\lim_{n\to\infty}\sup\frac{\#(\Omega^+\cap[0,n))}{\#(\Lambda\cap[0,n))}$$

is the upper density of the subset $\Omega^+=\{k\in N\cup\{0\},\delta_k=1\}$ with respect to the set $\Lambda=spec(U)=\{k\in N\cup\{0\},c_k(U)\neq0\}$, and $\#(E)$ is the number of elements of a finite set E,

4) **almost universal** for a space S with respect to the system $\{\varphi_k(x)\}_{k=0}^{\infty}$, if there exists a sequence of signs $\delta_k=\pm1$ with $\rho_\Lambda(\Omega)=0$, such that the series $\sum_{k=0}^{\infty}\delta_k c_k(U)\varphi_k(x)$ is universal in S, where

$$\rho_\Lambda(\Omega):=\lim_{n\to\infty}\frac{\#(\Omega\cap[0,n))}{\#(\Lambda\cap[0,n))}$$

is the density of the subset $\Omega=\{k\in N\cup\{0\},\delta_k=-1\}$ with respect to the set $\Lambda=spec(U)=\{k\in N\cup\{0\},c_k(U)\neq0\}$,

5) **universal in sense of signs**, if its Fourier series $\sum_{k=0}^{\infty}c_k(U)\varphi_k(x)$ in the system $\{\varphi_k(x)\}_{k=0}^{\infty}$ is universal in S **in sense of signs**: that is for each function $f\in S$ one can find a sequence of signs $\delta_k=\pm1$ such that the series $\sum_{k=0}^{\infty}\delta_k c_k(U)\varphi_k(x)$ converges to f in S,

6) **universal in sense of rearrangements**, if its Fourier series $\sum_{k=0}^{\infty}c_k(U)\varphi_k(x)$ in the system $\{\varphi_k(x)\}_{k=0}^{\infty}$ is universal in S in sense of rearrangements: that is for each function $f\in S$ one can

find $\{\sigma(k)\}_{k=1}^{\infty}$ some permutation of the natural numbers, such that the series $\sum_{k=1}^{\infty} c_{\sigma(k)}(U)\varphi_{\sigma(k)}(x)$ converges to f in S.

In recent years, we have obtained several results related to the existence and description of the structure of functions (universal functions), whose Fourier series with respect to a given classical system are universal in a certain sense for different function classes.

In particular, in [2], [3], [11], and [15] the following theorems were proved:

Theorem 1. There exists an integrable function U with monotonically decreasing Fourier–Walsh coefficients, which is universal in the sense of signs with respect to the Walsh system for the spaces $L^p[0,1]$ for all $p \in (0,1)$. In addition, the Fourier–Walsh series of the function U converges to it in $L^1[0,1]$.

Theorem 2. There exist an integrable function $U \in L^1[-\pi,\pi]$ and a sequence $\delta = \{\delta_k = \pm 1, k = 0,1,2,\dots\}$ of signs, which are form **universal pairs:** (U,δ) for space $L^p[-\pi,\pi]$, $p \in (0,1)$ with respect to the trigonometric system.

Theorem 3. For any $p \in (0,1)$ there exists an integrable function U that is both conditional universal and universal in the sense of signs with respect to the trigonometric system for the class $L^p[-\pi,\pi]$.

Theorem 4. There exists an integrable function U, with monotonically decreasing Fourier–Walsh coefficients, which is universal in the sense of signs with respect to the Walsh system for the space $L^0[0,1]$. In addition, the Fourier–Walsh series of the function U converges to it in $L^1[0,1]$.

Remark 3. It should be noted (this also follows from the above) that the existence of universal functions and universal triads depends on the type (sense) of universality, on the system, and on the space S. Therefore, questions in this direction are very comprehensive.

In this article we will prove

Theorem 5. There exist an integrable function $U \in L^1[0,1]$ and a sequence $\delta = \{\delta_k = \pm 1, k = 0,1,2,\dots\}$ of signs and a measurable set $E \subset [a,b]$ form **universal triads:** (U,δ,E) for space $L^0[0,1]$ with respect to the Walsh system.

Moreover, the following statement holds

Theorem 6. For any $\varepsilon \in (0,1)$ there exists a function $U \in L^1[0,1]$, with $\sup(U) \subset [0,\varepsilon]$, which has the following properties:

a) the Fourier coefficients of the function U in the Walsh system are positive and monotonically decreasing,

b) the Fourier–Walsh series of the function U converges to it in $L^1[0,1]$,

c) the function U is conditional universal for the class $M[0,1]$ with respect to the Walsh system,

d) for any $\delta \in (0,1)$ exists a measurable set $E \subset [0,1]$ with $|E| > 1-\delta$, so that for each function $g \in L^1[0,1]$ one can find such a function $f \in L^1[0,1]$ coinciding with $g(x)$ on E, and such that

$$|c_k(f)| = c_k(U), \quad k = 0,1,2,\dots,$$

e) the Fourier–Walsh series of the corrected function f converges to it in $L^1[0,1]$.

Remark 4. The proof method of Theorem 5 allows obtaining a new approach to constructing universal series in the Walsh system: by varying its values on a certain set of arbitrarily small measure, any measurable almost everywhere finite function can be turned into a function such that, after choosing the corresponding signs for the terms of the Fourier–Walsh series of the changed function, we can achieve the fact that the obtained series is universal in $M[-\pi,\pi]$.

The following questions arise, the answer to which is still unknown:

Question 2. Do there exist an orthonormal system $\{\varphi_k(x)\}_{k=1}^{\infty}$ of bounded functions and an integrable function $U(x)$ that is universal for the space $L^p[0,1]$ for some $p\in[0,1)$ (or at least for the space $M[0,1]$) with respect to the system $\{\varphi_k(x)\}_{k=1}^{\infty}$?

Question 3. Are the Theorems 4 and 6 true for the trigonometric system?

Question 4. Are the theorems 1-7 true for the Vilenkin system?

Question 5. Is it possible to construct a function that is universal for the space $L^0[0,1]$ with respect to the Walsh system in sense of rearrangements?

Question 6. Does a function $U\in L^1[-\pi,\pi]$ exist that, for the class $L^p[-\pi,\pi]$, with respect to the trigonometric system, is universal in the sense of permutations?

Question 7. Are the theorems 1-7 true for the Franklin system (for the Haar system)?

Question 8. Are the theorems 1-5 true for spherical harmonics?

In connection with Question 3, note that we can prove the following statement:

Theorem 7. There exist an integrable function $U\in L^1[0,1]$ and a sequence $\delta=\{\delta_k=\pm1, k=0,1,2,\dots\}$ of signs and a measurable set $E\subset[a,b]$ form **universal triads:** (U,δ,E) for space $L^0[0,1]$ with respect to the trigonometric system.

The proof of this theorem will be given in another paper by the author. In this paper, we will prove Theorem 6.

2. Auxiliary facts

The Walsh system, an extension of the Rademacher system, may be obtained in the following manner. Let r be the periodic function of least period 1 defined on $[0,1)$ by

$$r(x)=\chi_{[0,1/2)}(x)-\chi_{[1/2,1)}(x).$$

The Rademacher system $\{r_n(x)\}_{n=0}^{\infty}$ is defined by the conditions:

$$r_n(x)=r\left(2^n x\right),\ \ \forall x\in R,\ \ n=0,1,...$$

and, in the ordering employed by Paley (see [32], [33]), the n-th element of the Walsh system $\{\varphi_n(x)\}_{n=0}^{\infty}$ is given by

$$\varphi_n(x)=\prod_{k=0}^{\infty}\left(r_k(x)\right)^{\theta_k(n)}, \tag{2.1}$$

where $\sum_{k=0}^{\infty}\theta_k(n)2^k$ is the unique binary expansion of n, with each $\theta_k(n)$ either 0 or 1.

Note that (see [34]) the Walsh system is a basis for all $L^p[0,1]$ $p\in(1,\infty)$, i.e., every function $f(x)$ is $L^p[0,1]$ $p\in(1,\infty)$ uniquely representable by the series $\sum_{k=0}^{\infty}c_k\varphi_k(x)$ in the Walsh system by norm $L^p[0,1]$ convergent to $f(x)$.

Let $f\in L^1[0,1]$ and let

$$S_m(x,f)=\sum_{k=0}^{m-1} c_k(f)\varphi_k(x), \tag{2.2}$$

where

$$c_k(f)=\int_0^1 f(x)\varphi_k(x)\,dx. \tag{2.3}$$

In this article, we use the following lemma, which was proved in [4].

Lemma 1. Let numbers $n_0\in N$, $\left(N_0=2^{n_0}\right)$, $0<p_1<p_2<1$, $\varepsilon\in(0,1)$ and polynomial $W(x)$ in the Walsh system $\{\varphi_k(x)\}_{k=0}^{\infty}$ are given. Then there exist polynomials $U(x)$ and $B(x)$ in the Walsh system of the following form

$$U(x)=\sum_{k=2^{n_0}}^{2^n-1} b_k\varphi_k(x),\quad B(x)=\sum_{k=N_0}^{N-1}\varepsilon_k b_k\varphi_k(x),\quad N_0=2^{n_0},\quad N=2^n,$$

which satisfy the following conditions:

$$0<b_{k+1}<b_k<\varepsilon,\quad \varepsilon_k=\pm1,\ \forall k\in\left[2^{n_0},2^n\right)=[N_0,N), \tag{1}$$

$$B(x)=W(x)\ \forall x\in G,\ |G|\ge 1-\varepsilon-2^{-n_0}, \tag{2}$$

$$U(x)\chi_{[2^{-n_0},1)}(x)=0, \tag{3}$$

$$\max_{m\in[N_0,N)}\int_0^1\left|\sum_{k=N_0}^{m}\varepsilon_k b_k\varphi_k(x)\right|^p dx<4\int_0^1|W(x)|^p\,dx,\ \forall p\in(p_1,p_2), \tag{4}$$

$$\max_{m\in[N_0,N)}\int_0^1\left|\sum_{k=N_0}^{m}\varepsilon_k b_k\varphi_k(x)\right|dx<5\int_0^1|W(x)|\,dx, \tag{5}$$

$$\int_0^1|W(x)-B(x)|^p\,dx<\varepsilon\quad\forall p\in(p_1,p_2), \tag{6}$$

$$\max_{m\in[N_0,N)}\int_0^1\left|\sum_{k=N_0}^{m}a_k\varphi_k(x)\right|dx<\varepsilon. \tag{7}$$

We also use the following elementary result:

Lemma 2. For each function $g(x)\in M[0,1)$ one can find a sequence of polynomials $\{w_k(x)\}_{k=1}^{\infty}$ in the Walsh system with rational coefficients, which converges to $g(x)$ almost everywhere on $[0,1)$.

Proof of Lemma 2. We set

$$G_n=\{x\in[0,1);|g(x)|\le n\},\ G=\{x\in[0,1);\ |g(x)|<\infty\}, \tag{2.6}$$

$$G^{\pm\infty}=\left\{x\in[0,1);\ g(x)=\pm\infty\right\}, \tag{2.7}$$

$$g_n(x)=\begin{cases} g(x), & x\in G_n \\ sign\left\{g(x)\right\}n, & x\in G\setminus G_n \\ \pm n, & x\in G^{\pm\infty} \end{cases} \tag{2.8}$$

By (2.6)-(2.8), we have

$$G=\bigcup_{n=1}^{\infty}G_n,\ [0,1)=G\cup G^{+\infty}\cup G^{-\infty} \tag{2.9}$$

and

$$\lim_{n\to\infty}g_n(x)=g(x),\ \ x\in G,\ \ \lim_{n\to\infty}g_n(x)=\pm\infty,\ \ x\in G^{\pm\infty}. \tag{2.10}$$

For every natural number n one can find a polynomial $w_n(x)$ in the Walsh system with rational coefficients, such that

$$\left|\left\{x\in[0,1);\ \left|g_n(x)-w_n(x)\right|\le\frac{1}{n}\right\}\right|\ge 1-2^{-n}.$$

We set

$$E=\bigcup_{k=1}^{\infty}\bigcap_{n=k}^{\infty}\left\{x\in[0,1);\ \ \left|g_n(x)-w_n(x)\right|\le\frac{1}{n}\right\}.$$

Taking into account (2.9) and (2.10), we get that $|E|=1$ and on E

$$\lim_{n\to\infty}\left|g_n(x)-w_n(x)\right|=0.$$

From this and from (2.8) it follows that the sequence of polynomials $\{w_k(x)\}_{k=1}^{\infty}$ in the Walsh system with rational coefficients converges to $g(x)$ almost everywhere on $[0,1]$.

3. Proof of Theorem 6

Let

$$\{W_n(x)\}_{n=1}^{\infty} \tag{3.1}$$

be the sequence of all polynomials in the Walsh system $\{\varphi_k(x)\}_{k=0}^{\infty}$ with rational coefficients. It is easy to see the sequence $\{W_n(x)\}_{k=1}^{\infty}$ is dense in $L^p[0,1],\ p\in(0,\infty)$. Let $\theta,\delta\in(0,1)$ and let

$$m_1=\left[-\log_2\theta\right]+2\,. \tag{3.2}$$

We use Lemma 1, with

$$n_0=m_1\left(N_0=M_1=2^{m_1}\right),\ \ \theta=2^{-8(1+2)},\ \ p_1=\frac{1}{4},\ \ p_2=\frac{3}{4},\ \ W(x)=W_1(x)$$

in its formulation. Then there exist polynomials $U_1^{(1)}(x)$ and $B_1^{(1)}(x)$:

$$U_1^{(1)}(x)=\sum_{k=M_1}^{M_2-1}b_k^{(1)}\varphi_k(x)\,,\ \ B_1^{(1)}(x)=\sum_{k=M_1}^{M_2-1}\varepsilon_k^{(1)}b_k^{(1)}\varphi_k(x),\ \ M_1=2^{m_1},\ \ M_2=2^{m_2}$$

satisfying the following conditions:

$$0<b_{k+1}^{(1)}<b_k^{(1)},\ \ k\in\left[M_1,M_2-1\right),\ \ \varepsilon_k^{(1)}=\pm1,k\in\left[M_1,M_2\right),$$

$$B_1^{(1)}(x)=W_1(x)\forall x\in G_1,\ \ \left|G_1\right|\geq1-\frac{\delta}{2^2}-2^{-n_1}\geq1-\frac{\delta}{2^1},$$

$$U_1^{(1)}(x)\chi_{[\beta_1,1)}(x)=0,\ \ \beta_1=2^{-m_1}<\frac{\theta}{2},$$

$$\max_{m\in[M_1,M_2)}\int_0^1\left|\sum_{k=M_1}^{m}\varepsilon_k^{(1)}b_k^{(1)}\varphi_k(x)\right|dx<5\int_0^1\left|W_1(x)\right|dx,$$

$$\int_0^1\left|U_1^{(1)}(x)\right|dx<\max_{m\in[M_1,M_2)}\int_0^1\left|\sum_{k=M_1}^{m}b_k^{(1)}\varphi_k(x)\right|dx<4^{-2-1}.$$

Again, we use Lemma 1 with

$$n_0=\log_2M_2,\ \ \theta=\min\left\{b_{M_2-1}^{(1)},2^{-8(1+2)}\right\},\ \ p_1=\frac{1}{4},\ \ p_2=\frac{3}{4},\ \ W(x)=\left\{W_1(x)-U_1^{(1)}(x)\right\}$$

in its formulation. Then, we determine polynomials $U_1^{(2)}(x)$ and $B_1^{(2)}(x)$ of the form

$$U_1^{(2)}(x)=\sum_{k=M_2}^{M_3-1}b_k^{(1)}\varphi_k(x),\ \ B_1^{(2)}(x)=\sum_{k=M_2}^{M_3-1}\varepsilon_k^{(1)}b_k^{(1)}\varphi_k(x)$$

satisfying the following conditions:

$$0<b_{k+1}^{(1)}<b_k^{(1)}<b_{M_{2,}-1}^{(1)},\ \ k\in\left[M_2,M_3-1\right),\ \ \varepsilon_k^{(1)}=\pm1,\ \ k\in\left[M_2,M_3\right),$$

$$U_1^{(2)}(x)\chi_{[\beta_2,1)}(x)=0,\ \ \beta_2=\frac{1}{M_2},$$

$$\int_0^1\left|\left\{W_1(x)-U_1^{(1)}(x)\right\}-B_1^{(2)}(x)\right|^p dx<4^{-8(1+2)},\ \ p\in\left(\frac{1}{4},\frac{3}{4}\right),$$

$$\int_0^1\left|U_1^{(2)}\right|dx<\max_{m\in[M_2,M_3)}\int_0^1\left|\sum_{k=M_2}^{m}b_k^{(1)}\varphi_k(x)\right|dx<4^{-2-1},$$

It is clear that by using an induction, one can determine a sequence of polynomials $\{U_n^{(1)}(x)\}_{n=1}^{\infty}$, $\{U_n^{(2)}(x)\}_{n=1}^{\infty}$ $\{Q_n^{(1)}(x)\}_{n=1}^{\infty}$, $\{Q_n^{(2)}(x)\}_{n=1}^{\infty}$ of the form

$$U_n^{(1)}(x)=\sum_{k=M_{2n-1}}^{M_{2n}-1}b_k^{(n)}\varphi_k(x),\ \ U_n^{(2)}(x)=\sum_{k=M_{2n}}^{M_{2n+1}-1}b_k^{(n)}\varphi_k(x),\qquad(3.3)$$

$$B_n^{(1)}(x)=\sum_{k=M_{2n-1}}^{M_{2n}-1}\varepsilon_k^{(n)}b_k^{(n)}\varphi_k(x),\ \ B_n^{(2)}(x)=\sum_{k=M_{2n}}^{M_{2n+1}-1}\varepsilon_k^{(n)}b_k^{(n)}\varphi_k(x),\qquad(3.4)$$

which, for all $n=1,2,..$, satisfy the conditions:

$$M_n=2^{m_n},\ \ \{m_n\}_{n=1}^{\infty}\nearrow^{\infty},\ \ \varepsilon_k^{(n)}=\pm1,\ \ k\in\left[M_{2n-1},M_{2n+1}\right),\qquad(3.5)$$

$$0<b_{M_{2n+1}}^{(n)}<...b_{k+1}^{(n)}\leq b_k^{(n)}<...\leq b_{M_{2n-1}}^{(n)},\ \ k\in\left(M_{2n-1},M_{2n+1}-1\right),\qquad(3.6)$$

$$B_n^{(1)}(x)=W_n(x),\quad \forall x\in G_n,\ |G_n|\geq 1-\frac{\delta}{2^n}, \tag{3.7}$$

$$U_n^{(1)}(x)\chi_{[\beta_{2n-1},1)}(x)=U_n^{(2)}(x)\chi_{[\beta_{2n},1)}(x)=0,\quad \beta_j=\frac{1}{M_j}\leq\theta, \tag{3.8}$$

$$\max_{m\in[M_{2n-1},M_{2n})}\int_0^1\left|\sum_{k=M_{2n-1}}^{m}b_k^{(n)}\varphi_k(x)\right|dx+\max_{m\in[M_{2n},M_{2n+1})}\int_0^1\left|\sum_{k=M_{2n},}^{m}b_k^{(n)}\varphi_k(x)\right|dx<4^{-n}, \tag{3.9}$$

$$\max_{m\in[M_{2n-1},M_{2n})}\int_0^1\left|\sum_{k=M_{2n-1}}^{m}\varepsilon_k^{(n)}b_k^{(n)}\varphi_k(x)\right|dx\leq 5\int_0^1|W_n(x)|dx, \tag{3.10}$$

$$\int_0^1\left|W_n(x)-\sum_{j=1}^{n}\left(U_j^{(1)}(x)+B_j^{(2)}(x)\right)\right|^p dx<2^{-8n},\quad p\in\left(\frac{1}{4^n},1-\frac{1}{4^n}\right). \tag{3.11}$$

It is clear that (see (3.3), (3.9))

$$\sum_{n=1}^{\infty}\left(\int_0^1\left|U_n^{(1)}(x)\right|dx+\int_0^1\left|U_n^{(2)}(x)\right|dx\right)<\sum_{n=1}^{\infty}2^{-n}. \tag{3.12}$$

We define the function $U(x)$ and the sequence of numbers $\{b_k\}_{k=0}^{\infty}$ in the following way:

$$U(x)=U_0(x)+\sum_{n=1}^{\infty}\left(U_n^{(1)}(x)+U_n^{(2)}(x)\right)=\sum_{n=0}^{\infty}b_k\varphi_k(x), \tag{3.13}$$

where

$$U_0(x)=\sum_{k=0}^{M_{1,}-1}\varphi_k(x), \tag{3.14}$$

$$b_k=1,\ \forall k\in[0,M_1),\ b_k=b_k^{(n)},\ k\in\left[M_{2n-1},M_{2n+1}\right),\ n=1,2,... \tag{3.15}$$

Using $(3.3),(3.6)(3.8)$ and (3.12) – (3.15), we get that

$U(x)\in L^1[0,1]$, $U(x)=0$, $x\in[\theta,1)$, $b_k>0$, $\forall k\in\mathbf{N}\cup\{0\}$ and $\{b_k\}_{k=0}^{\infty}\searrow$.

From the conditions (3.3), (3.9) and (3.13) – (3.15) for all $m\in[M_{2n-1},M_{2n+1})$, $n=1,2,...$ it follows

$$\int_0^1\left|\sum_{k=0}^{m}b_k\varphi_k(x)-U(x)\right|dx\leq\sum_{j=n+1}^{\infty}\left(\int_0^1\left|U_j^{(1)}(x)\right|dx+\int_0^1\left|U_j^{(2)}(x)\right|dx\right)\leq$$

$$\leq\max_{m\in[M_{2n-1},M_{2n})}\int_0^1\left|\sum_{k=M_{2n-1}}^{m}b_k^{(n)}\varphi_k(x)\right|dx+\max_{m\in[M_{2n},M_{2n+1})}\int_0^1\left|\sum_{k=M_{2n},}^{m}b_k^{(n)}\varphi_k(x)\right|dx<2^{-n}.$$

From this it follows that the series $\sum_{k=0}^{\infty}b_k\varphi_k(x)$ converges to $U(x)$ in $L^1[0,1]$, and therefore

$$b_k=c_k(U),\ k=0,1,2,... \quad . \tag{3.16}$$

Thus, the Fourier series of the function $U(x)$ in the Walsh system converges in $L^1[0,1]$, and $\{c_k(U)\}_{k=0}^{\infty} \searrow 0$.

We set

$$\varepsilon_k = \begin{cases} 1, \text{if } k \in [0, M_1) \cup \left(\bigcup_{n=1}^{\infty} [M_{2n-1}, M_{2n}) \right), \\ \varepsilon_k^{(n)}, \text{ if } k \in [M_{2n}, M_{2n+1}), n \geq 1. \end{cases} \tag{3.17}$$

We will prove that the series (see (3.3), (3.4), (3.14) – (3.17))

$$\sum_{k=0}^{\infty} \varepsilon_k c_k(U) \varphi_k(x) = U_0(x) + \sum_{j=1}^{\infty} \left(U_j^{(1)}(x) + B_j^{(2)}(x) \right), \varepsilon_k = \pm 1 \tag{3.18}$$

is universal in $M[0,1)$ in the usual sense.

We set

$$E_n = \left\{ x \in [0,1]; \left| W_n(x) - \sum_{j=1}^{n} \left(U_j^{(1)}(x) + B_j^{(2)}(x) \right) \right| \leq 2^{-n} \right\}. \tag{3.19}$$

By (3.11) and (3.19) it follows that

$$2^{-n} \left| [0,1] \setminus E_n \right| \leq \int_0^1 \left| W_n(x) - \sum_{j=1}^{n} \left(U_j^{(1)}(x) + B_j^{(2)}(x) \right) \right|^{\frac{1}{2}} dx \leq$$

$$\leq \int_0^1 \left| W_n(x) - \sum_{j=1}^{n} \left(U_j^{(1)}(x) + B_j^{(2)}(x) \right) \right|^{\frac{1}{2}} dx \leq 2^{-3n}.$$

From this we have

$$\left| E_n \right| \geq 1 - 2^{-2n+1}. \tag{3.20}$$

We put

$$E = \bigcup_{k=1}^{\infty} \bigcap_{n=k}^{\infty} E_n. \tag{3.21}$$

It is clear that (see (3.20) and (3.21)) $|E| = 1$.

It is not hard to see that for all $x \in E$

$$\lim_{n \to \infty} \left(W_n(x) - \sum_{j=1}^{n} \left(U_j^{(1)}(x) + B_j^{(2)}(x) \right) \right) = 0. \tag{3.22}$$

Let $f(x) \in M[0,1)$.

Applying Lemma 2, one can find a subsequence $\{W_{n_q}(x)\}_{q=1}^{\infty}$ from the sequence (3.1), such that

$$\lim_{q \to \infty} W_{n_q}(x) = f(x) - U_0(x) \tag{3.23}$$

almost everywhere on $[0,1]$.

By (3.22) we have

$$\lim_{q\to\infty}\left(W_{n_q}(x)-\sum_{j=1}^{n_q}\left(U_j^{(1)}(x)+B_j^{(2)}(x)\right)\right)=0. \tag{3.24}$$

almost everywhere on $[0,1]$.

We put $N_q=M_{n_q}-1$. Taking into account (3.3), (3.4), (3.17), (3.23) and (3.24), it follows that

$$\sum_{k=0}^{N_q}\varepsilon_k c_k(U)\varphi_k(x)=U_0(x)+\sum_{j=1}^{n_q}\left(U_j^{(1)}(x)+B_j^{(2)}(x)\right)$$

converges to $f(x)$ almost everywhere on $[0,1]$. Thus, the series (3.18) is universal in $M[0,1)$, that is the function U is conditional universal for the class $M[0,1]$ with respect to the Walsh system.

Now we will prove assertions $c)$ and $d)$ of Theorem 6. We put

$$G=\bigcap_{n=1}^{\infty}G_n, \tag{3.25}$$

Obviously (see (3.7), (3.25))

$$|G|\ge 1-\delta. \tag{3.26}$$

Let $g(x)\in L^1[0,1)$. In the sequence (3.1) we select a subsequence $\{W_{k_q}(x)\}_{q=1}^{\infty}$ such that the following conditions

$$\lim_{N\to\infty}\int_0^1\left|\sum_{q=1}^{N}W_{k_q}(x)-\left(g(x)-U_0(x)\right)\right|dx=0, \tag{2.27}$$

$$\int_0^1\left|W_{k_q}(x)\right|dx<2^{-8q},\ \ \forall q\ge 2 \tag{3.28}$$

are satisfied.

Assume that the numbers $\nu_1=k_1<\ldots<\nu_{q-1}$, the functions $W_{\nu_1}(x),\ldots,W_{\nu_{q-1}}(x)$, $f_1(x),\ldots,f_{q-1}(x)$, and the polynomials $B_{\nu_1}^{(1)}(x), U_{\nu_1}^{(2)}(x)\ldots B_{\nu_{q-1}}^{(1)}(x), U_{\nu_{q-1}}^{(2)}(x)$ satisfying the following conditions:

$$f_n(x)=W_{k_n}(x),\ x\in G, 1\le n\le q-1,$$

$$\int_a^b\left|f_n(x)\right|dx<2^{-(n+1)},\ 1<n\le q-1,$$

$$\int_0^1\left|\sum_{j=1}^{l}\left[f_j(x)-\left(\sum_{n=\nu_{j-1}+1}^{\nu_j-1}U_n(x)+B_{\nu_j}^{(1)}(x)+U_{\nu_j}^{(2)}(x)\right)\right]\right|dx< \tag{3.29}$$

$$<2^{-2(l+1)},\ 1<l\le q-1,\ (\nu_0=0).$$

are already determined, where

$$U_n(x)=U_n^{(1)}(x)+U_n^{(2)}(x). \tag{3.30}$$

We choose a function $W_{\nu_q}(x)$, $\nu_q>\nu_{q-1}$ from the sequence (3.1) so that

$$\int_0^1\left|\left\{W_{k_q}(x)-\sum_{j=1}^{q-1}\left[f_j(x)-\left(\sum_{n=\nu_{j-1}+1}^{\nu_j-1}U_n(x)+B_{\nu_j}^{(1)}(x)+U_{\nu_j}^{(2)}(x)\right)\right]\right\}-W_{\nu_q}(x)\right|dx\le \tag{3.31}$$

$$\le 2^{-3(q+3)}.$$

By (3.28), (3.29) and (3.31), we obtain

$$\int_a^b\left|W_{\nu_q}(x)\right|dx<2^{-(q+1)}. \tag{3.32}$$

From this and (3.10) it follows that

$$\int_0^1\left|B_{\nu_q}^{(1)}(x)\right|dx\le \max_{m\in\left[M_{2\nu_q-1},M_{2\nu_q}\right)}\int_0^1\left|\sum_{k=M_{2\nu_q-1}}^{m}\varepsilon_k^{(\nu_q)}b_k^{(\nu_q)}\varphi_k(x)\right|dx\le 5\int_0^1\left|W_{\nu_q}(x)\right|dx< \tag{3.33}$$

$$<2^{-(q+1)}.$$

We put

$$f_q(x)=W_{k_q}(x)+\left[B_{\nu_q}^{(1)}(x)-W_{\nu_q}(x)\right],\ q\ge 1. \tag{3.34}$$

From (3.7) and (3.34) we have

$$f_q(x)=W_{k_q}(x),\ x\in G,\ q\ge 1. \tag{3.35}$$

Next, taking (3.3), (3.9), (3.29) – (3.31) and (3.34) into account for all $q\ge 1$ we find that

$$\left(\int_0^1\left|\sum_{j=1}^{q}\left[f_j(x)-\left(\sum_{n=\nu_{j-1}+1}^{\nu_j-1}U_n(x)+B_{\nu_j}^{(1)}(x)+U_{\nu_j}^{(2)}(x)\right)\right]\right|dx\right)\le$$

$$\le\int_0^1\left|\left\{W_{k_q}(x)-\sum_{j=1}^{q-1}\left[f_j(x)-\left(\sum_{n=\nu_{j-1}+1}^{\nu_j-1}U_n(x)+B_{\nu_j}^{(1)}(x)+U_{\nu_j}^{(2)}(x)\right)\right]\right\}-W_{\nu_q}(x)\right|dx+$$

$$+\left(\int_0^1\left|\sum_{j=1}^{q-1}\left[f_j(x)-\left(\sum_{n=\nu_{j-1}+1}^{\nu_j-1}U_n(x)+B_{\nu_j}^{(1)}(x)+U_{\nu_j}^{(2)}(x)\right)\right]\right|dx\right)+$$

$$+\sum_{k=\nu_{q-1}+1}^{\nu_q-1}\left(\int_0^1\left|U_k^{(1)}(x)\right|dx+\int_0^1\left|U_k^{(2)}(x)\right|dx\right)+\int_0^1\left|U_{\nu_q}^{(2)}(x)\right|dx<2^{-2q-2}. \tag{3.36}$$

Finally, it follows from (3.28), (3.32) – (3.34) for all $q\ge 1$ that

$$\int_a^b\left|f_q(x)\right|dx\le\int_a^b\left|W_{k_q}(x)\right|dx+\int_a^b\left|B_{\nu_q}^{(1)}(x)\right|dx+\int_a^b\left|W_{\nu_q}(x)\right|dx<$$

$$<2^{-8q}+6\int_a^b\left|W_{\nu_q}(x)\right|dx<2^{-q-1}\ . \tag{3.37}$$

Clearly, using induction we can define increasing natural numbers $\nu_1<\ldots<\nu_q<\ldots$, functions $W_{\nu_1}(x),\ldots,W_{\nu_q}(x)\ \ldots$, $g_1(x),\ldots,g_q(x)\ldots$, and polynomials $U_{\nu_1}^{(1)}(x),\ \ldots,\ U_{\nu_q}^{(1)}(x),\ldots$ to satisfy (3.31) – (3.37) for any $q\ge 1$.

It is clear that (see (3.37))

$$\sum_{q=1}^{\infty}\int_0^1\left|f_q(x)\right|dx<\infty. \tag{3.38}$$

We now determine the required function $f(x)$ and the sequence of numbers $\{\eta_k\}_{k=1}^{\infty}$ as follows:

$$f(x)=U_0(x)+\sum_{q=1}^{\infty}f_q(x), \tag{3.39}$$

$$\eta_k=\begin{cases}1,\ k\notin\bigcup\limits_{q=1}^{\infty}\left[M_{2\nu_q-1},M_{2\nu_q}\right)\\ \varepsilon_k^{(\nu_q)},\ k\in\left[M_{2\nu_q-1},M_{2\nu_q}\right),\ \ q=1,2,...\end{cases} \tag{3.40}$$

Using (3.27), (3.35), (3.38), and (3.39) we conclude that

$$f\in L^1[0,1];\ \ f(x)=g(x),\ \ \ x\in G.$$

Taking (3.3), (3.4), (3.13) – (3.16), (3.30), (3.36), (3.37), (3.39), and (3.40) into account, we find that

$$\left(\int_0^1\left|\sum_{k=0}^{M_{2\nu_q+1}-1}\eta_k c_k(U)\varphi_k(x)-f(x)\right|dx\right)\le$$

$$\le\left(\int_0^1\left|\sum_{j=1}^{q}\left[f_j(x)-\left(\sum_{n=\nu_{j-1}+1}^{\nu_j-1}U_n(x)+B_{\nu_j}^{(1)}(x)+U_{\nu_j}^{(2)}(x)\right)\right]\right|dx\right)+ \tag{3.41}$$

$$+\sum_{j=q+1}^{\infty}\left(\int_0^1\left|f_j(x)\right|dx\right)<2^{-q},$$

from this and (3.5) and (3.40) we have

$$\eta_k c_k(U)=c_k(f),\ \ \ \eta_k=\pm1,\ \ \left(\left|c_k(f)\right|=c_k(U)\right),\ \ k=0,1,2,...\ . \tag{3.42}$$

Let $m\ge1$. Then for some $q\ge1$, $m\in\left[M_{2\nu_q-1},M_{2\nu_q+1}\right)$, and therefore

$$\sum_{k=0}^{m}c_k(f)\varphi_k(x)=\sum_{k=0}^{M_{2\nu_q+1}}c_k(f)\varphi_k(x)+\sum_{k=M_{2\nu_q-1}}^{m}c_k(f)\varphi_k(x). \tag{3.43}$$

Taking (3.3), (3.4), (3.29), (3.30), (3.34), and (3.40) – (3.43) into account, we get

$$\left(\int_0^1\left|\sum_{k=0}^{m}c_k(f)\varphi_k(x)-f(x)\right|dx\right)\le\left(\int_0^1\left|\sum_{k=0}^{M_{2\nu_q+1}}\eta_k c_k(U)\varphi_k(x)-f(x)\right|dx\right)+$$

$$+\left(\int_0^1\left|\sum_{k=M_{2\nu_q-1}}^{m}\eta_k c_k(U)\varphi_k(x)\right|dx\right)\le2^{-q}+\left(\int_0^1\left|\sum_{k=M_{2\nu_q-1}}^{m}\varepsilon_k^{(\nu_q)}b_k^{(\nu_q)}\varphi_k(x)\right|dx\right)+$$

$$\sum_{n=\nu_{q-1}+1}^{\nu_q-1}\left(\max_{m\in[M_{2n-1},M_{2n})}\int_0^1\left|\sum_{k=M_{2n-1}}^{m}b_k^{(n)}\varphi_k(x)\right|dx+\max_{m\in[M_{2n},M_{2n}+1)}\int_0^1\left|\sum_{k=M_{2n}}^{m}b_k^{(n)}\varphi_k(x)\right|dx\right)\le 2^{-q-1}$$

From this (since if $m\to\infty$ then as $q\to\infty$) it follows that the Fourier–Walsh series of the corrected function f converges to it in $L^1[0,1]$.

Theorem 6 is proved.

References

[1] Grigoryan M. G., *On the universal and strong (L^1,L^∞)-property related to Fourier–Walsh series*, Banach J. Math. Anal. **11** (2017), no. 3, 698–712. https://doi.org/10.1215/17358787-2017-0012

[2] Grigoryan M. G., Sargsyan A. A., *On the universal function for the class $L^p[0,1]$, $p\in(0,1)$*, J. Funct. Anal. **270** (2016), no. 8, 3111–3133. https://doi.org/10.1016/j.jfa.2016.02.021

[3] Grigoryan M. G., *Functions, universal with respect to the classical systems*, Adv. Oper. Theory **5** (2020), no. 4, 1414–1433. https://doi.org/10.1007/s43036-020-00051-z

[4] Grigoryan M. G., Sargsyan, A. A., *The structure of universal functions for $L^p[0,1]$, $p\in(0,1)$-spaces*, Sb. Math. **209** (2018), no. 1, 35–55. https://doi.org/10.1070/SM8806

[5] Grigoryan M. G., Galoyan L. N., *On the universal functions*, J. Approx. Theory **225** (2018), 191–208. https://doi.org/10.1016/j.jat.2017.08.003

[6] Grigoryan M. G., Galoyan L. N.: *On Fourier series that are universal modulo signs*, Studia Math. **249** (2019), 215–231. https://doi.org/10.4064/sm180628-15-10

[7] Grigoryan M. G., *On universal Fourier series in the Walsh system*, Siberian Math. J. **63** (2022), 868–882. https://doi.org/10.1134/S0037446622050068

[8] Sargsyan A. A., Grigoryan M. G., *Universal function for a weighted space*, Positivity **21** (2017), 1457–1482. https://doi.org/10.1007/s11117-017-0479-8

[9] Grigoryan M. G., Konyagin S. V., *On Fourier series in the multiple trigonometric system*, Russian Math. Surveys **78** (2023), no. 4, 782–784. https://doi.org/10.4213/rm10112e

[10] Grigoryan M. G., Grigoryan T. M., Sargsyan A. A., *On the universal function for weighted spaces $L^p[0,1]$, $p\in[1,\infty)$*, Banach J. Math. Anal. **12** (2018), no 1, 104–125. https://doi.org/10.1215/17358787-2017-0044

[11] Grigoryan M. G., Galoyan L. N., *Functions universal with respect to the trigonometric system*, Izv. Math. **85** (2021), no. 2, 241–261. https://doi.org/10.1070/IM8964

[12] Grigoryan M. G., *On Fourier series almost universal in the class of measurable functions*, J. Contemp. Math. Anal. **57** (2022), no. 4, 215–221. https://doi.org/10.3103/S1068362322040069

[13] Grigoryan M. G., Sargsyan A. A., *On universal double Fourier series*, Math. Notes **117** (2025), no. 5, 874–879. https://doi.org/10.1134/S0001434625602837

[14] Grigoryan M. G., Galoyan L. N., *On conditionally universal functions*, J. Contemp. Math. Anal. **60** (2025), no. 2, 87–95. https://doi.org/10.3103/S1068362325700025

[15] Grigoryan M. G., *On universal (in the sense of signs) Fourier series with respect to the Walsh system*, Sb. Math. **215** (2024), no. 6, 717–742. https://doi.org/10.4213/sm10014e

[16] Birkhoff G. D., *Démonstration d'un théorème élémentaire sur les fonctions entières*, C. R. Acad. Sci. Paris **189** (1929), 473–475.

[17] Marcinkiewicz J., *Sur les nombres dérivés*, Fund. Math. **24** (1935), 305–308.

[18] Krotov V. G., *On the smoothness of universal Marcinkiewicz functions and universal trigonometric series*, Izv. Vyssh. Uchebn. Zaved. Mat. **8** (1991), 26–31.
[19] MacLane G. R., *Sequences of derivatives and normal families*, J. Anal. Math. **2** (1952), 72–87. https://doi.org/10.1007/BF02786968
[20] Luh W., *Universal approximation properties of overconvergent power series on open sets*, Analysis **6** (1986), 191–207. https://doi.org/10.1524/anly.1986.6.23.191
[21] Fekete M., *Untersuchungen über absolut konvergente Reihen mit Anwendung auf Dirichletsche und Fouriersche Reihen*, Math. Term. Ért. **32** (1914), 389–425.
[22] Grosse-Erdmann K.-G., *Holomorphe Monster und universelle Funktionen*, Mitt. Math. Semin. Giessen **176** (1987), 1–84.
[23] Men'shov D. E., *Universal sequences of functions*, Sb. Math. **65** (1964), no. 2, 272–312 (in Russian).
[24] Talalian A. A., *On the universal series with respect to rearrangements*, Izv. Akad. Nauk SSSR Ser. Mat. **24** (1960), 567–604 (in Russian).
[25] Ul'yanov P. L., *Representation of functions by series and classes $\phi(L)$*, Uspekhi Mat. Nauk **27** (1972), no. 2, 3–52 (in Russian). https://doi.org/10.1070/RM1972v027n02ABEH001370
[26] Krotov V. G., *Representation of measurable functions by series in the Faber–Schauder system and universal series*, Math. USSR-Izv. **11** (1977), no. 1, 205–218. https://doi.org/10.1070/IM1977v011n01ABEH001706
[27] Ivanov V. I., *Representation of functions by series in metric symmetric spaces without linear functionals*, Proc. Steklov Inst. Math. **189** (1990), 37–85.
[28] Grigorian M. G., *On the representation of functions by orthogonal series in weighted spaces*, Studia Math. **134** (1999), no. 3, 207–216. https://doi.org/10.4064/sm-134-3-207-216
[29] Gevorgyan G. G., Navasardyan K. A., *On Walsh series with monotone coefficients*, Izv. Math. **63** (1999), no. 1, 37–55. https://doi.org/10.1070/im1999v063n01ABEH000227
[30] Grigorian M. G., *On orthogonal series universal in* $L^p[0,1]$, $p>0$, J. Contemp. Math. Anal. **37** (2002), no. 2, 16–29.
[31] Kolmogoroff A. N., *Sur les fonctions harmoniques conjuguées et les séries de Fourier*, Fund. Math. **7** (1925), 24–29. https://doi.org/10.4064/fm-7-1-24-29
[32] Walsh J. L., *A closed set of normal orthogonal functions*, Amer. J. Math. **45** (1923), no. 1, 5–24.
[33] Paley R. E. A. C., *A remarkable set of orthogonal functions (I)*, Proc. Lond. Math. Soc. **34** (1932), no. 1, 241–264. https://doi.org/10.1112/plms/s2-34.1.241
[34] Watari C., *Mean convergence of Fourier–Walsh series*, Tohoku Math. J. **16** (1964), no. 2, 183–188.

Funding: This work was supported by the RA MSECS Higher Education and Science Committee, in the frames of the research: project 21AG-1A066.
Data Availability Statement: No data were generated or analyzed in this research.
Conflicts of Interest: The author declares no conflict of interest.

Reports of NAS RA
ՀՀ ԳԱԱ Զեկույցներ
NATIONAL ACADEMY OF SCIENCES OF THE REPUBLIC OF ARMENIA
ՀԱՅԱՍՏԱՆԻ ՀԱՆՐԱՊԵՏՈՒԹՅԱՆ ԳԻՏՈՒԹՅՈՒՆՆԵՐԻ ԱԶԳԱՅԻՆ ԱԿԱԴԵՄԻԱ

ԱՄՓՈՓԱԳԻՐ

Ուոլշի համակարգի նկատմամբ պայմանական ունիվերսալ ֆունկցիաների մասին

Մարտին Գրիգորյան[1,*]

[1]Երևանի պետական համալսարան, Ալեք Մանուկյան 1, 0025 Երևան, ՀՀ

[*]Հաղորդակցության համար՝ gmarting@ysu.am

Հոդվածում ապացուցվում է հեղինակի կողմից սահմանված պայմանական ունիվերսալ ֆունկցիաների և ունիվերսալ եռյակների գոյության վերաբերյալ թեորեմներ, որոնց ապացուցման համար կիրառված մեթոդը հանդիսանում է նոր մոտեցում չափելի ֆունկցիաների դասում Ուոլշի համակարգով ունիվերսալ շարքեր կառուցելու համար: Փոքր չափի բազմության վրա փոփոխելով գրեթե ամենուրեք վերջավոր, չափելի ցանկացած ֆունկցիայի արժեքները՝ ստանալ նոր ֆունկցիա, և այդ ուղղված ֆունկցիայի Ուոլշի համակարգով Ֆուրիեի շարքի անդամների համար համապատասխան նշաններ ընտրելով՝ այն դարձնել ունիվերսալ շարք չափելի ֆունկցիաների դասում:

Բանալի բառեր՝ Ունիվերսալ ֆունկցիա, Ֆուրիեի շարք, Ուոլշի համակարգ

Reports of NAS RA
ՀՀ ԳԱԱ Զեկույցներ
NATIONAL ACADEMY OF SCIENCES OF THE REPUBLIC OF ARMENIA
ՀԱՅԱՍՏԱՆԻ ՀԱՆՐԱՊԵՏՈՒԹՅԱՆ ԳԻՏՈՒԹՅՈՒՆՆԵՐԻ ԱԶԳԱՅԻՆ ԱԿԱԴԵՄԻԱ

2026 **Volume 126** **Issue 1** **Article No. 7**

Category: Chemistry
Type of Paper: Letter to the Editor
Received: January 24, 2026, **Revised:** January 29, 2026, **Accepted:** February 13, 2026
Published: April 16, 2026

DOI: 10.54503/0321-1339-2026.126.1-7

Pauling's Second Rule and Its Applications: From Inorganic Compounds to Understanding the Function of ATP

Artem R. Oganov[1,*]

[1]Skolkovo Institute of Science and Technology, Bolshoy Boulevard 30 bldg. 1, 121205 Moscow, Russia

[*]Correspondence: a.oganov@skoltech.ru

Abstract
Pauling's five rules for ionic crystals emerged as a generalization of the first experimentally determined crystal structures of inorganic compounds (primarily minerals). It was later discovered that the second rule (the rule of bond valence balance) is particularly powerful and universal. This essay explains how this rule can be used to explain very easily the differences in the chemistry of entire classes of chemical compounds (e.g., silicates and phosphates), as well as to elucidate the function of ATP as the universal energy currency for all life forms.

Keywords: mineralogy, biochemistry, chemical bonding

In Pauling's own words [1, 2] his second rule is stated as follows:

"Let *ze* be the electric charge of a cation and *v* its coordination number; we then define the strength of the electrostatic bond to each coordinated anion as

$$s = z/v \quad (1)$$

and make the postulate that in a stable ionic structure the valence of each anion, with changed sign, is exactly or nearly equal to the sum of the strengths of the electrostatic bonds to it from the adjacent cations, that is, that

$$\xi = \sum_i s_i = \sum_i z_i/v_i \ , \quad (2)$$

in which - ξe is the electric charge of the anion and the summation is taken over the cations at the centers of all the polyhedra of which the anion forms a corner".

Now it is well known that this rule is applicable not only to ionic crystals, but is universal. However, instead of electric charge in Eq. (1-2) one should use valence (i.e., the number of electrons donated or taken towards the formation of chemical bonds). The atomic charge is a vague concept with multiple possible definitions (see [3] for a very recently proposed new definition), whereas valence is well defined (at least in non-metallic substances). Also, *s* is now called bond valence – and it can be imagined that the valence of the cation is equally partitioned between all bonds formed by it, so each bond having the same valence *s*.

Let us illustrate how this rule works by considering silicates, all of which at normal pressure contain silicon in the tetrahedral coordination (Fig. 1a), surrounded by four oxygens (hence, silicon's coordination number v = 4). The valence of silicon is also equal 4, hence according to Eq. (1) the Si-O bond valence $s = 4/4 = 1$. Analogous calculation for the C-O bond in the CO_3-group (Fig. 1b) gives $s = 4/3$.

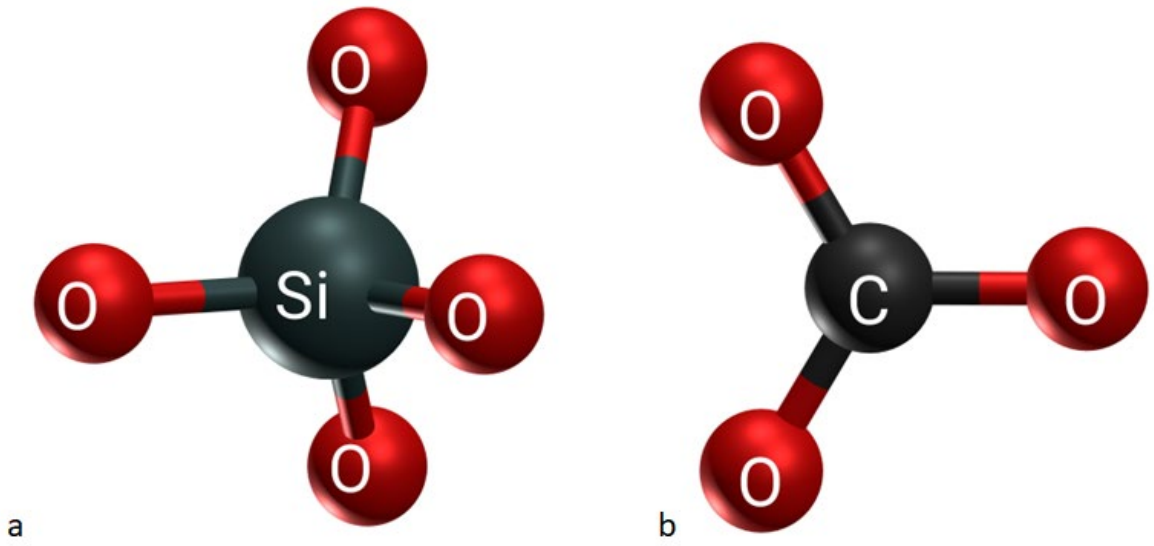

Figure 1. SiO_4-tetrahedron and CO_3 triangle found in all silicates and carbonates, respectively, at ambient pressure. The geometries shown here were taken from the crystal structure of minerals zircon ($ZrSiO_4$) and calcite ($CaCO_3$), but very similar geometries will be found in all other cases.

To satisfy Pauling's second rule, Eq. (2), the sum of bond valences on a given oxygen should equal oxygen's valence (equal to 2). How can this be satisfied? For silicates there are two ways – (1) an oxygen is shared by two SiO_4-tetrahedra, receiving one valence unit from each of the two neighboring silicon atoms (see Fig. 2a, where this is shown for SiO_2 quartz and $MgSiO_3$ enstatite), (2) an oxygen is shared by one SiO_4-tetrahedron (taking one valence unit from its silicon) and other cation polyhedra, the number of which is such that Eq. (2) is satisfied as precisely as possible. From these polyhedra the remaining one valence unit must come. Fig. 2c shows the structure of zircon $ZrSiO_4$, which can be assembled from SiO_4-tetrahedra and ZrO_8-units. The bond valence of each Zr-O bond is equal to the valence of Zr (it is equal to 4) divided by its coordination number (it is 8 in this structure), that is s(Zr-O)= ½. In the structure of zircon, each oxygen should therefore be bonded to one silicon and two zirconium atoms. Indeed, this is the case.

Note that it is forbidden for three SiO_4-tetrahedra to share the same oxygen atom – in this case the sum of Si-O bond valences on that oxygen would be equal to 3, which is very different from the valence of oxygen (two). Indeed, all the huge number of known silicate structures as well as all SiO_2 modifications (including glass) built from SiO_4-tetrahedra satisfy this rule. SiO_4-tetrahedra are allowed to polymerize sharing common oxygens, but no more than two tetrahedra can share the same oxygen.

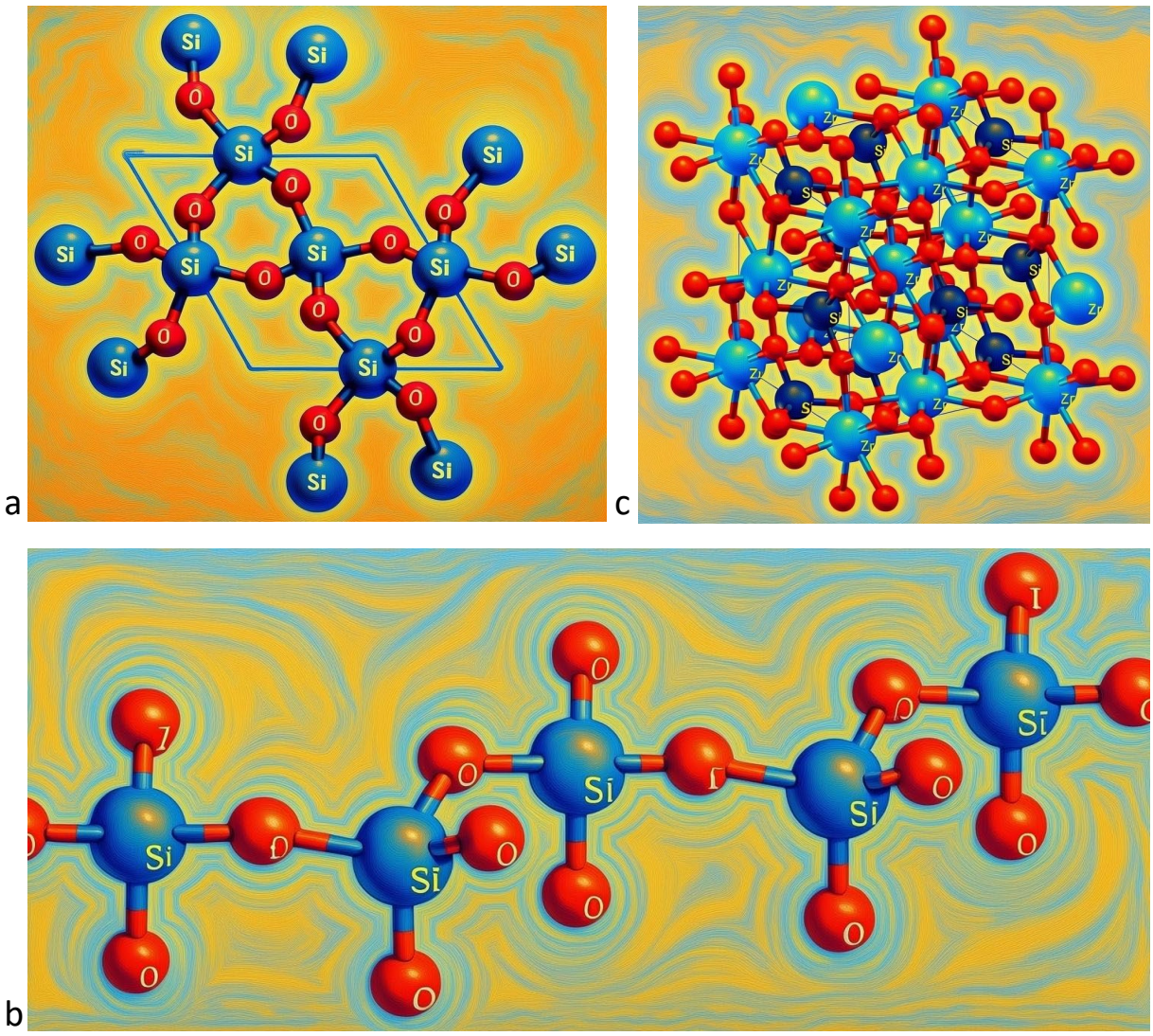

Figure 2. Some silicate motifs: (a) structure of quartz SiO_2, where corner-sharing SiO_4-tetrahedra form a 3D framework, (b) silicate chain from the structure of $MgSiO_3$ enstatite, where corner-sharing SiO_4-tetrahedra form an infinite 1D chain, (c) zircon $ZrSiO_4$, where there are no connections between SiO_4-tetrahedra.

Let us look at other classes of compounds. For example, carbonates at ambient pressure contain CO_3-triangles and (since carbon has valence 4) the valence of each C-O bond is equal to 4/3. If two such triangles share an oxygen, the oxygen will receive 8/3 = 2.67 valences from its neighboring carbons, which is much greater than oxygen's valence. Hence, Pauling's second rule forbids polymerization of CO_3-triangles, demanding that they be isolated from each other. The exceptions from this are extremely rare. At high pressures, however, coordination numbers increase and carbonates are based on CO_4-tetrahedra (e.g., [4]), the C-O bond valence is 4/4=1, just like in silicates, and polymerization of CO_4-tetrahedra is perfectly possible. All these expectations are fully consistent with both experimentally determined and predicted crystal structures.

Table 1 shows conclusions based on Pauling's second rule for various classes of compounds. This rule correctly predicts that borate ions (both BO_3-triangles and BO_4-tetrahedra) can polymerize, but nitrate-groups cannot (the only exception is the very reactive N_2O_5 molecule). This is again highly consistent with experiment. It is amazing how powerful this simple rule turns out to be.

Table 1. Inferences on crystal chemistry of various inorganic compounds from Pauling's second rule.

Class of compounds	Anionic group /cation-anion bond valence	Allowed to polymerize? /sum of bond valences on oxygen	Is polymerization observed?
Silicates	SiO_4 /1	Yes / 2	Yes, widely
Carbonates	CO_3 /1.33	No / 2.67	Almost never
High-pressure carbonates	CO_4 /1	Yes / 2	Yes, widely
Borates	BO_3 /1, BO_4 /0.75	Yes / 1.5-2.0	Yes, widely
Nitrates	NO_3 /1.67	No / 3.33	No, except N_2O_5
Phosphates	PO_4 /1.25	No / 2.5	Yes, sometimes
Sulfates	SO_4 /1.5	No / 3	Seldom
Chromates	CrO_4 /1.5	No / 3	Seldom
Perchlorates	ClO_4 /1.75	No / 3.5	No, except Cl_2O_7
Permanganates	MnO_4 /1.75	No / 3.5	No, except Mn_2O_7

Now let us step into a very interesting gray zone, going from the already discussed silicates (with SiO_4-groups) to phosphates (PO_4-groups) to sulfates (SO_4-groups) to perchlorates (ClO_4-groups). Along this series the valence of the central cation increases, and so does the bond valence, making polymerization of these tetrahedral ions more and more in violation of Pauling's second rule – by 0.5, 1.0, 1.5 valence units, respectively. Polymerization of MO_4-tetrahedra is unfavorable for M = P, S, Cl, progressively increasing in this series and making the polymeric structures highly reactive. For example, Cl_2O_7 molecule, the only known case of polymerization of ClO_4-groups, has a notoriously high enthalpy of formation from the elements, +238.1 kJ/mole in the liquid and +272.0 kJ/mole in the gaseous state [5], meaning that its formation from the elements is highly unfavorable. Cl_2O_7 exothermically reacts with water forming perchloric acid:

$$Cl_2O_7 + H_2O = 2HClO_4 \quad (3)$$

This can be viewed as hydrolytic cleavage of the Cl-O-Cl brigde. The experimental enthalpy of reaction (3) at room temperature is -33.43 kJ/mole [5]. Pyrosulfate-ion $S_2O_7^{2-}$ is well known, but is prone to hydrolysis similar to (3) and also exothermic by 68.55 kJ/mole [5]:

$$H_2S_2O_7 + H_2O = 2H_2SO_4 \quad (4)$$

Phosphate tetrahedra more easily polymerize forming well-known pyrophosphoric acid $H_4P_2O_7$, numerous oligophosphoric acids such as $H_5P_3O_{10}$ and $H_6P_4O_{13}$ and others, and metaphosphoric acid HPO_3 where corner-sharing PO_4-tetrahedra form infinite chains akin to metasilicate chain shown in Fig. 2b. Another limiting case is phosphoric anhydride P_4O_{10}, the structure of which is shown in Fig. 3a.

Hydrolysis reactions

$$H_4P_2O_7 + H_2O = 2H_3PO_4 \quad (5)$$

$$P_4O_{10} + 6H_2O = 4H_3PO_4 \quad (6)$$

have experimental enthalpies of -16.27 kJ/mole and -368.62 kJ/mole, respectively [5], at normal conditions, so both are exothermic. Unfavorable P-O-P linkages can be viewed as storing chemical energy. The former reaction corresponds to a hydrolysis of only one P-O-P linkage (carrying 16.3 kJ/mole worth of energy), whereas the latter has six (each one storing 61.4 kJ/mole worth of energy). The much greater value in the case of P_4O_{10} is due to its strained geometry. One can recall that P_4O_{10}

is widely used in chemical laboratories as a powerful dehydrating agent – precisely because of its highly exothermic reaction with water.

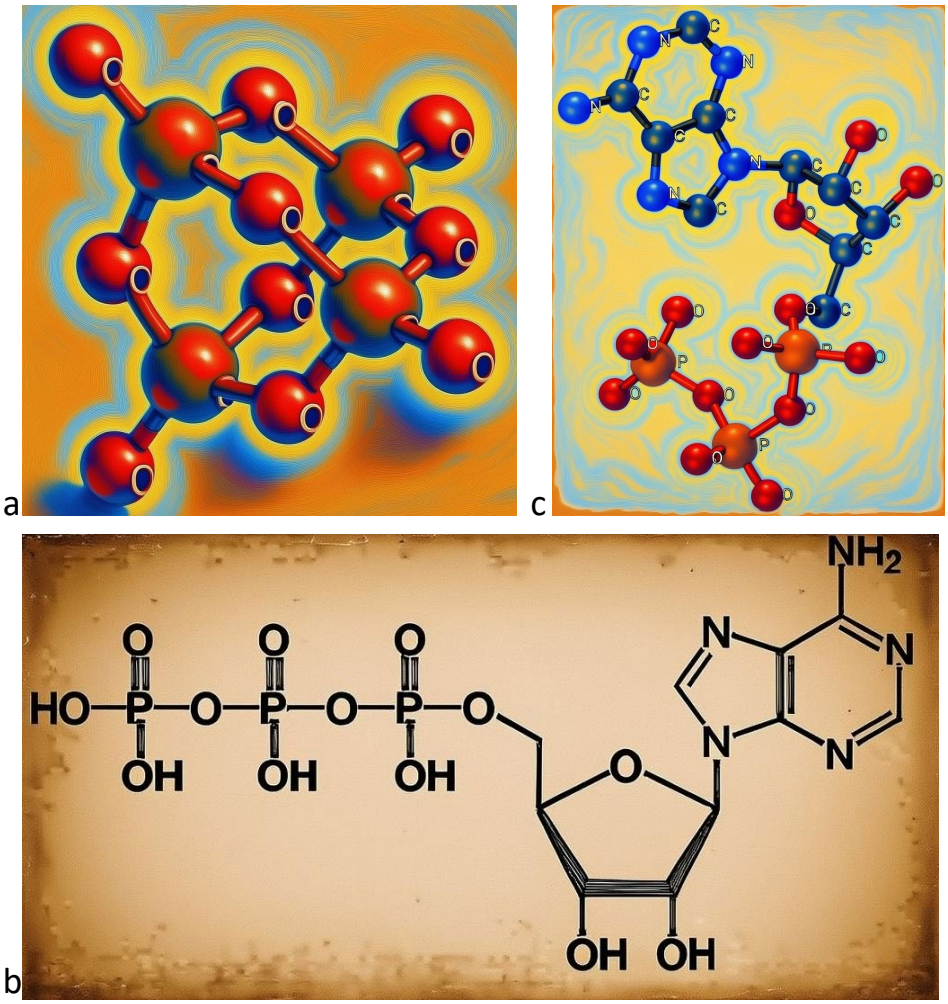

Figure 3. Polymerization of PO_4 tetrahedra: (a) in P_4O_{10}, (b,c) in adenosine triphosphate (ATP). (b) is a classical structural scheme of ATP, which does not reflect all aspects of 3D structure, (c) 3D-structure of ATP. The P-O-P angles in P_4O_{10} molecule and in ATP are 123° and 132-139°, respectively, reflecting the more strained bonding in P_4O_{10}. Note that hydrogen atoms are omitted in (c), as their positions were not reported in the experimental paper [6] (from which I plotted the structure) as X-ray is not sensitive to hydrogen atoms.

Another case is the sequential hydrolysis of adenosine triphosphate, ATP $(C_{10}H_{16}N_5P_3O_{13})^{4-}$ to adenosine diphosphate, ADP $(C_{10}H_{15}N_5P_2O_{10})^{3-}$ to adenosine monophosphate, AMP $(C_{10}H_{15}N_5P_2O_{10})^{2-}$:

$$ATP + H_2O = ADP + H_3PO_4 \quad (7)$$

$$ADP + H_2O = AMP + H_3PO_4 \quad (8)$$

The former reaction is exothermic by 30.5 kJ/mole, the latter by 15.1 kJ/mole [7]. Note that reactions (5) and (8) are directly analogous to each other, and their exothermic effects are very close.

Pauling's second rule not only explains structural chemistry of entire classes of inorganic compounds, but sheds light onto biological phenomena. All living cells share a small number of common, universal molecules – among them are ATP (the universal energy currency of all cells in all organisms), five nucleobases (building blocks of DNA and RNA), phospholipids (materials of cell membranes), twenty amino acids (building blocks of proteins), carbohydrates (structural polymers and fuel for cells). The most surprising thing in this list is the importance of phosphorylated organic molecules – ATP, nucleobases, phospholipids. Life is very economic and parsimonious, trying to use and reuse the same building blocks whenever possible. ATP and nucleobase adenosine have very different functions in the cell, but their sole chemical difference lies in the fact that ATP contains an inorganic triphosphate "tail". It is this triphosphate group that enables the energy storage/release function of ATP, as I discussed above. Why did nature choose phosphorus for that? Because abundant alternatives – silicon, carbon, sulfur, - are unsuitable. SiO_4-groups easily polymerize, but as the result of their polymerization is stable, no energy is stored. On the other hand, SO_4- and CO_3-groups tend not to polymerize at all, and whenever they do, the result is too unstable - yes, there is a great deal of energy stored in such compounds, but creating and keeping them is too difficult, as they are too easily hydrolyzed. Thus, the extraordinary biochemical role of phosphate is a result of a compromise. This extends even further: when nucleobases form a DNA or RNA molecule (which happens with direct participation of ATP), they join via phosphate PO_4-groups by means of phosphodiester linkages that act as a "glue" to hold DNA or RNA together. Each of these linkages is in slight violation of Pauling's second rule (with the sum of bond valences on the oxygen equal to 2.25), which makes it easier for enzymes to cleave DNA and RNA whenever needed. Once again, nature found a compromise – phosphodiester linkages are stable enough to be formed and maintained for a long time, but their small degree of instability (due to a slight violation of Pauling's rule) makes them suitable targets for enzymatic cleavage. DNA and RNA are thus easy to assemble and easy to disassemble, like a Lego constructor.

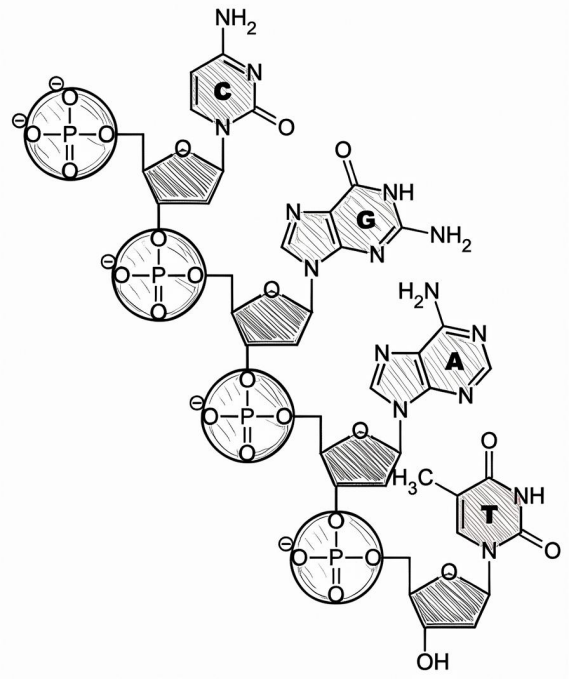

Figure 4. Four nucleobases (C = Cytozine, G = Guanine, A = Adenine, T = Thymine), joined by PO_4 tetrahedra to form a strand of DNA. RNA strand is made of the same nucleobases, except that instead of thymine it contains uracil.

I believe that this view, inspired by inorganic crystal chemistry, will prove fruitful in biochemistry and other fields. Such simple and universal rules have always been fruitful in science.

References

[1] Pauling, L. (1929). The principles determining the structure of complex ionic crystals. *J. Am. Chem. Soc.* 51, 1010-1026. https://doi.org/10.1021/ja01379a006

[2] Pauling, L., *The Nature of the Chemical Bond*, Cornell University Press Ithaca, New York, 1960.

[3] Anisimov, V. I., Oganov, A. R., Korotin, D. M., Novoselov, D. Y., Shorikov, A. O., Belozerov, A. S. (2024). First-principles definition of ionicity and covalency in molecules and solids. *J. Chem. Phys.* 160, 144113. https://doi.org/10.1063/5.0202481

[4] Oganov, A. R., Glass, C. W., Ono, S. (2006). High-pressure phases of $CaCO_3$: crystal structure prediction and experiment. *Earth Planet. Sci. Lett.* 241, 95-103. https://doi.org/10.1016/j.epsl.2005.10.014

[5] Wagman, D. D., Evans, W. H., Parker, V. B., Schumm, R. H., Halow, I., Bailey, S. M., Churney, K. L., Nuttall, R. L. (1982). The NBS taBles of chemical thermodynamic properties Selected values for inorganic and C1 and C2 organic substances in SI units. *J. Phys. Chem. Ref. Data* 11, Supplement No. 2.

[6] Kennard, O., Isaacs, N. W., Motherwell, W. D. S., Coppola, J. C., Wampler, D. L., Larson, A. C. (1971). The crystal and molecular structure of adenosine triphosphate. *Proc. Roy. Soc. London A* (1971) 325, 401–436. https://doi.org/10.1098/rspa.1971.0177

[7] Berg, J. M., Tymoczko, J. L., Stryer, L. (2007). *Biochemistry*. W. H. Freeman: New York, NY.

Acknowledgments: I am grateful to A.S. Saghyan and R.M. Aroutiounian for their invitation to write this article.

Conflicts of Interest: The author declares no conflicts of interest.

Reports of NAS RA
ՀՀ ԳԱԱ Զեկույցներ
NATIONAL ACADEMY OF SCIENCES OF THE REPUBLIC OF ARMENIA
ՀԱՅԱՍՏԱՆԻ ՀԱՆՐԱՊԵՏՈՒԹՅԱՆ ԳԻՏՈՒԹՅՈՒՆՆԵՐԻ ԱԶԳԱՅԻՆ ԱԿԱԴԵՄԻԱ

2026 **Volume 126** **Issue 1** **Article No. 8**

Category: Geology
Type of Paper: Original Research Article
Received: January 20, 2026, **Revised:** February 24, 2026, **Accepted:** March 16, 2026
Published: April 1, 2026

DOI: 10.54503/0321-1339-2026.126.1-8

Integrated Mapping of Active Faults and Seismic Hazard Evaluation for the example of Haiti

Ara Avagyan[1*], Samira Philip-Rebai[2], Claude Prepetit[3] and Roberte Monplaisir[4]

[1]Institute of Geological Sciences NAS RA, Baghramyan 24a, 0019 Yerevan, Armenia
[2]Independent Consultant in Natural Risk Reduction and Climate Change Adaptation: 80 rue de la Tour de Candelon, 34090 Montpellier, France
[3]Bureau des Mines et de l'Energie d'Haiti et de l'Unité Technique de Sismologie (UTS), Haiti
[4]Faculty of Sciences, State University of Haiti

[*]Correspondence: avagn1064@gmail.com

Abstract

This study presents a comprehensive mapping and analysis of active onshore and offshore faults in the North-West and South peninsula of Haiti, with implications for seismic hazard assessment. Field investigations (2017-2019), high-resolution satellite imagery, morphotectonic analysis, and structural data were integrated to identify and characterize major and secondary active faults. Kinematic analyses of onshore active faults indicate a dominant NNE–SSW compressional regime with oblique deformation. This pattern aligns with the regional stress field imposed by the relative motion of the Caribbean and North American plates. Despite limited historical seismicity, geomorphic and structural evidence demonstrates the recent and ongoing activity on the identified onshore faults. Deterministic seismic hazard assessment, incorporating fault geometry, segmentation, and kinematics, was conducted to estimate physically plausible maximum magnitudes (Mmax) and peak ground accelerations using multiple ground-motion prediction equations. Results indicate the highest onshore PGA values (up to ≥0.42 g) are associated with the Enriquillo–Plantain Garden Fault Zone, while secondary faults also contribute significantly to local ground motions. These highlight the critical role of both major and secondary active faults in controlling regional seismic hazard and underscore the importance of integrating detailed fault mapping into hazard models, particularly in regions with limited historical seismic records.

Keywords: Haiti, active fault mapping, geological hazard, PGA calculation

1. Introduction

Haiti's physiography is dominated by a rugged and highly varied terrain that shapes both its environmental dynamics and land-use patterns. Approximately three-quarters of the country consist of mountainous formations, with half of these highlands characterized by slopes exceeding 40%. Complementing these rugged highlands, several low-lying plains covering roughly 7,000 km² or about one-quarter of the national surface provide important geographic and economic spaces. Haiti's 1,500-km-long coastline further contributes to the country's complex physiographic mosaic. This diverse

topographic framework plays a central role in shaping environmental processes, resource distribution, and human activities across the country, making it a critical factor to consider in any geographical or environmental analysis.

Geology

The study area is situated on the island of Hispaniola, part of the Antillean arc, a geologically complex chain characterized by a crystalline basement overlain since the Mesozoic by 2,000-6,000 m of sedimentary formations and coral structures (Carte géologique, 1982-1988). This tectonic framework produces a series of NW–SE oriented folds that create alternating anticlinal hills and synclinal valleys arranged in an arcuate pattern and frequently bounded by active faults (Escuder Viruete et al., 2006).

Hispaniola's mountainous core consists primarily of schists, conglomerates, and limestones (Carte géologique, 1982-1988), cut in places by syenitic intrusions. To both the north and south of this central nucleus, extensive Tertiary deposits are flanked by more recent limestones and gravels. The central and northern mountain chains include diverse lithologies: metamorphic units, sandstones, conglomerates, limestones, clays, and in several central and western sectors, these formations are disrupted by dykes and quartz veins, some of which are gold-bearing. Approximately half of the island's surface is covered by Neogene-Quaternary alluvial deposits derived from erosion of the surrounding mountain slopes.

Coastal dynamics also contribute significantly to the island's geomorphic evolution. Coral growth and sediment input from rivers and torrents continually extend the coastline, resulting in widespread low-lying marshlands. The regional tectonic pattern is further shaped by a well-developed fault system, dominated in Haiti by major left-lateral strike-slip faults (Butterlin, 1954).

Current Geodynamic Setting

Haiti is located on the Caribbean Plate, within one of the most geodynamically active regions of the Americas. This zone marks the complex boundary between several interacting tectonic plates, most notably the Caribbean, North American, and South American plates (Fig. 1).

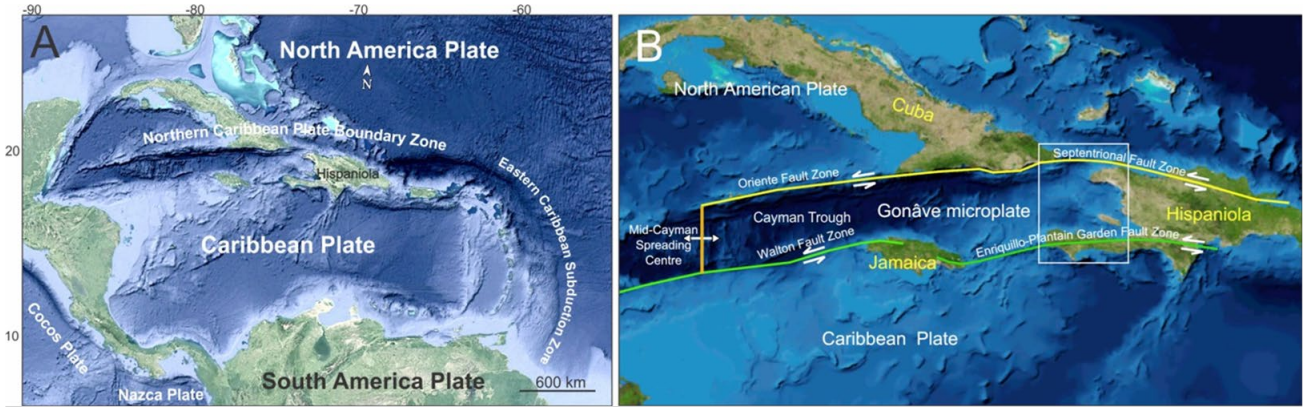

Figure 1. A-Tectonic setting of the Caribbean area on the Google satellite image. B-NASA World Wind Graphic (Public Domain) of faults around Haiti. The white rectangle indicates the study area.

The Caribbean Plate is being extruded eastward as a consequence of this confinement. Its movement is facilitated by the Eastern Caribbean Subduction Zone, which acts as a free boundary and accommodates ENE–WSW convergence with the Atlantic oceanic crust at a rate of approximately 2 cm/yr (DeMets et al., 2000).

Haiti lies within the Northern Caribbean Plate Boundary Zone (NCPBZ) (A, Fig. 1), a 250-km-wide deformation belt where the Caribbean Plate moves eastward relative to the North American Plate at roughly 20 mm/year (Calais, 1990). The oblique nature of this convergence generates a transpressional regime, producing both strike-slip motion and crustal shortening across Hispaniola (Mann et al., 2002).

Shortening is also significant, with GPS-derived rates of 5.2 ± 2 mm/year (Calais, 2002). It is expressed through folding and thrusting, including numerous structures identified during this study. The island is currently undergoing overall uplift, most pronounced in the northwest, where it has produced extensive sequences of Quaternary marine terraces (Carte géologique, 1982-1988) and alluvial fans. This uplift is accompanied by tectonically controlled fissural volcanism and by frequent deformation placed in Pliocene–Quaternary strata.

Seismicity reflects this active tectonic setting. Hispaniola's historical record shows at least one major earthquake per century: destructive events in 1751, 1771, 1842, 1887, 1904, 1946, and more recently the devastating 12 January 2010 earthquake.

The study area (white rectangle, B, Fig. 1) includes the most part of the Northern and Southern Peninsulas.

2. Methodology

Seismic hazard is particularly critical, motivating the development of a hazard analysis and the transfer of methodological expertise to national professionals.

Seismic-hazard assessment focuses on identifying seismic sources, estimating ground shaking, which can induce other phenomena as landslides, liquefactions, tsunamis etc. This requires an interdisciplinary framework combining structural geology, Quaternary geology, geomorphology, seismology, geophysics, and historical records extending the temporal window beyond the historical catalogue. The data are available from various sources, including archives, technical reports, previous studies and maps, satellite imagery, aerial photographs, field surveys, digital and non-digital databases, and local knowledge.

Existing information concerning abovementioned domains compiled, including historical and instrumental seismicity, geological and tectonic studies, maps, satellite and aerial imagery, and local knowledge obtained through a participatory approach.

Preliminary hazard evaluation realized throw active faults both onshore and offshore identification and characterization using document review, remote sensing, and field observations. Hazard scenarios is developed based on fault activity and potential magnitude. Distant sources capable of affecting the study area will also be considered.

Field investigations and GIS-based analysis refined the mapping and characterization of active faults, including those not historically documented. Methods include stratigraphic and structural analysis, morphotectonic mapping, surface geophysics.

Maximum magnitudes estimated using historical and empirical data (Coppersmith, 1991; Wells and Coppersmith, 1994). Ground-motion maps generated by modeling earthquake scenarios within each seismotectonic zone and applying appropriate attenuation relationships (Earthquake Spectra, 2008).

The following datasets were compiled for seismic hazard mapping and active fault analysis:

Seismicity Catalogs

- Historical and instrumental seismicity (USGS Open-File Report 2011–1133)
- Haiti seismicity catalog since 1973 (USGS)
- Instrumental seismicity, 2015-2018 (MBU)

Geological and Topographic Data

- Geological Map of the Republic of Haiti, 1:250,000 (Carte géologique, 1982-1988)

- Topographic maps at 1:50,000 scale
- Digital elevation models with 20 m contour intervals in GIS format (Centre Nationale De l'Information Géospatiale, CNIGS)
- Topographic map at 250 m resolution (CNIGS)

Remote Sensing and Imagery

- Aerial photographs
- LIDAR images at 0.5-1 m resolution (CNIGS)
- Google satellite imagery, 200 m resolution
- ESRI satellite imagery, 100 m resolution
- Aerial ortho-photographs, 1 m resolution (CNIGS)
- Satellite ortho-images at 15 m resolution (visible to thermal infrared), freely available from www.orthocoverage.com

Geophysical Data

- Marine geophysical survey images (Campagne océanographique HAITI-SIS N/O L'Atalante, Saint Domingue - Port au Prince Fort de France, 2012, Momplaisir, 1986; Leroy et al., 2015).

3. Tectonic Context

Thirtyfive GPS benchmarks were installed and repeatedly surveyed in Haiti, complemented by a network of 40 sites in the Dominican Republic, some of which record continuous displacement since 1994. These long-term geodetic observations provide quantification of elastic strain accumulation on major active faults (Manaker et al., 2008). Prior to 2010, these results already indicated that the Enriquillo–Plantain Garden Fault Zone (EPGFZ) in Haiti had accumulated sufficient strain to generate an earthquake of approximately Mw 7.2 (Manaker et al., 2008). The North American plate descends beneath the Caribbean—and dominantly strike-slip deformation along the Cayman Trough (B, Fig. 1) (Mann et al., 1984; Calais et al., 1992; Dolan et al., 1998). GPS measurements indicate that the Caribbean plate interior moves toward the ENE at 18-20 mm/year relative to the North American plate (Dixon et al., 1998; DeMets et al., 2000). This motion results in oblique convergence of Hispaniola and Puerto Rico with the oceanic lithosphere of North America (Mann et al., 2002).

In Hispaniola, this oblique convergence is partitioned between strike-slip motion along the Septentrional Fault Zone in the north and the EPGFZ in the south, and compressional deformation along the North Hispaniola thrust system (Dolan et al., 1998; Calais et al., 2002). The Mw 7.0 earthquake that devastated Port-au-Prince on 12 January 2010 (which resulted in more than 200,000 fatalities) and the Mw 7.2 earthquake on 14 August 2021 (with 2248 fatalities) occurred on one of the principal plate-boundary structures of the northern Caribbean: the EPGFZ (B, Fig. 1). Historical records suggest that the southern Haiti segment of the EPGFZ last ruptured during major earthquakes in 1751 and 1770, both likely near magnitude 7.5 (Ali et al., 2008). No comparable events have been reported since, although several moderate earthquakes (e.g., 1701, 1784, 1860, 1864, 1953) have affected the region. Thus, both the long-term kinematics of the plate boundary and the historical earthquake record consistently point to the EPGFZ as a major seismic source in Haiti, capable of generating damaging earthquakes at recurrence intervals on the order of centuries.

Kinematic block-model indicates slip rates of 9 ± 2 mm/year on the Septentrional Fault Zone and 7 ± 2 mm/year on the EPGFZ (Manaker et al., 2008). This left-lateral strike-slip system accommodates a significant portion of the relative motion between the Caribbean and North American plates (Mann et al., 1995; Dixon et al., 1998). Recent GPS measurements and high-resolution offshore seismic data within the transform Caribbean–North American plate boundary in southern Haiti, Greater Antilles, show 6-7 mm/year of plate boundary-normal shortening within a crustal sliver bounded to the south by the EPGFZ left-lateral strike-slip fault and to the north by a south-dipping reverse fault system offshore the northern coast of the Southern Peninsula of Haiti (Calais et al., 2023).

4. Active Fault Mapping

4.1. Regional-Scale Offshore Active Faults

Field investigations were conducted between 2017 and 2019 on the North and South Peninsulas of Haiti, within the Nord-Ouest, Grande-Anse, Nippes, and Sud departments (A, Fig. 2). The datasets used in this study are described in the Methodology section.

The contribution of offshore active structures to seismic hazard cannot be neglected, given their significance and high seismic potential (Fig. 1). Mercier et al. (2011) demonstrated the recent reactivation of one of these offshore faults located at the eastern extremity of the Southern Peninsula.

The investigation and mapping of offshore active faults were carried out through the analysis of bathymetric and marine geophysical data (e.g., Momplaisir, 1986; Leroy et al., 2015) (D, Fig. 2). A detailed morphotectonic analysis of these datasets allowed the clear identification of a set of submarine active faults framing both the North and South Peninsulas (B, C, Fig. 2).

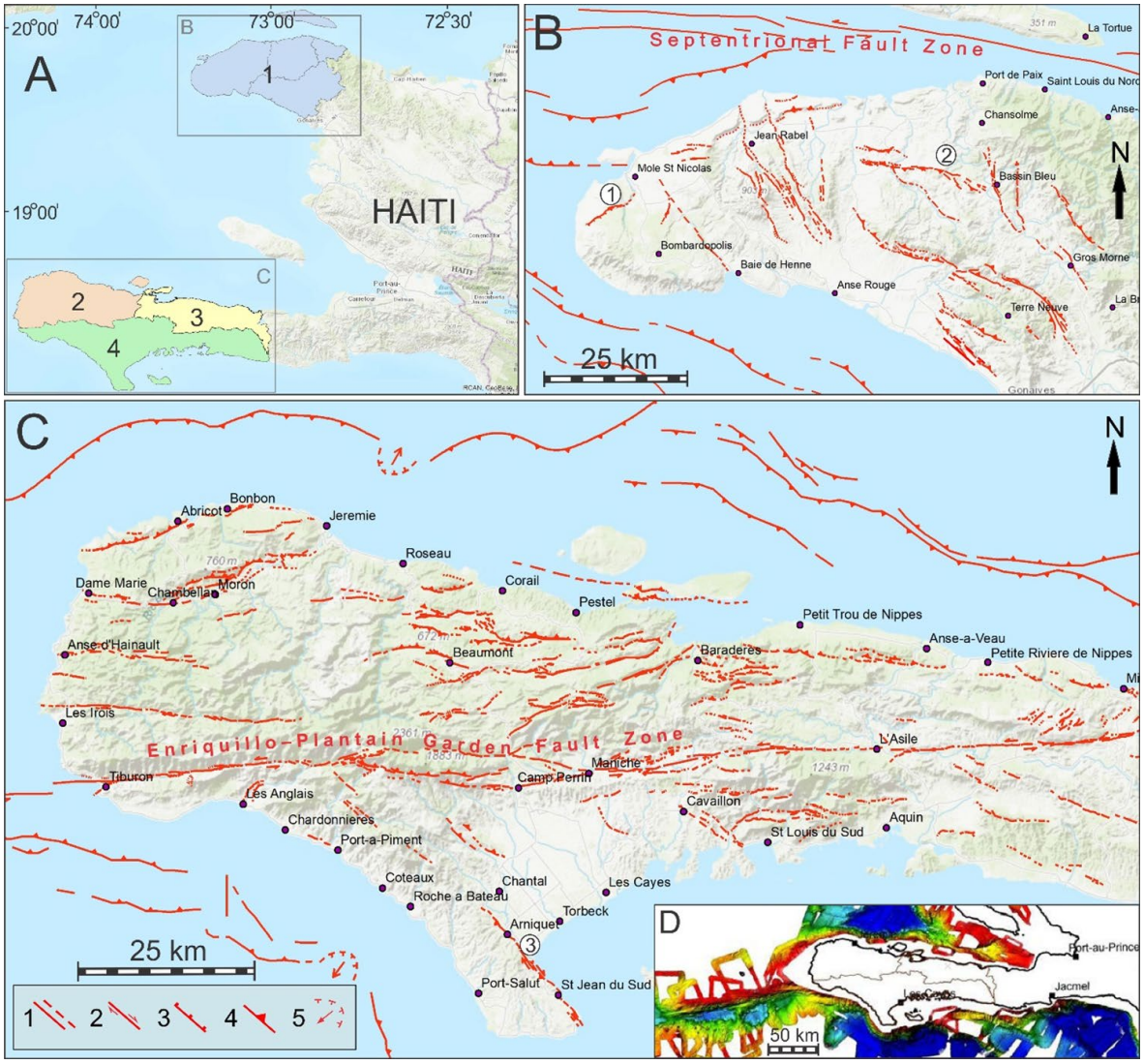

Figure 2. A-Departments of Haiti where the study was conducted: (1) Nord-Ouest, (2) Grande-Anse, (3) Nippes, (4) Sud. B, C-Synthesis maps of local- and regional-scale active onshore and offshore faults affecting the North-Western and Southern Peninsulas. (1) Active fault; (2) Active strike-slip fault; (3) Active normal fault; (4) Active reverse/thrust fault; (5) Landslide. D-3D bathymetric reconstruction of the coastal area of the Southern Peninsula (after the HAITI-SIS oceanographic campaign, R/V L'Atalante, Santo Domingo–Port-au-Prince–Fort-de-France, 2012; Momplaisir, 1986; Leroy et al., 2015).

Evidence for the activity of these faults is documented both directly—through their morphological expression on the seafloor based on bathymetric analysis and geophysical profiles—and indirectly, through morphostructural and geodynamic analyses of the coastlines of the North and South Peninsulas. Indeed, satellite image analysis and field observations reveal a series of uplifted marine terraces along the northern coastlines of both peninsulas. An example from the northwestern tip of the North Peninsula is shown in Figure 3. Seismogravitational fractures (indicated by white arrows) affect Quaternary reefal marine terraces.

These Quaternary (Carte géologique, 1982-1988) reefal limestone terraces testify to recent coastal uplift of approximately 0.19 mm/year, consistent with the kinematics of the offshore reverse faults identified in Figures 2B and 2C. The geometry and kinematics of these structures imply uplift of the southern block relative to the northern block, explaining the presence of raised terraces that record recurrent Quaternary activity. Very recent submarine landslides were also identified along these structures, likely associated with their recent reactivation (B, C, Fig. 2).

4.2. Identification of the Main Onshore Active Faults

The identification of active faults is generally based on instrumental and historical seismicity, morphostructural interpretation of satellite images, aerial photographs, and digital elevation models (DEMs). This approach allows the selection of major tectonic structures most likely to rupture in the future and, where possible, the characterization of their extent, segmentation, geometry, and kinematics.

The study area is characterized by numerous seismogravitational structures (normal faults, tilted terraces, etc.) (A, Fig. 3). Structures of purely tectonic origin (active faults) were distinguished from those of gravitational origin.

Numerous geological faults have been identified and mapped in the study area (Fig. 2), some of which were previously inferred to be active (Goreau, 1983; Momplaisir, 1986; Amilcar, 1997). In the present study, active fault identification and mapping were conducted at a scale of 1:50,000, locally refined to 1:10,000 and, in some cases, to outcrop scale (Figs. 4, 5, 6).

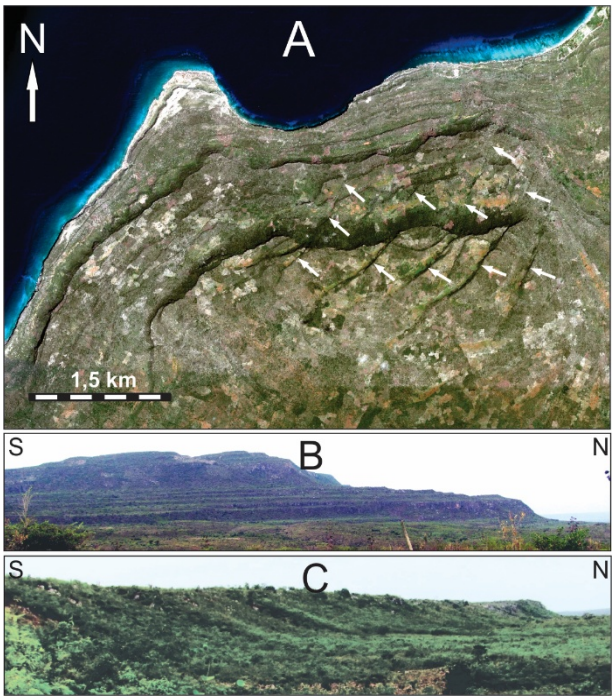

Figure 3. A-Seismogravitational fractures (white arrows) affecting Quaternary reef marine terraces along the northern margin of the North Peninsula, west of the town of Môle-Saint-Nicolas (B, Fig. 1), shown on a Google Earth image. B-Panoramic view of marine terraces from Môle-Saint-Nicolas. C-Detail of a marine terrace scarp.

One example is the Morne Basse active fault system (1 in B, Fig. 2), located in the northwestern part of the North-Western Peninsula, southwest of the town of Môle-Saint-Nicolas (Fig. 4). This normal fault strikes NE–SW (N61°) and extends for approximately 9.8 km. The western segment is particularly well expressed morphologically in aerial imagery, DEMs, and field observations (Fig. 4). The southeastern block is downthrown. Morphological analysis of LiDAR data indicates a cumulative vertical offset of $\leq 65 \pm 2$ m. The recent activity of this fault is demonstrated by stratigraphic, morphotectonic, and structural evidence, as it cuts Quaternary marine terraces after their uplift and deformation.

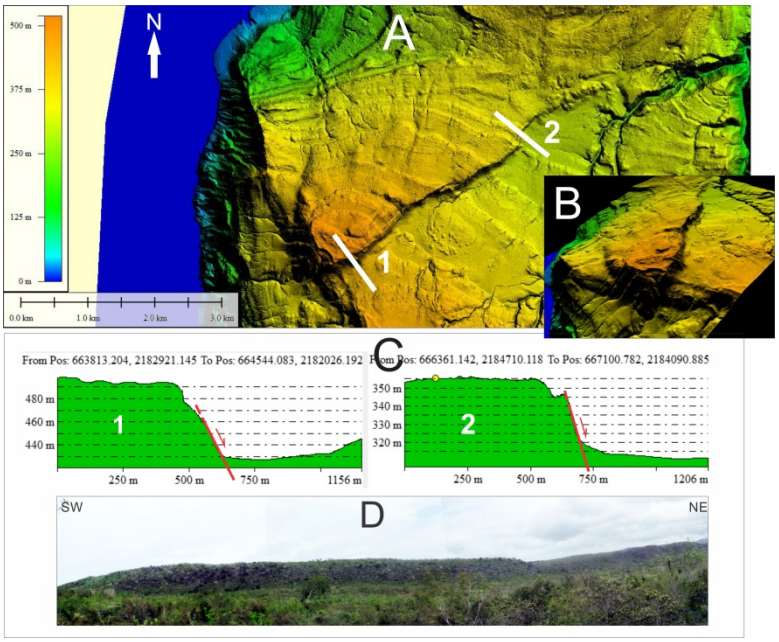

Figure 4. Morphological expression of the Morne Basse Fault system (location is indicated by circle 1 in B, Fig. 2) revealed by high-resolution DEMs (1 m) in 3D views (A, B) and topographic profiles (C: 1, 2). D-Field photograph of the fault scarp.

Another example studied at outcrop scale is the Morne Fouco–Morne Rampas Fault system (2 in B, Fig. 2; Fig. 5). This fault system extends for approximately 22 km, with an overall E–W orientation. It is segmented and exhibits reverse kinematics with a left-lateral strike-slip component. The fault juxtaposes Lower Cretaceous limestones against Upper Miocene marls. Morphologically, it is marked by a sharp and continuous topographic break, clearly visible in both satellite imagery and the field (Fig. 5).

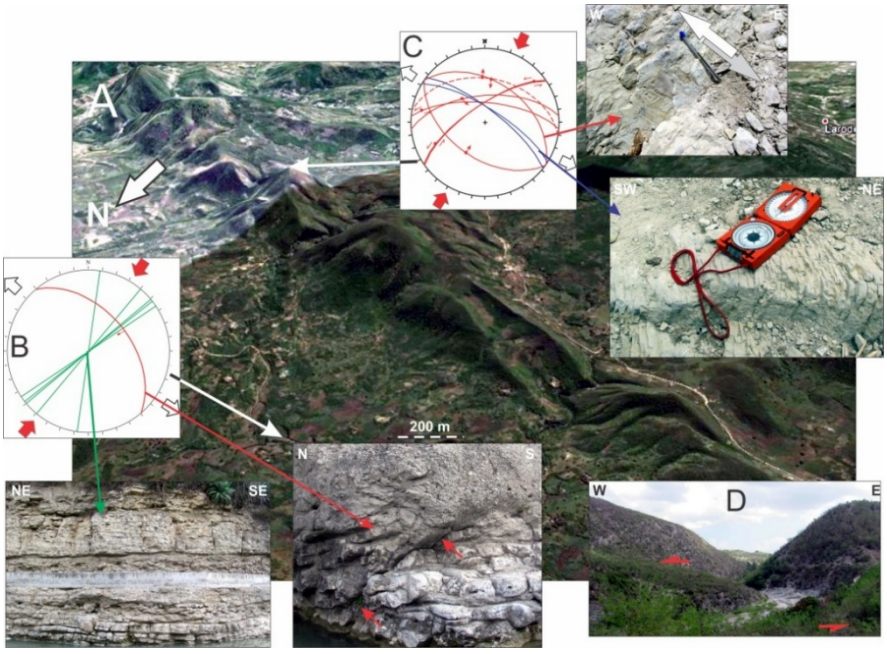

Figure 5. Central part of the Morne Fouco–Morne Rampas Fault segment (location is indicated by circle 2 in B, Fig. 2). This segment is expressed morphologically in satellite imagery (A-Google Earth view). Microtectonic analysis (on the lower hemisphere) of stations (B) and (C), located along the axis of this fault segment, indicates NNE-oriented compression and NW-oriented extension, based on both fracture analysis (green) and fault-slip data (red). D-Morphological expression of the eastern part of the Morne Rampas fault segment in the field, and left-lateral deflection of the Moustique River at the fault crossing.

Microtectonic analysis at two stations (B, C, Fig. 5) indicates NNE-directed compression and NW-directed extension, based on both fracture (green) and fault-slip (red) analyses. This implies oblique motion on the Morne Fouco–Morne Rampas Fault system, corresponding to reverse faulting with a left-lateral strike-slip component. This kinematics is further supported by the left-lateral offset of the Moustique River at the fault crossing (D, Fig. 5).

Despite the absence of known historical or instrumental earthquakes associated with this fault, its recent activity is unequivocal.

A third example is the Belsue–Saint-Jean-du-Sud Fault (3 in C, Fig. 2), approximately 50 km long and trending NNW–SSE. In its southern part, Mann et al. (1995) reported the presence of a fault segment, while Amilcar (1997) suggested a potential fault. Structural analysis conducted in this study confirms the presence of an active reverse fault with a right-lateral strike-slip component, consistent with the current regional stress field.

Towards the eastern basin filled with Quaternary sediments, the dip of limestones progressively increases from 35°E to 60°NE, eventually becoming near vertical. These limestones define a north-verging fold structure consistent with reverse fault kinematics. Approximately 2 km northwest of Saint-Jean-du-Sud (C, Fig. 2), a reverse fault striking N121° and dipping 21°SW was identified (B, C, D, Fig. 6). Secondary N017° strike-slip faults were also observed (E, Fig. 6).

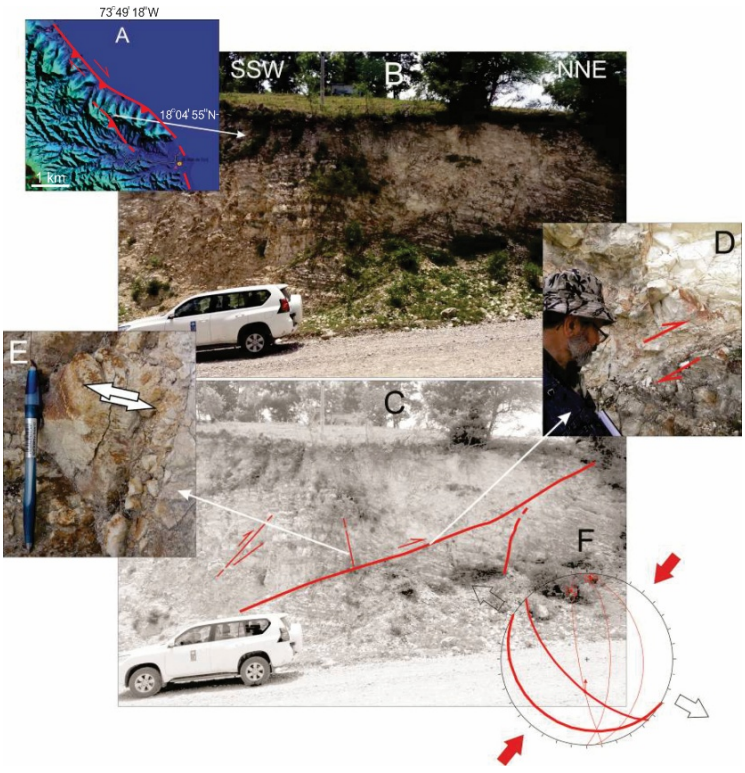

Figure 6. Reverse fault (B, C, D) striking N121° and dipping 21°SW was identified 2 km northwest of Saint-Jean-du-Sud (A) (Belsue–Saint-Jean-du-Sud Fault zone (3 in C, Fig. 2)). Location is indicated by circle 3 in C, Fig. 2. E-Secondary right-lateral strike slip fault. F- Faults representation on the lower hemisphere indicating NNE-oriented compression and NW-oriented extension.

Regarding the Haitian sector, the Enriquillo–Plantain Garden Fault Zone (EPGFZ) (C, Fig. 2) has long been recognized as a major seismic hazard. This fault system cuts across the entire Southern Peninsula of Haiti. To the east, it extends offshore toward eastern Jamaica, bounding the Gonâve microplate to the south (Fig. 1). To the west, it terminates offshore south of Hispaniola. Together with the Septentrional Fault Zone, it represents one of the two most significant fault systems in Haiti and has hosted major historical earthquakes.

These faults accommodate plate motion by accumulating elastic strain over decades to centuries before releasing it abruptly during earthquakes. Moreau de Saint-Méry (1797-1798) provided detailed accounts of the catastrophic destruction of Port-au-Prince and Léogâne during the 1751 and 1770 earthquakes. Since then, the region has repeatedly experienced seismic activity, including a major earthquake (estimated $M > 7$) in 1862 in the central Southern Peninsula (USGS Open-File Report 2011–1133).

In this study, particular attention was given to the EPGFZ in order to refine its seismogenic potential. Analysis of fault geometry, kinematics, and aerial photographs allowed the identification of three major segments, two of which cross the Nippes and Sud departments (Fig. 2).

5. Seismic Hazard Assessment

Seismic hazard assessment, including determination of maximum magnitude (Mmax) and peak ground acceleration (PGA), was carried out for the Nippes and Sud departments.

5.1. Evaluation of Maximum Magnitudes of Seismic Sources

Based on detailed mapping of seismic sources (active faults) in the study area, plausible rupture scenarios were defined for each structure, considering their geometry, kinematics, and segmentation (Fig. 2). Using a conservative approach and assuming the most plausible segmentations, maximum magnitudes were calculated using empirical relationships proposed by Coppersmith (1991) and Wells and Coppersmith (1994).

Twelve seismic sources were selected as having the greatest potential impact and were therefore included in the PGA calculations (Table 1; A, Fig. 7).

Table 1. Selected seismic sources (1-12, Fig. 12) and estimated Mmax values used for bedrock seismic acceleration (seismic hazard) assessment in the Sud and Nippes departments.

seismic zones	Id	Fault (length. km)	Segm.	Seg. len-gth. (km)	Kine - mat.	M max Cop. 91	Sig.	Mw max WC 94	Sig. 1	M max	Sig.
EPGFZ	1	EPGFZ, ~1000	West	102 ±8	-	7.41	0.03	7.4	0.04	7.41	0.03
	2	EPGFZ, ~1000	East	127 ±13	SS	7.52	0.05	7.52	0.04	7.52	0.05
Trois Baies	3	Trois-Baies, 107±7	-	-	R	7.43	0.03	7.47	0.03	7.47	0.03
Port salut-Tiburon	4	Port-Salut-Tiburon, 172±15	-	-	R	7.68	0.04	7.72	0.05	7.72	0,05
Ile a Vache	5	Ile a Vache, 115±15	-	-	R	7.47	0.06	7.51	0.06	7.51	0.06
Saint Louis du Sud-Bainet Nord	6	St Luis du Sud-Bainet Nord, 82±7	East - North	-	R	7.29	0.04	7.33	0.04	7.33	0.04
Bainet	7	Bainet, 122±9	-	122 ±9	SS	7.5	0.04	7.49	0.04	7.5	0.04
Baraderes	8	Baraderes, 60±10	-	-	R	7.13	0.08	7.25	0.09	7.25	0,09
Marcelline	9	Marcelline-Baraderes, 28±4	-	28± 4	-	6.73	0.07	6.75	0.07	6.75	0.07
Petite Rivière des Nippes	10	Petite Riviere de Nippes-Miragoane-GrandGoave, 55±10	-	55± 10	R	7.08	0.09	7.12	0.09	7.12	0.09
Cavaillon Nord	11	Cavaillon Nord, 43±3	-	-	R	6.96	0.03	6.99	0.03	6.99	0.03
Belsue-St Jean du Sud	12	Belsue-St Jean du Sud, 49±3	-	-	All	7.02	0.05	7.06	0.05	7.06	0.05

In practice, the maximum plausible earthquake is estimated from the largest known historical event, if it exceeds the magnitude derived from fault length. Due to the lack of well-documented historical earthquakes, magnitudes were inferred using empirical relationships linking fault geometry and kinematics (rupture length, coseismic displacement) to earthquake magnitude.

Accordingly, maximum physically plausible magnitudes were recalculated for all identified structures in the Sud and Nippes departments using the relationships of Coppersmith (1991) and Wells and Coppersmith (1994). Under a conservative assumption, fault segments 7, 8, 9, and 10 were assumed to rupture along their entire lengths. Similarly, major fault systems in the Nippes and Sud

departments were divided into two principal segments, each approximately 100 km long. The resulting updated maximum plausible magnitudes were then used for PGA calculations (Table 1).

5.2. Bedrock PGA Evaluation

To obtain results as close to reality as possible, four ground-motion attenuation models were applied (Earthquake Spectra, 2008):

- Abrahamson–Silva NGA model
- Boore–Atkinson NGA model
- Campbell–Bozorgnia NGA model
- Chiou–Youngs NGA model

The mean value of these calculations was adopted as the final PGA estimate.

Two approaches can be used to assess regional-scale seismic hazard (Philip, 2007):

Deterministic approach: This method is based on determining the maximum plausible earthquake and requires detailed knowledge of the location and characteristics of seismic sources. It does not account for earthquake recurrence frequency and may lead to over- or underestimation of hazard.

Probabilistic approach: This method estimates the probability of exceeding specific ground-motion values over a given time period (e.g., 100 or 500 years). Its main limitation is the representativeness of seismic catalogs, particularly in regions of low to moderate seismicity or regions such as Haiti, where historical data cover only approximately three centuries.

Given these limitations, the deterministic approach was adopted in this study. Dominant earthquake scenarios controlling ground acceleration in the Sud and Nippes departments were identified. Using the defined reference earthquakes and the ground-motion models described above, bedrock PGA values were calculated across the entire study area. Dominant scenarios were then identified for each location.

PGA calculations considered 12 seismic sources to evaluate the individual contribution of each fault (Fig. 7). Calculated bedrock PGA values range from approximately 0.09 g to ≥0.42 g. The highest accelerations affecting the Sud and Nippes departments are associated with segments of the EPGFZ. Faults 7, 8, 9, 10, and 12 also exert a significant local influence on PGA values.

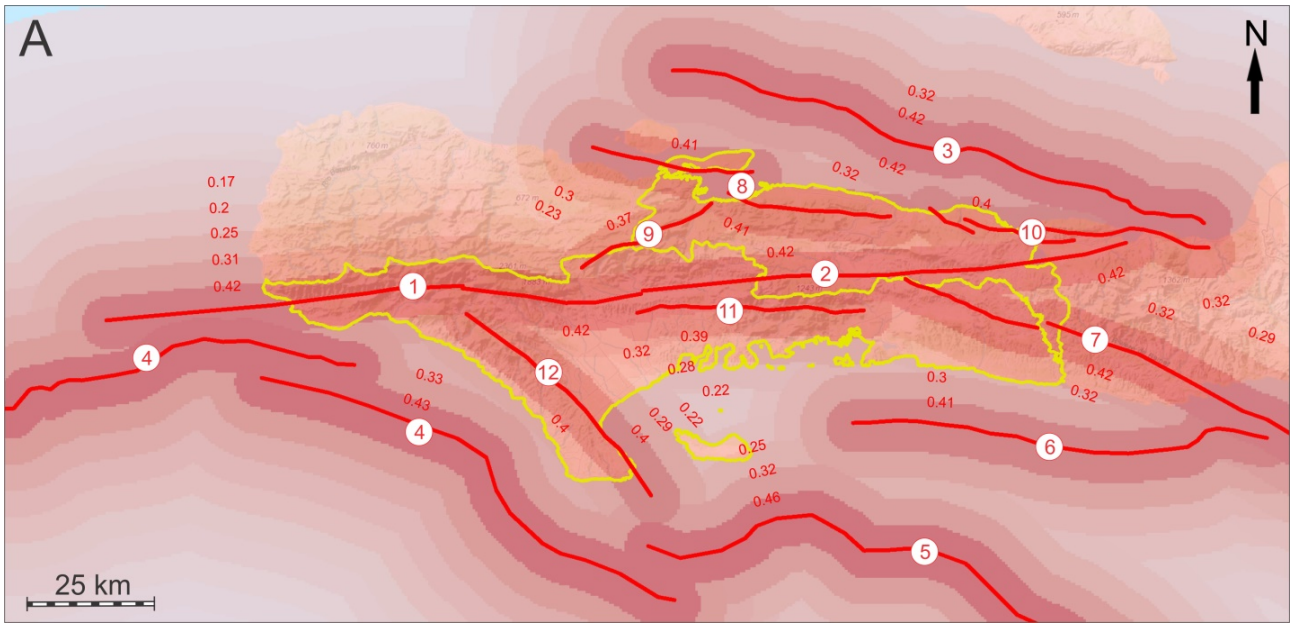

Figure 7. The 12 selected seismic sources considered in the hazard assessment and the resulting PGA calculations for the Nippes and Sud departments.

6. Discussion

The results of this study demonstrate that both offshore and onshore active faults play a critical role in controlling the seismic hazard of the North-West and South peninsulas of Haiti. Offshore structures exhibit clear morphotectonic evidence of recent activity, including fault scarps, submarine landslides, and deformation of the seafloor. These observations, combined with the uplifted Quaternary marine terraces observed along the coastlines, indicate ongoing tectonic coastal uplift of approximately 0.19 mm/year consistent with the regional stress regime.

The coherence between offshore fault kinematics and onshore deformation patterns strongly suggests mechanical coupling between these structures. The uplift of reef terraces along the northern margins of the North-West and South peninsulas is consistent with reverse faulting identified offshore, implying recurrent activity throughout the Quaternary. The presence of recent submarine landslides along these faults further supports their potential for coseismic reactivation and associated secondary hazards, such as tsunamis or coastal instability.

Onshore, the detailed mapping carried out at multiple scales (from regional to outcrop scale) allowed discrimination between purely tectonic faults and seismogravitational structures. Several fault systems previously inferred or poorly constrained were confirmed as active, with clear morphologic, stratigraphic, and structural evidence and new ones mapped. The earthquake of 24 January 2022 of magnitude 5.3 and its aftershocks of magnitude 4.1-5.1 confirmed the existence and activity of the Baraderes fault (8, Fig. 7).

The kinematic analysis of the mapped faults indicates a dominant compressional regime with oblique deformation, expressed by reverse faulting associated with strike-slip components. Microtectonic data consistently indicate NNE–SSW compression and NW–SE extension, in agreement with the regional tectonic framework imposed by the relative motion between the Caribbean and North American plates.

This behavior of secondary active faults reflects the complex interaction between major structures, such as the Enriquillo–Plantain Garden Fault Zone (EPGFZ), and secondary faults accommodating deformation at a more local scale.

Despite the lack of documented historical earthquakes on some of these faults, their geomorphic expression and structural relationships clearly indicate recent and potentially ongoing activity. This highlights the limitation of relying solely on historical and instrumental seismicity catalogs in regions with short observation periods, such as Haiti.

The deterministic seismic hazard assessment conducted in this study emphasizes the importance of integrating detailed fault geometry, segmentation, and kinematics into hazard models. The recalculated maximum plausible magnitudes (Mmax), derived from empirical relationships based on seismic source length, provide physically realistic upper bounds for seismic scenarios in the absence of well-constrained historical events.

The PGA results show significant spatial variability across the Sud and Nippes departments, with the highest accelerations associated with segments of the EPGFZ. However, several secondary faults (notably sources 7, 8, 9, 10, and 12) also contribute substantially to local ground-motion levels. This finding underscores that seismic hazard in the region is not controlled by a single, even secondary fault system but rather by a network of active structures.

The use of multiple ground-motion prediction equations and the adoption of their mean value reduce model-related uncertainty and provide robust PGA estimates at bedrock level. The resulting acceleration values (up to ≥ 0.42 g) indicate a high level of seismic hazard, particularly for areas located near major fault segments.

7. Conclusion

This study provides a comprehensive characterization of active onshore and offshore faults in the North-West and South peninsulas of Haiti and evaluates their implications for seismic hazard. High-resolution morphotectonic analysis, combined with field observations and structural data, allowed the identification and detailed mapping of numerous active faults, many of which were previously poorly constrained or underestimated.

The results demonstrate that offshore faults are an integral component of the regional seismotectonic system and significantly contribute to seismic hazard. The consistency between offshore deformation, coastal uplift, and onshore fault kinematics indicates long-term, recurrent activity throughout the Quaternary.

The deterministic seismic hazard assessment for the departments Nippes and Sud, based on conservative rupture scenarios and physically plausible maximum magnitudes, reveals that the highest PGA values are associated with the Enriquillo–Plantain Garden Fault Zone, while several secondary fault systems exert a strong local influence. These findings highlight the necessity of incorporating both major and secondary faults into seismic hazard models.

Overall, this work underscores the critical need for detailed active fault mapping in regions with limited historical seismic records and important instrumental devastated earthquake of 12 January 2010 (which resulted in more than 200,000 fatalities) and 14 August 2021 (with 2248 fatalities). The results provide essential constraints for seismic hazard mitigation, land-use planning, and risk reduction strategies in southern Haiti and constitute a robust framework for future probabilistic assessments and site-specific studies.

References

Ali, S. T.; Freed, A. M.; Calais, E.; Manaker, D. M.; McCann, W. R. Coulomb Stress Evolution in the Northeastern Caribbean over the Past 250 Years Due to Coseismic, Postseismic, and Interseismic Deformation. *Geophys. J. Int.* **2008**, *174*, 904–918. https://doi.org/10.1111/j.1365-246X.2008.03634.x

Amilcar, H. Étude géologique de l'Ouest du Massif de la Hotte (Haïti, Grandes Antilles) dans son cadre terrestre et marin: Implications géodynamiques. Université Paul Sabatier, Toulouse, 1997.

Baker, J. W.; Jayaram, N. Correlation of Spectral Acceleration Values from NGA Ground Motion Models. *Earthquake Spectra* **2008**, *24*, 299–317. https://doi.org/10.1193/1.2857544

Butterlin, J. (1954). La géologie de la République d'Haïti et ses rapports avec celle des régions voisines. PhD thesis, Jouve, 1954, 446 p.

Calais, E.; Mercier de Lépinay, B. A Natural Model of Active Transpressional Tectonics: The En Échelon Structures of the Oriente Deep along the Northern Caribbean Transcurrent Plate Boundary. *Rev. Inst. Fr. Pét.* **1990**, *45* (2), 147–160. https://doi.org/10.2516/ogst:1990013

Calais, E.; Béthoux, N.; Mercier de Lépinay, B. From Transcurrent Faulting to Frontal Subduction: A Seismotectonic Study of the Northern Caribbean Plate Boundary from Cuba to Puerto Rico. *Tectonics* **1992**, *11*, 114–123. https://doi.org/10.1029/91TC02364

Calais, E.; Mazabraud, Y.; Mercier de Lépinay, B.; Mann, P.; Mattioli, G.; Jansma, P. Strain partitioning and fault slip rates in the Northeastern Caribbean from GPS measurements. *Geophys. Res. Lett.* **2002**, *29* (18), 1856. https://doi.org/10.1029/2002GL015397

Calais, E.; Symithe, S. J.; Mercier de Lépinay, B. Strain Partitioning within the Caribbean–North America Transform Plate Boundary in Southern Haiti: Tectonic and Hazard Implications. *Bull. Seismol. Soc. Am.* **2023**, *113* (1), 131–142. https://doi.org/10.1785/0120220121

Carte géologique à 1/250 000 de la République d'Haïti (en 4 feuilles) B.M.E. (1982-1988). Editeur C.E.R.C.G. IMAGEO, CNRS, Paris: 1- Bien Aimé Monplaisir R., Boisson D. (1987) : feuille Sud-Est (feuille de Port-au-Prince), 2- Boisson D., Pubellier M. (1987) : feuille Nord-Est (feuille de Cap-Haïtien), 3- Pubellier M., Boisson D. (1988) : feuille Nord-Ouest (feuille de Môle St Nicolas), 4- Amilcar H., Bien Aimé Monplaisir R. (1988) : feuille du Sud-Ouest (feuille des Cayes).

Coppersmith, K. J. Seismic Source Characterization for Engineering Seismic Hazard Analysis. In *Proceedings of the 4th International Conference on Seismic Zonation*; 1991; Vol. 1, pp 3–60. Earthquake Engineering Research Institute.

DeMets, C.; Jansma, P. E.; Mattioli, G. S.; Dixon, T. H.; Farina, F.; Bilham, R.; Calais, E.; Mann, P. GPS geodetic constraints on Caribbean–North America Plate Motion. *Geophys. Res. Lett.* **2000**, *27*, 437–440. https://doi.org/10.1029/1999GL005436

Dixon, T. H.; Farina, F.; DeMets, C.; Jansma, P.; Mann, P.; Calais, E. Relative motion between the Caribbean and North American plates and related boundary zone deformation from a decade of GPS observations. *J. Geophys. Res.* **1998**, *103*, 15157–15182. https://doi.org/10.1029/97JB03575

Dolan, J. F.; Wald, D. J. The 1943–1953 North-Central Caribbean Earthquakes: Active tectonic setting, seismic hazards, and implications for Caribbean-North America plate motions. In J. F. Dolan, & P. Mann (Eds.), Active strike-slip and collisional tectonics of the Northern Caribbean Plate Boundary Zone. *Geol. Soc. Am. Spec. Pap.* **1998**; Vol. 326, pp 143–169.

Earthquake Spectra. Special issue on NGA ground motion models. *Earthquake Spectra* **2008**, *24* (1), 1–341.

Escuder Viruete, J.; Díaz de Neira, J. A.; Hernáiz Huerta, P. P.; Monthel, J.; García Senz, J.; Joubert, M.; et al. Magmatic relationships and ages of Caribbean Island arc tholeiites, boninites and related felsic rocks, Dominican Republic. *Lithos* **2006**, *90* (3-4), 161–186. https://doi.org/10.1016/j.lithos.2006.02.001

Goreau, P. D. The tectonic evolution of the North-Central Caribbean plate margin. PhD thesis, Massachusetts Institute of Technology, 1983.

Leroy, S.; Ellouz-Zimmermann, N.; Corbeau, J.; Rolandone, F.; De Lépinay, B. M.; Meyer, B.; et al. Segmentation and kinematics of the North America–Caribbean plate boundary offshore Hispaniola. *Terra Nova* **2015**, *27*, 467–478. https://doi.org/10.1111/ter.12181

Manaker, D. M.; Calais, E.; Freed, A. M.; Ali, S. T.; Przybylski, P. Interseismic Plate coupling and strain partitioning in the Northeastern Caribbean. *Geophys. J. Int.* **2008**, *174*, 889–903. https://doi.org/10.1111/j.1365-246X.2008.03819.x

Mann, P.; Burke, K.; Matumoto, T. Neotectonics of Hispaniola: plate motion, sedimentation, and seismicity at a restraining bend. *Earth Planet. Sci. Lett.* **1984**, *70*, 311–324. https://doi.org/10.1016/0012-821X(84)90016-5

Mann, P.; Taylor, F. W.; Edwards, R. L.; Ku, T.-L. Actively evolving microplate formation by oblique collision and sideways motion along strike-slip faults: An example from the northeastern Caribbean plate margin. *Tectonophysics* **1995**, *246*, 1–69. https://doi.org/10.1016/0040-1951(94)00268-E

Mann, P.; Calais, E.; Ruegg, J.-C.; DeMets, C.; Jansma, P. E.; Mattioli, G. S. Oblique collision in the northeastern Caribbean from GPS measurements and geological observations. *Tectonics* **2002**, *21* (6), 7-1–7-26. https://doi.org/10.1029/2001TC001304

Momplaisir Bien-Aimé, R. (1986). Contribution à l'étude géologique de la partie orientale du Massif de la Hotte (Presqu'île du Sud d'Haïti). PhD thesis, Université Paris VI. 1986.

Philip, H.; Bousquet, J.-C.; Masson, F. Séismes et risques sismiques: Approche sismotectonique. Dunod, Paris, 2007. ISBN 978-2-10-049581-8

Pubellier, M.; Vila, J. M.; Boisson, D. North Caribbean neotectonic events: The Trans-Haitian fault system. Tertiary record of an oblique transcurrent shear zone uplifted in Hispaniola. *Tectonophysics* **1991**, *194* (3), 217–236. https://doi.org/10.1016/0040-1951(91)90262-Q

Wells, D. L.; Coppersmith, K. J. New empirical relationships among magnitude, rupture length, rupture width, rupture area, and surface displacement. *Bull. Seismol. Soc. Am.* **1994**, *84* (4), 974–1002. https://doi.org/10.1785/BSSA0840040974

Author Contributions: Ara Avagyan: Writing – original draft, Methodology, Investigation, Data curation, Supervision. Samira Philip-Rebai: Writing – review & editing, Methodology, Investigation, Data curation, Supervision. Claude Prepetit: Writing – review & editing, Data curation. Roberte Monplaisir: Writing – review & editing, Data curation.

Funding: This study was funded by Programme des Nations Unis pour le développement d'Haïti et Unité Technique de Sismologie.

Acknowledgments: The authors thank the UNDP-Haïti (Programme des Nations Unis pour le développement d'Haïti et Unité Technique de Sismologie), haïtien technical institutions Bureau des Mines et de l'Energie (BME/UTS), Laboratoire National du Bâtiment et des Travaux Publics (LNBTP), Centre National de l'Information Géo-Spatiale (CINGS) and Université d'Etat d'Haïti-Faculté des Sciences (UEH-FDS) for support of the study. We also thank Standelet Ceus and Jerry Charles Pierre for UNDP-Haïti and Marceau Jean-Baptiste et Phedy Jean for BME. The authors thank Klaus Reicherter for constructive and valuable review.

Conflicts of Interest: All authors declare no conflict of interest.

ԱՄՓՈՓԱԳԻՐ

Ակտիվ խզվածքների ինտեգրված քարտեզագրում և սեյսմիկ վտանգի գնահատում. Հայիթիի օրինակը

Արա Ավագյան[1,*], Սամիրա Ֆիլիպ-Ռեբաի[2], Կլոդ Պրեպետիտ[3], Ռոբերտ Մոնպլեզիր[3]

[1]ՀՀ ԳԱԱ երկրաբանական գիտությունների ինստիտուտ, Բաղրամյան 24ա, 0019 Երևան, ՀՀ
[2]Բնական ռիսկերի նվազեցման և կլիմայի փոփոխության հարմարվողականության անկախ խորհրդատու, Մոնպելյե, Ֆրանսիա
[3]Հայիթիի օգտակար հանածոների և էներգիայի բյուրո և Սեյսմոլոգիայի Տեխնիկական Միավոր (UTS), Հայիթի
[4]Գիտությունների ֆակուլտետ, Հայիթիի պետական համալսարան, Հայիթի

[*]Հաղորդակցության համար՝ avagn1064@gmail.com

Սույն հետազոտությունը ներկայացնում է Հայիթիի հյուսիս-արևմտյան հատվածում և հարավային թերակղզում գտնվող ցամաքային և ափամերձ ծովային ակտիվ խզվածքների քարտեզագրումն ու վերլուծությունը՝ սեյսմիկ վտանգի գնահատման համատեքստում: Դաշտային հետազոտությունները (2017-2019 թթ.), բարձր լուծաչափի արբանյակային պատկերները, մորֆոտեկտոնական վերլուծությունը և կառուցվածքային տվյալները ինտեգրվել են՝ հիմնական և երկրորդային ակտիվ խզվածքները հայտնաբերելու և բնութագրելու նպատակով: Ցամաքային ակտիվ խզվածքների կինեմատիկ վերլուծությունները ցույց են տալիս գերիշխող Հյուսիս-հյուսիսարևելք–Հարավ-հարավարևմուտք ուղղված սեղմման ռեժիմ՝ թեք դեֆորմացիայով: Այս օրինաչափությունը համապատասխանում է Կարիբյան և Հյուսիսամերիկյան տեկտոնական սալերի հարաբերական շարժմամբ պայմանավորված տարածաշրջանային լարվածության դաշտին: Չնայած պատմական սեյսմիկության սահմանափակ տվյալներին, գեոմորֆոլոգիական և կառուցվածքային ապացույցները վկայում են հայտնաբերված ցամաքային խզվածքների ժամանակակից ակտիվության մասին: Կատարվել է դետերմինիստական սեյսմիկ վտանգի գնահատում, հաշվի են առնված խզվածքների երկրաչափությունը, սեգմենտավորումը և կինեմատիկան: Գնահատվել են ֆիզիկապես հնարավոր առավելագույն մագնիտուդները (Mmax) և արագացումները՝ կիրառելով գետնային շարժումների կանխատեսման մի քանի հավասարումներ: Արդյունքները ցույց են տալիս, որ ամենաբարձր ցամաքային PGA արժեքները (մինչև ≥ 0.42 g) կապված են Էնրիկիլյո–Պլանտեն Գարդեն խզվածքային գոտու հետ, մինչդեռ երկրորդային խզվածքները նույնպես էական ներդրում ունեն տեղական գետնային շարժումների մեջ: Այս արդյունքները ընդգծում են ինչպես հիմնական, այնպես էլ երկրորդային ակտիվ խզվածքների կարևոր դերը տարածաշրջանային սեյսմիկ վտանգի վերահսկման գործում և ցույց են տալիս խզվածքների մանրամասն քարտեզագրման ինտեգրման կարևորությունը վտանգի մոդելներում, հատկապես այն տարածաշրջաններում, որտեղ պատմական սեյսմիկ տվյալները սահմանափակ են:

Բանալի բառեր՝ Հայիթի, ակտիվ խզվածքների քարտեզագրում, երկրաբանական վտանգ, PGA հաշվարկ

Reports of NAS RA
ՀՀ ԳԱԱ Զեկույցներ
NATIONAL ACADEMY OF SCIENCES OF THE REPUBLIC OF ARMENIA
ՀԱՅԱՍՏԱՆԻ ՀԱՆՐԱՊԵՏՈՒԹՅԱՆ ԳԻՏՈՒԹՅՈՒՆՆԵՐԻ ԱԶԳԱՅԻՆ ԱԿԱԴԵՄԻԱ

2026 **Volume 126** **Issue 1** **Article No. 9**

Category: Mathematics
Type of Paper: Original Research Article
Received: December 5, 2025, **Revised:** March 1, 2026, **Accepted:** March 9, 2026
Published: April 14, 2026

DOI: 10.54503/0321-1339-2026.126.1-9

On UC-multipliers for multiple trigonometric systems

Grigori A. Karagulyan[1,*]

[1]Institute of Mathematics of NAS RA, 24/5 Marshal Baghramian ave., Yerevan 0019, Armenia

[*]Correspondence: g.karagulyan@gmail.com

Abstract

We investigate the class of sequences $w(n)$ that can serve as almost-everywhere convergence Weyl multipliers for all rearrangements of multiple trigonometric systems. We show that any such sequence must satisfy the bounds $\log n \lesssim w(n) \lesssim \log^2 n$. Our main result establishes a general equivalence principle between one-dimensional and multidimensional trigonometric systems, which allows one to extend certain estimates known for the one-dimensional case to higher dimensions.

Keywords: multiple trigonometric system, non-overlapping polynomials, Weyl multiplier, Menshov-Rademacher theorem
MSC (2010): 42C05, 42C10, 28D05

1. Introduction

1.1. Weyl multipliers

Let

$$\Phi = \{\phi_n : n = 1, 2, \ldots\} \subset L^2(0,1) \tag{1.1}$$

be an orthonormal system. Recall that a sequence of positive numbers $w(n) \nearrow \infty$ is called an almost everywhere convergence Weyl multiplier (or simply a Weyl multiplier) for Φ if every series

$$\sum_{n=1}^{\infty} a_n \phi_n(x), \tag{1.2}$$

whose coefficients satisfy

$$\sum_{n=1}^{\infty} a_n^2 w(n) < \infty \tag{1.3}$$

converges almost everywhere (see [16] or [8]). The classical Menshov-Rademacher theorem ([18, 27]) asserts that the sequence $\log^2 n$ is a Weyl multiplier for every orthonormal system. The optimality of $\log^2 n$ of this sequence was also shown by Menshov in [18], where he constructed an orthonormal system for which any sequence $w(n) = o(\log^2 n)$ fails to be Weyl multiplier. The following concepts are standard in the theory of orthogonal series.

Definition 1.1. *A sequence of positive numbers $w(n) \nearrow \infty$ is called an almost everywhere convergence Weyl multiplier for rearrangements (RC-multiplier) of an orthonormal system*

$\Phi = \{\phi_n\}_{n\ge 1}$ *if it is a Weyl multiplier for every system* $\{\phi_{n_k}\}$, *where* $\{n_k\}$ *is a sequence of distinct naturals (not necessarily increasing).*

Definition 1.2. *A sequence of positive numbers* $w(n) \nearrow \infty$ *is called an almost everywhere unconditional convergence Weyl multiplier (UC-multiplier) for an orthonormal system* $\Phi = \{\phi_n\}_{n\ge 1}$ *if under condition* (1.3) *series* (1.2) *converges almost everywhere after every rearrangement of its terms.*

By the Menshov-Rademacher theorem, the sequence $\log^2 n$ is RC-multiplier for any orthonormal system Φ and Menshov's counterexample shows that $\log^2 n$ is optimal in this sense. The study of RC- and UC-multipliers for classical orthonormal systems is a longstanding topic in the theory of orthogonal series. It is well known that the constant sequence $w(n) \equiv 1$ is a Weyl multiplier for trigonometric, Walsh, Haar and Franklin systems, yet it is not an RC-multiplier for any of them. Kolmogorov [17] was the first to observe that the sequence $w(n) \equiv 1$ is not RC-multiplier for the trigonometric system. However, he has never published the proof of this fact. A proof of this assertion was later given by Zahorski [40]. Afterward, developing Zahorski's argument, Ul'yanov [33, 34] established such a property for Haar and Walsh systems. Using the Haar functions technique, Olevskii [24] succeeded proving that such a phenomenon occurs for every complete orthonormal system. Ul'yanov [32, 36] found the optimal growth of the RC and UC multipliers of Haar system. This technique of the proof became a key argument in the study of the analogous problems for other classical systems.

Theorem A (Ul'yanov, [36]). *The sequence* $\log n$ *is an RC-multiplier for the Haar system.*

Theorem B (Ul'yanov, [36]). *A non-decreasing sequence* $w(n)$ *is a UC-multiplier for the Haar system if and only if*

$$\sum_{n=1}^{\infty} \frac{1}{nw(n)} < \infty. \tag{1.4}$$

In fact, if $\log n$ is a RC-multiplier for an orthonormal system, then any non-decreasing sequence $w(n)$ satisfying (1.4) is UC-multiplier for the same orthonormal system. This follows from a general result that is established in later papers [26, 35].

The results of Theorems A and B have extensions for some other orthonormal systems of wavelet type. In particular, G.Gevorkyan in [5, 6] established the analogue of Theorem B for the Franklin and Ciesielski systems of wavelet type. For arbitrary wavelet type systems the similar results were recently proved by the author in [9]. Moreover, in paper [9] authors provide a new approach that enables one to get analogues of both Theorems A and B for systems of non-overlapping polynomials with respect to general wavelet type systems (some details of the papers is given below).

For character type orthogonal systems, such as the trigonometric and Walsh systems, the problem of characterization of RC and UC multipliers is not completely solved yet. These problems were first posed in Ul'yanov's 1964 survey [37] and revisited in several later papers (see [36], p. 1041, [38], p. 80, [39], p. 57). The Menshov-Rademacher theorem implies that $\log^2 n$ is a RC-multiplier for both the trigonometric and Walsh systems, and no sequence $w(n) = o(\log^2 n)$ is known to be RC-multiplier for either system. Lower bounds for the RC and UC multipliers of the Walsh system were studied in [2, 22, 23, 30]. The best result, proved independently by Bochkarev [2, 3] and Nakata [22], shows that if an increasing sequence $w(n)$ fails to satisfy Ul'yanov's condition (1.4), then it is not a UC-multiplier for the Walsh system. For the trigonometric system the lower bounds for the RC and UC multipliers were studied in [4, 11, 12, 19-21, 29]. The analogous of the Bochkarev-Nakata [2, 22] theorem for the trigonometric system was recently proved by the author in [11]. We also mention a

recent paper [13], where it was proved that for dyadic orthonormal trigonometric polynomials the sequence $\sqrt{\log n}$ is RC-multiplier.

For a fixed orthonormal system (1.1) one can consider orthonormal systems formed by non-overlapping polynomials

$$p_n(x) = \sum_{k \in G_k} a_k \phi_k(x), \quad k = 1, 2, \ldots, \tag{1.5}$$

i.e. G_k are pairwise disjoint sets of natural numbers.

Definition 1.3. *A sequence of positive numbers* $w(n) \nearrow \infty$ *is said to be a strong RC-multiplier (SRC-multiplier) for an orthonormal system* (1.1) *if it is a Weyl multiplier for any orthonormal system of non-overlapping polynomials* (1.5).

Observe that if $w(n)$ is SRC-multiplier of an orthonormal system Φ, then it is also RC-multiplier for Φ, since any subsequence $\{\phi_{n_k}\}$ corresponds to (1.5) with each $G_k = \{n_k\}$. It is of recent interest finding the best SRC-multiplier for a given orthonormal system. It was proved in [10] that for the general martingale difference systems the optimal SRC-multiplier is the sequence $\log n$. An analogous result for general wavelet-type systems was proved in [9]. Hence, we have $\log n$ is a Weyl multiplier for any orthonormal system of non-overlapping polynomials with respect Haar, Franklin and all other wavelet type systems (see definition in [9]). The optimal growth of a sequence $w(n)$ that can serve as an RC or SRC multiplier for the trigonometric or Walsh systems is still unknown. From the Menshov-Rademacher theorem together with the results of [2, 13, 22], it follows only that any such sequence must satisfy

$$\log n \lesssim w(n) \lesssim \log^2 n. \tag{1.6}$$

In this paper, we study the RC(SRC)-multiplier problem for the multiple trigonometric system. Namely, we prove that this problem coincides with the corresponding problem for the one-dimensional trigonometric system.

Theorem 1.1. *Let* $w(n)$ *be an increasing numerical sequence satisfying* $w(n^2) \le Cw(n)$. *Then* $w(n)$ *is an RC(SRC)-multiplier for the one-dimensional trigonometric system if and only if it is an RC(SRC)-multiplier for the multiple trigonometric system.*

Remark 1. Note that the bound $w(n^2) \le Cw(n)$ is natural, since Weyl multipliers are known to have at most logarithmic growth, and this inequality is satisfied for any sequence $w(n)$ with logarithmic behavior.

Remark 2. Observe that for the Walsh system the result of Theorem 1.1 is immediate, since the Walsh system is probabilistically equivalent to its multiple system. Indeed, the functions in both systems are generated by all possible products of independent random variables taking the values ± 1 with equal probability. Such an equivalence does not hold for the trigonometric system. Nevertheless, in this paper we develop a technique that effectively replaces this equivalence principle in the trigonometric setting.

Applying Theorem 1.1, one can extend the bound (1.6), known for the one-dimensional trigonometric system, to the multidimensional case.

Corollary 1.1 *If a sequence* $w(n)$ *is a RC-multiplier of a multiple trigonometric system, then* $\log n \lesssim w(n) \lesssim \log^2 n$.

Remark 3. Theorem 1.1 and Corollary 1.1 provide an example of reducing a multidimensional problem to the one-dimensional case. A phenomenon of a similar nature appears in a different context in the theory of orthogonal series. In particular, papers [1, 7, 25, 28, 31] have developed techniques that allow

one to deduce multidimensional Carleson-type almost everywhere convergence theorems from their one-dimensional counterparts. For general orthogonal series, this phenomenon was first observed by Tevzadze, who proved that if an orthonormal system is a convergence system, then its tensor product system is also a convergence system with respect to cubical partial sums. Analogous results for more general partial sums were later obtained by Goginava and Oniani. A similar passage from the one-dimensional to the multidimensional case was first considered by Sjölin for trigonometric Fourier series, including in the setting of general Orlicz spaces. Antonov subsequently refined the Orlicz classes ensuring almost everywhere convergence of one-dimensional and multidimensional Fourier series, and in particular obtained an implicit result guaranteeing such a dimensional passage. In papers [14, 15] by the author and Mkoyan, a related approach was used to determine the optimal class of functions for which almost everywhere strong summability holds. The result of Theorem 1.1, however, differs substantially from the works cited above. In particular, we do not deal with multiple series; rather, we consider a multiple trigonometric system within a one-dimensional series framework. Moreover, the realization of this dimensional reduction is based on a purely number-theoretic argument, relying on the Chinese remainder theorem.

2. Probabilistically equivalence and measure-preserving maps

Definition 2.1. *Let* $(X,\mathcal{A},\mu)$ *and* $(Y,\mathcal{B},\nu)$ *be probability spaces. Sequences of measurable functions* $f_k : X \to \mathbb{R}$ *and* $g_k : Y \to \mathbb{R}$, $k = 1,2,\ldots$, *are said to be probabilistically equivalent if they share the same joint cumulative distribution function, i.e. we have*

$$\mu\left(\bigcap_{k=1}^{n} f_k^{-1}(E_k)\right) = \nu\left(\bigcap_{k=1}^{n} g_k^{-1}(E_k)\right)$$

for every choice of Borel sets $E_k \subset \mathbb{B}$, $k = 1,2,\ldots,n$.

A natural way to obtain probabilistically equivalent sequences is to use a measure-preserving map, as shown in Lemma 2.2 below.

Definition 2.2. *Let* $(X,\mathcal{A},\mu)$ *and* $(Y,\mathcal{B},\nu)$ *be probability spaces. We say a function* $\Theta : \mathcal{A} \to \mathcal{B}$ *is measure-preserving map (MP-map), if for any measurable sets* $E,F \in \mathcal{A}$ *we have*

$$\begin{aligned} &1)\ \mu(E) = \nu(\Theta(E)), \\ &2)\ \mu(E \cup F) = \nu(\Theta(E) \cup \Theta(F)). \end{aligned} \tag{2.1}$$

Remark 4. Note that this definition of a measure-preserving map differs from the classical definition, in which the mapping is given as a function from X to Y. However, as we will see below (Lemma 2.2), such a mapping induces the same basic correspondence between functions on X and Y as in the classical case. The use of this definition simplifies the construction of measure-preserving maps, which we will employ several times in the proofs below

Lemma 2.1. *If* Θ *is a MP-map from a probability space* $(X,\mathcal{A},\mu)$ *to* $(Y,\mathcal{B},\nu)$, *then for any measurable sets* $E,F \in \mathcal{A}$, $E_k \in \mathcal{A}$, $k = 1,2,\ldots$,

$$\mu(E \setminus F) = \nu(\Theta(E) \setminus \Theta(F)), \tag{2.2}$$

$$\mu\left(\bigcup_k E_k\right) = \nu\left(\bigcup_k \Theta(E_k)\right), \tag{2.3}$$

$$\mu\left(\bigcap_k E_k\right) = \nu\left(\bigcap_k \Theta(E_k)\right). \tag{2.4}$$

Proof. Using the definition of MP-map, we obtain

$$\begin{aligned}\mu(F)+\mu(E\setminus F)&=\mu(F\cup E)=\nu(\Theta(F)\cup\Theta(E))\\&=\nu(\Theta(F))+\nu(\Theta(E)\setminus\Theta(F))\\&=\mu(F)+\nu(\Theta(E)\setminus\Theta(F)).\end{aligned}$$

Thus (2.2) follows. Similarly,

$$\begin{aligned}\mu(E)+\mu(F)-\mu(E\cap F)&=\mu(E\cup F)=\nu(\Theta(E)\cup\Theta(F)))\\&=\nu(\Theta(E))+\nu(\Theta(F)))-\nu(\Theta(E)\cap\Theta(F)))\\&=\mu(E)+\mu(F)-\nu(\Theta(E)\cap\Theta(F))).\end{aligned}$$

This implies (2.4) for two sets and so for a finite collection of measurable sets. Then passing to a limit we will get (2.4) for any countable collection of sets. Similarly (2.1) implies (2.3).

Let Θ be a MP-map from a probability space $(X,\mathcal{A},\mu)$ to $(Y,\mathcal{B},\nu)$. Then Θ induces a map that takes any indicator function $\mathbf{1}_E$, $E\in\mathcal{A}$, to $\mathbf{1}_{\Theta(E)}$. The following lemma gives a suitable extension of Θ to entire space $L^0(X)$ of measurable functions.

Lemma 2.2. *If Θ is a MP-map from a probability space $(X,\mathcal{A},\mu)$ to a probability space $(Y,\mathcal{B},\nu)$, then it can be uniquely extended as an operator from $L^0(X)$ into $L^0(Y)$ such that every sequence $\{f_k\}_{k\ge1}\subset L^0(X)$ is probabilistically equivalent to its image sequence $\{\Theta(f_k)\}_{k\ge1}$.*

Proof. Let $s(x)$ be a simple function, i.e.

$$s(x)=\sum_{i=1}^{m}\alpha_i\mathbf{1}_{E_i}(x),$$

where $E_i\in\mathcal{A}$, $i=1,2,\dots,m$, are pairwise disjoint measurable sets and $\alpha_i\in\mathbb{B}$. Then we define

$$\Theta s(x)=\sum_{i=1}^{m}\alpha_i\mathbf{1}_{\Theta(E_i)}(x).$$

For an arbitrary $f\in L^0_{\mathbb{B}}(X)$, one can find a sequence of simple functions $s_n(x)$, such that

$$f(x)=\lim_{n\to\infty}s_n(x)\text{a.e.}. \tag{2.5}$$

Using Lemma 2.1 and a standard argument one can observe that the sequences $s_n(x)$ and $\Theta s_n(x)$ are probabilistically equivalent. Consequently, $\Theta s_n(x)$ converges almost everywhere and the limit doesn't depend on the particular choice of simple functions s_n in (2.5). We therefore define this limit as $\Theta f(x)$. It is also clear that any sequence $\{f_k\}_{k\ge1}\subset L^0_{\mathbb{B}}(X)$ is probabilistically equivalent to its image sequence $\{\Theta(f_k)\}_{k\ge1}$.

3. A decomposition for discrete trigonometric systems

For an integer $l\ge1$ we denote $\mathbb{N}_l=\{0,1,\dots,l-1\}$ and let

$$\mathbb{N}_{p_1,\dots,p_d}=\mathbb{N}_{p_1}\times\cdots\times\mathbb{N}_{p_d}$$

be the Cartesian product of the sets $\mathbb{N}_{p_k}$, $k=1,\dots,d$. The discrete trigonometric system (DTS) of order l is the collection of l orthonormal functions on $\mathbb{T}=\mathbb{R}/\mathbb{Z}$ defined by

$$\mathcal{D}^{(l)}=\left\{t_n^{(l)}(x)=\sum_{k=0}^{l-1}\exp\left(2\pi i\frac{nk}{l}\right)\cdot\mathbf{1}_{\delta_k^{(l)}}(x):\quad n\in\mathbb{N}_l\right\}, \tag{3.1}$$

where $\delta_k^{(l)} = [k/l, (k+1)/l)$. The orthogonality of the system (3.1) is a direct consequence of the orthogonality of the discrete Fourier matrix.We consider those as 1-periodic functions on $\mathbb{R}$. For integers $p_k \geq 2$, $k = 1, 2, \ldots, d$, consider the multiple DTS $\mathcal{D}^{(p_1,\ldots,p_d)}$, which is the tensor product of the one dimensional systems $\mathcal{D}^{(p_k)}$. This system consists of the functions

$$t_{\mathbf{n}}^{(p_1,\ldots,p_d)}(\times) = \prod_{k=1}^{d} t_{n_k}^{(p_k)}(x_k)$$
$$= \sum_{u_1=1}^{p_1} \cdots \sum_{u_d=1}^{p_d} \exp 2\pi i \left(\frac{n_1 u_1}{p_1} + \cdots + \frac{n_d u_d}{p_d}\right) \cdot \mathbf{1}_{\delta_{u_1}^{(p_1)} \times \cdots \times \delta_{u_d}^{(p_d)}}(\times)$$
$$\times = (x_1, \ldots, x_d) \in \mathbb{T}^d, \qquad \mathbf{n} = (n_1, \ldots, n_d) \in \mathbb{N}_{p_1,\ldots,p_d},$$

where $\delta_{u_1}^{(p_1)} \times \cdots \times \delta_{u_d}^{(p_d)}$ is the Cartesian product of the intervals $\delta_{u_k}^{(p_k)}$. In the sequel the notation $\{a\}$ denotes the fractional part of a number a. For positive integers n and p let denote by $\langle n \rangle_p$ the remainder when n is divided by p.

Proposition 3.1 *If $p_1, \ldots, p_d$ are mutually coprime numbers and $p = p_1 \ldots p_d$, then the systems $\mathcal{D}^{(p)}$ and $\mathcal{D}^{(p_1,\ldots,p_d)}$ are probabilistically equivalent. Moreover, this equivalence is generated by a measure-preserving map $\Theta : \mathbb{T}^d \to \mathbb{T}$.*

Proof. According to the Chinese remainder theorem for any integers $n_j \in \mathbb{N}_{p_j}$, $j = 1, 2, \ldots, d$ there is a unique integer $l \in \mathbb{N}_p$ such that

$$l = n_j \bmod p_j, \quad j = 1, 2, \ldots, d.$$

This defines a one-to-one mapping $\tau : \mathbb{N}_{p_1,\ldots,p_d} \to \mathbb{N}_p$ such that $\tau(n_1, n_2, \ldots, n_d) = l$. Consider the mapping $\overline{\tau} : \sqcap_{j=1}^{d} \mathbb{N}_{p_j} \to \mathbb{N}_p$ defined by

$$\overline{\tau}(u_1, \ldots, u_d) = \left\langle \tau(u_1, \ldots, u_d) \sum_{j=1}^{d} \frac{p}{p_j} \right\rangle_p .$$

Observe that this is a one-to-one mapping. Since the sets $\sqcap_{j=1}^{d} \mathbb{N}_{p_j}$ and $\mathbb{N}_p$ both have cardinality p it remains to show that $\overline{\tau}$ is injective. For $(u_1, \ldots, u_d) \neq (u_1', \ldots, u_d')$ we have

$$\left\langle \overline{\tau}(u_1, \ldots, u_d) - \overline{\tau}(u_1', \ldots, u_d') \right\rangle_p$$
$$= \left\langle (\tau(u_1, \ldots, u_d) - \tau(u_1', \ldots, u_d')) \sum_{j=1}^{d} \frac{p}{p_j} \right\rangle_p . \tag{3.2}$$

One can check that $\tau(u_1, \ldots, u_d) - \tau(u_1', \ldots, u_d')$ is not divisible by p, as well as $\sum_{j=1}^{d} \frac{p}{p_j}$ and p are coprime numbers. This implies that (3.2) can not be 0 and so $\overline{\tau}$ is injective. Using $\overline{\tau}$ we define a MP-map $\Theta : \mathbb{T}^d \to \mathbb{T}$ by choosing

$$\Theta(\delta_{u_1}^{(p_1)} \times \cdots \times \delta_{u_d}^{(p_d)}) = \delta_u^{(p)} \text{ if } u = \bar{\tau}(u_1, \ldots, u_d),$$

while inside of each $\delta_{u_1}^{(p_1)} \times \cdots \times \delta_{u_d}^{(p_d)}$ the map Θ is defined arbitrarily, provided that the measure-preserving property is maintained. Using the definitions of τ and $\overline{\tau}$, we obtain

$$\left\{\frac{\tau(n_1,\dots,n_d)\overline{\tau}(u_1,\dots,u_d)}{p}\right\}$$
$$=\left\{\frac{\tau(n_1,\dots,n_d)\tau(u_1,\dots,u_d)\sum_{j=1}^{d}\frac{p}{p_j}}{p}\right\}$$
$$=\left\{\sum_{j=1}^{d}\frac{\tau(n_1,\dots,n_d)\tau(u_1,\dots,u_d)}{p_j}\right\}=\left\{\sum_{j=1}^{d}\frac{n_ju_j}{p_j}\right\}.$$

Thus for $n=\tau(n_1,\dots,n_d)$ and $u=\overline{\tau}(u_1,\dots,u_d)$ we have

$$\exp\left(2\pi i\cdot\frac{nu}{p}\right)=\exp\left(2\pi i\cdot\frac{\overline{\tau}(n_1,\dots,n_d)\tau(u_1,\dots,u_d)}{p}\right)$$
$$=\prod_{j=1}^{d}\exp\left(2\pi i\cdot\frac{n_ju_j}{p_j}\right).$$

This implies that

$$\Theta(t_{n_1,\dots,n_d}^{(p_1,\dots,p_d)})=t_n^{(p)},\text{whenever } n=\tau(n_1,\dots,n_d).$$

Therefore the systems $\mathcal{D}^{(p)}$ and $\mathcal{D}^{(p_1,\dots,p_d)}$ are probabilistically equivalent.

4. Auxiliary lemmas and the proof of Theorem 1.1

Denote by $\mathcal{T}_d$ the d-dimensional trigonometric system, which consists of the functions

$t_{\mathbf{n}}(\times)=exp(2\pi i(n_1x_1+\cdots+n_dx_d))$, where
$\times=(x_1,\dots,x_d)\in\mathbb{T}^d$, $\mathbf{n}=(n_1,\dots,n_d)\in\mathbb{Z}^d$.

The one-dimensional trigonometric system (when $d=1$) will be simply denoted by $\mathcal{T}$.

Definition 4.1. *Let $(X,\mathcal{A},\mu)$ and $(Y,\mathcal{B},\nu)$ be probability spaces. Sequences of measurable functions $f_k:X\to\mathbb{R}$ and $g_k:Y\to\mathbb{R}$, $k=1,2,\dots,n$, are said to be probabilistically equivalent with an error $\varepsilon>0$ if there is a sequence $\overline{g}_k:Y\to\mathbb{R}$, $k=1,2,\dots,n$, probabilistically equivalent to $\{f_k\}$ such that $\|\overline{g}_k-g_k\|_2<\varepsilon$, $k=1,2,\dots,n$.*

Lemma 4.1. *Let $f_k\in\mathcal{T}_d$, $k=1,2,\dots,n$ be an arbitrary choice of d-dimensional trigonometric functions. Then for any $\varepsilon>0$ there exist an integer p and a sequence of discrete one-dimensional trigonometric functions $g_k\in\mathcal{D}^{(p)}$, $k=1,2,\dots,n$, such that the sequences $\{f_k\}$ and $\{g_k\}$ are probabilistically equivalent with an error ε.*

Proof. Let

$$f_k(\times)=t_{n_1^k,\dots,n_d^k}(x),\quad k=1,2,\dots,n. \tag{4.1}$$

We will find p in the form $p=p_1\cdots p_d$, where p_k are mutually coprime integers. By choosing the numbers $p_j\geq\max_{1\leq k\leq n}n_j^k$ large enough, we may achieve a good approximation of functions (4.1) by the corresponding discrete trigonometric functions, that is

$$\left|t_{n_1^k,\dots,n_d^k}(\times)-t_{n_1^k,\dots,n_d^k}^{(p_1,\dots,p_d)}(\times)\right|<\varepsilon \text{ for all } k=1,2,\dots,n,\quad \times\in\mathbb{T}^d. \tag{4.2}$$

Then applying Proposition 3.1, we can say that the sequence $t^{(p_1,\dots,p_d)}_{n_1^k,\dots,n_d^k}$, $k=1,2,\dots,n$, is probabilistically equivalent to a sequence of discrete one-dimensional trigonometric functions $g_k \in \mathcal{D}^{(p)}$. This together with (4.2) implies that the sequences $\{f_k\}$ and $\{g_k\}$ are probabilistically equivalent with an error $\varepsilon > 0$, completing the proof of lemma.

Let $c_k(f)$, $k \in \mathbb{Z}$, be the Fourier coefficients of a function $f \in L^2(\mathbb{T})$ with respect to one dimensional trigonometric system $\mathcal{T}$ and denote the spectrum of f by

$$spec(f) = \{k \in \mathbb{Z} : c_k(f) \neq 0\}.$$

Lemma 4.2. *For every integer $l \geq 1$ the functions $t_n^{(l)} \in \mathcal{D}^{(l)}$, $n = 0,1,\dots,l-1$, have non-overlapping spectrums with respect to $\mathcal{T}$. Moreover, there are non-overlapping one-dimensional trigonometric polynomials g_k, $k = 0,1,\dots,l-1$, each is a linear combination of l trigonometric functions and*

$$\| g_n \|_{L^2(\mathbb{T})} \leq 1, \quad \| t_n^{(l)} - g_n \|_{L^2(\mathbb{T})} \lesssim 1/\sqrt{l}, \quad n = 0,1,\dots,l-1.$$

Proof. For the Fourier coefficients of the functions $t_n^{(l)}$ (see (3.1)) we have

$$\begin{aligned} c_m(t_n^{(l)}) &= \int_0^1 t_n^{(l)}(x) \exp\left(-2\pi i m x\right) dx \\ &= \sum_{k=0}^{l-1} \exp\left(2\pi i \frac{nk}{l}\right) \int_{k/l}^{(k+1)/l} \exp\left(-2\pi i m x\right) dx \\ &= \exp\left(\frac{2\pi i m}{l}\right) \sum_{k=0}^{l-1} \exp\left(2\pi i \frac{(n-m)k}{l}\right) \int_0^{1/l} \exp\left(2\pi i m x\right) dx \\ &= \exp\left(\frac{2\pi i m}{l}\right) \frac{\exp(2\pi i m/l) - 1}{2\pi i m} \sum_{k=0}^{l-1} \exp\left(2\pi i \frac{(n-m)k}{l}\right). \end{aligned} \tag{4.3}$$

If $m \neq n \bmod l$ the sum in (4.3) is zero and therefore $c_m(t_n^{(l)}) = 0$. Thus we obtain $spec(t_n^{(l)}) = \{n + lj : j \in \mathbb{Z}\}$, $n = 0,1,\dots,l-1$, are non-overlapping. On the other hand, choosing $m = n + lj$ in (4.3) we get

$$| c_{n+Nj}(t_n^{(l)}) | \lesssim \frac{1}{|j|+1}, \quad j \in \mathbb{Z}.$$

Thus for the polynomials

$$g_n(x) = \sum_{|j| < l/2} c_{n+lj}(t_n^{(l)}) \exp\left(2\pi i (n+lj) x\right), \quad n = 0,1,\dots,l-1,$$

we get

$$\| t_n^{(l)} - g_n \|_2^2 \lesssim \sum_{|j| \geq l/2} \frac{1}{j^2} \lesssim \frac{1}{l}.$$

This completes the proof of the lemma.

Lemma 4.3. *Let $\{\phi_n(x)\}_{n=1}^{\infty}$ be an orthonormal system on $(0,1)$ and suppose that $w(n)$ is an increasing sequence satisfying $w(n) \geq c \log n$ for a constant $c > 0$. Then $w(n)$ is a Weyl multiplier for $\{\phi_n(x)\}$ if and only if under condition* (1.3)*,*

$$\lim_{k \to \infty} \max_{2^k \leq m < 2^{k+1}} \left| \sum_{n=2^k}^{m} a_n \phi_n(x) \right| = 0. \tag{4.4}$$

Proof. Without loss of generality the condition $w(n) \geq c \log n$ can be replaced by

$$w(n) \geq \log n. \tag{4.5}$$

Hence we can suppose that $w(n)$ satisfies (4.5). It is known that under the condition (4.5) from (1.3) it follows that

$$\lim_{k\to\infty} \sum_{n=1}^{2^k} a_n \phi_n(x) \text{ exists a.e..} \tag{4.6}$$

(see [8], Lemma [5.3.2]). From (4.4) and (4.6) one can get the a.e. convergence of series (1.2) . Hence, $w(n)$ is a Weyl multiplier for the system $\{\phi_n\}$. Now suppose conversely that $w(n)$ satisfies (4.5) and it is a Weyl multiplier for $\{\phi_n\}$. Then under the condition (1.3) series (1.2) converges a.e., which immediately implies (4.4).

Proof of Theorem 1.1. Let $\{f_n\}_{n\geq 1} \subset \mathcal{T}_d$ be an arbitrary choice of d -dimensional trigonometric functions. Applying first Lemma 4.1, then Lemma 4.2 , for every k we find a collection of non-overlapping one-dimensional trigonometric polynomials $\{\overline{f}_n : 2^k < n \leq 2^{k+1}\}$ such that each $\overline{f}_n$ is a linear combination of 4^k trigonometric functions,

$$\| \overline{f}_n \|_2 \leq 1, \quad n = 1, 2, \ldots,$$

and the blocks

$$\{f_n : 2^k \leq n < 2^{k+1}\} \text{and} \{\overline{f}_n : 2^k \leq n < 2^{k+1}\}, \quad k = 0, 1, 2, \ldots \tag{4.7}$$

are probabilistically equivalent with an errors $\lesssim 2^{-k}$. Note that some polynomials in $\{\overline{f}_n\}_{n\geq 1}$ may have overlapping spectrums and it may only happen when those polynomials belong to different blocks. It is clear that there exist integers n_k such that the new polynomial system defined by

$$g_n(x) = \overline{f}_n(x) \cdot e^{2\pi n_k x}, \quad 2^k \leq n < 2^{k+1}, \tag{4.8}$$

are non-overlapping. Thus the polynomials g_n can be written in the form

$$g_n(x) = \sum_{s=s_n+1}^{s_{n+1}} b_s \exp(2\pi i m_s x), \quad \sum_{s=s_n+1}^{s_{n+1}} b_s^2 \leq 1. \tag{4.9}$$

where m_k, $k = 1, 2, \ldots$, is a sequence of different integers (not necessarily increasing) such that

$$s_1 = 0, \quad s_{n+1} - s_n = 4^k \text{ if } 2^k \leq n < 2^{k+1}. \tag{4.10}$$

Observe that from (4.10) it follows that

$$s_n \leq 1 + 8 + 8^2 + \cdots + 8^k \text{ whenever} 2^k \leq n < 2^{k+1}.$$

Therefore we have

$$s_n \leq n^4. \tag{4.11}$$

Now let $w(n)$ be a RC-multiplier for the trigonometric system. Hence, according to the result of [11] we can suppose that

$$w(n) > c \log n. \tag{4.12}$$

Let us show that $w(n)$ is a Weyl multiplier for $\{g_n\}_{n\geq 1}$ as well. Let the sequence $\{a_n\}$ satisfies (1.3). By (4.9) we may formally write

$$\sum_{n=1}^{\infty} a_n g_n(x) = \sum_{n=1}^{\infty} \sum_{s=s_n+1}^{s_{n+1}} a_n b_s \exp(2\pi i m_s x), \tag{4.13}$$

where the second sum can be considered as a series in a rearranged one-dimensional trigonometric system with the coefficients

$c_s = a_n b_s$ if $s_n < s \le s_{n+1}$.

From (4.11) and the condition $w(n^2) \le Cw(n)$ it follows that $w(s_{n+1}) \le Cw(n)$. Thus we obtain

$$\sum_{s=1}^{\infty} c_s^2 w(s) = \sum_{n=1}^{\infty} a_n^2 \sum_{s=s_n+1}^{s_{n+1}} b_s^2 w(s)$$

$$\le C \sum_{n=1}^{\infty} a_n^2 w(n) \sum_{s=s_n+1}^{s_{n+1}} b_s^2$$

$$\le C \sum_{n=1}^{\infty} a_n^2 w(n) < \infty$$

and therefore, by the assumption that $w(n)$ is a RC-multiplier for the trigonometric system, we get that both series in (4.13) converge a.e.. Hence, we conclude that $w(n)$ is a Weyl multiplier for $\{g_n\}_{n\ge 1}$. Taking into account (4.12) we can apply Lemma 4.3. Then, using also (4.8), we obtain

$$\lim_{k\to\infty} \max_{2^k \le m < 2^{k+1}} \left| \sum_{n=2^k}^{m} a_n \overline{f}_n(x) \right| = \lim_{k\to\infty} \max_{2^k \le m < 2^{k+1}} \left| \sum_{n=2^k}^{m} a_n g_n(x) \right| = 0 \text{a.e..} \tag{4.14}$$

for any sequence a_n satisfying (1.3). Since two systems in (4.7) are probabilistically equivalent with an error $\lesssim 2^{-k}$, there exists an intermediate sequence $\{\overline{\overline{f}}_n : 2^k \le n < 2^{k+1}\} \subset L^2(\mathbb{T})$, which is probabilistically equivalent to $\{f_n : 2^k \le n < 2^{k+1}\}$ and $\| \overline{\overline{f}}_n - \overline{f}_n \|_2 \le 2^{-k}$. This implies

$$\max_{2^k \le m < 2^{k+1}} \left| \sum_{n=2^k}^{m} a_n f_n(x) \right| = \max_{2^k \le m < 2^{k+1}} \left| \sum_{n=2^k}^{m} a_n \overline{\overline{f}}_n(x) \right|$$

$$\le \max_{2^k \le m < 2^{k+1}} \left| \sum_{n=2^k}^{m} a_n \overline{f}_n(x) \right| + \delta_k(x) \tag{4.15}$$

where

$$\| \delta_k \|_2^2 \le \sum_{n=2^k}^{2^{k+1}-1} a_n^2 \cdot \sum_{n=2^k}^{2^{k+1}-1} \| \overline{f}_n - \overline{\overline{f}}_n \|_2^2 \le 2^{-k} \cdot \sum_{n=2^k}^{2^{k+1}-1} a_n^2.$$

Hence, it becomes clear that $\delta_k(x) \to 0$ a.e.. Combining this with (4.14) and (4.15), we obtain

$$\lim_{k\to\infty} \max_{2^k \le m < 2^{k+1}} \left| \sum_{n=2^k}^{m} a_n f_n(x) \right| = 0.$$

Then once again applying Lemma 4.3 we conclude that $w(n)$ is a Weyl multiplier for the system $\{f_n\}_{n\ge 1}$.

Now consider the part of the theorem concerning the SRC-multipliers. In this case, we use a simplified version of the argument employed in the previous part and omit the details. Let $\{f_n\}_{n\ge 1}$ be an arbitrary orthonormal system of non-overlapping d-dimensional trigonometric polynomials. Applying Lemmas 4.1 and 4.2, for every k we find a collection of non-overlapping one-dimensional trigonometric polynomials $\{\overline{f}_n : 2^k \le n < 2^{k+1}\}$ such that $\| \overline{f}_n \|_2 \le 1$, $n = 1, 2, \ldots$, and the systems (4.7) are probabilistically equivalent with an errors $\lesssim 2^{-k}$. Note that in this case the number of representation terms in the polynomials $\overline{f}_n$ is not important. Then similarly we define the sequence (4.8). If $w(n)$ is a SRC-multiplier for the trigonometric system, then it is Weyl multiplier for the

polynomial system $\{g_n\}_{n\geq 1}$. Thus, applying Lemma 4.3, we can immediately write (4.14). Then continuing exactly the same procedure after (4.14) we conclude that $w(n)$ is a Weyl multiplier for our arbitrarily chosen non-overlapping polynomial system $\{f_n\}_{n\geq 1}$. This completes the proof of the theorem.

References

[1] N. Yu. Antonov, *Almost everywhere convergence over cubes of multiple trigonometric Fourier series*, Izv. Ross. Akad. Nauk Ser. Mat. **68** (2004), no. 2, 3–22. DOI https://doi.org/10.1070/IM2004v068n02ABEH000472 (Russian, with Russian summary); English transl., Izv. Math. **68** (2004), no. 2, 223–241. MR2057997

[2] S. V. Bočkarev, *Rearrangements of Fourier-Walsh series*, Izv. Akad. Nauk SSSR Ser. Mat. **43** (1979), no. 5, 1025–1041, 1197. DOI https://doi.org/10.1070/IM1980v015n02ABEH001226 (Russian). MR552550

[3] S. V. Bočkarev, *A majorant of the partial sums for a rearranged Walsh system*, Dokl. Akad. Nauk SSSR **239** (1978), no. 3, 509–510 (Russian). MR0487239

[4] S. Sh. Galstyan, *Convergence and unconditional convergence of Fourier series*, Dokl. Akad. Nauk **323** (1992), no. 2, 216–218 (Russian); English transl., Russian Acad. Sci. Dokl. Math. **45** (1992), no. 2, 286–289 (1993). MR1191534

[5] G. G. Gevorkyan, *On Weyl factors for the unconditional convergence of series in the Franklin system*, Mat. Zametki **41** (1987), no. 6, 789–797, 889 (Russian). MR904246

[6] G. G. Gevorkyan, *On Weyl factors for the unconditional convergence of series in the Cicielskii system*, Mat. Zametki **116** (2024), no. 5, 707–713, DOI https://doi.org/10.4213/mzm14418 (Russian).

[7] Ch. Fefferman, *On the convergence of multiple Fourier series*, Bull. Amer. Math. Soc. **77** (1971), 744–745, DOI https://doi.org/10.1090/S0002-9904-1971-12793-3. MR435724

[8] S. Kačmaž and G. Šteıngauz, *Teoriya ortogonalnykh ryadov*, Gosudarstv. Izdat. Fiz.-Mat. Lit., Moscow, 1958 (Russian). MR0094635

[9] A. Kamont and G. A. Karagulyan, *On wavelet polynomials and Weyl multipliers*, J. Anal. Math. **150** (2023), no. 2, 529–545, DOI https://doi.org/10.1007/s11854-023-0281-4. MR4645048

[10] G. A. Karagulyan, *On systems of non-overlapping Haar polynomials*, Ark. Math. **58** (2020), no. 1, 121–131, DOI https://doi.org/10.4310/ARKIV.2020.v58.n1.a8.

[11] G. A. Karagulyan, *On Weyl multipliers of the rearranged trigonometric system*, Sbornik Mathematics **211** (2020), no. 12, 1704-1736, DOI https://doi.org/10.1070/SM9422.

[12] G. A. Karagulyan, *A sharp estimate for the majorant norm of a rearranged trigonometric system*, Russian Math. Surveys **75** (2020), no. 3, 569-571, DOI https://doi.org/10.1070/RM9946.

[13] G. A. Karagulyan, M. T. Lacey, and K. V. Navoyan, *Maximal Calderón-Zygmund operators and Weyl multipliers*, Sbornik Mathematics **216** (2025), no. 10, 42–61, DOI https://doi.org/10.4213/sm10277.

[14] U. Goginava, L. Gogoladze, and G. Karagulyan, *BMO-estimation and almost everywhere exponential summability of quadratic partial sums of double Fourier series*, Constr. Approx. **40** (2014), no. 1, 105–120, DOI https://doi.org/10.1007/s00365-014-9234-6. MR3229996

[15] G. A. Karagulyan and A. A. Mkoyan, *An exponential estimate for the cubic partial sums of multiple Fourier series*, Izv. Ross. Akad. Nauk Ser. Mat. **83** (2019), no. 2, 83–96, DOI https://doi.org/10.4213/im8769 (Russian, with Russian summary); English transl., Izv. Math. **83** (2019), no. 2, 273–286. MR3942799

[16] B. S. Kashin and A. A. Saakyan, *Orthogonal series, Translations of Mathematical Monographs*, vol. **75**, American Mathematical Society, Providence, RI, 1989. Translated from the Russian by Ralph P. Boas; Translation edited by Ben Silver. MR1007141
[17] A. Kolmogoroff and D. Menchoff, *Sur la convergence des séries de fonctions orthogonales*, Math. Z. **26** (1927), no. 1, 432–441, DOI https://doi.org/10.1007/BF01475463 (French). MR1544864
[18] D. E. Menshov, *Sur les series de fonctions orthogonales I*, Fund. Math. **4** (1923), 82–105 (Russian).
[19] F. Móricz, *On the convergence of Fourier series in every arrangement of the terms*, Acta Sci. Math. (Szeged) **31** (1970), 33–41. MR271617
[20] S. Nakata, *On the divergence of rearranged Fourier series of square integrable functions*, Acta Sci. Math. (Szeged) **32** (1971), 59–70. MR0435711
[21] S. Nakata, *On the divergence of rearranged trigonometric series*, Tohoku Math. J. **27** (1975), no. 2, 241–246, DOI https://doi.org/10.2748/tmj/1178240990. MR407519
[22] S. Nakata, *On the unconditional convergence of Walsh series*, Anal. Math. **5** (1979), no. 3, 201–205, DOI https://doi.org/10.1007/BF01908903 (English, with Russian summary). MR549237
[23] S. Nakata, *On the divergence of rearranged Walsh series*, Tohoku Math. J. **24** (1972), 275–280, DOI https://doi.org/10.2748/tmj/1178241538. MR340941
[24] A. M. Olevskiı, *Divergent Fourier series*, Izv. Akad. Nauk SSSR Ser. Mat. **27** (1963), 343–366 (Russian). MR0147834
[25] U. Goginava and G. Oniani, *On the almost everywhere convergence of multiple Fourier series of square summable functions*, Publ. Math. Debrecen **97** (2020), no. 3-4, 313–320, DOI https://doi.org/10.5486/PMD.2020.8680. MR4194063
[26] S. N. Poleščuk, *On the unconditional convergence of orthogonal series*, Anal. Math. **7** (1981), no. 4, 265–275, DOI https://doi.org/10.1007/BF01908218 (English, with Russian summary). MR648491
[27] H. Rademacher, *Einige Sätze über Reihen von allgemeinen Orthogonalfunktionen*, Math. Ann. **87** (1922), no. 1-2, 112–138, DOI https://doi.org/10.1007/BF01458040 (German). MR1512104
[28] P. Sjölin, *Convergence almost everywhere of certain singular integrals and multiple Fourier series*, Ark. Mat. **9** (1971), 65–90, DOI https://doi.org/10.1007/BF02383638. MR336222
[29] K. Tandori, *Beispiel der Fourierreihe einer quadratisch-integrierbaren Funktion, die in gewisser Anordnung ihrer Glieder überall divergiert*, Acta Math. Acad. Sci. Hungar. **15** (1964), 165–173, DOI https://doi.org/10.1007/BF01897034 (German). MR161082
[30] K. Tandori, *Über die Divergenz der Walshschen Reihen*, Acta Sci. Math. (Szeged) **27** (1966), 261–263 (German). MR208265
[31] N. R. Tevzadze, *The convergence of the double Fourier series at a square summable function*, Sakharth. SSR Mecn. Akad. Moambe 58 (1970), 277–279 (Russian, with English and Georgian summaries). MR298338
[32] P. L. Ul′yanov, *Weyl factors for unconditional convergence*, Mat. Sb. (N.S.) **60** (102) (1963), 39–62 (Russian). MR0145265
[33] P. L. Ul′yanov, *Divergent Fourier series*, Uspehi Mat. Nauk **16** (1961), no. 3 (99), 61–142 (Russian). MR0125398
[34] P. L. Ul′yanov, *Divergent Fourier series of class L^p ($p \geq 2$)*, Soviet Math. Dokl. **2** (1961), 350–354. MR0119026
[35] P. L. Ul′yanov, *On Weyl multipliers for unconditional convergence of orthogonal series*, Dokl. Akad. Nauk SSSR **235** (1977), no. 5, 1038–1041 (Russian). MR0450886
[36] P. L. Ul′yanov, *Exact Weyl factors for unconditional convergence*, Dokl. Akad. Nauk SSSR **141** (1961), 1048–1049 (Russian). MR0132966

[37] P. L. Ul′yanov, *Solved and unsolved problems in the theory of trigonometric and orthogonal series*, Uspehi Mat. Nauk **19** (1964), no. 1 (115), 3–69 (Russian). MR0161085
[38] P. L. Ul′yanov, *A. N. Kolmogorov and divergent Fourier series*, Uspekhi Mat. Nauk **38** (1983), no. 4 (232), 51–90 (Russian). MR710115
[39] P. L. Ul′yanov, *The work of D. E. Men'shov on the theory of orthogonal series and its further development*, Vestnik Moskov. Univ. Ser. I Mat. Mekh. **4** (1992), 8–24, 101 (Russian, with Russian summary); English transl., Moscow Univ. Math. Bull. **47** (1992), no. 4, 8–20. MR1215456
[40] Z. Zahorski, *Une série de Fourier permutée d'une fonction de classe L^2 divergente presque partout*, C. R. Acad. Sci. Paris **251** (1960), 501–503 (French). MR147833

Funding: The research is supported by the Higher Education and Science Committee of RA, in the frames of the research project 21AG-1A045.
Conflicts of Interest: The author declares no conflicts of interest.

Reports of NAS RA
ՀՀ ԳԱԱ Զեկույցներ
NATIONAL ACADEMY OF SCIENCES OF THE REPUBLIC OF ARMENIA
ՀԱՅԱՍՏԱՆԻ ՀԱՆՐԱՊԵՏՈՒԹՅԱՆ ԳԻՏՈՒԹՅՈՒՆՆԵՐԻ ԱԶԳԱՅԻՆ ԱԿԱԴԵՄԻԱ

2026 **Volume 126** **Issue 1** **Article No. 10**

Category: Chemistry
Type of Paper: Original Research Article
Received: November 22, 2025, **Accepted:** April 15, 2026, **Published:** April 23, 2026

DOI: 10.54503/0321-1339-2026.126.1-10

Features of non-catalytic conversion of light alkanes

Vladimir Arutyunov[1,2,*], Valery Savchenko[2], Aleksey Nikitin[1,2], Aleksey Ozerskii[1], Igor Sedov[2], Ludmila Strekova[1]

[1]Semenov Federal Research Center for Chemical Physics, Russian Academy of Sciences, Moscow, 119991, Russia
[2]Federal Research Center of Problems of Chemical Physics and Medicinal Chemistry, Russian Academy of Sciences, Chernogolovka, Moscow Region, 142432, Russia

[*]Correspondence: v_arutyunov@mail.ru

Running title: Features of non-catalytic conversion

Abstract

The kinetics of non-catalytic gas-phase pyrolysis and oxidative conversion of light hydrocarbons in the temperature range of 1400-1800 K. has been analyzed. Their fundamental difference from the kinetics of the corresponding catalytic processes has been established. Unlike catalytic processes, at these temperatures the oxidative conversion of C_2+ hydrocarbons does not begin with the oxidative stages, but with their pyrolysis, which proceeds much faster than oxidation; and in the specified temperature range C_2+ hydrocarbons transform faster than oxygen. The thermal stage of conversion of C_2+ alkanes leads to the formation of ethylene, and then the oxidation process proceeds almost identically for all these hydrocarbons. Therefore, the additives of all C_2+ alkanes have the same effect on the oxidation and ignition of methane and, consequently, their impurities have the same effect on the knock characteristics of methane. Unlike its homologues, the oxidation of methane proceeds much more slowly and directly when interacting with oxygen, so the conversion of methane and oxygen proceeds similarly. When there is a lack of oxygen, after oxygen conversion is completed, thermal methane pyrolysis occurs at the reached temperature, mainly into acetylene. The subsequent conversion of latter into hydrogen and CO occurs as a result of its interaction with H_2O and CO_2 formed in the mixture.

Keywords: light hydrocarbons, alkanes, non-catalytic processes, thermal conversion, oxidative conversion, kinetic modeling

Introduction

The scale of modern energy and the low energy efficiency EROI (Energy Return On Invested) values of renewable energy sources (RES), usually not exceeding 3,[1] exclude the possibility of its transition to alternative energy sources. Therefore, fossil hydrocarbons remain the main source of energy for the foreseeable future. Contrary to the concerns that arose at the end of the last century, which initiated a series of studies commissioned by the Club of Rome,[2] it is now obvious that the lack of hydrocarbon resources does not threaten the global economy, but the majority of them are represented by unconventional natural gas resources, primarily shale gas and gas hydrates.[1] This makes

it inevitable that gaseous hydrocarbons and, above all, methane will be used more widely, not only for the production of energy, but also as a raw material for producing a wide range of petrochemicals.

Main components of natural and associated gases, which are the resource base of gas chemistry, are light alkanes, which, as a rule, have lower free energy than the target products of their chemical conversion. This is especially true for methane, the principal component of natural gases, which is the most thermodynamically stable hydrocarbon under normal conditions. Therefore, gas-chemical processes require high temperatures and consumes a lot of energy for their implementation, and even in the presence of catalysts, the role of gas-phase reactions in their course can be significant, and in some cases, predominant.

The most difficult and energy-consuming stage of most large-scale methane conversion processes is the initial stage, its activation, which requires breaking the very strong (104 kcal/mol) first C-H bond in this molecule. If we exclude the relatively low-tonnage processes of producing halides-containing, sulfur-containing and nitrogen-containing compounds, then the list of products that can be obtained directly from methane is small (Fig. 1). It is represented by two main groups. The first is products formed as intermediates in the nonequilibrium kinetic processes of methane oxidation and pyrolysis, such as oxygenates (methanol, formaldehyde, peroxides), ethane, ethylene, and aromatic compounds. Their maximum achievable yield is usually low, so it is difficult to count on the possibility of creating economically attractive technological processes based on them.

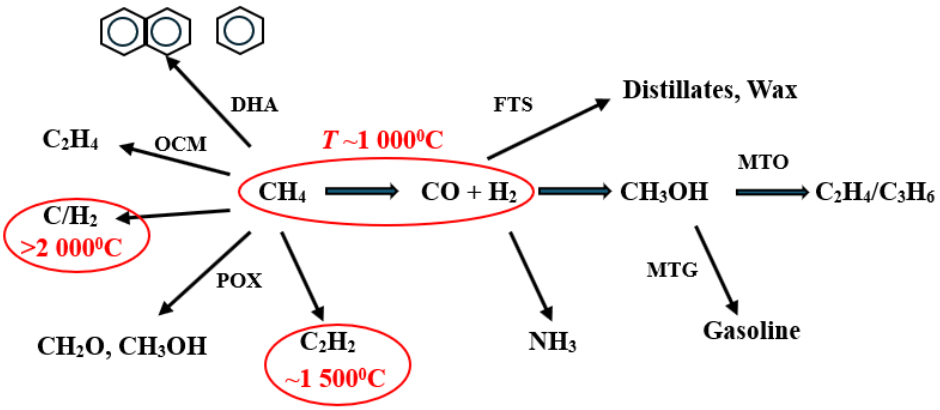

Figure 1. Possible products of methane conversion.

The second group consists of products into which methane can be converted under certain conditions with almost complete or sufficiently high selectivity. At temperatures above 2000 °C, the equilibrium products of methane pyrolysis are solid carbon and hydrogen. The process is considered as one of the possible industrial sources of hydrogen. However, high energy costs and the formation of a large volume of fine carbon, the real need for which is insignificant, raise doubts about its prospects.

At temperatures in the region of ~1500 °C, acetylene becomes one of the equilibrium products of methane pyrolysis. This is the basis of a number of industrial processes for producing this valuable product, but along with significant consumption of energy, the carbon yield of acetylene is relatively low, about 30%.

The most attractive product for gas chemistry, which can be obtained directly from methane, is syngas, into which methane can be converted almost entirely at a relatively moderate temperature of ~1000 °C. In addition to the high selectivity of formation and not very high production temperature, syngas is attractive as an intermediate product, on the basis of which there are already well-developed large-scale synthesis processes for the most large-scale chemical products: ammonia, hydrogen,

methanol, synthetic liquid hydrocarbons (synthetic oil). The last two processes open up a practical way to obtain all other petrochemicals from natural gas.

However, despite the formally existing possibility of using significantly cheaper and more affordable compared to oil natural gas resources for the production of petrochemicals, the contribution of gas chemistry to their production remains small. The reason is the high energy consumption and the great complexity of the existing technologies of the basic process of gas chemistry – the conversion of methane into syngas, associated with overcoming its thermodynamic stability. Currently, in the production from natural gas of such basic gas chemistry products as methanol and synthetic liquid hydrocarbons, this stage accounts for up to 60-70% of their cost.[3]

Thus, the prospects for expanding the contribution of gas chemistry to the production of petrochemicals depend on increasing energy efficiency and reducing the technological complexity of industrial processes for converting natural gas into syngas. The purpose of this paper is to analyze the features and prospects of alternative processes based on non-catalytic conversion of light hydrocarbons.

Matrix reforming as an example of non-catalytic conversion of light hydrocarbons

Gas-phase matrix reforming has been developed as one of the promising opportunities to increase energy efficiency and reduce the technological complexity of converting natural gas into syngas.[4,5] In matrix reforming, the possibility of converting very rich mixtures of hydrocarbon gases with an oxidizer, necessary to obtain a high yield of syngas, is realized through internal heat recuperation from hot conversion products into a fresh gas mixture entering the conversion. Such preheating of the reagents makes it possible to significantly expand the limits of stable oxidation (combustion) of hydrocarbons and, consequently, to ensure a high yield of syngas.

In matrix reformers, such recuperation is realized by organizing flameless near-surface combustion of natural gas. The flame front is stabilized at a short distance from the surface of the matrix made of a heat-resistant material permeable to a gas mixture of hydrocarbons and oxidizer (Fig. 2). Such materials can be perforated ceramics, foam metals, metal felt or pressed metal wire. Heat recuperation occurs due to intensive convective and (in the presence of a screen or in a geometrically closed matrix) radiative heat exchange between the flame front and the solid matrix. As a result, the temperature of the outgoing conversion products is reduced by 400-500 °C, and the working surface of the matrix is heated to 900-1000 °C. Due to this, the fresh reaction mixture, passing through the matrix, heats up and enters the flame front already preheated.

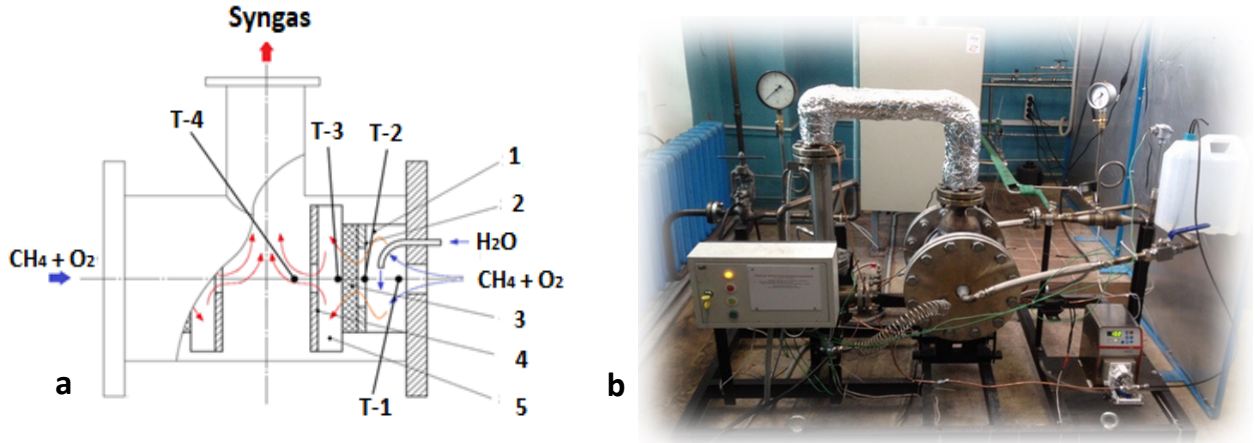

Figure 2. a) The scheme of matrix reformer: 1 – mixing chamber; 2 – inlet diaphragm; 3 – matrix; 4 – radiation screen; 5 – reaction volume; T-1 – T-4 – thermocouples. b) General view of the matrix reformer with an operating pressure of up to 10 atm and a gas flow up to 10 m^3/h.

The most complete conversion of methane and the maximum yield of syngas components H_2 and CO are achieved at the values of the oxidant excess coefficient $\alpha = [O_2]/2[CH_4] = 0.34\text{-}0.36$, which are optimal for this process. At lower α values, the syngas yield decreases due to a decrease in methane conversion, and at higher values, due to an increase in the yield of products of complete oxidation. The H_2/CO ratio, which is very important for the subsequent use of syngas, does not strongly depend on the value of α and is in the range of 1.7-1.8. The reforming process, with the exception of the thermal regime of the matrix, is practically independent of the presence of nitrogen, the concentration of which in the oxidizer affects only the concentration of the components of the syngas produced, therefore atmospheric air, oxygen-enriched air and oxygen can be used as an oxidizer.[4,5]

We briefly note the main advantages of matrix reforming of natural gas, which make it attractive for many technological applications. First of all, it is an autothermal process that does not require external heat or energy sources. The transformation of rich mixtures of hydrocarbon gas (methane) with an oxidizer occurs due to the fact that, in parallel with weakly exothermic reaction (1) of its partial oxidation into syngas

$$CH_4 + 0.5O_2 \rightarrow CO + 2H_2 \qquad \Delta H^0_{298} = -36 \text{ kJ/mol} \qquad (1)$$

a small part of it undergoes complete oxidation by reaction (2):

$$CH_4 + 2O_2 \rightarrow CO_2 + 2H_2O \qquad \Delta H^0_{298} = -802 \text{ kJ/mol}, \qquad (2)$$

thereby providing the necessary energy to maintain the autothermal process, ensuring maximum energy efficiency of hydrocarbon raw materials in this technological process.

The conversion takes place completely in the gas phase behind the surface of the matrix, which makes the process easily controllable and removes the problem of carbon formation, which is critical for catalytic processes of natural gas conversion.

The absence of a catalyst not only simplifies the process, but also significantly reduces the requirements for gas preparation and purification, making it insensitive to many impurities, which are catalytic poisons, and allowing the direct use of hydrocarbon gases of almost any composition, including associated and refinery gases.

Matrix conversion has a very high specific volumetric capacity, at least an order of magnitude higher than the specific capacity of catalytic steam reforming of methane, which makes it possible to reduce specific capital costs accordingly and create cost-effective low-tonnage installations based on it.

The use of atmospheric air, enriched air, or oxygen does not change the nature of the process, its kinetics, or the H_2/CO ratio, affecting only the content of ballast nitrogen in the resulting syngas. The possibility of using atmospheric air not only significantly reduces the cost of the technological process, but also makes it safe to use directly in places of production and processing of combustible hydrocarbons.

Efficient heat recuperation of products makes it possible to convert gases with a high content of inert components (N_2, CO_2, H_2O), including biogas, into syngas,[6] which opens up the possibility of obtaining petrochemicals from renewable bioproducts or waste.

By subsequent catalytic steam reforming of part of the formed CO into hydrogen by the water gas shift reaction (WGSR) (3):

$$CO + H_2O \leftrightarrow CO_2 + H_2, \qquad (3)$$

it is possible not only to regulate the ratio of H_2/CO in the resulting syngas in accordance with the requirements of subsequent processes of its use, but also to obtain hydrogen-containing gas with an H_2 concentration of up to 75%.[7] Moreover, the process remains autothermal, even taking into account the heat consumption for steam generation in a volume sufficient to completely convert the resulting carbon monoxide into hydrogen. At the same time, in comparison with the production of hydrogen by

catalytic steam reforming of methane, the specific consumption of fuel gas is reduced by almost 4 times, the consumption of steam is almost 3 times, and the specific volumetric productivity is increased by an order of magnitude.

A combined process has been developed and patented that combines gas-phase matrix and subsequent catalytic steam reforming of methane and a portion of CO into syngas,[8] which further allows the production of methanol and hydrogen with virtually zero CO_2 formation.[7,9] The possibility of using enriched air with a given N_2/O_2 ratio in the matrix reformer makes it possible to obtain in one stage a hydrogen-nitrogen mixture for the synthesis of ammonia.

Features of kinetics of non-catalytic conversion of light hydrocarbons

The prospects of practical use of matrix reforming of natural gas and a number of other non-catalytic gas-phase processes based on pyrolysis and oxidative conversion of light hydrocarbons have stimulated interest in studying their kinetics in the region of relatively moderate temperatures of 1400-1800 K.[10–12] Kinetic analysis of non-catalytic processes of C_1–C_4 hydrocarbons conversion: their thermal pyrolysis, partial oxidation, steam and carbon dioxide reforming was carried out on the basis of the most detailed and reliable kinetic mechanism of light hydrocarbons oxidation NUI Galway (2010),[13] and its results were qualitatively confirmed by experiments on matrix reforming of hydrocarbon gases.

As a result of kinetic modeling of these processes, it was found that at temperatures of 1400-1800 K under isothermal conditions, the processes of non-catalytic conversion of all C_2+ hydrocarbons begin with the stage of their thermal pyrolysis, which proceeds approximately the same way in the presence of various gases (Ar, N_2, O_2, H_2O, CO_2). This is a consequence of the fact that during the pyrolysis of C_2+ hydrocarbons, the breakaway of atom $H^{\bullet}$ and the subsequent conversion of alkyl radical $C_nH_{2n+1}^{\bullet}$ proceed at a higher rate than their reactions with other components of the reaction mixture, including with oxygen-containing compounds O_2, H_2O, CO_2. Figure 3 shows that the conversion of C_2–C_4 hydrocarbons proceeds much faster than the conversion of oxygen, and is completed long before its complete conversion.

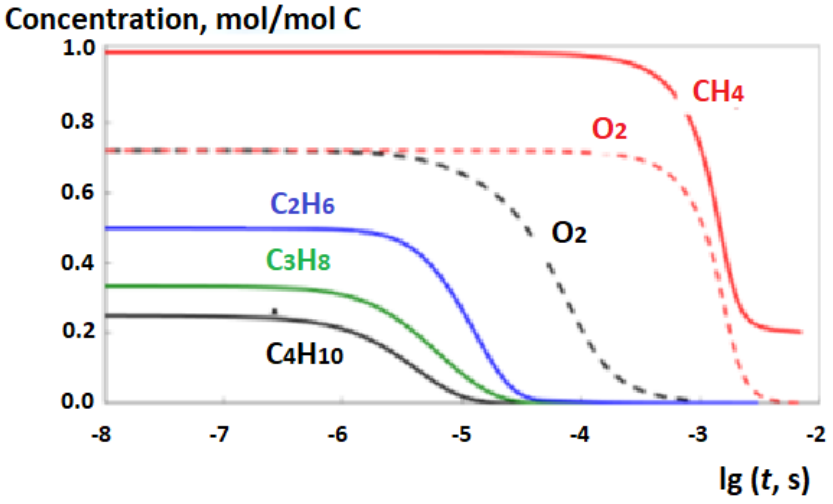

Figure 3. Kinetics of isothermal (T = 1600 K) non-catalytic partial (oxidant excess coefficient α = 0.36) oxidation of C_1–C_4 hydrocarbons. The solid curves represent the conversion of the corresponding hydrocarbon, and the dotted curves represent the conversion of oxygen. For C_2–C_4 hydrocarbons, the oxygen conversion curves practically coincide.[12]

The Figure 4 is clearly demonstrating that the kinetics of butane conversion during its partial oxidation and thermal pyrolysis practically coincide, while the rate of oxygen conversion is significantly lower compared to the rate of butane conversion. Thus, under these conditions, oxygen

has practically no effect on the conversion of light alkanes, and the conversion of oxygen itself occurs as a result of its interaction with products of pyrolysis of C_2+ alkanes, mainly ethylene, which is a more stable hydrocarbon in this temperature range, along with acetylene.

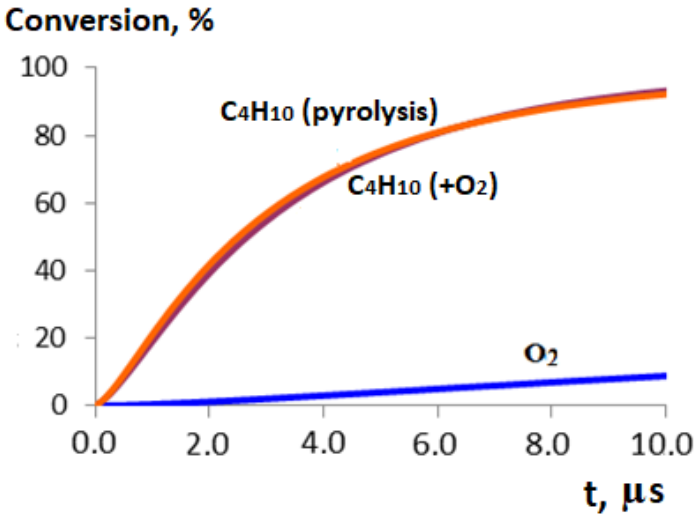

Figure 4. The conversion of reagents in a mixture of 0.25 C_4H_{10} + 0.72 O_2 + 1.0 Ar and at thermal pyrolysis of C_4H_{10}. T = 1600 K, P = 1 atm.

Ethylene formed at the initial stage of C_2+ alkane conversion (pyrolysis stage) in the chain of rapid reactions $C_nH_{2n+1}^{\bullet} \rightarrow C_nH_{2n} \rightarrow C_2H_4$ is the main compound interacting with O_2 at the next oxidation stage. When there is a lack of oxygen, this leads mainly to the formation of CO and H_2O. Therefore, the rate of O_2 consumption during the partial non-catalytic oxidation of all light C_2+ hydrocarbons, including ethylene, is approximately the same. Partially, C_2H_4 is also consumed by the sequence of reactions $C_2H_4 \rightarrow C_2H_3^{\bullet} \rightarrow C_2H_2$, turning into the most stable hydrocarbon under these conditions, acetylene.

Unlike C_2+ alkanes, the conversion of methane in the presence of O_2 proceeds significantly faster than in its absence, since the reaction

$$CH_4 (+M) <=> CH_3^{\bullet} + H^{\bullet} (+M) \quad (4)$$

is slower than the reactions of CH_4 with $O^{\bullet}$ and $OH^{\bullet}$ radicals. The presence of H_2O and CO_2 at T < 1800 K has little effect on the rate of CH_4 conversion, since under these conditions its oxidative conversion is much faster. During the partial oxidation of methane, ethylene is also one of the compounds that interact with O_2, but it is formed as a result of slower stages of pyrolysis of CH_4: $CH_4 \rightarrow CH_3\bullet \rightarrow C_2H_6 \rightarrow C_2H_5^{\bullet} \rightarrow C_2H_4 \rightarrow C_2H_3^{\bullet} \rightarrow C_2H_2$. Therefore, methane oxidation proceeds much slower than that of C_2+ alkanes, and similarly with oxygen conversion (Fig. 3).

After complete oxygen conversion, the gas mixture with T = 1400-1800 K contains H_2, CO, H_2O, CO_2, minor amounts of C_2H_2 and unreacted CH_4 in a ratio far from equilibrium. Subsequent much slower conversion of C_2H_2 and CH_4, in which the main oxidizing agents are H_2O and CO_2, lead to the establishment of thermodynamic equilibrium between the components of the water gas shift reaction (WGSR): H_2, CO, H_2O, CO_2. Next, the system slowly approaches thermodynamic equilibrium. Under adiabatic conditions or at a given temperature profile, this sequence of stages is maintained.

In the case of an adiabatic process, at the initial stage of establishing thermodynamic equilibrium between the components of WGSR for mixtures of C_2+ hydrocarbons with a high concentration of H_2O, due to the exothermic reaction (3), proceeding at a higher rate than the endothermic conversion

of C_2H_2 and CH_4, there is a region of temperature increase in the gas mixture outside the flame zone. Such an increase in temperature is not observed during partial oxidation of methane.

During non-catalytic steam or carbon dioxide reforming of methane in the temperature range of 1400-1800 K, unlike similar catalytic processes, its pyrolysis initially proceeds with the predominant formation of acetylene, which is practically not affected by the concentration of H_2O or CO_2 in the reaction mixture. And only then does the formed acetylene interact with these oxygen-containing components to form hydrogen and CO, i.e. syngas. In this case, the conversion of H_2O and CO_2 occurs mainly in reactions with radicals

$$H_2O + H^{\bullet} \rightarrow H_2 + OH^{\bullet}, \quad (5)$$

$$CO_2 + H^{\bullet} \rightarrow CO + OH^{\bullet}. \quad (6)$$

The indicated sequence of processes occurring during the oxidative conversion of C_1–C_4 hydrocarbons made it possible to explain the reasons for the previously established identical effect of impurities of various C_2–C_6 alkanes on the ignition delay of methane in the temperature range $T < 900$ K,[14] in which fuel mixtures ignite in gas piston engines.[15] At these temperatures, the process of degenerate branched chain oxidation of methane begins, in which the leading role is played by $CH_3OO^{\bullet}$ radicals formed in the equilibrium reaction

$$CH_3^{\bullet} + O_2 \leftrightarrow CH_3OO^{\bullet}. \quad (7)$$

The subsequent formation of methyl hydroperoxide CH_3OOH in this process and its thermal decomposition provide a degenerate branching

$$CH_3OOH \rightarrow CH_3O^{\bullet} + OH^{\bullet}. \quad (8)$$

This process develops relatively slowly, with a long induction period, but leads to a gradual increase in temperature, with an increase in which rapid pyrolysis of heavier methane homologues begins, leading to the formation of mainly ethylene. The subsequent rapid interaction of ethylene with oxygen leads to a sharp increase in the oxidation rate, a shortening of the induction period, and subsequent ignition of the entire mixture. Pyrolysis of C_2–C_6 alkanes into ethylene C_2H_4 before their interaction with oxygen explains their almost identical effect on the ignition of methane and, accordingly, the same effect of the admixtures of these alkanes on the knock resistance of gas-engine fuels.

For the C_2+ alkanes themselves, a similar mechanism of low-temperature branching through the corresponding $RO_2^{\bullet}$ peroxide radicals is not realized due to the rapid isomerization of such alkyl peroxide radicals, followed by their decomposition into olefin $Q^{=}$ and the weakly reactive $HO_2^{\bullet}$ radical

$$R^{\bullet} + O_2 <=> RO_2^{\bullet}, \quad (9)$$

$$RO_2^{\bullet} => Q^{=} + HO_2^{\bullet}, \quad (10)$$

the formation of which at these relatively low temperatures is equivalent to chain termination.

Conclusions

The study of the kinetics of non-catalytic gas-phase processes of pyrolysis and oxidative conversion of light hydrocarbons has shown their fundamental difference from the kinetics of the corresponding catalytic processes. In addition, in the considered temperature range, until a sufficiently high concentration of radicals is formed as a result of reactions involving more reactive compounds (ethylene, acetylene) H_2O and CO_2 are not actually active reagents.

Unlike catalytic processes, the oxidative conversion of C_2+ hydrocarbons begins with their pyrolysis, rather than with oxidative stages. Pyrolysis at these temperatures proceeds much faster than oxidation, so they transform faster than oxygen. The thermal stage of the C_2+ alkane conversion leads

to the formation of ethylene, and therefore their further oxidation proceeds in almost the same way. As a result, the additives of all C_2+ alkanes have the same effect on the oxidation and ignition of methane and, consequently, its knock characteristics.

References

(1) Arutyunov, V.S.; Lisichkin, G.V. Energy resources of the 21st century: problems and forecasts. Can renewable energy sources replace fossil fuels? Russ. Chem. Rev. 2017, 86 (8), 777–804. https://doi.org/10.1070/RCR4723
(2) Meadows, D.H.; Meadows, D.L.; Randers, J.; Behrens, W.W. III. The Limits to Growth. Universe Books: New York, NY, 1972.
(3) Arutyunov, V. Direct Methane to Methanol: Foundations and Prospects of the Process. Elsevier B.V.: Amsterdam, The Netherlands, 2014. ISBN: 978-0-444-63253-1.
(4) Arutyunov, V.S.; Savchenko, V.I.; Sedov, I.V.; Shmelev, V.M.; Nikitin, A.V.; Fokin, I.G.; Eksanov, S.A.; Shapovalova, O.V.; Timofeev, K.A. Experimental studies of natural gas to synthesis gas converters based on permeable cavity matrices. Russian Journal of Applied Chemistry 2016, 89 (11), 1816−1824. https://doi.org/10.1134/S1070427216110124
(5) Nikitin, A.; Ozersky, A.; Savchenko, V.; Sedov I.; Shmelev, V.; Arutyunov, V. Matrix conversion of natural gas to syngas: The main parameters of the process and possible applications. Chem. Eng. J. 2019, 377, article 120883 https://doi.org/10.1016/j.cej.2019.01.162
(6) Arutyunov, V.; Nikitin, A.; Strekova, L.; Savchenko, V.; Sedov, I. Utilization of renewable sources of biogas for small-scale production of liquid fuels. Catalysis Today 2021, 379, 23–27. https://doi.org/10.1016/j.cattod.2020.06.057
(7) Arutyunov, V.S.; Nikitin, A.V.; Savchenko, V.I.; Sedov, I.V. Combined Production of Hydrogen and Methanol without CO_2 Emission Based on Matrix Conversion of Natural Gas. Doklady Chemistry 2023, 513 (2), 361–366. https://doi.org/10.1134/S0012500823601018
(8) Patent RU 217582 U1, 2023.
(9) Patent RU 2801162 C1, 2023.
(10) Savchenko, V.I.; Nikitin, A.V.; Zimin, Ya.S.; Ozerskii, A.V.; Sedov, I.V.; Arutyunov, V.S. Impact of post-flame processes on the hydrogen yield in partial oxidation of methane in the matrix reformer. Chem. Eng. Res. Des. 2021, 175, 250–258. https://doi.org/10.1016/j.cherd.2021.09.009
(11) Savchenko, V.I.; Ozerskii, A.V.; Nikitin, A.V.; Sedov, I.V.; Arutyunov, V.S. Non-Catalytic Partial Oxidation of C_{2+} Hydrocarbon/H_2 Mixtures. Petroleum Chemistry 2023, 63 (11), 1353–1364. https://doi.org/10.1134/S0965544123110014
(12) Savchenko, V.I.; Ozerskii, A.V.; Nikitin, A.V.; Sedov, I.V.; Arutyunov, V.S. Comparative Analysis of Non-Catalytic Processes for Methane and C_2+ Hydrocarbon Conversion: Thermal Pyrolysis, Partial Oxidation, Steam Reforming, and Dry Reforming. Petroleum Chemistry 2025, 65, 761–777 https://doi.org/10.1134/S0965544125600468
(13) NUI Galway. Combustion Chemistry Center. Mechanism. https://c3.universityofgalway.ie/combustionchemistrycentre/mechanismdownloads/
(14) Arutyunov, V.S.; Arutyunov, A.V.; Belyaev, A.A.; Troshin, K.Ya. Controlled ignition of low-carbon gas engine fuels based on natural gas and hydrogen: process kinetics. Russ. Chem. Rev. 2023, 92 (7), RCR5084 https://doi.org/10.59761/RCR5084
(15) Arutyunov, V.S.; Arutyunov, A.V. On antiknock rating of gas engine fuel. Gazovaya Promyshlenost (Gas Industry) 2023, No. 12 (858), 102–109 (in Russian).

Author's Contributions: V.S. Arutyunov: conceptualization, original draft preparation, revision and finalization for publication; V.I. Savchenko: conceptualization, methodology; A.V. Nikitin: experimental

studies; analysis and description of reaction routes; A.V. Ozerskii: kinetic simulation of gas-phase processes, interpretation and visualization of results; I.V. Sedov: analysis and interpretation of kinetic data, conclusions on common and distinct behavioral trends in non-catalytic conversion processes for hydrocarbons; L.N. Strekova: review of literature, graphical presentation.

Funding: This study was funded by the Russian Science Foundation (project no. 22-13-00324).

Conflicts of Interest: The authors declare no conflicts of interest.